UNIVERSITI TEKNOLOGI MARA

COMPARATIVE STUDY OF HYDROTHERMAL-ASSISTED SCHIFF BASE CROSSLINKED AND GRAFTED CHITOSAN-MICROALGAE-KRONOS COMPOSITES FOR THE REMOVAL OF BRILLIANT GREEN DYE

ELMIRA KASHI

PhD

June 2026

UNIVERSITI TEKNOLOGI MARA

COMPARATIVE STUDY OF HYDROTHERMAL-ASSISTED SCHIFF BASE CROSSLINKED AND GRAFTED CHITOSAN-MICROALGAE-KRONOS COMPOSITES FOR THE REMOVAL OF BRILLIANT GREEN DYE

ELMIRA KASHI

Thesis submitted in fulfilment
of the requirements for the degree of
Doctor of Philosophy
(Science)

Faculty of Applied Sciences

June 2026

CONFIRMATION BY PANEL OF EXAMINERS

I certify that a Panel of Examiners has met on 20 January 2026 to conduct the final examination of Elmira Kashi on her Doctors of Philosophy thesis entitled "Comparative Study of Hydrothermal-Assisted Schiff Base Crosslinked and Grafted Chitosan-Microalgae-Kronos Composites for the Removal of Brilliant Green Dye" in accordance with Universiti Teknologi MARA Act 1976 (Akta 173). The Panel of Examiners recommends that the student be awarded the relevant degree. The Panel of Examiners was as follows:

Wan Nazihah Wan Ibrahim, PhD
Associate Professor
Faculty of Applied Sciences
Universiti Teknologi MARA
(Chairman)

Yong Soon Kong, PhD
Associate Professor
Faculty of Applied Sciences
Universiti Teknologi MARA
(Internal Examiner)

Mohd Hazwan Hussin, PhD
Professor
Pusat Pengajian Sains Kimia
Universiti Sains Malaysia
(External Examiner)

PROFESSOR DR HJH ZURAEDA IBRAHIM
Dean
Institute of Postgraduates Studies
Universiti Teknologi MARA

Date: 8 June 2026

AUTHOR'S DECLARATION

I declare that the work in this thesis was carried out in accordance with the regulations of Universiti Teknologi MARA. It is original and is the results of my own work, unless otherwise indicated or acknowledged as referenced work. This thesis has not been submitted to any other academic institution or non-academic institution for any degree or qualification.

I, hereby, acknowledge that I have been supplied with the Academic Rules and Regulations for Post Graduate, Universiti Teknologi MARA, regulating the conduct of my study and research.

Name of Student	:	Elmira Kashi
Student ID. No.	:	2020832376
Programme	:	Doctor of Philosophy (Science) - AS950
Faculty	:	Applied Sciences
Thesis Title	:	Comparative Study of Hydrothermal-Assisted Schiff Base Crosslinked and Grafted Chitosan-Microalgae-Kronos Composites for the Removal of Brilliant Green Dye
Signature of Student	:	……..
Date	:	June 2026

ABSTRACT

The constant depletion of water resources on earth has been a growing concern for the continuous existence of humans and other life forms on the planet. Due this the urgency of the current situation around the globe the United Nations has included this area of research in the 17 Sustainable Development Goals (SDGs) pertaining the 17 global goals addressing the most pressing challenges the world is facing and promoting a more sustainable future for all (sixth goal: Ensure availability and sustainable management of water and sanitation for all). Meanwhile, textile industries are one of the major contributors to the pollution of global water resources with the discharge of effluents containing various chemicals and dyes into natural water resources. Majority of dyes used in industries are synthetic and organic dyes due to their lower cost, however the complex chemical structure of these dyes makes them resistant to biodegradation. Hence, in this research the feasibility of the employment and efficiency of dye removal (brilliant green (BG) dye) by four different chemically crosslinked (crosslinking agents used: glyoxal and benzil) or grafted (grafting agents used: salicylaldehyde and benzaldehyde) chitosan-microalgae-kronos (TiO_2). The physicochemical properties of the four synthesised adsorbents have been investigated using various analytical techniques (FT-IR analysis, XRD analysis, FE-SEM imaging with EDX analysis, pH_{pzc} determination analysis, and elemental (CHNS/O) analysis) and the impact of the main adsorption parameters (adsorbent dose, pH and time) on the dye removal of each adsorbent was determined. Box-Behnken Design from Response Surface Methodology was used for design of experiments and parameter optimisation and the optimised parameter values were used to investigate the adsorption equilibrium behaviour. The pseudo-first order and pseudo-second order kinetic models' parameters for each adsorbent (for the removal of BG dye) were calculated to determine the rate determining factor in the adsorption systems. Furthermore, the adaptability of the adsorption equilibrium data with Langmuir, Freundlich and Temkin isotherm models was investigated to better understand the adsorption process of BG removal by the four synthesised adsorbents. Moreover, the feasibility and spontaneity of the adsorption process was investigated by calculating the thermodynamic parameters for the BG removal process by the adsorbents. Additionally, based on the obtained data from all analyses a plausible adsorption mechanism has been proposed for each adsorbent. Finally, the results of the analyses for all adsorbents have been compared to determine the better approach (crosslinking or grafting) to achieve a more efficient adsorption system for the removal of BG dye. The obtained results revealed that amongst the four modified adsorbents in this study, the salicylaldehyde-grafted adsorbent has the highest efficiency (q_{max}=957mg/g) towards the removal of the target pollutant (BG dye), while the glyoxal-crosslinked adsorbent, despite yielding the lowest dye removal capacity (q_{max}=88.3mg/g), exhibits efficient removal in acidic pH values (highest removal achieved at pH=4) which can prove efficient for the removal of pollutants in acidic environments without the need for pH adjustments.

ACKNOWLEDGEMENT

Firstly, I wish to thank God for giving me the opportunity to embark on my PhD and for completing this long and challenging journey successfully.

I wish to express my deepest gratitude to my supervisor Dr. Ali H. Jawad Al-Taie for all his sincere help and support throughout this arduous journey, reaching the end of this path wouldn't have been possible without him. I would also like to express my gratitude to my co-supervisor Dr. Siti Norasmah Binti Surip for providing support whenever needed.

I would like to express my sincere gratitude to my mother who believed in me and gave me strength no matter how many times I wanted to give up, my father who silently supported me through the most difficult times, and my brother who always made me strive to be better.

My appreciation goes to the Advanced Biomaterials and Carbon Development (ABCD) Research Group and the faculty of applied sciences who provided the facilities and assistance during the experimental phase of this project. Special thanks to my colleagues and friends for helping me throughout my PhD journey.

Finally, this thesis is dedicated to my loving husband, Hayder, who helped and supported me unconditionally throughout this journey.

TABLE OF CONTENTS

		Page
CONFIRMATION BY PANEL OF EXAMINERS		**ii**
AUTHOR'S DECLARATION		**iii**
ABSTRACT		**iv**
ACKNOWLEDGEMENT		**v**
TABLE OF CONTENTS		**vi**
LIST OF TABLES		**x**
LIST OF FIGURES		**xiii**
LIST OF SYMBOLS		**xvii**
LIST OF ABBREVIATIONS		**xviii**
CHAPTER 1 INTRODUCTION		**1**
1.1	Research Background	1
1.2	Motivation for This Work	3
1.3	Problem Statement	3
1.4	Research Objectives	4
1.5	Research Question	5
1.6	Significance of Study	5
CHAPTER 2 LITERATURE REVIEW		**7**
2.1	Background	7
2.2	Dyes as Water Pollutant	9
2.3	Synthetic Organic Dyes as Water Pollutants	11
	2.3.1 Brilliant Green (BG) Dye	13
2.4	Treatment Methods for Dye Removal from Wastewater	14
2.5	Adsorption for Dye Removal	17
2.6	Chitosan (CS) as an Adsorbent	18
2.7	Modifications of Chitosan	19
	2.7.1 Physical Modifications of chitosan	23

2.7.2 Chemical Modifications of chitosan 26
2.7.3 Hydrothermal Method for Synthesis of Crosslinked and Grafted Chitosan Derivatives 34
2.7.4 Benzaldehyde (BD) as a Grafting Agent 34
2.7.5 Salicylaldehyde (SD) as Grafting Agent 36
2.7.6 Glyoxal as a Crosslinking Agent 37
2.7.7 Benzil as a Crosslinking Agent 38
2.8 Algae as an Adsorbent 40
2.8.1 Algae (Spirulina sp.) as a Modifying Agent 41
2.9 Titanium Dioxide as an Adsorbent 42
2.10 Dye Adsorption Mechanisms on Chitosan Derivatives 44
2.11 Optimisation by Response Surface Methodology (RSM) 44

CHAPTER 3 RESEARCH METHODOLOGY 46
3.1 Materials and Methods 46
3.1.1 Chemicals and Reagents 46
3.1.2 Apparatus 46
3.2 Methods 47
3.2.1 Preparation of Cs-Ma-Tk Beads 47
3.2.2 Grafting of Cs-Ma-Tk with SD 47
3.2.3 Grafting of Cs-Ma-Tk with BD 47
3.2.4 Cross-linking Cs-Ma-Tk with Bz_2 48
3.2.5 Cross-linking Cs-Ma-Tk with Gly 48
3.3 Characterisation of the Adsorbents 48
3.3.1 X-Ray Diffraction Analysis 48
3.3.2 FT-IR Spectra Analysis 49
3.3.3 Physical Properties 49
3.3.4 Surface Morphology and elemental composition 50
3.3.5 Surface Charge (pHpzc) Analysis 51
3.4 Design of Experiments using Box-Behnken design (BBD) 51
3.5 Equilibrium Studies 53
3.5.1 Kinetic Study 53
3.5.2 Isotherm Study 54
3.5.3 Thermodynamic Study 55

CHAPTER 4 RESULTS AND DISCUSSION **57**
4.1 Salicylaldehyde grafted Cs-Ma-Tk (Cs/SD-Ma-Tk) 57
4.1.1 Surface Properties of Cs/SD-Ma-Tk 57
4.1.2 X-Ray Diffraction Analysis of Cs/SD-Ma-Tk 59
4.1.3 FT-IR Spectrum Analysis of Cs/SD-Ma-Tk 60
4.1.4 Surface Morphology of Cs/SD-Ma-Tk 62
4.1.5 Statistical Optimisation and Analysis 63
4.1.6 Adsorption Equilibrium Studies of BG Removal by Cs/SD-Ma-Tk 71
4.1.7 Proposed Mechanism of BG Removal by Cs/SD-Ma-Tk 75
4.2 Benzaldehyde grafted Cs-Ma-Tk (Cs/BD-Ma-Tk) 77
4.2.1 Surface Properties of Cs/BD-Ma-Tk 77
4.2.2 X-Ray Diffraction Analysis of 78
4.2.3 FT-IR Spectrum Analysis of Cs/BD-Ma-Tk 79
4.2.4 Surface Morphology of Cs/BD-Ma-Tk 80
4.2.5 Statistical Optimisation and Analysis 82
4.2.6 Adsorption Equilibrium Studies of BG Removal by Cs/BD-Ma-Tk 88
4.2.7 Proposed Mechanism of BG Removal by 92
4.3 Glyoxal Crosslinked Cs-Ma-Tk (Cs/Gly-Ma-Tk) 94
4.3.1 Surface Properties of Cs/Gly-Ma-Tk 94
4.3.2 X-Ray Diffraction Analysis of Cs/Gly-Ma-Tk 95
4.3.3 FT-IR Spectrum Analysis of Cs/Gly-Ma-Tk 96
4.3.4 Surface Morphology of Cs/Gly-Ma-Tk 98
4.3.5 Statistical Optimisation and Analysis 99
4.3.6 Adsorption Equilibrium Studies of BG Removal by Cs/Gly-Ma-Tk 107
4.3.7 Proposed Mechanism of BG Removal by Cs/Gly-Ma-Tk 111
4.4 Benzil Crosslinked Cs-Ma-Tk (Cs/Bz_2-Ma-Tk) 113
4.4.1 Surface Properties of Cs/Bz_2-Ma-Tk 113
4.4.2 X-Ray Diffraction Analysis of Cs/Bz_2-Ma-Tk 114
4.4.3 FT-IR Spectrum Analysis of Cs/Bz_2-Ma-Tk 115
4.4.4 Surface Morphology of Cs/Bz_2-Ma-Tk 116
4.4.5 Statistical Optimisation and Analysis 118

4.4.6 Adsorption Equilibrium Studies of BG Removal by Cs/Bz_2-Ma-Tk 125
4.4.7 Proposed Mechanism of BG Removal by Cs/Bz_2-Ma-Tk 130
4.5 Comparison 132

CHAPTER 5 CONCLUSION AND FUTURE WORK 137
5.1 Conclusion 137
5.2 Future Work Recommendations 139

REFERENCES 140

APPENDICES 179

AUTHOR'S PROFILE 187

LIST OF TABLES

Tables	Title	Page
Table 2.1	Several Treatment Methods for Dye Effluents [2]	15
Table 2.2	Examples of Modifications Done by Researchers on Chitosan for Dye Adsorption	20
Table 2.3	Several Modifications Done by Researchers on Chitosan Using Algae	25
Table 2.4	Several Cross-Linking and Grafting Agents Used to Improve the Properties of Cs	30
Table 2.5	Applications of Algae in Dye Removal	41
Table 2.6	Examples of Applications of TiO_2 in Dye Removal	43
Table 3.1	Factors and Their Levels	52
Table 4.1	Physicochemical Characteristics of Cs/SD-Ma-Tk	58
Table 4.2	Factor Levels of the BBD Design for BG Removal by Cs/SD-Ma-Tk	64
Table 4.3	BBD Design Coded and Actual Values Alongside Predicted and Experimental Response for BG Removal by Cs/SD-Ma-Tk	64
Table 4.4	ANOVA Test Results for BG Removal by Cs/SD-Ma-Tk	66
Table 4.5	Kinetic Model Data for BG Adsorption by Cs/SD-Ma-Tk	72
Table 4.6	Isotherm Model Parameters for BG Removal by Cs/SD-Ma-Tk	74
Table 4.7	Thermodynamic Parameters of BG Removal by Cs/SD-Ma-Tk	74
Table 4.8	Surface Properties of Cs/BD-Ma-Tk	78
Table 4.9	Factor Levels of the BBD Design for BG Removal by Cs/BD-Ma-Tk	82
Table 4.10	Experimental Matrix Based on BBD Approach for Designing Experiments and the Corresponding Response (BG Removal (%) by Cs/BD-Ma-Tk)	83

Table 4.11	Analysis of Variances (ANOVA) for BG Dye Removal by Cs/BD-Ma-Tk	85
Table 4.12	Kinetic Model Parameters for BG Dye Removal by Cs/BD-Ma-Tk	89
Table 4.13	The Parameters of Isotherm Models for BG Dye Adsorption by Cs/BD-Ma-Tk	90
Table 4.14	Thermodynamic Parameters for the Adsorption of BG Dye by Cs/BD-Ma-Tk	92
Table 4.15	Surface Properties of Cs/Gly-Ma-Tk	95
Table 4.16	Factor Levels of the BBD Design for BG Removal by Cs/Gly-Ma-Tk	100
Table 4.17	Experimental Design Based on BBD for BG Removal (%) by Cs/Gly-Ma-Tk	100
Table 4.18	Analysis of Variance (ANOVA) for BG Dye Removal by Cs/Gly-Ma-Tk	102
Table 4.19	PFO and PSO Kinetic Parameters for BG Adsorption by Cs/Gly-Ma-Tk	108
Table 4.20	Isotherm Model Parameters for BG Adsorption by Cs/Gly-Ma-Tk	109
Table 4.21	Thermodynamic Parameters of BG Removal by Cs/Gly-Ma-Tk	110
Table 4.22	Surface Properties and Elemental Composition of Cs/Bz_2-Ma-Tk	114
Table 4.23	Three Levels of the Three Independent Variables in the Removal of BG Dye by Cs/Bz_2-Ma-Tk	119
Table 4.24	BBD Design Coded and Actual Values Alongside Predicted and Experimental Response for BG Removal by Cs/Bz_2-Ma-Tk (with Desirability Test Results (Last Row)	119
Table 4.25	ANOVA Test Results for BG Removal by Cs/Bz_2-Ma-Tk	121
Table 4.26	PFO and PSO Kinetic Models' Terms for the Removal of BG Dye by Cs/Bz_2-Ma-Tk	127
Table 4.27	Isotherm Model Parameters for BG Removal by Cs/Bz_2-Ma-Tk	128

Table 4.28 Thermodynamic Parameters of BG Removal by Cs/Bz_2-Ma-Tk 129
Table 4.29 Comparison of the Analyses Results for the Four Synthesised Adsorbents 135

LIST OF FIGURES

Figures	Title	Page
Figure 2.1	Industries Responsible for the Discharge of Dye Effluents in the Environment [2]	8
Figure 2.2	Dangerous Chemicals Used in Conjunction With Colorants for Dyeing Industries [2]	10
Figure 2.3	Chemical Structure of Brilliant Green (BG) [45]	13
Figure 2.4	Chemical Structure of Ideal Chitosan [118]	18
Figure 2.5	Hybrid Composite Preparation Methods: (A) Mechanical Stirring, (B) Surface Coating, and (C) Nanocomposite [170]	24
Figure 2.6	Chemical Structure of Benzaldehyde [232]	35
Figure 2.7	Schiff Base of Chitosan-Benzaldehyde [235]	35
Figure 2.8	The Chemical Structure of Salicylaldehyde [237]	36
Figure 2.9	Schiff Base of Chitosan-Salicylaldehyde [237]	37
Figure 2.10	The Chemical Structure of Glyoxal [240]	37
Figure 2.11	Schiff Base of Chitosan-Glyoxal [240]	38
Figure 2.12	The Chemical Structure of Benzil [248]	39
Figure 2.13	Schiff Base of Chitosan-Benzil [6]	39
Figure 2.14	The Primitive Cells of Rutile, Brookite and Anatase (from Left to Right) [261]	42
Figure 2.15	General steps of using RSM	45
Figure 4.1	N_2 Adsorption/Desorption Plot of Cs/Sd-Ma-Tk with Pore Width Distribution Inset	59
Figure 4.2	XRD Pattern of Cs/SD-Ma-Tk	60
Figure 4.3	FT-IR Spectra of Cs/SD-Ma-Tk (a) Before and (b) After the Adsorption of BG Dye	61
Figure 4.4	FE-SEM Images at Two Magnification Powers of 3kx (a and d) and 10kx (b and e) of (a-b) Cs/SD-Ma-Tk, (d-e) Cs/SD-Ma-Tk+BG and EDX Profiles of (c) Cs/SD-Ma-Tk and (f) Cs/SD-Ma-Tk+BG	63
Figure 4.5	Desirability Ramps of BG Removal by Cs/SD-Ma-Tk	65

Figure 4.6	BBD Plots of (a) Predicted vs. Actual, (b) Normal Plot of Residuals, and (c) Cook's Distance; for BG Removal by Cs/SD-Ma-Tk	67
Figure 4.7	Impact of Independent Variables (a) Cs/SD-Ma-Tk Dose, (b) pH, and (c) Time on BG Removal Response	68
Figure 4.8	3D Surface Plots and 2D Contour Curves of the Interactive Impact of Variable Pairs with Significant Impact on BG Removal Response by Cs/SD-Ma-Tk (Plus pHpzc Plot of Cs/SD-Ma-Tk)	71
Figure 4.9	Impact of Initial Concentration and Kinetic Model Regressions of BG Removal by Cs/SD-Ma-Tk	72
Figure 4.10	Langmuir, Freundlich and Temkin Isotherm Regressions for BG Removal by Cs/SD-Ma-Tk	73
Figure 4.11	Van't Hoff Plot of BG Removal by Cs/SD-Ma-Tk	75
Figure 4.12	Suggested Mechanism of Adsorption for the Removal of BG Dye by Cs/SD-Ma-Tk	76
Figure 4.13	N_2 Adsorption/Desorption Profile of Cs/BD-Ma-Tk	78
Figure 4.14	XRD Pattern of Cs/BD-Ma-Tk	79
Figure 4.15	FT-IR Analysis of (a) Cs/BD-Ma-Tk, and (b) Cs/BD-Ma-Tk+BG dye	80
Figure 4.16	FE-SEM Images at Two Magnification Powers of 3kx (a and d) and 10kx (b and e) of (a-b) Cs/BD-Ma-Tk, (d-e) Cs/BD-Ma-Tk+BG and EDX Profiles of (c) Cs/BD-Ma-Tk and (f) Cs/BD-Ma-Tk+BG	81
Figure 4.17	Desirability Ramps of BG Removal by Cs/BD-Ma-Tk	84
Figure 4.18	BBD Model Validation Plots of (a) Normal Plot of Residual (b) Predicted vs Actual for BG Dye Removal by Cs/BD-Ma-Tk	85
Figure 4.19	3D Images of Interactive Effects Of Parameters (a) AB (Dose vs pH), (b) AC (Dose vs Time), and (c) BC (pH vs Time) on BG Removal by Cs/BD-Ma-Tk and (d) pH_{pzc} Test of Cs/BD-Ma-Tk	87
Figure 4.20	Effect of Concentration and Time Variations on Cs/BD-Ma-Tk Adsorption Capacity Alongside the Regression Fits of the PFO and PSO Kinetic Models to the Experimental Data	88

Figure 4.21	Isotherm Model (Langmuir, Freundlich and Temkin) Regression Fits to the Equilibrium Data of BG Adsorption by Cs/BD-Ma-Tk	90
Figure 4.22	Van't Hoff Plot of BG Removal by Cs/BD-Ma-Tk	91
Figure 4.23	The Proposed Interaction Mechanism of BG Dye with Cs/BD-Ma-Tk	93
Figure 4.24	N_2 Adsorption-Desorption Isotherm of Cs/Gly-Ma-Tk	95
Figure 4.25	XRD Pattern of Cs/Gly-Ma-Tk	96
Figure 4.26	FT-IR Spectra of (a) Cs/Gly-Ma-Tk, and (b) Cs/Gly-Ma-Tk+BG	97
Figure 4.27	FE-SEM Images at Two Magnification Powers of 3kx (a and d) and 10kx (b and e) of (a-b) Cs/Gly-Ma-Tk and (d-e) Cs/Gly-Ma-Tk After BG Adsorption and EDX Mapping of (c) Cs/Gly-Ma-Tk and (f) Cs/Gly-Ma-Tk after BG Dye Adsorption	99
Figure 4.28	Desirability Ramps of BG Removal by Cs/Gly-Ma-Tk	101
Figure 4.29	(a) Normal Plot of Residual (b) Predicted versus Actual Removal of BG Dye with Cs/Gly-Ma-Tk (c) Residual vs Run of BG Removal	103
Figure 4.30	3D Surface Plots and 2D Contours of (a-b) AB (Adsorbent Dose*pH), and (d-e) BC (pH*Time) Interactions on BG Dye Removal by Cs/Gly-Ma-Tk (and (c) pH_{pzc} Test of Cs/Gly-Ma-Tk)	106
Figure 4.31	Effect of the Contact Time on BG Adsorption by Cs/Gly-Ma-Tk at Several Concentrations Alongside PFO and PSO Regression Fits to the Experimental Data	107
Figure 4.32	The Langmuir, Freundlich and Temkin Adsorption Isotherm Regression Fits of BG Dye Adsorption by Cs/Gly-Ma-Tk	109
Figure 4.33	The Van't Hoff Plot of the Equilibrium Thermodynamic Data for BG Adsorption by Cs/Gly-Ma-Tk	110
Figure 4.34	Illustration of the Plausible Interactions Contributing to the Adsorption of BG Dye by Cs/Gly-Ma-Tk	112
Figure 4.35	N_2 Adsorption/Desorption Plot of Cs/Bz_2-Ma-Tk	114
Figure 4.36	XRD Pattern of Cs/Bz_2-Ma-Tk	115

Figure 4.37	FT-IR Spectra of Cs/Bz_2-Ma-Tk (a) Before and (b) After BG Dye Adsorption	116
Figure 4.38	FE-SEM Images at Two Magnification Powers of 3kx (a and d) and 10kx (b and e) of (a-b) Cs/Bz_2-Ma-Tk and (d-e) Cs/Bz_2-Ma-Tk After BG Adsorption and EDX Mapping of (c) Cs/Bz_2-Ma-Tk and (f) Cs/Bz_2-Ma-Tk After BG Dye Adsorption	118
Figure 4.39	Desirability Ramps of BG Removal by Cs/Bz_2-Ma-Tk	120
Figure 4.40	BBD Plots of (a) Normal Plot of Residuals, (b) Predicted vs. Actual, and (c) Cook's Distance; for BG Removal by Cs/Bz_2-Ma-Tk	122
Figure 4.41	The Impact of Independent Variables on BG Removal Response by Cs/Bz_2-Ma-Tk	123
Figure 4.42	pH_{pzc} Plot of Cs/Bz_2-Ma-Tk	124
Figure 4.43	3D Plot and 2D Contour of Interactive Impact of pH and Time for BG Dye Removal Response by Cs/Bz_2-Ma-Tk	125
Figure 4.44	Impact of Initial Dye Concentration and Kinetic Model Regressions of BG Dye Removal by Cs/Bz_2-Ma-Tk	126
Figure 4.45	Langmuir, Freundlich and Temkin Isotherm Regressions for BG Removal by Cs/Bz_2-Ma-Tk	128
Figure 4.46	Van't Hoff Plot of BG Removal by Cs/Bz_2-Ma-Tk	129
Figure 4.47	Suggested Mechanism of Adsorption for the Removal of BG Dye by Cs/Bz_2-Ma-Tk	131

LIST OF SYMBOLS

Symbols	
%	Percentage
g	Gram
m	Milli
min	Minute
mol	Mole
nm	Nanometre
μm	Micrometre

LIST OF ABBREVIATIONS

Abbreviations

BBD	Box-Behnken Design
BD	Benzaldehyde
BET	Brunauer-Emmett-Teller Method
BG	Brilliant green
Bz_2	Benzil
Cs	Chitosan
FE-SEM/EDX	Field Emission Scanning Electron Microscope with Energy Dispersive X-ray
FT-IR	Fourier Transform Infrared
Gly	Glyoxal
Ma	Microalgae
pH_{pzc}	Point of Zero Charge pH
RSM	Response Surface Methodology
SD	Salicylaldehyde
TK	TiO_2 (Kronos)
XRD	X-ray Diffractometer

CHAPTER 1
INTRODUCTION

1.1 Research Background

Water is the most important resource for the survival of humankind. The water resources on the planet are limited and with continuous discharge of effluents from different industries into the water bodies many of the water resources have been contaminated; hence in the past decades water treatment has become an increasingly important field. As the urgent issue of water contamination persists, finding a proper way for permanently removing dye molecules from the effluents has become a pressing matter. There are many different approaches that have been investigated for dye removal from wastewater such as biological treatment, oxidation, adsorption, filtration, and photo-degradation to minimise the negative effects of dyes on the water resources on earth [1], [2]. In recent years, removal of dyes using adsorption approach has attracted attention for the purpose of separating dye molecules from the dye effluent and returning the treated water for reuse.

From the materials that have been investigated for the removal of dyes from effluents through adsorption technique, biopolymers are of the most economically and environmental-friendly ones. One of the notable biopolymers that has received considerable attention in recent years is Chitosan (Cs) or β-(1-4)-2-amino-2-deoxyd-glucose). Chitosan is a derivative of chitin that is initially obtained from the exoskeleton of crustaceans such as crabs and shrimps [3]. As the pressing issue of water contamination requires abundantly available resources for treatment, chitosan is a promising biopolymer to utilise as it is the second most abundant biopolymer in nature only after cellulose. Chitosan is a bioactive polymer with many desirable characteristics such as anti-bacterial activity, non-toxicity, easy modification, cost-efficiency, being eco-friendly and biodegradability. Its desirable characteristics have made chitosan a widely used material in medicinal applications, food industries, water treatment and many other fields. Furthermore, Cs has been preferred over many other compounds due to its high adsorption capacity and quicker adsorption rates [4]. However, Cs also possesses certain undesirable properties such as high swelling in aqueous environments

and low stability in acidic pH that need to be addressed by modification processes such as cross-linking or grafting [5], [6].

Microbial biomasses (dead or alive) have been investigated extensively for the removal of dyes from effluents. Microbial biomass such as bacteria, micro algae and fungi can be used for dye effluent treatment as they can either adsorb dye molecules or use the enzymes that they secrete to destroy the chromophores of dye molecules resulting to decolouration [7]. Algal biomasses are widely grown and cost-efficient. Their biosorption activity for the extraction of toxic colourants has been studied and they have proven to be power adsorbents [8], [9].

On the other hand, titanium dioxide (TiO_2) is an abundant catalyst widely utilised in degradation of toxic mineral and dyes from wastewater. The different microscopic structures on it allow this material unique properties such as chemical stability, low toxicity, high reactivity, high hydrolytic and mechanical stability which in return deem it as a suitable material for various applications. In addition, the surface of TiO_2 contains Lewis's acid and base centres that majorly determine the adsorptive and catalytic properties of this material [10], [11]. Additionally, kronos is a commercial, carbon-doped, microscale TiO_2 that will be used in this research.

This study aims to synthesise a promising and cost-effective crosslinked and grafted composites of chitosan/microalgae/TiO_2 (kronos) (Cs-Ma-Tk) for the removal of Brilliant Green dye. All materials used in this study are abundantly available in nature, cost-efficient and non-toxic. There has been extensive research done on chitosan but composites of chitosan with algal biomass have been less reported for wastewater treatment. In most research done on composites of chitosan with TiO_2, nanoparticles were used, and the commercial microscale Kronos has little reported use in literature up to the date of writing this thesis. Moreover, the grafting of aromatic aldehydes on the polymeric matrix of chitosan through Schiff base reaction has minimal reports in literature and there are no studies performed to compare the two processes of cross-linking and grafting (to the extent of my knowledge) for synthesis of promising dye adsorbents. Hence, this study aims to fill the above-mentioned gaps in existing literature.

1.2 Motivation for This Work

Clean water resources on our green planet are extremely limited and with the indiscriminate discharge of various pollutants (such as dyes, harsh chemicals, heavy metals, pesticides, etc.) from different industries into the freshwater bodies during the previous decades, the available water resources are running ever thinner. According to the United Nations all humans are entitled to the right to clean water, hence with the ever-increasing need to access clean water with the growth in human population it has become imperative to address the water remediation issue. Amongst the many water pollutants, dyes (specifically synthetic organic dyes) not only affect the drinkability of water due to their toxic nature which can endanger human health, but also severely impact aquatic creatures by reducing sunlight penetration which consequently hinders photosynthesis by aquatic plants. Synthetic organic dyes, generally containing aromatic rings in their structure, are extremely resistant to decomposition and so their presence in water resources can bring about long lasting consequences. To avoid the major negative impacts imposed on the environment and human life due to the discharge of dye containing effluents the field of water remediation has become increasingly active during the recent decade with various water remediation methods proposed by different researchers from all around the globe. This work is in an effort to join this cause and strive to better the environment.

1.3 Problem Statement

The clean water resources on the planet are limited and as time goes by more water bodies get polluted by chemicals, heavy metals and other polluting agents. One of the major contributors to the pollution of water resources is the discharge of dye-containing water from different industries. The discharge of untreated dye effluents into the water bodies is an urgent and pressing issue for the aquatic life and humans due to the harmful effects of these compounds. Removal of these dyes from wastewater prior to discharge needs to be considered to avoid further contamination of the water resources. Chitosan (Cs) is a bio-polymer material that can be used as an adsorbent for dye treatment. However, natural chitosan's high solubility in many organic acids, high swelling index in water, compressibility at high operating pressure, and poor surface area limits its use in water treatment technologies. On the other hand, Cs has low

porosity and weak mechanical properties, which are the main drawbacks for high adsorption capabilities. Another downside of Cs is that it has high affinity towards anionic dyes, but not to cationic dyes. However, due to the abundance of this material in nature and its low cost, the use of this biopolymer as an adsorbent is very beneficial. In the recent years, various methods have been employed by researchers to overcome the disadvantages of chitosan for more efficient adsorption results. The addition of algal biomasses and TiO_2 nanoparticles have been investigated by researchers in recent years, however a ternary composite system containing chitosan, algae and TiO_2 has not been studied before. Furthermore, many studies have been made regarding the effects of Schiff base crosslinking and grafting on the adsorptive properties of chitosan derivatives, however a concise comparison of the two modes is currently missing in literature. This study aims to fill the above-mentioned gap in knowledge by developing a novel ternary composite system of chitosan/algae/TiO_2 and crosslinking/grafting the synthesised composite to achieve a more chemically stable, durable, effective, and cost-efficient adsorbent. Additionally, the efficiency of the synthesised composites towards the removal of BG dye were compared to determine the more advantageous approach between chemical crosslinking and grafting for the synthesis of Cs-based adsorbents towards pollutant (cationic species) removal. Furthermore, the properties of the developed adsorbents, as well as their behaviour in the adsorption system, have been studies in details to better understand the differences between the two modification methods.

1.4 Research Objectives

The general purpose of this study is to compare the efficiency of brilliant green dye removal by grafted and crosslinked chitosan composites. However, the specific aim of this study is to fulfil the following objectives:

a) To synthesise Schiff base chitosan-microalgae-TiO_2 (kronos) composites modified by cross-linking (by Glyoxal and Benzil) and grafting (by Salicylaldehyde and Benzaldehyde) reactions via hydrothermal method to be used as promising adsorbents for the removal of Brilliant Green dye from aqueous environments.
b) To study the physicochemical properties of the synthesised crosslinked and

grafted composites via various analytical methods such as FT-IR, FE-SEM/EDX, XRD, BET, pHpzc and elemental (CHNS/O) analyses.

c) To perform statistical optimisation for the key adsorption parameters (adsorbent dose, contact time and pH) using RSM-BBD and investigate the impact of individual and dual parameters on the BG removal response.
d) To study the adsorption equilibrium behaviour through kinetic, isotherm and thermodynamic studies and determine the pathways leading to the adsorption of BG by each adsorbent and propose a plausible adsorption mechanism.
e) To compare the obtained results for each adsorbent and determine the more efficient modification method (crosslinking or grafting) to achieve a more efficient BG removal.

1.5 Research Question

i) What changes occur to the ternary composite system when put through the hydrothermal grafting and crosslinking process?
ii) How does the crosslinking/grafting process affect the adsorption efficiency of the synthesised adsorbents?
iii) What are the optimal conditions for achieving the highest BG dye removal for each adsorbent?
iv) What are the differences in the adsorptive behaviour of the four adsorbents and why do these differences exist?
v) What are the advantages and disadvantages of each of the synthesised adsorbents?

1.6 Significance of Study

In this study, novel chitosan-composites have been introduced and modified through chemical crosslinking and grafting approaches *via* hydrothermal process utilising two example agents representing each category (Benzaldehyde and Salicylaldehyde as representatives of grafting approach and Benzil and Glyoxal as representatives of cross-linking approach) for the removal of Brilliant Green dye from aqueous environments. The differences in the resulting materials after hydrothermal process in terms of adsorptive properties, surface charge, and chemical composition

have been compared to determine the most advantageous method for improving the synthesised material (Cs-Ma-Tk) for Brilliant Green dye removal. The comparison between these two types of materials using the same hydrothermal process on chitosan derivatives has never been studied before (to the extent of my knowledge) and hence it is the contribution to knowledge of this research. Furthermore, this research falls under the sixth goal in the 17 Sustainable Development Goals (SDGs), a shared blueprint for peace and prosperity for the people and the planet, an agenda started by the United Nations.

CHAPTER 2
LITERATURE REVIEW

2.1 Background

In recent years, there are frequent discussions going on in the world on environmental issues regarding water as an essential need for the survival of humans and other organisms. Environmental pollution has a strong relation with industrialisation and there are several contributors to the discharge of toxic water contaminants to the water bodies. The afore mentioned contributors are mainly the industries that include the production of toxic water contaminants in the process of manufacturing their products, such water contaminants include untreated chemicals and harmful dyes. out of the industries that release harmful dyes into the environment, textiles, plastics, printing, oil and gas can be mentioned as some of the most responsible contributors [12]. vast amounts of coloured wastewater are created in the process of colouring products in these industries. Figure 2.1 exhibits the distribution of dye usage in different industries. The textile industries take the most responsibility (54%) for the discharge of dye effluents to the environment compared to the other responsible industries. Different stages and processes in textile industries use specific mixtures of chemicals, dyestuff, and water. Mostly after each process in textile industries, the products will be rinsed, and the remainder of chemicals and dyes will be directly discharged to the environment as effluents. As an example, in the dyeing process in textile industries, nearly 85% of the initially prepared dye mixture (dye molecules and chemicals) cannot bind to the textiles and is finally ejected as dye effluent [2]. Thus, the textile sector is the most responsible for the discharge of water contaminants (mainly dye effluents) to the environment and this issue needs to be addressed.

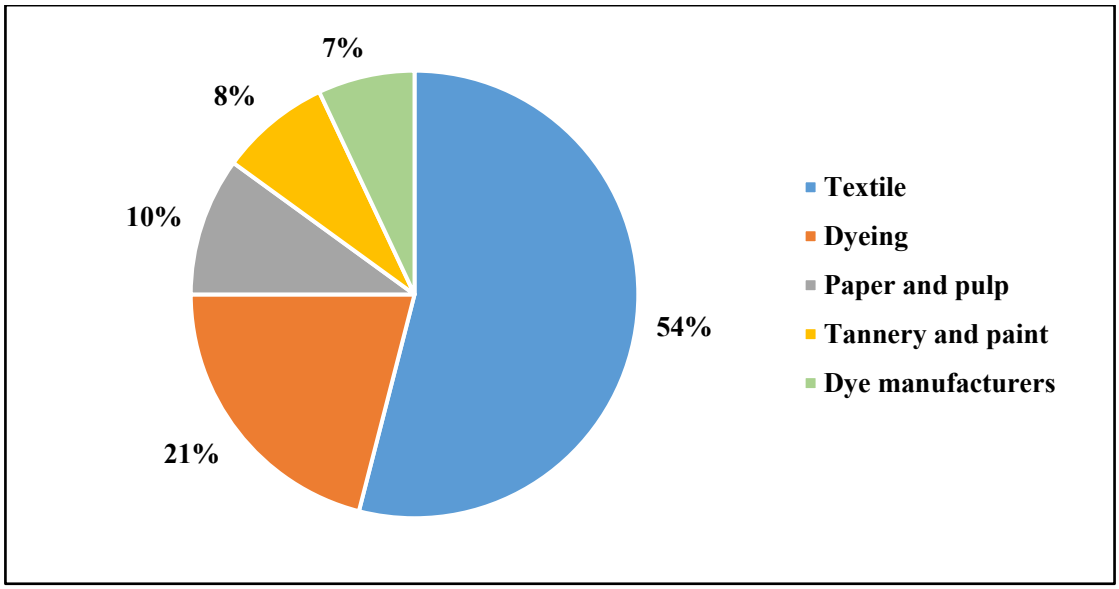


Figure 2.1 Industries Responsible for the Discharge of Dye Effluents in the Environment [2]

Generally, dyes are categorised under two major categories of natural dyes and synthetic (artificial) dyes. Natural dyes refer to dyes extracted from the many colourful substances available in nature and as they are from the environment and their most positive feature is that they do not pose any harm to the environment. Natural dyes can be extracted from many different resources such as fruits (e.g., berries), flowers (e.g., roses), minerals (e.g., malachite), insects (e.g., Cochineal) and animals (e.g., shellfish) [13], they would then be cooked, watered down, and turned into basic organic clothing colours. But due to the low affinity of natural dyes towards textiles, they require the use of metallic salts as mordants to facilitate the attachment of the pigment or dye to the fibres. While the natural dyes are non-toxic and cause no harm to the environment, the resources for their production are limited and due to their low affinity to textiles, the dying process requires more time, hence the need for more abundant dyeing resources became apparent. Synthetic dyes, on the other hand, are chemically made and they are typically derived from petroleum and coal tar [8]. The search for an alternative resource to replace the natural dyes started due to rising demand from the society for vibrant colours in clothing and the limited resources of natural dyes could not meet such high demands [14]. Synthetic dyes vary greatly based on their chemical structure as different materials need specific chemicals to conform to the dye. However, as the synthetic dyes are chemically treated to achieve a colouring substance, they can be highly toxic and harmful to the environment. This study targets the concerns regarding the toxic dyes

discharged into the water bodies from textile industry as this industry is one of the most polluting industrial sectors regarding wastewater due to the fact that the dye effluents are generally discharged into the environment without any treatment.

Brilliant green (BG) is a water-soluble basic triphenylmethane dye that is used to colour silk, wool, jute, leather, cotton, and paper, among other materials. It works as an antifungal, antibacterial, and anti-parasitic agent in aquaculture [15]. It has been categorised as a Class II health hazard, but due of its low cost, it is still utilised in several nations. The inability to biodegrade makes it essential to remove BG from effluents prior to discharge. Carcinogenesis, mutagenesis, chromosomal breakage, and pulmonary toxicity have all been mentioned as the hazardous effects of this dye.

2.2 Dyes as Water Pollutant

Many industries use synthetic dyes excessively and the estimated production amount of these dyes is around 700,000 metric tons per annum, while according to reports, the textile industry alone uses over 40,000 tons of the synthetic dyes generated annually worldwide [16], [17], [18], [19], [20]. Effluents discharged by the textile industries carry high amounts of dyes. This amount ranges from 2% for simpler dyes up to as high as 50% for reactive dye effluents. The discharge of these effluents, untreated, into the water bodies causes high dye contamination in the vicinity of the discharge point from the surface of the body to the groundwater [21], [22], [23], [24]. The presence of dyes in water brings diverse negative effects on all living organisms in the area such as chemical oxygen demand, visual emissions, cytotoxicity, genotoxicity, mutagenicity, and carcinogenicity [25], [26], [27], [28]. There are many industries responsible for the discharge of untreated effluents to the water bodies that consequently leads to the pollution of water by increasing the level of biological oxygen demand (BOD) and chemical oxygen demand (COD) in the water composition [29], [30], [31]. Figure 2.1 demonstrates the different polluting chemicals that can be found in dye effluents discharged by textile industries. The discharge of these chemicals and reagents into water bodies can bring about severe environmental impacts, such as harsh pH levels impacting the aquatic life, presence of soaps and other surfactants causing eutrophication due to nutrient rich additives which prompt excessive growth in algae, oil-in-water emulsions blocking sunlight and degrading water quality, etc.

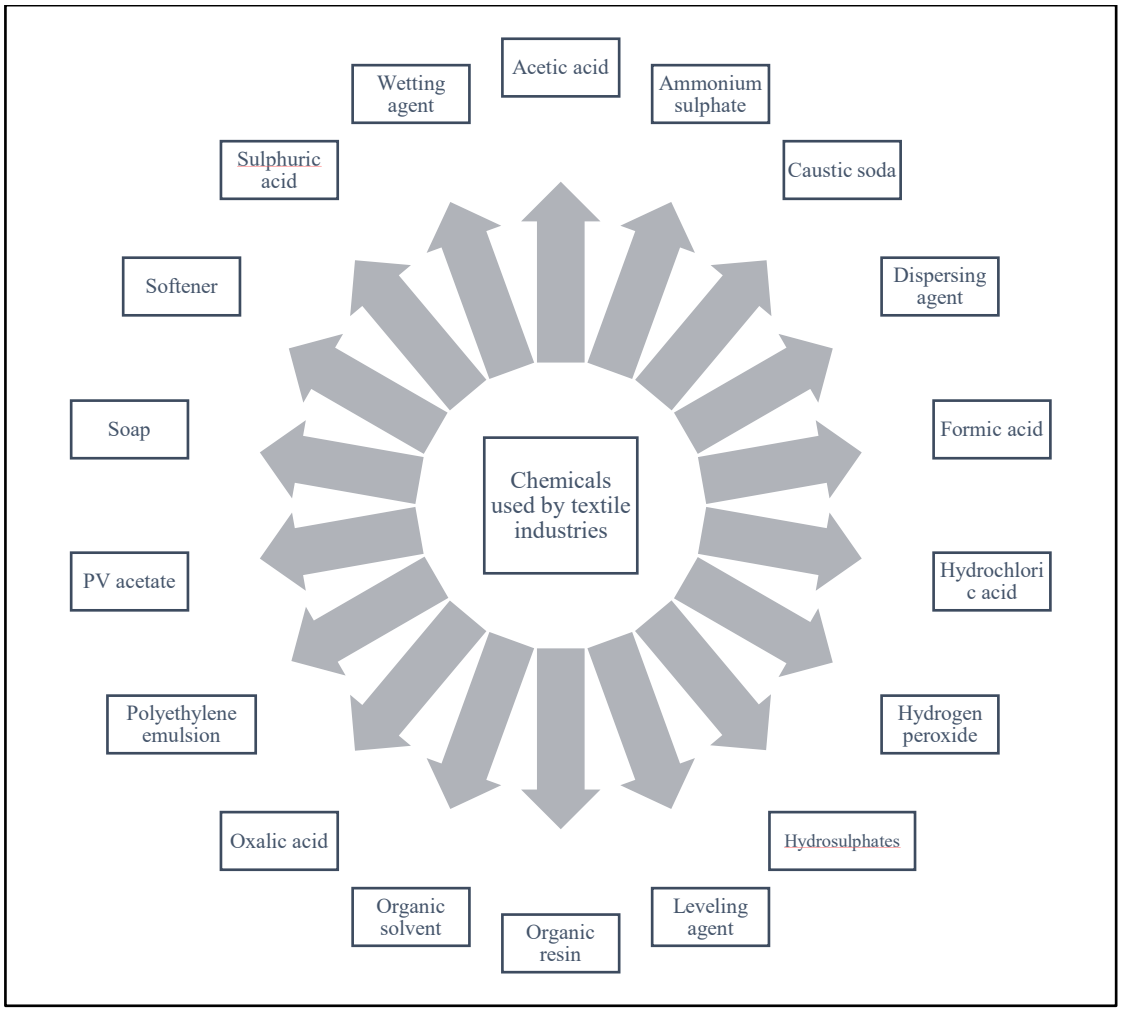


Figure 2.2 Dangerous Chemicals Used in Conjunction With Colorants for Dyeing Industries [2]

As can be seen from Figure 2.2 the dye effluents discharged by textile industries contain many toxic chemicals which can harm the lives of animals and humans alike. It is worth mentioning that the toxicity levels of the dye effluents discharged are especially high for synthetic dyes as compared to their natural counterpart [32], [33]. The amount of water used during different manufacturing processes in textile industries is enormously high. Expectedly, that high amount of water would turn to polluted water after the end of every process [34]. This polluted water is highly contaminated by high values of COD and BOD, salts, pigments, and organic matter. However, as synthetic dyes are not biodegradable, their presence in the discharged effluents creates a more complex issue of biodegradability and raises the need for their removal prior to discharge [35].

Synthetic organic dyes are man-made chemical compounds used to impart color to a wide range of materials, including textiles, paper, leather, plastics, cosmetics, and

food. Derived primarily from petrochemical sources, these dyes are valued for their vibrant hues, high stability, and cost-effectiveness. Among the most common types are azo dyes, anthraquinone dyes, and triphenylmethane dyes, with azo dyes accounting for nearly 60–70% of all synthetic dyes produced globally. In the textile industry, synthetic organic dyes are particularly widespread due to their compatibility with various natural and synthetic fibers, such as cotton, polyester, nylon, and rayon. They are applied through dyeing and printing processes, often involving large volumes of water and chemicals to ensure even and lasting coloration. However, a significant portion of these dyes does not bind completely to the fabric. It is estimated that up to 30% of the dyes used are lost in the dye bath and discharged as part of industrial wastewater, or effluent. When dye-containing effluents are not properly treated before being released into the environment, they cause serious problems. One of the most immediate effects is water pollution. The intense coloration from synthetic dyes reduces sunlight penetration in water bodies, disrupting photosynthesis in aquatic plants and leading to oxygen depletion. This results in ecological imbalances and can cause the death of fish and other aquatic life.

Many synthetic organic dyes are also toxic, carcinogenic, or mutagenic. For example, azo dyes can degrade under anaerobic conditions to form aromatic amines—some of which are known carcinogens. Heavy metals and other auxiliary chemicals used in dye formulations further exacerbate the toxicity of the effluents. When such effluents are released into rivers, lakes, or soil without proper treatment, they pose long-term health risks to animals, plants, and humans alike. In many developing regions, communities living near textile factories are exposed to contaminated drinking water and suffer from increased rates of skin disorders, respiratory issues, and other chronic illnesses.

2.3 Synthetic Organic Dyes as Water Pollutants

Synthetic organic dyes are widely used in textile, leather, paper, printing, cosmetic, and related industries to impart vibrant and durable colours. Their large-scale manufacture and extensive use make them a significant class of environmental pollutants: it is estimated that industrial dye processes annually release tens to hundreds of thousands of tonnes of dye and dye-containing wastewater globally [33], [36], [37]. These substances are problematic for several reasons.

First, many synthetic dyes are persistent and resistant to biodegradation. Their complex aromatic structures, often incorporating azo (–N=N–), anthraquinone, sulfonated, or nitro functional groups, render them chemically stable under many environmental conditions; conventional wastewater treatment plants frequently fail to remove or degrade them completely [33], [36].

Second, even at low concentrations (often $\ll 1$ mg L^{-1}), dyes impart strong colours to water bodies, reducing light penetration and disturbing aquatic ecosystems. Reduced light inhibits photosynthesis in phytoplankton and aquatic plants, lowering oxygen production and upsetting the oxygen balance in water, which can lead to hypoxic or anoxic conditions harmful to fish and invertebrates [33], [38], [39].

Third, synthetic organic dyes exhibit various toxic, mutagenic, and carcinogenic effects on organisms. Some dye molecules or their breakdown products (such as aromatic amines from azo dye cleavage) have been shown to damage DNA, disrupt reproduction, affect organ function (liver, kidney, skin), and in some cases contribute to cancer risk in animals and humans [33], [40], [41]. Exposures may occur through ingestion of contaminated water, accumulation in aquatic organisms, or occupational contact in dyeing industries.

Fourth, due to their chemical nature, some dyes also interfere with the physical, chemical, and biological parameters of water. Dye effluents often carry high biological oxygen demand (BOD) and chemical oxygen demand (COD) because of both the dyes themselves and various auxiliary chemicals used in dyeing (e.g. salts, surfactants, fixing agents, heavy metal salts). The discharge of such effluents can alter pH, salinity, turbidity, and dissolved oxygen levels in water [33], [36], [39].

Fifth, dyes can accumulate in sediments and living tissues. Aquatic organisms like algae, invertebrates, and fish may bioaccumulate dye molecules or their toxic metabolites. This has implications not only for the health of the organisms themselves (e.g. reduced growth, impaired photosynthesis or reproduction), but also for higher trophic levels, including humans who consume contaminated fish and water. There is evidence for mutagenic and genotoxic effects in biota exposed to contaminated waters [33], [40].

Finally, the environmental and health effects are compounded by the sheer volume of dye effluent. It is common for textile dyeing operations to lose 5-15% of dyes to effluent in dyeing, fixing, and washing steps; in some cases, losses are significantly greater depending on dye class and process efficiency. Such continuous inputs maintain

dye presence in the environment, limiting opportunities for natural attenuation [33], [36], [37].

2.3.1 Brilliant Green (BG) Dye

Brilliant Green, also known as Zelyonka, is a cationic dye with the chemical formula C27H33N2.HO4S, a colour index of 42,040, a maximum wavelength of 625 nm, and a molecular weight of 482.63 g/mol. Its IUPAC name is [4-[[4-(diethylamino) phenyl]-phenylmethylidene] cyclohexa-2, 5dien-1-ylidene] diethylazanium [25], [42], [43]. It has a glittering surface with small golden crystals. It is water and alcohol soluble and used to treat Gram-positive bacteria as an antiseptic [44].

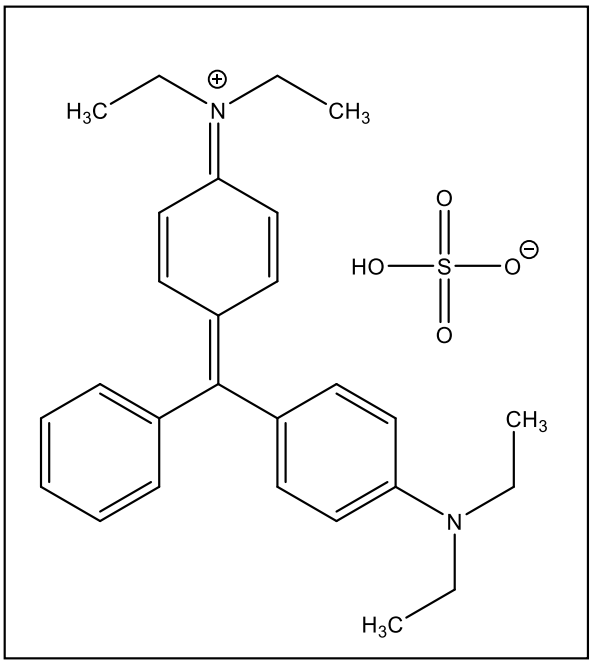


Figure 2.3 Chemical Structure of Brilliant Green (BG) [45]

Brilliant green (BG) dye is a synthetic organic dye commonly used for a variety of purposes e.g., biological stain, veterinary medicine, dermatological agent, an additive to poultry feed to inhibit propagation of mould, intestinal parasites and fungus, textile dying and paper printing [46], [47], [48]. Via inhalation, it is poisonous to the lungs. Carbon dioxide, nitrogen oxide, and sulphur oxides are all possible by-products of its decomposition. As almost indestructible toxicants, dye accumulation in the soil is a major concern [44], [49], [50]. Because of its high solubility (100 g/L), BG, a commonly

used dye, finds its way into aquatic environments. Because of its high volatility, it pollutes the environment as well. BG is an organic dye that belongs to the triphenyl methane family and appears as a golden crystal [51]. When injected into humans and animals, brilliant green is toxic. The gastrointestinal tract is commonly irritated by BG, with long-term exposure resulting in organ damage [52]. The toxic and hazardous substances created by dyes after oxidation and reduction in water pose an even greater health risk, necessitating immediate action to remove them from wastewater. BG dye was selected for research because it is widely used in fabric manufacturing and is hazardous to the environment and human health. As a result, it is important to eliminate or reduce BG from effluents prior to their discharge into bodies of water. Traditional water treatment methods for BG abatement (such as biological treatment and chemical precipitation) are limited due to its complex nature [42]. Hence, the research field has been constantly searching for different methods of removing such toxic dyes from the water bodies in the last few decades and several methods have been suggested for the removal of dyes from the dye-polluted effluents.

2.4 Treatment Methods for Dye Removal from Wastewater

There have been several approaches proposed in different research articles that have proven effective for the removal of dyes from effluents; e.g., such as bacterial degradation [53], [54], [55], biological treatment [43], [56], membrane filtration [57], [58], [59], [60], coagulation/flocculation [61], [62], [63], [64], advanced oxidation [65], [66], [67], [68], [69], and adsorption [70], [71], [72]. However, every method has its own drawbacks so they cannot always be effective and suitable for the target dye and environment [2]. An optimal dye removal system is a system capable of removing significant amounts of dyes effectively and within a limited span of time without causing the creation of secondary contamination (e.g., sludge). Hence, it is encouraged to extract the pollutants from effluents using a method that will not cause any harm such as creating toxic by-products in water. Table 2.1 exhibits advantages and disadvantages of several methods of dye removal from effluents.

Table 2.1
Several Treatment Methods for Dye Effluents [2]

Methods	**description**	**Advantages**	**Disadvantages**
Oxidation	Oxidising agents are used to break down the chemical structure of dye molecules to CO_2 and H_2O. catalysts can be employed to improve the process.	This method can achieve complete degradation of dye molecules, take a short amount of time and its application is straightforward.	It is an expensive and pH dependant process. Activation of hydrogen peroxide as an oxidation agent is difficult and effective dye removal requires the presence of catalysts.
Adsorption	Adsorbent materials fit to adsorb dye molecules with high capacity are used.	A brilliant method for the removal of different types of dyes.	Some adsorbents could be costly.
Coagulation-flocculation	Agents capable of inducing coagulation-flocculation are supplemented to the dye effluent to create clumps of dye particles which can then be removed using a filtering method.	Cost-efficient and effective towards disperse, vat and sulphur dye effluents.	The clumps of dye particles leave high amounts of sludge. The system is pH dependant and ineffective for the removal of reactive, basic and azo dyes from effluents.
Irradiation	Dye molecules are removed from effluents using radiation.	It is an effective method at laboratory scale.	Massive amounts of dissolved oxygen are needed in this process.
Membrane filtration	Effluents are made to pass through a membrane that splits the particles of dyes from water.	An effective method for recovery and reusability of water.	expensive system installation and high sludge formation make it unsuitable for the removal of dyes.
Nano filtration and ultra-filtration	Dye molecules are separated from clean water after passing the effluents through a thin-pored membrane.	It is an effective method for the removal of all types of dyes.	An expensive method with high consumption of energy as well as constant clogging of membrane pores that reduces the lifespan of the system.

Methods	description	Advantages	Disadvantages
Reverse osmosis	Water is pushed through a thin membrane by high pressure causing the contaminants to stay on one side of the membrane while water passes to the other side.	It is a common method for recycling water which can produce pure water. It is an efficient way decolouring and desalting different types of dyes.	It is a costly procedure that requires high pressure.
Microbial adsorption	A blend of organic living organisms fit to adsorb dye molecules.	Certain dyes show brilliant attraction towards such microbial biomass.	Limited by the affinity of the dye towards the biomass and not effective for all dyes.
Enzymatic degradation	Enzymes are extracted and employed for degradation of dye molecules.	It is a cost-efficient, effective, reusable and non-toxic method.	The amount of enzyme production is unreliable.
Algae degradation	Algae achieve self-growth through the consumption of dye molecules.	A cheap and eco-friendly system that can effectively remove dyes from effluents.	The system shows instability.

In most countries, the commonly used method for removal of colour from dye effluents prior to discharge is the typical biological method, also commonly regarded as the traditional route, which consists of a mixture of aerobic and anaerobic processes. However, the use of solely this treatment has proven to be insufficient to remove hazardous particles from dye effluents as coloured water can still be seen in the discharge of treated dye effluents [73], [74]. Although the use of traditional route can help in reducing the need for chemical oxygen present in wastewater, it fails to make the discharged water dye-free or free of toxicity.

Chemical dye removal methods are generally methods based on chemistry and its theories as the base for dye removal. Most of the chemical dye removal methods are costly compared with biological and physical dye removal methods, except for electrochemical dye removal methods [60], [75]. Moreover, it was reported by Katheresan, et al., (2018) that these methods are often commercially unattractive as they have requirements for equipment and electrical power consumption.

However, physical dye removal methods are generally simpler and employed by the process of mass transfer. Standard methods for the extraction of visible dyes

include reverse osmosis [76], [77], [78], irradiation [79], [80], [81], [82], [83], nanofiltration [83], [84], [85], [86], [87], or ultrafiltration [78], [88], membrane filtration [57], [89], [90], [91], coagulation or flocculation [92], [93], [94] and adsorption [72], [95], [96], [97]. Of the three methods mentioned (biological, chemical, and physical) the most used methods are branches of physical dye removal due to their simplicity and efficacy as they require the least amount of chemicals compared to the biological or chemical methods for extracting dyes.

2.5 Adsorption for Dye Removal

Adsorption can be said to be one of the most widely used methods for dye removal. It has been mentioned by many researchers that adsorption process has been widely implemented for the treatment of dye effluents due to its cost-effectiveness and high efficiency of removal [18], [98], [99]. Although adsorption is an effective method for successful extraction of dyes from industrial wastewater, the effectiveness of the process is highly dependent on the choice of an adequate adsorbent. Compared to other contaminant elimination methods, adsorption is preferred in most cases due to its high efficiency, selectivity, cost-efficiency, high accessibility of raw material, low initial capital investment, simplicity in design and operation, and non-toxicity [100]. The efficiency of the adsorption process is highly reliant on the type of adsorbent used and their affinity with the targeted pollutant for removal, hence, a thorough evaluation of the adsorbent type and assessing its effectiveness is necessary. Various adsorbent materials have been employed for the removal of toxic dyes from effluents, e.g., clay minerals [101], [102], [103], biochar [104], [105], [106], activated carbon [107], [108], [109], natural biopolymers such as algal biomasses and chitosan [110], [111], [112], [113], [114]. Generally, in an adsorption process the factors that affect the uptake of dye molecules are adsorbent dosage, contact time between adsorbate and adsorbent, dye concentration, temperature, and pH of solution. The adsorption process is an economically efficient physical-chemical process for dye-polluted wastewater treatment. The choice of an adequate adsorbent is a very important factor as the physical and chemical properties of the adsorbent such as pore structure and chemical surface groups determine the efficacy of the adsorption process.

2.6 Chitosan (CS) as an Adsorbent

Cs is a glucosamine, an N-acetyl glucosamine copolymer branched by β-(1-4) bonds. Chitosan is derived from chitin, the second most abundant biopolymer on the planet. In 1859 the deacetylation product of chitin was discovered by Rouget and several years later it was named chitosan by Hoppe-Seyler [115], [116]. Due to the abundance of -OH, -O- and NH_2 groups in its structure, there exist various intramolecular and intermolecular hydrogen bonds which immensely affect the crystallinity, viscosity and solubility of this substance[116]. The abundant presence of primary amines in the structure of Cs makes it a rare polycationic polymer in nature (pK_a~6.5), which makes it clearly distinguishable from other polysaccharides [117]. The ideal structure of chitosan has been shown in Figure 2.4.

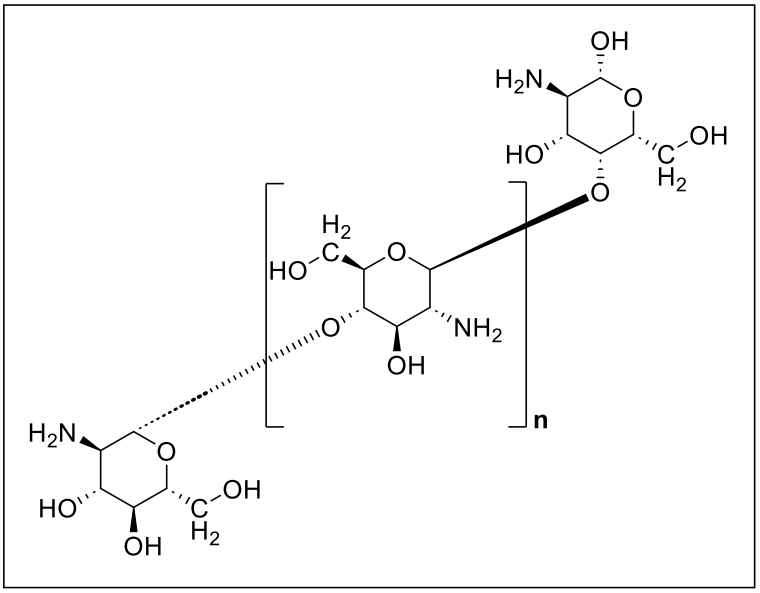


Figure 2.4 Chemical Structure of Ideal Chitosan [118]

After the deacetylation degree of chitin exceeds 50%, it turns into a soluble material in aqueous acidic solutions and its name is directly transformed into chitosan. When in acidic media, the amine ($-NH_2$) group protonation makes chitosan a polyelectrolyte, giving it great potential for the adsorption of water contaminants [119], [120], [121]. Moreover, chitosan is an abundantly available biopolymer in existence and a bio-functional polysaccharide that has a promising potential to be employed in various fields. Furthermore, the biodegradability and biocompatibility of Cs allow it to act as an eco-friendly adsorbent for water treatment purposes [122], [123], [124], [125].

2.7 Modifications of Chitosan

Chitosan (Cs) is produced through the deacetylation of chitin, the most abundant biopolymer found in nature after cellulose, commonly found in the exoskeleton of eukaryotic species such as insects and crustaceans as well as the cell walls of fungi [126], [127]. Cs possesses strong mechanical qualities as well as the capacity to stop bleeding (haemostasis), heal wounds, kill germs, and absorb organic and inorganic contaminants [128], [129], [130]. Furthermore, the biodegradability and biocompatibility of Cs allow it to act as an eco-friendly adsorbent for water treatment purposes [122], [123], [124], [125]. Despite the great characteristics of Cs, there are various shortcomings that make effective application of Cs in water treatment challenging, e.g., acid solubility, lack of adsorption affinity towards cationic dye species, low surface area which limits the access of dye molecules to active adsorption sites, high swelling index, and low mechanical strength [131], [132], [133], [134]. Furthermore, the biodegradability and biocompatibility of Cs allow it to act as an eco-friendly adsorbent for water treatment purposes [122], [123], [124], [125]. Despite the great characteristics of Cs, there are various shortcomings that make effective application of Cs in water treatment challenging, e.g., acid solubility, lack of adsorption affinity towards cationic dye species, low surface area which limits the access of dye molecules to active adsorption sites, high swelling index, and low mechanical strength [131], [132], [133], [134]. Cross-linking reaction can improve many limiting characteristics of chitosan but due to the nature of cross-linking reaction which would restrict more functional groups on the backbone of Cs that can negatively impact the adsorptive properties of Cs [135]. Whereas the grafting approach can result into improved chemical stability in a broader pH range and better mechanical properties of Cs and the grafted material can further increase the adsorptive properties of Cs based on the active adsorption sites available in its structure [136]. Table 2.2 contains some modifications done by researchers on chitosan for dye adsorption purposes.

Table 2.2
Examples of Modifications Done by Researchers on Chitosan for Dye Adsorption

Base	Modification method	Materials added to composite	Cross-linking agent	Grafting agent	Dye	Reference
Chitosan	Hydrogel beads	−	Glutaraldehyde	−	Malachite Green, Indigo Carmine	[137]
Chitosan	Magnetic hydrogel beads	Fly ash, $FeCl_2.4H_2O$, $FeCl_3.6H_2O$	Poly vinyl alcohol	−	Reactive orange 16	[138]
Chitosan	Nanocomposite hydrogel beads	TiO_2 nano particles	Glyoxal	−	Methyl Orange	[139]
					Reactive Red 120	[140]
Chitosan	Aerogel	Cellulose	−	−	Congo Red	[141]
Chitosan	Hydrogel beads	Coir pith activated carbon, sodium dodecyl sulphate	−	−	Malachite Green	[142]
Chitosan	Hydrogel beads	Alunite (silica)	−	−	Acid Red 1 and Reactive Red 2	[143]

Base	Modification method	Materials added to composite	Cross-linking agent	Grafting agent	Dye	Reference
Chitosan	Composite precipitate	Alginate	Glutaraldehyde	Aniline	Brilliant Green, Methyl Orange, Patent Blue V	[144]
Chitosan	Magnetising by Fe_2O_3 nanoparticles	$FeCl_2.4H_2O$, $FeCl_3.6H_2O$	–	–	Acid Blue 113	[145]
Chitosan	Composite film	Sodium zeolite	–	–	Methyl Orange	[98]
Chitosan	Microwave assisted bio nanocomposite	Bentonite	–	–	Reactive Violet 5R	[146]
Chitosan	Magnetic biochar	Corn stalk biochar	Glutaraldehyde	–	Amaranth	[147]
Chitosan	Hydrogel beads	Magadiite (a polysilicate)	–	–	Congo Red, Methylene Blue	[148]
Carboxymethyl chitosan	Composite hydrogels	Phytic acid, ammonium persulphate	–	–	Methyl Orange, Congo Red	[149]
Chitosan	Nanocomposite	Co_2O_3	–	Phthalic anhydride	Brilliant Green	[150]
Chitosan	Biocomposite	*Lactobacillus Casei* Bacteria	–	Benzaldehyde	Acid Red 88	[151]

Base	Modification method	Materials added to composite	Cross-linking agent	Grafting agent	Dye	Reference
Chitosan	Hydrogel beads	−	−	Benzaldehyde	Reactive Orange 16	[152]
Chitosan	Hydrogel beads	−	−	Salicylaldehyde	Reactive Orange 16	[5]
Chitosan	Biocomposite	Montmorillonite, algae	−	Benzaldehyde	Reactive Blue 19	[153]
Chitosan	Hydrogel	Guar gun	Glyoxal	−	Auramine O, Malachite Green	[154]
Chitosan	Hydrogel	−	Barbituric acid	−	Remazol Brilliant Blue	[155]

2.7.1 Physical Modifications of chitosan

Physical modifications have been employed on chitosan to improve the physical characteristics of the resulting product due to their convenience and efficiency. Physical modifications can affect the physical properties of Cs (e.g., pore structure, specific surface area, etc.) and due to the ease of operations and the ability to apply in a multitude of operational modes they are vastly applied [116]. These modifications methods are reversible and generally divided into two categories of blending and physical crosslinking. In the process of physical crosslinking, physical interactions (such as electrostatic attraction, formation of hydrogen bonds, and hydrophobic interactions) are taken advantage of to develop the physical properties of the resultant product. Physical crosslinking process can be achieved by pH variations [116], use of ionic crosslinkers [156], polyanions [157], and temperature variations [158]. On the other hand, the blending approach is the process of physically mixing Cs with other materials to create Cs-based composites to improve the characteristics of the final product. Several materials, such as biopolymers [159], microorganisms [151], magnetic materials [160], nanoparticles [161], etc. have been employed to modify Cs in literature.

2.7.1.1 Chitosan Modification by Titanium Dioxide

Titanium dioxide (TiO_2) is one of the most widely used materials of the last few decades applicable in all fields such as biomedical applications [162], [163], coating materials [164], building blocks [165], waste water treatment [166], [167], etc. due to its great characteristics of antibacterial activity, photodegradation, physical strength, chemical stability, heat resistance, eco-friendliness and high surface area. The use of titanium dioxide as a compositing material for chitosan derivatives is widely practiced for improving the physicochemical properties of pristine chitosan, i.e., achieving higher mechanical and chemical performance, higher surface area and porosity and increasing the adsorptive capacity of chitosan [168], [169]. In recent years, hybrid composites synthesised by immobilisation of inorganic compounds (most commonly metal oxides such as TiO_2, ZnO and CuO nanoparticles) onto organic materials (such as chitosan, gums, protein and starch) have become increasingly important [170]. The preparation of such hybrid composites is generally done in three methods (mechanical stirring, surface coating and creation of nanocomposites) as shown in Figure 2.5.

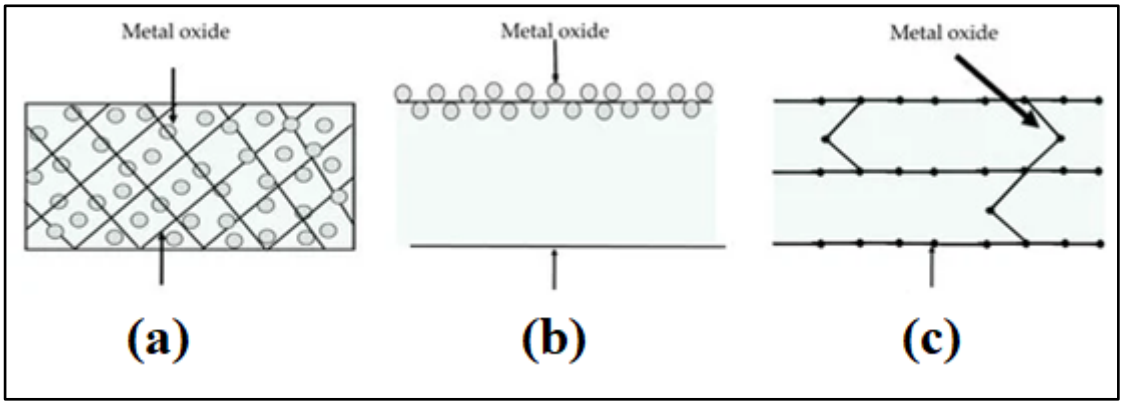


Figure 2.5 Hybrid Composite Preparation Methods: (A) Mechanical Stirring, (B) Surface Coating, and (C) Nanocomposite [170]

The first method is achieved by entrapping the molecules of the metal oxide in the polymeric matrix of the supporting material (organic compound) by mechanical stirring (Figure 2.5a). The properties of the final product synthesised by this method is highly dependent on the ratios of the two compounds (organic and inorganic) used. It is worth mentioning that although this method involves simple mechanical stirring, but the two compounds may also form chemical bonds. In the second method, electrochemical and/or physical deposition are utilised to deposit the metal oxide in the polymeric surface matrix (Figure 2.5b), whereas, in the third method which involves the creation of a nanocomposite, the metal oxide and the organic compound would be chemically bonded and the metal oxide can also improve the physico-chemical properties of the mixture by acting as a cross-linking agent [171].

Incorporating TiO_2 on the polymer matrix of chitosan can increase the roughness and porosity of the surface of the resulting hybrid composite and develop better structural properties [172]. Moreover, the crystallinity of chitosan hybrid composite is lower than that of pristine chitosan which is caused by the introduction of TiO_2 in the polymeric matrix of chitosan and the formation of hydrogen bonds between the two compounds [173]. Additionally, a TiO_2 dose dependent decrease in the pore volume [174] and pore size [175] as well as an increase in specific surface area [176] were observed for the hybrid composite of Cs-TiO_2. Furthermore, the thermal stability of the resulting composite would be enhanced [174] and the degradation rate reduced [177] due to the strong intermolecular interactions that appear after the introduction of TiO_2 to the polymeric matrix of chitosan resulting into higher decomposition and glass transition temperatures for the hybrid composite compared to chitosan. Although there

have been many studies on the formation of Cs and TiO_2 composites, most are focused on the use of TiO_2 nanoparticles which is not the case in this study. The TiO_2 material used in this study is a commercial carbon-doped TiO_2 (Kronos TiO_2) (henceforth referred to as Tk) with a micro particle size.

2.7.1.2 Chitosan Modification by Microalgae

Microalgae (Ma) are photosynthetic microorganism that are vastly responsible for the production of oxygen in aquatic environments and widely available with short growth cycles. Producing a vast array of biotic materials has allowed various applications of Ma in food, biofuel, chemical, carbon sequestration, and pharmaceutical industries to develop [178], [179]. Hence, Ma is comprised of unicellular organisms, with their cell walls containing proteins, polysaccharides, and lipid molecules providing a variety of active functional groups, such as hydroxyl, amine, amino, sulphate, and phosphate groups that are greatly responsible for the potential of Ma in pollutant adsorption [180], [181], [182], [183], [184]. The abundance and eco-friendly nature of Ma makes it a great biopolymer to act as an addition to Cs in the composite formation stage which has been a popular field of research for the potential of the resulting chitosan-microalgae biocomposite in various fields, such as food packaging and the removal of pollutants (such as dyes and heavy metals) from contaminated water [159], [185], [186], [187], [188], [189]. The resulting biocomposite would benefit from a higher surface area which allows for more contact between the dye molecules and the active adsorption sites available of the surface of the biocomposite, and greater affinity to a wider range of dye species due to the addition of the surface functional groups and better electronegativity of the resulting biocomposite [113], [190]. Table 2.3 consists of several reports on modifications of chitosan by algae found in literature.

Table 2.3
Several Modifications Done by Researchers on Chitosan Using Algae

Base	Modification method	Type of algae	Purpose	Reference
Chitosan	Film	Spirulina sp.	Removal of Cr^{6+} and Pb^{2+}	[191]
Chitosan	Foam	Spirulina sp.	Removal of phenol	[192]

Base	Modification method	Type of algae	Purpose	Reference
Chitosan	Film	Arthrospira Spirulina sp.	Removal of Methylene Blue, Tartrazine Yellow and Reactive Black 5 dyes	[193]
Chitosan and montmorillonite	Hydrogels	Spirulina (Sp)	Cr(IV) adsorption	[194]
Chitosan	Edible films	Spirulina extract	Food packaging	[195]
Chitosan	Algae doped magnetic nanoparticles	Microalgae biomass	Removal of Direct Red 31 and Direct Red 28 azo dyes	[196]
Chitosan	Glutaraldehyde cross-linked microbeads	Cladophora sp.	Removal of heavy metals (Cd(II), Cr(III), Cu(II), Ni(II) and Zn(II)	[188]
Chitosan	imprinting bio-composite pellets	Ulva lactuca	Removal of Cd (II)	[159]
Chitosan	Glass particle coating	Spirulina sp.	Removal of Allura Red and Methylene Blue dyes	[197]
Chitosan	Magnetic nanocomposite	Spirulina	Removal of Mercury ions	[198]
Chitosan	Film	Spirulina sp.	Removal of Pb^{2+} ions	[199]
Chitosan	Film	Spirulina LEB-18 sp.	Removal of Methylene Blue dye	[200]

2.7.2 Chemical Modifications of chitosan

There are various functional groups in the structure of Cs backbone including: -NH_2 located on C2, two -OH groups located in C3 and C6 positions, β(1→4) glycosidic linkages, and some *N*-acetylamino groups. Amongst these groups, the -NH_2 and -OH are chemically active and can bonds with other materials for the generations of various Cs derivatives [116]. The -OH located in the C3 position has lower activity than the C6 positioned -OH due to the steric hindrances which prevents its free rotation, while the stability of the glycosidic bonds is very high and they won't easily break and hence they

cannot act as a modification site. Hence, the formation of chemical bonds between Cs and other materials mainly occurs through the -NH_2 and C6-OH (with -NH_2 having higher chemical activity) functional groups. Various chemical reactions can occur on the chemically active functional groups, such as: *N*-alkylation or acylation, Schiff base formation, functionalisation to thiosemicarbazone, esterification, quaternisation, O-acylation, etc [201]. Schiff base formation (CH=N) is a result of a condensation reaction between the *N*-amino groups of Cs with aromatic, aliphatic, heterocyclic ketones and aldehydes. The formation of Schiff bases can greatly enhance the process of chemical crosslinking and grafting of Cs [116].

2.7.2.1 Chemical Modification of Chitosan by Grafting

Chemical grafting is the most effective and frequent way of altering the functional and structural characteristics of natural polymers. Graft copolymerisation of natural polysaccharides can improve the functional characteristics of natural polymers, making it a valuable resource for creating new materials [201]. Because synthetic polymeric chains are attached to the backbone of natural polysaccharides during grafting, the characteristics of both polymers are combined [202]. The natural characteristics of Cs are improved when pure Cs is modified by grafting. Cs grafted copolymers have a wide range of applications and are widely utilised in a variety of industries.

Furthermore, grafting reaction can be done between chitosan and a monomer containing an active carbonyl group from aldehydes or ketones to form a Schiff base (−RCN−) with the amine group present in the polymeric matrix of chitosan [153]. The feasibility of such Schiff base reactions achieved by grafting of an aldehyde monomer to the backbone of chitosan have been studied by researchers. In a study conducted by Normi, et al., [5], it was found that the Schiff base reaction does indeed occur between the carbonyl group of salicylaldehyde and the amino group of chitosan. Moreover, during the reaction between SD and Cs, there are reversible addition and depolymerisation reactions taking place, and with the increase of temperature reaction rate increases greatly. Furthermore, the feasibility of the formations of Schiff base between benzaldehyde and chitosan through grafting was studied by Agha, et al., (2017) [151], and it was shown that the formation of Schiff base was successful. Additionally, the grafting of both salicylaldehyde and benzaldehyde on the polymeric matrix of

chitosan increases its antibacterial and antifungal properties greatly. Moreover, the incorporation of 2,3-dihydroxyl-benzaldehyde into the polymeric chain of chitosan causes a great increase in the BET surface are, total pore volume and pore radius of the synthesised material compared to pristine chitosan increasing its potential as a promising adsorbent in wastewater treatment [203]. Furthermore, the successful grafting of chitosan (by Schiff base reaction) results into the formation of imine groups, this in return, would increase the thermal stability of the produce and increase the decomposition temperature [204]. Additionally, a decrease in crystallinity of the Schiff base chitosan-benzaldehyde was observed which was attributed to the breakage of hydrogen bonds between amino ($-NH_2$) and hydroxy ($-OH$) groups present in the polymeric matrix of chitosan [203]. Additionally, a recent research done on the thermal stability and photostability of chitosan grafted by 4 different aromatic aldehydes [205] revealed that the aromatic moieties attached to the polymeric matrix of chitosan through grafting absorb UV light irradiations and turn it into harmless heat which consequently reduces photo-degradation in the grafted chitosan samples. Moreover, the same trend was observed for thermal stability of the samples grafted by aromatic aldehydes and a noticeable increase in the decomposition temperature proves the improved thermal stability of the grafted samples. The grafting approach can result into improved chemical stability in a broader pH range and better mechanical properties of Cs and the grafted material can further increase the adsorptive properties of Cs based on the active adsorption sites available in its structure [136]. Furthermore, the addition of an aromatic ring would allow π-π interactions between the aromatic structure of the dye and the grafting agent and resultantly elevate the dye contaminant adsorption [151].

2.7.2.2 Chemical Modification by Crosslinking

Similar to grafting, the crosslinking process is a good approach to improve the chemical stability of Cs in an acidic environment while lowering swelling and leachability in aqueous solution. Chemical cross-linking is a simple approach for making chitosan-based hydrogels with relatively low-cost ingredients. During a copolymerisation reaction, covalent chemical connections are formed in all directions in space, resulting in a three-dimensional network. Cross-linking agents are molecules having at least two reactive functional groups that facilitate the creation of bridges between polymer chains in this chemical process [206]. The difference between grafting

and cross-linking reactions lies in the fact that the materials used for cross-linking can create links with two polymeric chains of chitosan connecting to amino groups from the two ends while grafting agents have one bonding site that they can attach to the amino groups of chitosan polymeric matrix with.

One of the commonly used cross-linkers is ethylene glycol diglycidyl ether (EGDE). By combining the epoxide groups of EGDE with the amino groups ($–NH_2$) supplied by the D-glucosamine units in the polymeric matrix of CS biopolymer, an effective crosslinking reaction may be accomplished [3]. Additionally, epichlorohydrin is another commonly used cross-linker for chitosan. Furthermore, the main advantage of using this cross-linking agent with chitosan rises from the fact that epichlorohydrin reacts strongly with the hydroxyl groups on the Cs backbone and allows the amino groups that are the main cationic adsorption sites of Cs to bind to the dye molecules. This cross-linking agent is especially useful when the target dye is of anionic nature as the cationic amine function of Cs is the main factor for the adsorption of anionic dyes. Moreover, there have been numerous studies done on effects of various cross-linking agents on adsorption properties of chitosan and chitosan composites and a summary of such studies can be found in Table 2.4 exhibiting several cross-linking and grafting agents used to improve the properties of chitosan synthesised in various forms such as beads, films, nanocomposites and hydrogels.

Table 2.4
Several Cross-Linking and Grafting Agents Used to Improve the Properties of Cs

Form of Modification	Cross-linking agent	Grafting agent	Additives	Adsorbate	Reference
Hydrogel Beads	–	Ethyl acrylate	–	Basic Blue 41 and Basic Red 18	[207]
	Glutaraldehyde	–	Lysozyme	Methyl Orange and Cr(VI)	[208]
	Tripolyphosphate	–	Fly ash	Reactive Red 120	[209]
	Glyoxal	–	Kaolin clay	Remazol Brilliant Blue R (RBBR)	[30]
	Epichlorohydrin	–	Kaolin clay	Reactive Blue 19	[210]
	Epichlorohydrin	–	Carbon clay	Acid Blue 29 and Methylene Blue	[211]
	Citric acid	–	–	Cu(II) and Phosphate anions	[212]
	Tricarboxylic citric acid	–	–	Cr(VI)	[213]
	Bio-hydroxyapatite	–	–	Orange G	[214]

Form of Modification	Cross-linking agent	Grafting agent	Additives	Adsorbate	Reference
		Benzaldehyde	Montmorillonite and algae	Brilliant Green	[153]
Hydrogel beads	epichlorohydrin	4-aminobenzoic acid	–	Pb(II), Cu(II), Ni(II), Zn(II) and Cd(II) ions	[215]
	–	Benzaldehyde	–	Reactive Orange 16	[152]
	–	Salicylaldehyde	–	Reactive Orange 16	[5]
	Benzil	–	–	Reactive Orange 16	[6]
Magnetisation	Glutaraldehyde	–	CS_2 (xanthate modification of chitosan), Al_2O_3, Iron Oxide	Methylene Blue and Safranin O	[216]
	glutaraldehyde	itaconic acid	Magnetite (Fe_3O_4) nanoparticles and a rhodium metal-organic framework	Trimethoprim	[217]

Form of Modification	Cross-linking agent	Grafting agent	Additives	Adsorbate	Reference
Hydrogel	Poly (N-isopropylacrylamide) and N,N′-methylenebisacrylamide	–	TiO_2 nano particles	Acid Fuchsin	[218]
	–	Salicylaldehyde	–	Crystal Violet and Rose Bengal	[219]
Nanocomposite	Glutaraldehyde and epichlorohydrin	Melamine	Montmorillonite nanoparticles	Ferric ions	[220]
	Ethylene glycol diglycidyl ether (EDGE)	–	TiO_2 nano particles	Reactive Orange 16	[3]
	Glyoxal	–	TiO_2 nano particles	Methyl Orange	[221]
	Benzil	–	ZnO nanoparticles and FeCl3.6H2O	Remazol Brilliant Blue R (RBBR)	[222]
	Tripolyphosphate	–	TiO_2 nanoparticles	Reactive Orange 16	[139]
	Glyoxal		Magnetite (Fe_3O_4) and ZnO nanoparticles	Reactive Blue 19	[223]

Form of Modification	Cross-linking agent	Grafting agent	Additives	Adsorbate	Reference
		Acrylamide, acrylic acid, 4-styrene sulfonic acid	Graphene oxide and TiO_2 nanoparticles	Pb^{2+}	[224]
		phthalic anhydride	Co_2O_3 nanoparticles	Brilliant Green	[150]
Film	Glyoxal		-	Reactive Orange 16 and Methyl Orange	[225]
	EGDE		-	Reactive Red 120 and Methyl Orange	[226]

2.7.3 Hydrothermal Method for Synthesis of Crosslinked and Grafted Chitosan Derivatives

Hydrothermal synthesis is a simple, cost-efficient, and eco-friendly process performed under controlled conditions of temperature and pressure and it is essentially a solution-reaction-based method. Hydrothermal synthesis, often known as "hydrothermal technique", is a unique process for creating crystalised compounds utilising high-temperature aqueous solutions at high vapour pressures. Hydrothermal synthesis is a single-crystal synthesis process that relies on the solubility of minerals in hot water under high pressure [227], [228].

Nanomaterials can be synthesised using hydrothermal process in a wide range of temperatures (from ambient to extremely high temperatures). The morphology of the synthesised material can be controlled by the pressure conditions during the synthesis process. Meanwhile, the pressure condition is determined by the vapour pressure of the major component placed inside the hydrothermal reactor. Moreover, hydrothermal method has been employed successfully for the synthesis of a wide range of nanomaterials as this synthesis method has several advantages compared to other methods. Although, at high temperatures, hydrothermal synthesis can result into the production of unstable nanomaterials, this process can generate nanomaterials with high vapour pressures with minimal material loss. In comparison to traditional crosslinked composite synthesis, hydrothermal synthesis is a straightforward procedure that yields homogeneous, fine, and non-agglomerated powder in a single step. The characteristics of particles are regulated, and desirable repeatability is attained by modifying the reaction parameters and procedure. Meanwhile, the cost of instruments, energy, and precursors is substantially cheaper, making the process more environmentally benign [229]. Even though there are a variety of advanced synthesising ways for producing high-quality biocomposite nanomaterials, the hydrothermal method is the most widely employed due to its ease of use and low cost.

2.7.4 Benzaldehyde (BD) as a Grafting Agent

One of the most essential and flexible chemical molecules in the economy is benzaldehyde (BD; C_7H_6O; Figure 2.6), the simplest aromatic aldehyde and parent of the benzaldehyde class, which is an arenecarbaldehyde composed of benzene with a

single formyl group. It can be found in many different sources, including apricot, almond glycoside, peach seeds, and cherry [230], [231].

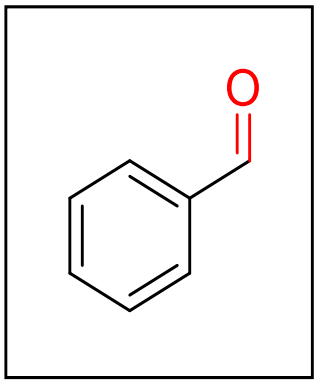


Figure 2.6 Chemical Structure of Benzaldehyde [232]

Benzaldehyde is currently produced primarily using toluene as a raw material in two procedures: the hydrolysis of benzal chloride and the partial oxidation of toluene [233]. Furthermore, the most common application of BD is in the production of various organic compounds. This simple molecule is a key precursor in the production of fragrances, epoxy resins, synthetic polymers, medicines, sweeteners, and petrochemical [230], [231]. The emissions of combustion activities such as incinerators, gasoline and diesel engines, and wood burning may emit benzaldehyde into the ecosystem. The synthesis of BD in the environment can be aided by photochemical oxidation of aromatic hydrocarbons like toluene. The development of long-term, efficient catalytic systems for benzaldehyde manufacturing is thus a critical task in both academic and industrial sectors [234]. Schiff base form of Cs-BD can be seen in Figure 2.7.

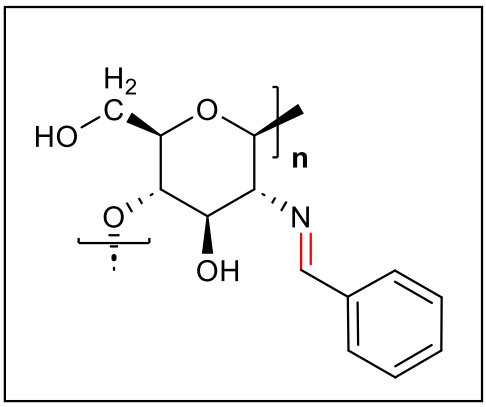


Figure 2.7 Schiff Base of Chitosan-Benzaldehyde [235]

2.7.5 Salicylaldehyde (SD) as Grafting Agent

Salicylaldehyde (SD; also known as salicylic aldehyde and salicylal) is the ortho isomer of monohydroxybenzaldehyde and high commercial importance. SD is a colourless and oily liquid with a pungent odour. The natural occurrences of SD can be found in beer, cassia, bird cherries, spirea oils, tomatoes, tea, grapes, and coffee. SD and its derivatives have vast areas of use as ingredients in various industries, such as electroplating, agricultural chemicals, fibres, polymers, petroleum chemicals, and perfumes. The main method for the production of SD is through air oxidation of saligenin (obtained through a base-catalysed reaction between formaldehyde and phenol) in the presence of a suitable catalyst, such as palladium or platinum [236].

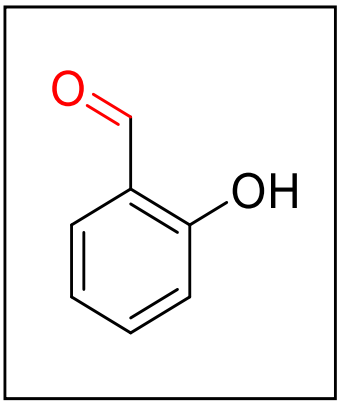


Figure 2.8 The Chemical Structure of Salicylaldehyde [237]

Moreover, SD is an important reactant in a variety of reactions, including the production of cyclic organic compounds like coumarin and organic ligands like salen ligand (a tetradentate C2-symmetric ligand produced from the Schiff base reaction between SD and ethylenediamine) [236], [238]. Schiff base is formed when the amino groups of Cs combine with the aromatic aldehyde groups of SD. The condensation reaction between primary amine from Cs and an active aldehyde from SD produces Schiff base compounds with imine groups (–RC=N) as shown in Figure 2.9 [189]. Moreover, SD linked Cs is an effective adsorbent because of its lightweight, high surface porosity, low-cost and non-glucose properties. By Schiff base modification of CS, a lightweight and porous SD linked Cs was produced as a bio adsorbent with good efficacy in removing colours from aqueous solution [219].

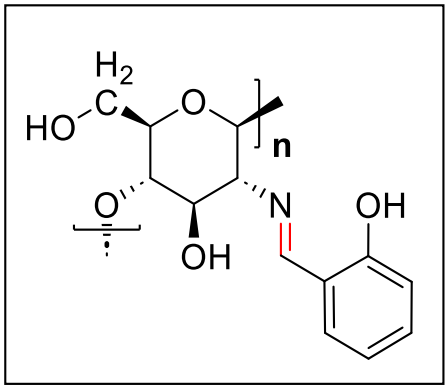


Figure 2.9 Schiff Base of Chitosan-Salicylaldehyde [237]

2.7.6 Glyoxal as a Crosslinking Agent

Glyoxal (OHC–CHO) is a dialdehyde (Figure 2.10) that can be procured from numerous natural resources, e.g., from the oxidation of lipids or as a by-product of biological processes. The two adjacent carbonyl groups in the chemical structure of this material, make it highly reactive [239]. In recent years, glyoxal has attracted the attention of many researchers as a promising cross-linking agent due to its various advantageous features such as abundant availability, cost-efficiency, high functionality and high solubility in water [225].

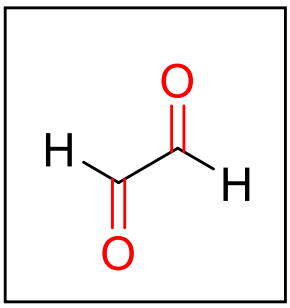


Figure 2.10 The Chemical Structure of Glyoxal [240]

The high functionality of glyoxal is due to its acetal formation ability between the aldehyde groups of glyoxal with the hydroxyl groups in the glucosamine units of chitosan on top of the Schiff's base formation ability between the aldehyde groups of glyoxal and the free amino groups in chitosan's backbone. Glyoxal is assumed to have a steric effect on the network structure of the cross-linked fibre as compared to

glutaraldehyde resulting in a tight supramolecular structure with higher crystallinity [241]. The Schiff base of Cs-Gly is shown in Figure 2.11.

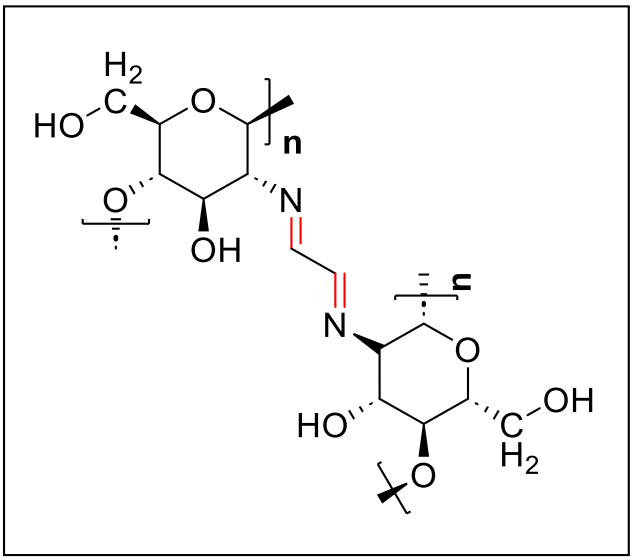


Figure 2.11 Schiff Base of Chitosan-Glyoxal [240]

The effects of cross-linking reaction of chitosan in different forms have been studied by different researchers. Yang, et al., (2005) studied the effects of cross-linking with glyoxal on chitosan fibre and observed an enhancement in the mechanical properties of the fibre after the cross-linking reaction which occurred due to the acetalisation and Schiff base reaction taking place [241]. Jawad, et al., (2019) studied the effect of cross-linking with glyoxal on chitosan film for dye removal. They found that the cross-linking reaction reduced the swelling index of chitosan dramatically due to it blocking some of the hydrophilic groups in the polymeric structure of chitosan [225]. There have been multiple studies performed with glyoxal as a successful cross-linking agent for composites of chitosan [30], [154], [221], [223], [242], [243], [244], [245], [246].

2.7.7 Benzil as a Crosslinking Agent

Benzil (Bz_2; 1,2-diphenylethane-1,2-dione) is an organic compound with the formula (C6H5CO)2, generally abbreviated as $(PhCO)_2$ is one of the most common diketones and in physical appearance of it is in the form of a yellow solid material [247]. The chemical structure of Benzil can be seen in Figure 2.12. Benzil is mostly used in

the free-radical curing of polymer networks and ultraviolet radiation causes a decomposition in this material resulting in the generation of free-radical species which in return promote the formation of cross-links. Benzil is made of two ketone groups side by side (alpha-diketone), making it the simplest aromatic diketone. Diketones are responsible for creating various fragrances.

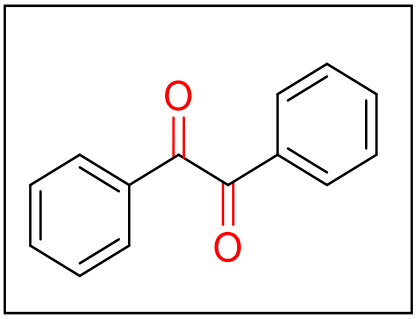


Figure 2.12 The Chemical Structure of Benzil [248]

Benzil has the chemical formation suitable for acting as a cross-linking agent, by converting the amine group in the chitosan backbone into imine and thus achieve the formation of Schiff base chitosan derivative through cross-linking reaction [6], [222]. The resulting material would possess increased chemical stability and high mechanical resistance. The Schiff base of Cs-Bz_2 is shown in Figure 2.13. The amount of research done on benzil as a cross-linking agent for chitosan derivatives is very limited and there is room for growth in this field.

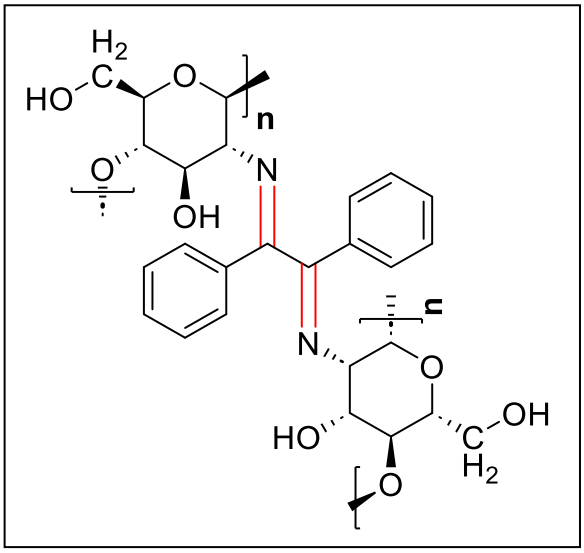


Figure 2.13 Schiff Base of Chitosan-Benzil [6]

2.8 Algae as an Adsorbent

Multiple microbial biomasses (dead or living) have been extensively studied for their ability to remove dyes from wastewater. The methods for controlling biomasses and modified biomasses primarily include chelation, complexion, surface adsorption, ion exchange, etc [27]. When referring to microbial biomasses, this category includes bacteria, micro algae and fungi among other biomasses. These materials/organisms are capable of adsorbing dye molecules and/or destruction of chromophores of the dye molecule by secretion of enzymes resulting into decolouration [7]. Algal biomasses are broadly grown in nature with short growth cycles, making them cost-efficient. Hence, they have attracted the attention of researchers to study their efficiency as an adsorbent for dye removal processes which consequently resulted into discovering their strong adsorption properties [8], [9]. However, even though they can expand utilising wastewater as a cultivation medium added to their great binding affinity and sorption selectivity towards contaminants compared to activated carbon and typical ion exchange resins, they have often been given attention only as alternative biosorbents [249]. According to Soni, et al., (2019) and Gerhardt , et al., (2020) the biomass of microalgae mainly comprises of proteins, carbohydrates, and lipids which would consequently mean that many functional groups such as hydroxyl, carboxyl, phosphate and sulphate are available in the chemical structure of this biomass and these functional groups are associated with the high binding affinity of micro algae towards the water pollutants [191], [250].

Moreover, *Arthrospira maximum* is a spiral shaped, filamentous, water-blue-green microalgae, with an almost 8mm diameter that has been investigated by researchers for wastewater treatment purposes [251].In research conducted by Balti, et al., (2017), it was found that *spirulina* is a multicellular microalgae cyanobacteria that takes the shape of a spiral. Additionally, *Spirulina* can survive and function in sea water as well as fresh water [195]. Furthermore, *Spirulina platensis* is categorised as a blue-green microalgae (cyanobacteria) that can be commonly found in tropical and subtropical lakes with high levels of bicarbonate and carbonate [252]. Blue-green algae are commonly used in animal feed, nutritious food, diagnostics, and therapy due to their high levels of pigments and phytonutrients. Such desirable characteristics have brought the importance of this material into the spotlight, resulting to increased demand for the

blue-green algae in the global market. Moreover, *Chlorella sp.* (Green algae; chlorophyta) is a single cell (small globular cell) microalga with a diameter averaging 2-10 μm that has been utilised most (compared to other microalgae) in wastewater treatment [253]. Table 2.5 consists of some of the applications of algae for dye removal studied by researchers.

Table 2.5
Applications of Algae in Dye Removal

Algae type	Modifications	Target dye	Reference
Fucus vesiculosus, Spirulina maxima and *Chlorella pyrenoidosa*	Chemically modified with orthophosphoric acid (H_3PO_4) and zinc chloride ($ZnCl_2$)	Methylene Blue	[254]
Spirulina sp.	Modified with hexadecyltrimethylammonium bromide (HDTMA) surfactant	Crystal Violet and Safranin	[8]
Spirulina platensis	Incubation	Indigo Blue	[9]
Scenedesmus obliquus	Biochar-algae microspheres coated with sodium alginate	Malachite Green	[255]
Chlorella sorokiniana strain HIN-3	–	Congo Red and Red-S3B	[256]
Chlorella vulgaris	–	Direct Black-22	[257]
Lipid free *chlorella vulgaris*	Lipid extraction from *chlorella vulgaris* and TPP crosslinked composite formation with magnetite (Fe^{2+} and Fe^{3+}) and chitosan	Crystal Violet	[258]

2.8.1 Algae (Spirulina sp.) as a Modifying Agent

Spirulina is a multicellular cyanobacterium alga with a filamentous form that was first discovered at Lack Chad (Central Africa) in 1940 as its major natural source and it was found to be one of the first-generation photosynthetic life forms [259]. Due

to its abundant contents of antioxidants, minerals, fats, lipids, sugars, essential amino acids, macro, and micronutrients as well as the short time required for its growth and harvest, Spirulina has gathered ample attention in different industrial sectors such as food, hygiene and aquaculture [250]. Hence, due to all the desirable features of this material, it has been extensively used by researchers to investigate its adsorption and toxin removal potentials. Additionally, nanomaterials are the trending topic in chemical processing in recent years due to their high rates of active surface area cause by their small scale [250], [259]. As micro algae have been recommended to be used as alternative biosorbents, this low-cost microalga that is vastly available and grown globally can be considered as an additive to the chitosan composite to improve the desirable properties of the blend [191], [259].

2.9 Titanium Dioxide as an Adsorbent

Titanium dioxide, also known as titanium (IV) oxide or titania is in the inorganic compound with the chemical formula TiO_2. TiO_2 is a semiconductor, and it is well known for its photocatalytic properties that can be used for splitting water into hydrogen and oxygen, building self-cleaning facades, decontaminating water, etc [260]. This material is a white, water insoluble solid which is commonly used as a pigment with a wide range of applications such as paint, sunscreen and food colouring. Moreover, TiO_2 is available in three main dioxide forms; namely anatase, rutile and brookite. In all these forms, titanium exhibits an octahedral geometry, being bonded to six oxide anions. Figure 2.14 shows the three main dioxide forms of titanium in their primitive cell form.

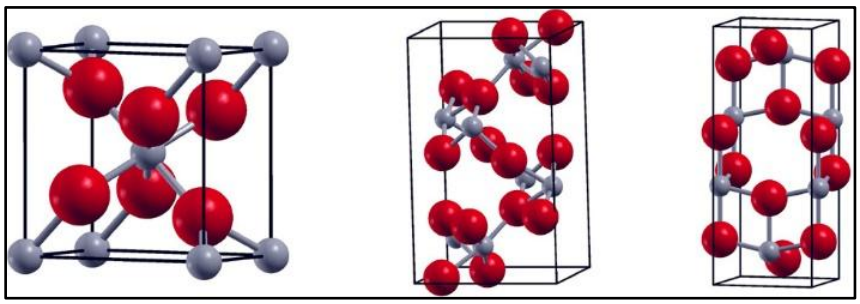


Figure 2.14 The Primitive Cells of Rutile, Brookite and Anatase (from Left to Right) [261]

The most abundant and most extensively studied polymorph of TiO_2 is the rutile phase. Over the past decade titanium dioxide has received much attention due to its competitive cost, non-toxicity, excellent stability, and ability to produce high oxidising radicals [262]. Furthermore, titanium dioxide has been widely used as an additive to the chitosan derivatives to increase the chemical stability, surface area and adsorption in wastewater treatment. Table 2.6 illustrates some of the research done in this field.

Table 2.6
Examples of Applications of TiO_2 in Dye Removal

Type of adsorbent	**Application in wastewater treatment**	**Reference**
Nanocomposite	Chitosan/TiO_2 nanocomposite was synthesised and successfully implemented for the removal of thorium (IV) from aqueous solutions	[263]
Nanocomposite	TiO_2 nanoparticles were dispersed in the polymer matrix of grafted chitosan-polyacrylamide for the effective removal of Sirius yellow K-FC dye in 6 cycles of reusability with minimal drop in efficiency	[161]
Thin film	Chitosan, extracted from crab shells, was used in the fabrication of CS-TiO_2 thin films and tested for the removal of methylene blue dye and proved as an effective adsorbent.	[264]
Nanocomposite	Hybrid cross-linked chitosan-epichlorohydrin/TiO_2 nanocomposite was synthesised and applied for the effective removal of Reactive Red 120 dye.	[265]
Nanocomposite	Molecular imprinted chitosan-TiO_2 nanocomposite was synthesised with chitosan as the imprinting carrier and TiO_2 as support/carrier by sol-gel route for selective removal of Rose Bengal dye.	[266]
Nanocomposite	A low-cost nanocomposite with TiO_2/hydrogel core utilising the free radical graft copolymerisation method as a promising adsorbent for Brilliant Green dye.	[11]
Nanocomposite	Chitosan/TiO_2 nanocomposite cross-linked by EGDE were synthesised and applied for the removal of Reactive Orange 16 dye and the material was found as a successful candidate for efficient removal of acid dyes from aqueous solutions.	[3]

2.10 Dye Adsorption Mechanisms on Chitosan Derivatives

Chitosan is a material with abundant binding sites along its polymeric matrix. The abundance of active amino ($-NH_2$) and hydroxyl ($-OH$) groups on chitosan makes it an excellent material for adsorption of different pollutants from wastewater [267]. Furthermore, the formation of Ti−OH groups after compositing chitosan with kronos can also add to the active adsorption sites [170]. Moreover, the main responsible force for the adsorption of dyes on the surface of chitosan composites is the electrostatic attraction caused by the formation of positive or negative charges on the surface of Cs composite which can bond with the opposing charge of the dye molecules [268]. Another possible interaction responsible for the adsorption of dyes is the hydrogen bonds that can occur due to the abundance of hydrogen in the polymeric matrix of chitosan which can create hydrogen bonds with O and N atoms available in the chemical structure of dye molecules [223]. Moreover, the presence of nucleophiles with free electron pairs in the structure of chitosan (O and N) that can react with the electrophile benzene rings present in the chemical structure of dyes leads to a plausible n-π stacking interaction which plays an extra role in the adsorptive removal of dyes by chitosan composites. Additionally, the crosslinking and grafting reactions with materials containing aromatic rings allows the occurrence of π-π interactions between the aromatic rings available in the structure of BG dye molecules and the aromatic rings added to the Cs backbone [189], [269].

2.11 Optimisation by Response Surface Methodology (RSM)

Response Surface Methodology (RSM) initially consists of certain mathematical and statistical methods for the purpose of designing experiments, creating models with consideration for interactions of the model parameters and optimisation to reach maximum output. In recent years, the use of experimental design has become essential in the field of research as it reduces the number of experiments that need to be performed to reach a final verdict on optimum operating conditions to maximise the target output. Due to the many advantages of experimental design, researchers are increasingly relying on these statistical methods, such as RSM, to ease the process of research [270].

One of the available designs in RSM is Box-Behnken Design (BBD). Furthermore, when the number of experimental variables (factors) are equal or higher than three, BBD is more labour efficient and ideal for fitting a second-order polynomial equation for the model. Hence, it is easier to achieve optimum output of the response (dye removal in case of this research) with minimalistic number of runs (experiments) and expectedly using less volumes of chemicals [269]. Moreover, in BBD the range of variables that are set in experiments will not exceed the range that was pre-configured to the software so the operation range can be controlled better while using BBD compared to other models available in RSM. In Figure 2.15, the basic steps in the use of RSM in any research can be seen.

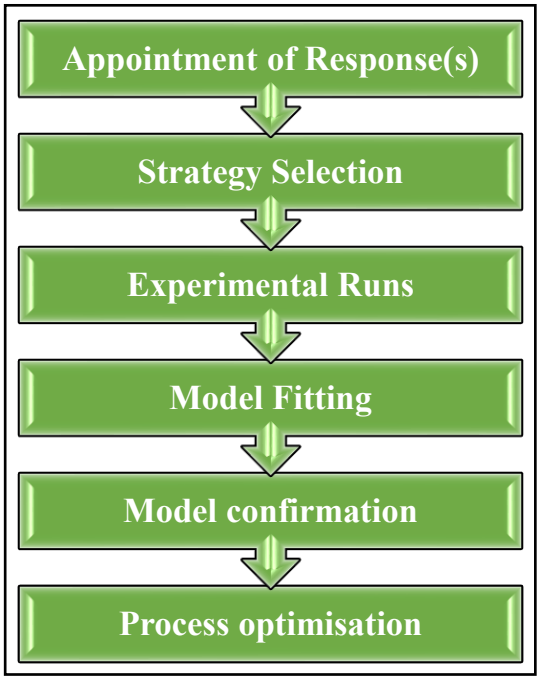


Figure 2.15 General steps of using RSM

CHAPTER 3
RESEARCH METHODOLOGY

3.1 Materials and Methods

3.1.1 Chemicals and Reagents

Chitosan (Cs) flakes (medium MW; degree of deacetylation ≥ 75%), C-doped TiO_2 kronos (Tk) particles (1< particle size <10 μm), benzaldehyde (C6H5CHO; assay ≥ 99%; MW= 106.12 g mol^{-1}), salicylaldehyde ($C_7H_6O_2$; MW: 122.12 g mol^{-1}) and benzil $(C_6H_5CO)_2$; 98%; MW= 210.23 g mol^{-1}) were supplied by Sigma Aldrich. Glyoxal ($C_2H_2O_2$; 40% solution in water; density: 1.27 g cm^{-3} (20 °C)) was acquired from Merck. Brilliant green dye (C27H34N2O4S; MW: 482.64 g mol^{-1}), sodium hydroxide (NaOH) pellets (MW: 40 g mol^{-1}), sodium chloride (NaCl) powder (MW: 58.44 g mol^{-1}) and Acetic Acid (CH3COOH) solution (99.8%) were purchased from R&M chemicals. Microalgae (Ma) powder was provided by Microalgae Research Laboratory (MRL) (Faculty of Applied Sciences, UiTM Shah Alam, Malaysia). Double-distilled water was used for washing and dilution as necessary throughout the research. Brilliant green dye stock solution of 1000 mg L^{-1} was diluted as necessary for adsorption studies. All reagents used in this study were pure and of analytical grade without the need for any further purification.

3.1.2 Apparatus

The apparatus that utilised in this research consist of pH meter (827 pH Lab, Metrohm Swiss Made), standard test sieve (ASTM E-11 Standard, 250μm), field emission scanning electron microscope equipped with energy dispersive X-ray spectroscopy (Thermo-Scientific Apreo 2 S), Direct Reading Spectrophotometer (HACH DR 2800), Fourier transform infrared (FTIR) analyser (Perkin-Elmer, Spectrum RX I, at wavenumbers ranging between 4000 cm^{-1} and 450 cm^{-1}), CHNS/O analyser (Flash 2000, Thermo-Scientific) and X-ray diffractometer (XRD, PANalytical X'Pert PRO in the 5°- 90° range and Cu Kα radiation (λ = 1.54 Å)).

3.2 Methods

3.2.1 Preparation of Cs-Ma-Tk Beads

Initially, 5 g of Chitosan flakes (Cs), 2.5 g of microalgae (Ma) and 2.5 g of C-doped TiO_2 kronos (Tk) (ratio of 50%-25%-25%, respectively) were mixed well and 175 mL of acetic acid solution (5%) was then added to the mixture. The resulting viscous solution was mixed under mechanical stirring for 24 h. This step is undertaken to rectify complete dissolution of chitosan flakes in the acetic acid solution. Afterwards, a 10ml syringe was used to transfer the viscous solution as droplets (manually) to 1L of 0.5 M NaOH solution. The beads were then left in the NaOH solution for 1h before being washed thoroughly with double-distilled water to remove all traces of NaOH solution and reach neutral pH.

3.2.2 Grafting of Cs-Ma-Tk with SD

The grafting reaction was performed by placing the Cs-Ma-Tk beads inside a hydrothermal reactor submerged in 100mL salicylaldehyde (2% v/v) solution. Subsequently, the hydrothermal reactor was placed inside an oven set at 100ºC for 4hrs. The beads were then thoroughly washed with double-distilled water and oven dried at 50ºC overnight. Finally, the dry grafted Cs/SD-Ma-Tk beads were ground using a mortar and pestle and the resulting powder was sieved to a constant 150 µm < particle size < 250 µm and kept in an airtight container for further applications.

3.2.3 Grafting of Cs-Ma-Tk with BD

The grafting reaction was performed by placing the Cs-Ma-Tk beads inside a hydrothermal reactor submerged in 100mL benzaldehyde (2% v/v) solution. Subsequently, the hydrothermal reactor was placed inside an oven set at 100ºC for 4hrs. The beads were then thoroughly washed with double-distilled water and oven dried at 50ºC overnight. Finally, the dry grafted Cs/BD-Ma-Tk beads were ground using a mortar and pestle and the resulting powder was sieved to a constant 150 µm < particle size < 250 µm and kept in an airtight container for further applications.

3.2.4 Cross-linking Cs-Ma-Tk with Bz_2

The Cs-Ma-Tk hydrogel beads were put in a hydrothermal reactor (submersed in 100 mL benzil (2% w/v; 50% water and 50% acetone solution) solution which was then placed inside an oven at 100°C for 16 h to allow for the crosslinking reaction between Cs and Bz_2 to occur. The beads were then extracted from the reactor and rinsed thoroughly to remove any excess Bz_2. The Cs/Bz_2-Ma-Tk were then placed inside an oven at 50°C overnight to dry. The dried Cs/Bz_2-Ma-Tk beads were then crushed using a pestle and mortar and passed through a sieve to achieve a consistent particle size of about 250 μm. The obtained Cs/Bz_2-Ma-Tk powder was then kept inside an airtight container for further application.

3.2.5 Cross-linking Cs-Ma-Tk with Gly

The Cs-Ma-Tk hydrogel beads were put in a hydrothermal reactor (submersed in 100 mL glyoxal (2% v/v) solution which was then placed inside an oven at 100°C for 16 h to allow for the crosslinking reaction between Cs and Gly to occur. The beads were then extracted from the reactor and rinsed thoroughly to remove any excess Gly. The Cs/Gly-Ma-Tk were then placed inside an oven at 50°C overnight to dry. The dried Cs/Gly-Ma-Tk beads were then crushed using a pestle and mortar and passed through a sieve to achieve a consistent particle size of about 250 μm. The obtained Cs/Gly-Ma-Tk powder was then kept inside an airtight container for further application.

3.3 Characterisation of the Adsorbents

3.3.1 X-Ray Diffraction Analysis

The crystalline phase of the composites was characterised utilising X-ray Diffractometer (XRD, X'Pert PRO, PAnalytical). The XRD spectra were obtained and the peaks a different 2θ values (5-90 degrees) were utilised to confirm the successful incorporation of the composite components into the polymeric matrix of Cs. The analysis was carried out using Cu Kα radiation with a wavelength of 1.5406 Å, operated under appropriate accelerating voltage and current conditions. The powdered samples were placed on a sample holder and scanned over the selected 2θ range at a constant

scanning rate to obtain the diffraction patterns. The resulting diffractograms were analysed by examining the position, intensity, and shape of the diffraction peaks. These features provide information regarding the crystalline and amorphous regions present in the materials. Changes in peak position or intensity were used to evaluate structural modifications and interactions between the incorporated components and the chitosan matrix. The obtained diffraction patterns were further compared with standard reference data where necessary to assist in identifying the crystalline phases present in the composites.

3.3.2 FT-IR Spectra Analysis

FT-IR analysis is an important step in characterisation to identify the functional groups of the adsorbent as well as confirm the incorporation of the added compositing materials into the matrix of Cs. The functional groups of the samples before and after dye adsorption were identified via Fourier transform infrared (FTIR, Perkin-Elmer, Spectrum RX I) Spectroscopy. The FTIR analysis was performed by creating KBR pellets and in the range of 4000-450cm^{-1}. Prior to analysis, the powdered samples were finely ground and mixed with potassium bromide (KBr) to form transparent pellets suitable for infrared transmission measurements. The spectra were recorded within the selected wavenumber range at an appropriate resolution to obtain clear absorption bands corresponding to the vibrational modes of the chemical bonds present in the materials. The obtained FTIR spectra were analysed by identifying the characteristic absorption peaks associated with functional groups such as hydroxyl, amino, and other chemical bonds present in the adsorbent structure. Comparison of the spectra before and after dye adsorption was carried out to evaluate possible interactions between the adsorbent surface and the dye molecules, as indicated by shifts in peak positions or changes in peak intensity. This analysis provides insight into the surface chemistry of the materials and the functional groups involved in the adsorption process.

3.3.3 Physical Properties

Surface properties and pore structure are essential determinants of adsorbent performance. Adsorbents with higher surface area and better pore structure can more effectively capture dye molecules. The Brunauer, Emmett, and Teller (BET) method

was employed to calculate the surface area and the pore size distribution of the composites. Furthermore, the N_2 adsorption-desorption isotherms of the synthesised composites were plotted and analysed to better evaluate the porosity of the composites. The specific surface area of the materials was determined from the nitrogen adsorption data using the Brunauer–Emmett–Teller (BET) model. Prior to analysis, the samples were degassed to remove physically adsorbed moisture and impurities, ensuring that the measured adsorption corresponded only to nitrogen molecules interacting with the accessible surface of the adsorbent. Nitrogen adsorption measurements were conducted at 77 K, and the BET equation was applied to the adsorption data within the appropriate relative pressure range to obtain a linear plot from which the monolayer adsorption capacity was determined. The BET surface area was subsequently calculated from this monolayer capacity by considering the molecular cross-sectional area of nitrogen. In addition, the total pore volume and average pore diameter were derived from the adsorption–desorption isotherm data to provide further information on the pore structure of the materials. This approach enabled a consistent evaluation of the surface properties of all adsorbents investigated in this study.

3.3.4 Surface Morphology and elemental composition

The surface morphology and elemental composition of the composites were investigated using a field emission scanning electron microscope equipped with an energy dispersive X-ray analyser (FESEM–EDX, Thermo-Scientific Apreo 2 S). Prior to observation, the samples were mounted onto conductive stubs and coated with a thin layer of gold using a gold sputterer to enhance surface conductivity and minimise charging effects during imaging. The FESEM analysis was performed under appropriate accelerating voltage and magnification conditions to obtain high-resolution micrographs, allowing detailed examination of the surface texture, particle distribution, and structural features of the composites. In addition, the integrated EDX detector was used to qualitatively identify the elemental composition of the samples by analysing the characteristic X-ray signals emitted from the specimen when exposed to the electron beam. The elemental distribution and relative presence of elements within the composites were evaluated from the obtained spectra. Further quantitative elemental analysis was conducted using a CHNS elemental analyser (Flash 2000, Thermo-Scientific), which was employed to determine the carbon (C), hydrogen (H), nitrogen

(N), and sulphur (S) contents of the materials, while the oxygen (O) content was calculated by difference. This combined analysis provided complementary information on both the morphological characteristics and the elemental composition of the prepared composites.

3.3.5 Surface Charge (pHpzc) Analysis

The surface charge (pHpzc) of the adsorbents was investigated utilising the pH drift method with a pH meter. The synthesised composites were treated with 100ml 0.01M NaCl solutions of varying pH (3-12) for 24 hours and tested for changes in the solution pH after the treatment in order to determine the point of zero charge on the surface of each composite material.

3.4 Design of Experiments using Box-Behnken design (BBD)

After preparing the five target adsorbents of this research, experimental design is implemented to investigate the adsorptive behaviour of the adsorbents. This study carries out the process optimisation of experimental design in three steps. In the first step, preliminary experiments are performed to mark the effective range of the three variables (adsorbent dose, contact time and solution pH) to be utilised for the design of experiments [3]. The second step is to utilise the results of the preliminary tests in the design of a three-level three-factors (with five centre points) Box-Behnken design using a statistical analysis computer software (Design Expert software version 13.0; StatEase). There are 17 experimental runs (for a three-level three factor design) produced by BBD to investigate the solo and interactive effects of the factors on the response (dye removal) as well as to determine the quadratic model fit for the response. There are three variables, and each variable has three levels of values generally known as -1,0 and +1 levels for low, medium and high values of each variable respectively. The general scheme of the factorial design can be seen in Table 3.1.

Table 3.1
Factors and Their Levels

Factors	Description	Low (-1)	Medium (0)	High (+1)
A	Adsorbent dose (g/100 mL)			
B	pH			
C	Contact time (min)			

Furthermore, a second-degree polynomial is employed to determine the correlation between the input variables and the output as shown in equation (3.1).

$$Y = \beta_0 + \sum \beta_i X_i + \sum \beta_{ii} X_i^2 + \sum \sum \beta_{ij} X_i X_j \quad (3.1)$$

Where Y represents the predicted response, X_i and X_j are the independent variables, β_0 β_i, β_{ii}, and β_{ij} denote the intercept, linear, quadratic, and interactive regression coefficients, respectively.

The third step is to perform the experiments produced by BBD. The adsorption experiments were performed in batch study mode to investigate the values of response (dye removal (%)) and adsorption capacity of the composites. The BG dye removal experiments were performed by adding the specified masses of the adsorbents inside 250mL Erlenmeyer flasks containing 100mL BG dye solution (50mg/L). The flasks were then placed inside a thermostatic water bath shaker (Memmert WNB7-45) and agitated at a constant speed of 80 strokes/min for the specified periods of time at the controlled temperature of 25°C. The dye removal was then calculated after measuring the final concentration of each sample utilising a spectrophotometer (HACH DR 3800) at λmax = 623 nm. The samples were passed through a 0.22 μm nylon syringe filter to obtain solutions devoid of any adsorbent particles. The equation used to calculate dye removal (%) is displayed below.

$$\mathrm{R}\,\% = \frac{(\mathrm{C_o} - \mathrm{C_e})}{\mathrm{C_o}} \times 100 \quad (3.2)$$

Where R represents dye removal (%) and C_o and C_e indicate the initial and equilibrium BG concentrations (mg/L), respectively.

3.5 Equilibrium Studies

Adsorption experiments were performed in batch mode to evaluate the adsorption capacity of the adsorbents towards BG at different initial concentrations. The experiment parameters were determined after performing desirability test on the results of the experimental design to maximise response (BG removal) within the range of the three parameters. The suggested conditions were then tested three times to confirm the reliability and repeatability of the obtained dye removal values. Adsorption equilibrium studies were conducted to determine the adsorption capacity and the adsorption model followed by the system using the optimised values of adsorbent dosage and pH for the adsorption of BG from dye solutions with various initial concentrations (20-250mg/L). The experiments were conducted in the same manner as described in section 3.4 and the equilibrium adsorption capacities (q_e, mg/g) of the adsorbents were calculated using the following equation (3.3):

$$q_e = \frac{(\mathrm{C_o} - \mathrm{C_e})\mathrm{V}}{\mathrm{W}} \tag{3.3}$$

Where q_e represents adsorption capacity (mg/g). $\mathrm{C_o}$ and $\mathrm{C_e}$ indicate the initial and equilibrium dye concentrations (mg/L) respectively. V (L) refers to the volume of BG solution used, and W (g) denotes the amount of the adsorbent added to the dye solution.

3.5.1 Kinetic Study

In order to fully comprehend the BG dye adsorption behaviour on the crosslinked and grafted Cs-Ma-Tk composites and investigate the adsorption mechanism, the compatibility of two standard kinetic models, namely pseudo-first order (PFO) [271] and pseudo-second order (PSO) [272], with the experimental adsorption data was investigated. The non-linear forms of PFO and PSO models are shown in equations (3.4) and (3.5), respectively.

pseudo-first-order: $$q_t = q_e(1 - exp^{-k_1^t}) \tag{3.4}$$

pseudo-second-order: $$q_t = \frac{q_e^2 k_2^t}{1 + q_e k_2^t} \quad (3.5)$$

Where q_e and q_t represent adsorption capacity (mg/g) at equilibrium and time respectively and *k1* and *k2* denote the PFO and PSO rate constants (1/min), respectively.

3.5.2 Isotherm Study

The investigation of the adsorption isotherm followed by the adsorption process is an important milestone in determining the correct pathways of the adsorption process and mechanism. Furthermore, the adsorption isotherm parameters can provide help in the understanding of the interactions between the adsorbent and adsorbate [273]. The most widely applied isotherms (Langmuir [274], Freundlich [275], and Temkin [276]) were employed to analyse the equilibrium adsorption data and calculate the maximum adsorption capacity of the adsorbents towards BG dye. The Langmuir isotherm model represents a monolayer adsorption process occurring on a homogenous surface [274], while the Freundlich isotherm model is characteristic of a multi-layered adsorption process ensuing on a heterogenous surface with differing adsorption energies [275]. Whereas the Temkin adsorption isotherm model assumes that there exists a linear decrease in the required energy for adsorption with the increase of coverage [276]. The non-linear expressions of Langmuir, Freundlich, and Temkin isotherms are presented in equations (3.6), (3.7) and (3.8), respectively.

Langmuir Adsorption Isotherm: $$q_e = \frac{q_{max} K_a C_e}{1 + K_a C_e} \quad (3.6)$$

Freundlich Adsorption Isotherm: $$q_e = K_f C_e^{1/n} \quad (3.7)$$

Temkin Adsorption Isotherm: $$q_e = \frac{RT}{b_T} \ln(K_T C_e) \quad (3.8)$$

Where q_e and C_e represent the amount of BG dye adsorbed at equilibrium (mg/g) and the equilibrium BG concentration (mg/L), respectively. While q_{max} denotes the maximum adsorbed quantity of BG (mg/g) and *Ka* is the Langmuir constant associated with the affinity of the active adsorption sites (L/mg). Furthermore, K_f is the

Freundlich constant related to the adsorption capacity (mg/g) while n provides information concerning the favourability of the adsorption process. R (J/mol K) signifies the universal gas constant (8.314), T (K) implies temperature, while the Temkin constants b_T and K_T (L/mg) relay information regarding the heat of adsorption and the equilibrium binding, respectively.

Non-linear forms of the isotherm models have been chosen for this study because most adsorption isotherm equations, such as the Langmuir and Freundlich models, are inherently non-linear with respect to their parameters. Transforming these equations into linear forms to apply linear regression can distort the original mathematical structure of the model and modify the statistical properties of the experimental errors. As reported in the literature, linearisation may alter the error distribution, violate the assumptions of constant variance and normality required for least-squares regression, and introduce statistical bias that can lead to inaccurate parameter estimation and misleading model selection. In contrast, non-linear regression fits the original isotherm equations directly to experimental data, preserving their theoretical form and providing more reliable parameter estimates, improved statistical interpretation, and a more accurate representation of adsorption behaviour. Furthermore, with modern computational tools readily available, the numerical solution of non-linear regression problems has become straightforward, making non-linear modelling a more robust and reliable approach for adsorption isotherm analysis [277], [278].

3.5.3 Thermodynamic Study

Adsorption thermodynamic parameters were calculated to investigate the adsorption process of BG dye onto the surface of the grafted and crosslinked Cs-Ma-Tk composites regarding the feasibility and spontaneity of the process as well as the randomness of the adsorption system at the solid/fluid interface [279]. Equations (3.9), (3.10) and (3.11) are used to determine the parameters of adsorption thermodynamics, namely, Gibbs free energy change ($\Delta G°$), entropy change ($\Delta S°$), and enthalpy change ($\Delta H°$).

$$\Delta G° = -RT \ln K_d \tag{3.9}$$

$$k_d = \frac{q_e}{C_e} \tag{3.10}$$

$$\ln k_d = \frac{\Delta S°}{R} - \frac{\Delta H°}{RT} \tag{3.11}$$

where T and R represent the absolute temperature (K) and the universal gas constant (8.314 J/mol K), respectively. k_d signifies the distribution coefficient, q_e denotes the amount of dye adsorbed by the adsorbent at equilibrium (mg/g) and C_e stands for the concentration of BG remaining in the aqueous solution at equilibrium (mg/L). The values of thermodynamic parameters ($\Delta H°$ and $\Delta S°$) are calculated from plotting $\ln k_d$ against 1/T, where slope and intercept are utilised to determine $\Delta H°$, and $\Delta S°$, respectively.

CHAPTER 4
RESULTS AND DISCUSSION

4.1 Salicylaldehyde grafted Cs-Ma-Tk (Cs/SD-Ma-Tk)

In this section, a new composite material of Chitosan- Microalgae- Kronos TiO_2 was synthesised and put through a hydrothermal grafting process to create salicylaldehyde-grafted Chitosan- Microalgae- Kronos TiO_2 (henceforth referred to as Cs/SD-Ma-Tk) for the adsorption of brilliant green dye. The use of biodegradable and abundantly available resources in this study is an effort to achieve a cost-efficient and biofriendly adsorbent with high efficiency towards the removal of pollutants (specifically BG dye in this study) from effluents. The addition of Tk and Ma would help alleviate chemical instability and low affinity of Cs towards cationic pollutant species, while the Schiff base reaction occurring during the grafting process would further enhance the structural stability of the resultant composite. The dye removal conditions (adsorbent dosage, pH, contact time) have been optimised using RSM-BBD methodology and the optimal conditions have been applied for kinetic, isotherm, and thermodynamic studies. Based on the findings of the analyses, a plausible adsorption mechanism has been proposed.

4.1.1 Surface Properties of Cs/SD-Ma-Tk

Surface properties and pore structure are essential determinants of adsorbent performance. Adsorbents with higher surface area and better pore structure can more effectively capture dye molecules. The Brunauer, Emmett, and Teller (BET) method was employed to calculate the surface area and the pore size distribution of the Cs/SD-Ma-Tk composite as portrayed in Table 4.1. The results show a surface area of 9.1 (m^2/g), Langmuir surface area of 13.1 (m^2/g), pore volume of 0.02 (cm^3/g) and average pore diameter of 8.2 (nm). The obtained average pore diameter classifies Cs/SD-Ma-Tk as a mesoporous material according to IUPAC classifications.

Table 4.1
Physicochemical Characteristics of Cs/SD-Ma-Tk

Parameters	**CsMaTk/S**
Surface Area (m^2/g)	9.1
Langmuir Surface Area (m^2/g)	13.1
Pore Volume (cm^3/g)	0.02
Average Pore Diameter (nm)	8.2
Carbon	40.35%
Hydrogen	4.56%
Nitrogen	4.51%
Sulphur	0.05%
Oxygen (by difference) (%)	50.53%

The N_2 adsorption-desorption isotherm of Cs/SD-Ma-Tk were plotted and displayed in Figure 4.1 (with pore width distribution inset) and it is found to be compatible with type IV isotherm which further affirms the mesoporosity of the synthesized adsorbent. The compatibility of the plot with H3 hysteresis loop which is associated with the existence of macropores in the pore network reveals a very broad distribution of pore size in Cs/SD-Ma-Tk [280]. The wide range of pore width distribution can be seen in Figure 4.1 inset as well. Elemental analysis was performed to measure the C, H, N, S and O contents of Cs/SD-Ma-Tk and the results present 40.35%, 4.56%, 4.51%, 0.05% and 50.53% content, respectively (as displayed in Table 4.1).

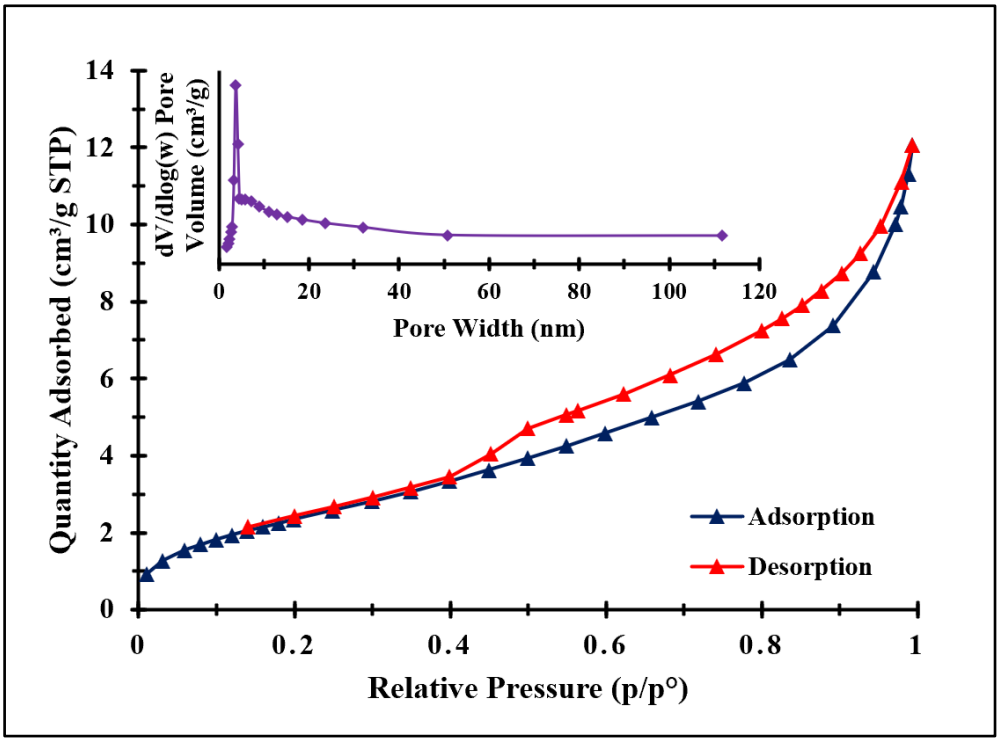


Figure 4.1 N_2 Adsorption/Desorption Plot of Cs/Sd-Ma-Tk with Pore Width Distribution Inset

4.1.2 X-Ray Diffraction Analysis of Cs/SD-Ma-Tk

The crystallographic nature of Cs/SD-Ma-Tk was studied using XRD analysis and exhibited in Figure 4.2. The two characteristic peaks observed at 2θ=10.7 and 20.7 are associated with the (020) and (110) crystal planes of Cs [281]. The distinctive peak observed at 2θ=22.48 can be attributed to the crystalline phase of cellulose associated with Microalgae [190]. The peaks observed at 2θ=25.7, 38.1, 48.3, 54.3, 55.4, 63.2, 69.2, 70.5, 75.1 and 82.8 can be attributed to the (101), (004), (200), (105), (211), (213), (116), (220), (215) and (224) crystal planes of TiO_2, respectively [46–48]. The observation of the characteristic peaks of cellulose and TiO_2 can affirm the successful incorporation of Ma and Tk into the matrix of chitosan.

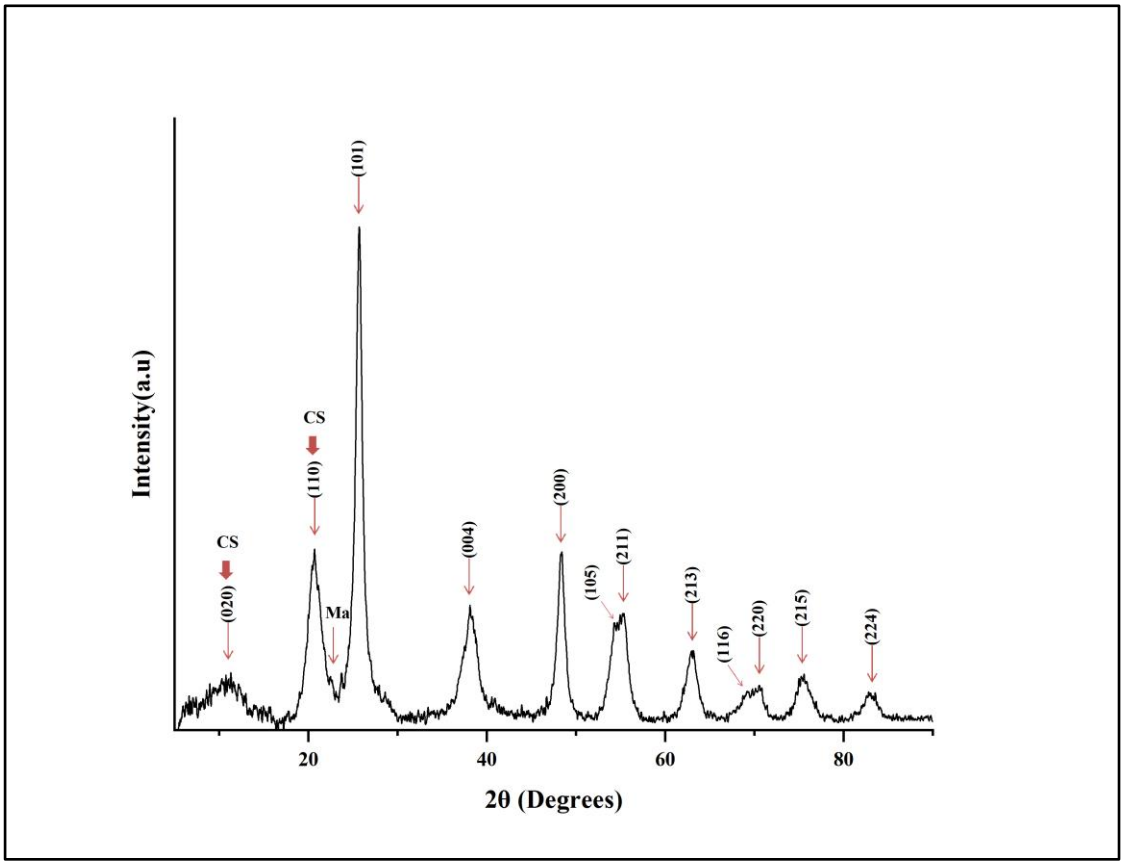


Figure 4.2 XRD Pattern of Cs/SD-Ma-Tk

4.1.3 FT-IR Spectrum Analysis of Cs/SD-Ma-Tk

FT-IR analysis is an important step in characterisation to identify the functional groups of the adsorbent as well as confirm the incorporation of the added compositing materials into the matrix of Cs. Figure 4.3 exhibits the FT-IR spectra of Cs/SD-Ma-Tk before and after the adsorption of BG dye. The broad peak observed at 3350-3670 cm^{-1} is a characteristic peak attributed to the stretching vibrations of -OH and -NH groups [285]. As observed from the figure, the intensity of the broad peak in this region has decreased after the adsorption of BG dye which can attest to the occupation of these surface functional groups by the dye molecules. The peak at 2900 cm^{-1} is affiliated with -CH stretching vibrations of the aliphatic group [286]. The sharp peak at 1640 cm^{-1} is the clear indicator of the presence of Schiff Base reaction in the grafting process and the formation of C=N bonds, furthermore, this peak also represents the stretching vibration carbonyl groups (C=O) present in esters, carboxylic acids, etc. [287]. The peak observed at 1414 cm^{-1} can be attributed to the stretching vibrations of sulphate (S=O) groups of Ma [288], while the peak observed at 1270 cm^{-1} can be ascribed to the C-N

stretching vibrations of amide II [289]. The asymmetric stretching vibrations of the C-O-C bridge are the attributing factor for the peak appearing at 1152 cm^{-1}, whereas the peak observed at 896 cm^{-1} is attributed to C-H bending [287]. The characteristic peaks of TiO_2 can be observed in the 800-400 cm^{-1} region. The peak observed at 792 cm^{-1} can be associated with the vibration of the Ti-O mode while the peaks at 768 cm^{-1} and 525 cm^{-1} can be ascribed to Ti-O-Ti vibrations [289], [290]. All major peaks in Cs/SD-Ma-Tk before and after the adsorption of BG appear to be similar, though the intensity of many peaks relating to surface functional groups show a decrease as can be observed in the highlighted areas in Figure 4.3. Therefore, it can be derived that the abundant functional groups of Cs/SD-Ma-Tk effectively contributed to the removal of BG from the dye solution.

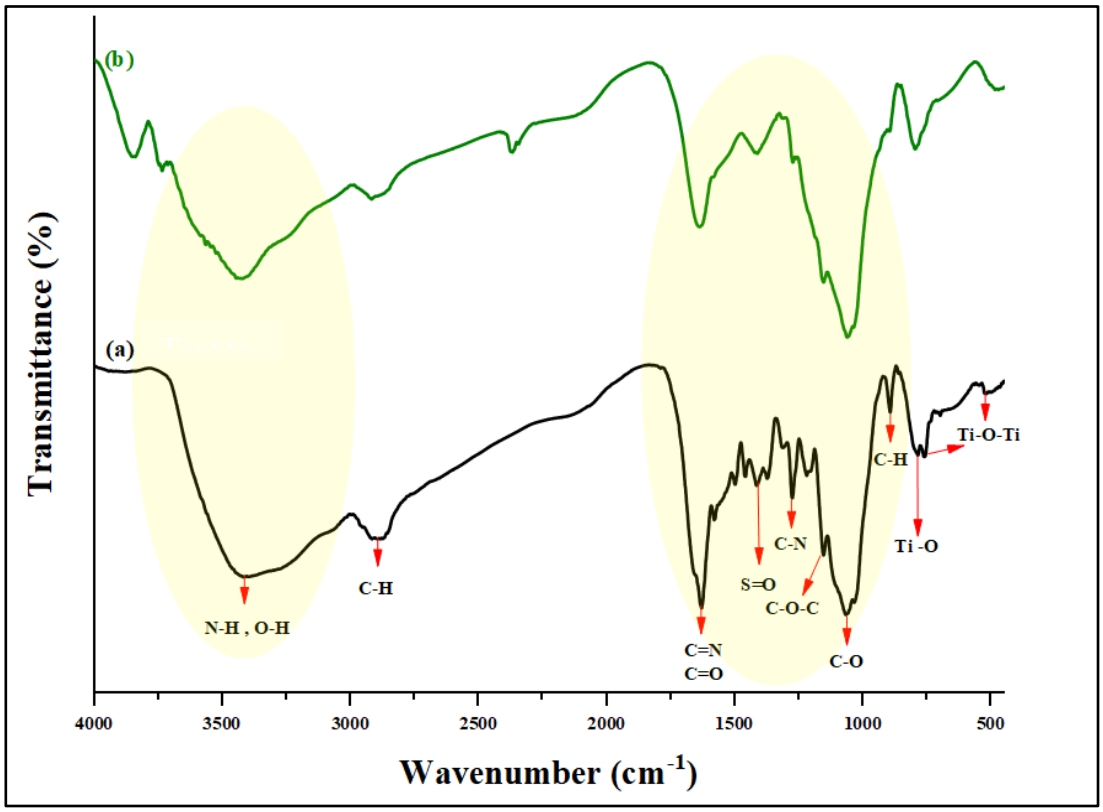
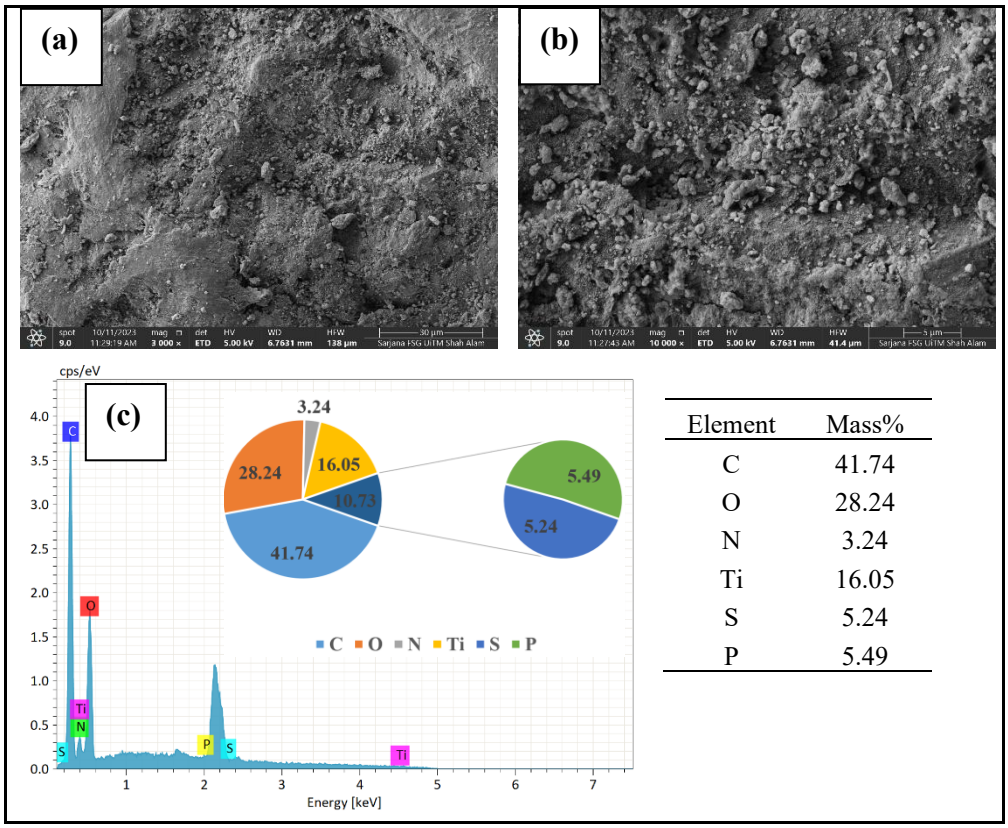


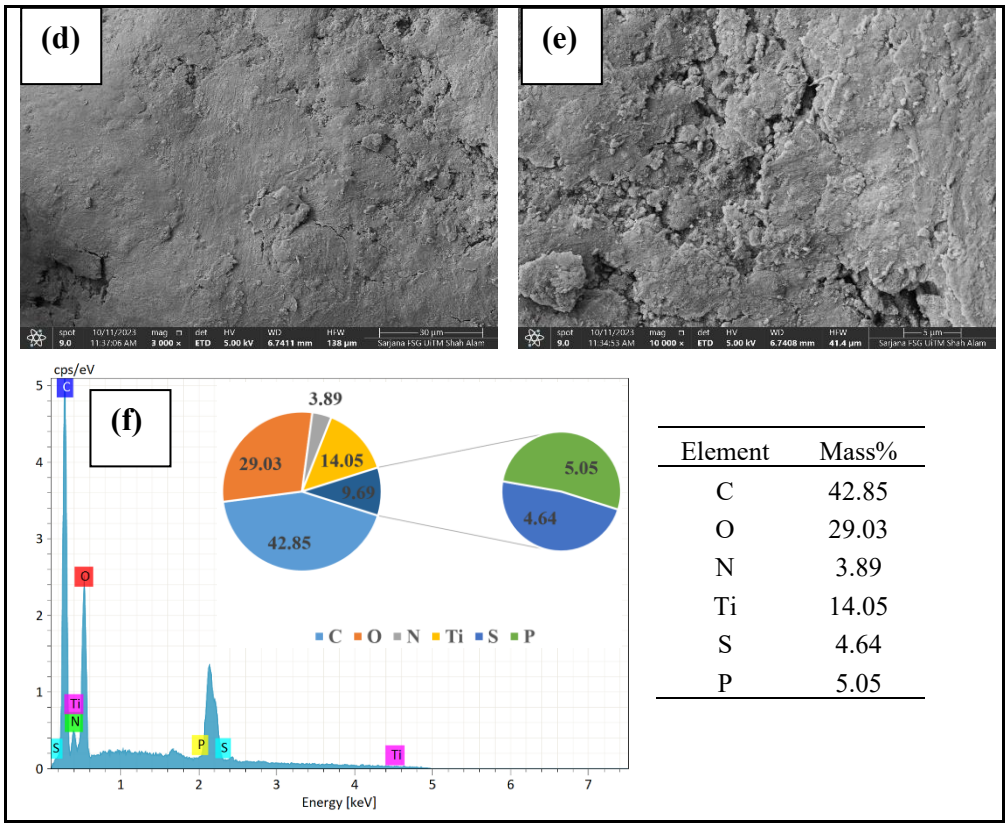
Figure 4.3 FT-IR Spectra of Cs/SD-Ma-Tk (a) Before and (b) After the Adsorption of BG Dye

4.1.4 Surface Morphology of Cs/SD-Ma-Tk

To identify the morphological changes to the surface of Cs/SD-Ma-Tk after the adsorption of BG, FE-SEM images (at two magnification powers of 3000x and 10000x) of Cs/SD-Ma-Tk before and after the adsorption process were obtained and provided in Figure 4.4. As can be observed in Figure 4.4a and b, the surface of Cs/SD-Ma-Tk before adsorption is rough and uneven in the presence of evenly distributed TiO_2 particles. It can be surmised from the surface morphology that the uneven surface can increase the contact area with the BG dye molecules and subsequently result to a higher capture rate by Cs/SD-Ma-Tk surface functional groups. Evidently, in Figure 4.4d and e, it is observed that after the adsorption process the surface of Cs/SD-Ma-Tk becomes smooth with minimal roughness and visible particles. This observation can be attributed to the dye molecules being trapped by the surface functional groups of Cs/SD-Ma-Tk and filling the uneven surface areas, resulting into a smooth surface. Furthermore, the EDX data of Cs/SD-Ma-Tk after the adsorption of BG dye molecules (Figure 4.4f) displays a noticeable increase in the C, O and N contents compared to the EDX data of Cs/SD-Ma-Tk (Figure 4.4c) which is in line with the chemical structure of BG dye molecules and further affirms the presence of BG dye molecules on the surface of Cs/SD-Ma-Tk.



Element	Mass%
C	41.74
O	28.24
N	3.24
Ti	16.05
S	5.24
P	5.49



Element	Mass%
C	42.85
O	29.03
N	3.89
Ti	14.05
S	4.64
P	5.05

Figure 4.4 FE-SEM Images at Two Magnification Powers of 3kx (a and d) and 10kx (b and e) of (a-b) Cs/SD-Ma-Tk, (d-e) Cs/SD-Ma-Tk+BG and EDX Profiles of (c) Cs/SD-Ma-Tk and (f) Cs/SD-Ma-Tk+BG

4.1.5 Statistical Optimisation and Analysis

4.1.5.1 Experimental Design and Process Optimisation for BG dye Removal by Cs/SD-Ma-Tk

Box Behnken Design (BBD) from Response Surface Methodology (RSM) was utilised for statistical analysis and optimisation of three input factor (A: Cs/SD-Ma-Tk dose, B: pH, and C: contact time) to maximise the output (dye removal%). The experimental design was developed using the computer software Design Expert (ver. 13.0, Stat-Ease, USA) which generated 17 experiments for three levels of the three input factors. The range of the input variables were initially determined by performing premonitory experiments prior to the experimental design. The values of the three levels of the input variables (-1, 0 and 1) are illustrated in Table 4.2.

Table 4.2
Factor Levels of the BBD Design for BG Removal by Cs/SD-Ma-Tk

Factor name	Factor code	Level of factor		
		-1	0	1
Cs/SD-Ma-Tk Dose (g/100mL)	A	0.02	0.06	0.1
pH	B	4	6.5	9
Time (min)	C	10	35	60

Furthermore, Table 4.3 provides the generated experimental design including the coded and actual values of the three variables as well as the experimental and predicted values for the response. The optimal parameter values were determined after performing desirability test on the results of the experimental design. Figure 4.5 and the last row of Table 4.3 exhibit the results of the desirability test. Figure 4.5 illustrates the suggested experimental conditions within the range of the three parameters to maximise the response (BG removal). The suggested conditions (Cs/SD-Ma-Tk dose=0.066 g/100mL; pH=8.6; time=58min) were then tested three times to confirm the reliability and repeatability of the obtained dye removal values. Table 4.3 (last row) exhibits the results of the desirability test with the comparison of the expected and obtained results. The values obtained for dye removal are closely related to the expected results and hence these parameters (Cs/SD-Ma-Tk dose=0.066 g/100mL; pH=8.6) will be employed for the adsorption studies.

Table 4.3
BBD Design Coded and Actual Values Alongside Predicted and Experimental Response for BG Removal by Cs/SD-Ma-Tk

Run	Coded Values			Actual values			Removal of BG (%)	
	A	B	C	A	B	C	Observed	Predicted
1	-1	-1	0	0.02	4	35	10.8	12.5
2	+1	-1	0	0.1	4	35	16.7	15.5
3	-1	+1	0	0.02	9	35	46.3	47.5
4	+1	+1	0	0.1	9	35	74.1	72.4
5	-1	0	-1	0.02	6.5	10	50.5	48.7
6	+1	0	-1	0.1	6.5	10	53.5	54.6
7	-1	0	+1	0.02	6.5	60	52.1	51.0
8	+1	0	+1	0.1	6.5	60	70.9	72.7
9	0	-1	-1	0.06	4	10	16.4	16.5
10	0	+1	-1	0.06	9	10	55.2	55.8
11	0	-1	+1	0.06	4	60	20.6	20.0

Run	Coded Values			Actual values			Removal of BG (%)	
	A	B	C	A	B	C	Observed	Predicted
12	0	+1	+1	0.06	9	60	72.8	72.7
13	0	0	0	0.06	6.5	35	55.1	54.6
14	0	0	0	0.06	6.5	35	57.2	54.6
15	0	0	0	0.06	6.5	35	54.5	54.6
16	0	0	0	0.06	6.5	35	53.4	54.6
17	0	0	0	0.06	6.5	35	52.7	54.6
Desirability test run				0.066	8.6	58	72.4±1.9	74.7

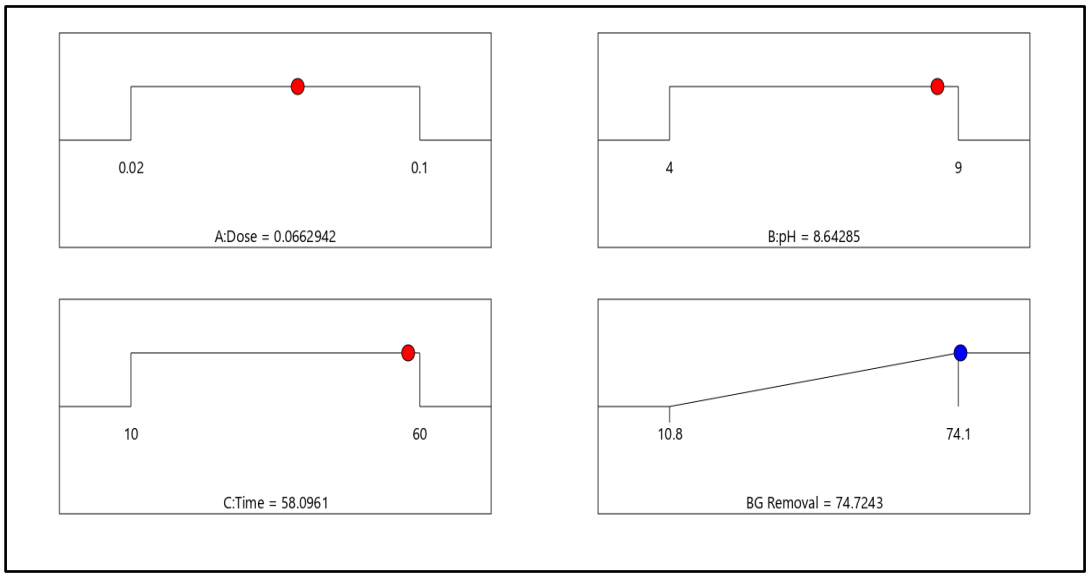


Figure 4.5 Desirability Ramps of BG Removal by Cs/SD-Ma-Tk

4.1.5.2 Statistical Analysis of BG Removal by Cs/SD-Ma-Tk

The validity of the model to be applied for the experimental data as well of the individual and interactive impact of the input model variables and their statistical significance were investigated. ANOVA test was performed on the generated quadratic model to affirm the adequacy of the model as well as determine the statistical significance of various model parameters and the results are reported in Table 4.4. The statistical evaluation of the model displayed a high f-value and a low p-value (155.51 and <0.0001) which can be interpreted as the model being adequate to explain the experimental data [291]. Furthermore, the reported coefficient of correlation (R^2) for the model is 0.9950 which further affirms the ability of the employed quadratic model to explain the experimental data. Additionally, the high p-value of Lack-of-Fit (LoF)

renders it statistically insignificance which further validates the reliability of the proposed model. Typically, all model parameters with p-values lower than 0.05 are statistically significant and capable of affecting the response value [292].

Table 4.4
ANOVA Test Results for BG Removal by Cs/SD-Ma-Tk

Source	Sum of Squares	df	Mean Square	F-value	p-value	Significance
Model	6238.3	9	693.1	155.5	< 0.0001	*
A-Dose	385.0	1	385.0	86.4	< 0.0001	*
B-pH	4227.4	1	4227.4	948.4	< 0.0001	*
C-Time	208.1	1	208.1	46.7	0.0002	*
AB	119.9	1	119.9	26.9	0.0013	*
AC	62.4	1	62.4	14.0	0.0072	*
BC	44.9	1	44.9	10.1	0.0156	*
A^2	4.7	1	4.7	1.1	0.3404	#
B^2	1153.6	1	1153.6	258.8	< 0.0001	*
C^2	43.7	1	43.7	9.8	0.0166	*
Residual	31.2	7	4.5			
Lack of Fit	19.1	3	6.4	2.11	0.2412	#
Pure Error	12.1	4	3.0			
Cor total	6269.5	16				
R^2	0.9950					
Adjusted R^2	0.9886					

* significant; # not significant.

As observed from Table 4.4, all model terms save for A^2 are statistically significant model terms. In other words, the individual variables dose (A), pH (B) and time (C), the interactive effect of pairs of variables dose*pH (AB), dose*time (AC) and pH*time (BC) and the squared effect of pH (B2) and time (C2) are all statistically significant model terms. The generated 2nd order polynomial expression for predicting the response by BBD is exhibited in equation (4.1).

$$\text{BG Removal (\%)} = + 54.58 + 6.94A + 22.99B + 5.10C + 5.47AB + 3.95AC + 3.35BC - 16.55B2 + 3.22C2 \quad (4.1)$$

Additionally, various analytical graphs were utilised to further affirm the suitability of the employed model to explain the data. The correlation between the model predicted and experimental response values is depicted in Figure 4.6a and the close fit of all data points to the regression line proves that the suggested quadratic model is capable of consistently predicting the response value [293]. The plot of normal probability of residuals displayed in Figure 4.6b further affirms the suitability of the model as the regular and precise distribution of data points demonstrates that errors are normally distributed, and the residuals are independent [294]. Additionally, Cook's distance plot (Figure 4.6c) was used for validation of the model. Generally, in Cook's distance plots, if the model can accurately explain the data, then all points would have values lower than unity, whereas the existence of points with values greater than unity questions the reliability of the proposed model [295]. The observed results of Figure 4.6c further validate the suitability of the model to explain the experimental results.

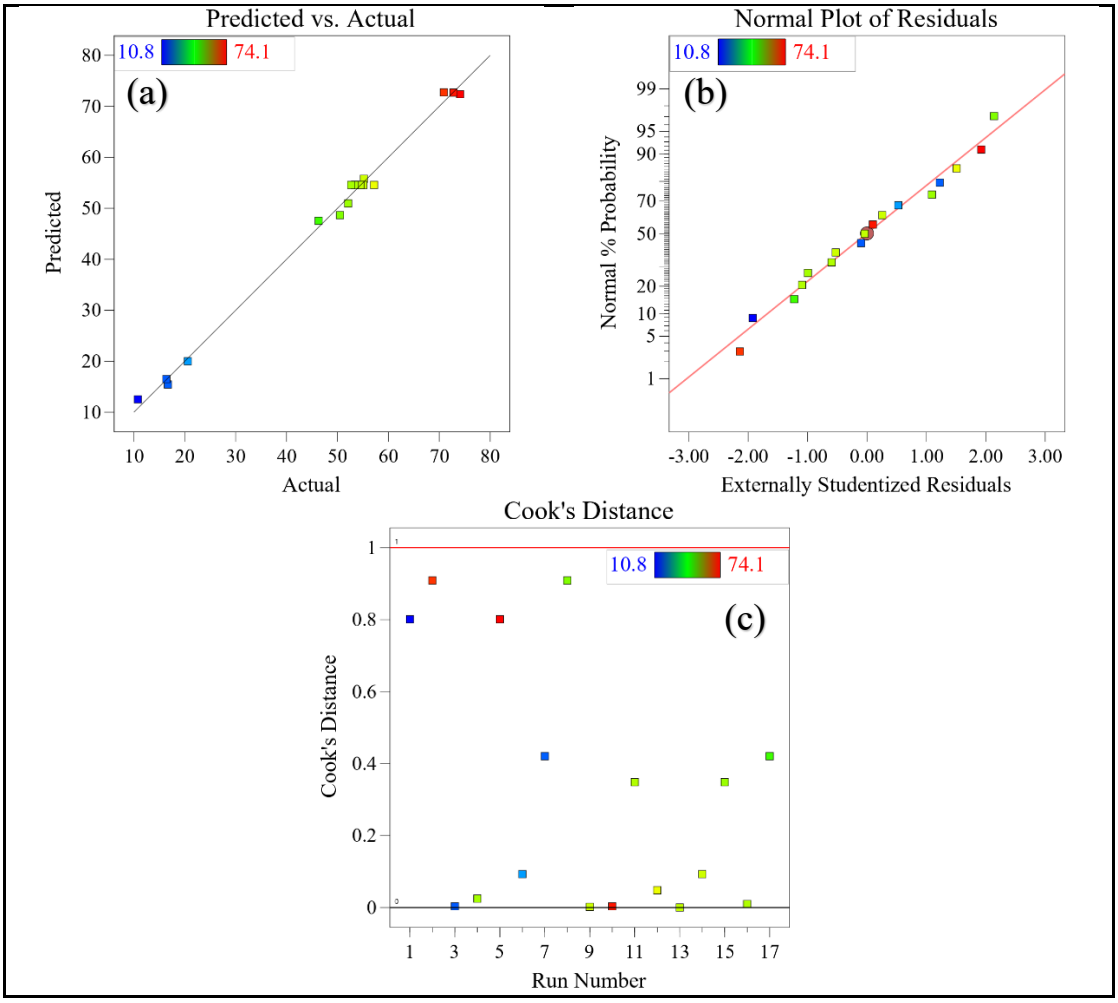


Figure 4.6 BBD Plots of (a) Predicted vs. Actual, (b) Normal Plot of Residuals, and (c) Cook's Distance; for BG Removal by Cs/SD-Ma-Tk

4.1.5.3 Individual Impact of Variables

The impact of the three individual model terms, namely Cs/SD-Ma-Tk dose, pH, and contact time were investigated, and the results are reported in Figure 4.7. It can be observed from Figure 4.7a that the increase of Cs/SD-Ma-Tk dose causes a consistent increment in BG removal throughout all dose values. Whereas the increase of pH (Figure 4.7b) from 4 to 6.5 triggered a sharp increase in BG removal which decelerated after the middle point. The plots reveal that pH has the highest impact on BG removal values which can be explained by the surface charges changing in pH values higher/lower than pH of point of zero charge (pHpzc=6.9). The influence of time on BG removal can be seen in Figure 4.7c which displays a consistent increase before the mid-point which accelerated afterwards. It can be concluded that the removal of BG by Cs/SD-Ma-Tk is not a quick process and requires adequate time to achieve its potential.

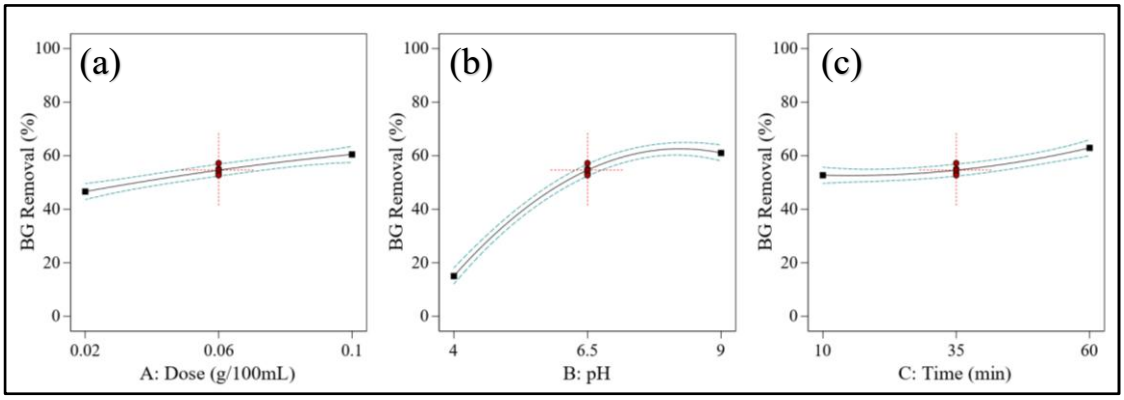
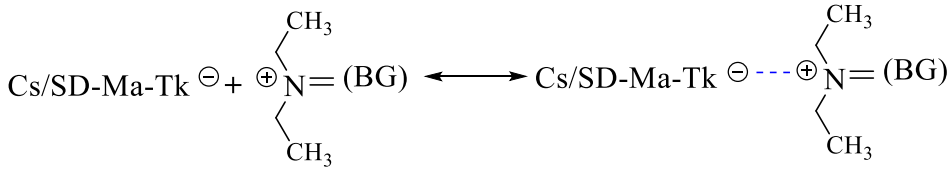


Figure 4.7 Impact of Independent Variables (a) Cs/SD-Ma-Tk Dose, (b) pH, and (c) Time on BG Removal Response

4.1.5.4 Interactive Impact of Variables

The interactive impact of each pair of variables on BG dye removal was investigated through 3D surface plots and 2D contour curves and displayed in Figure 4.8. The 3D surface plot and 2D contour curve of the interactive effect of dose and pH (AC) while keeping time constant at 35 min (Figure 4.8a and b) display that the increase of pH from 4 to 9 at the minimum dose value resulted into a sharp increase in BG removal from 10.8% to 46.3%. Moreover, the increase of Cs/SD-Ma-Tk dose from 0.02 to 0.1(g/100 mL) at minimum pH value caused a mild increment from 10.8% to 16.7%

to BG dye removal. However, the simultaneous rise of the two variables of pH and dose triggered a sharp increase of BG removal from 10.8% to 74.1%. The strong effect of pH on BG removal can be attributed to the changes in surface charge of Cs/SD-Ma-Tk in different pH values. As displayed in Figure 4.8c the point of zero charge for Cs/SD-Ma-Tk was observed at pH value of 6.9, meaning that at this pH the surface of Cs/SD-Ma-Tk is devoid of any charges and at pH values higher and lower than this value the surface would gain negative and positive charges, respectively. Consequently, the presence of positive charges in acidic environments would create a repulsive effect with the positively charged BG dye molecules, limiting the adsorptive efficacy of Cs/SD-Ma-Tk. Meanwhile, in alkaline environments the limitations imposed by the electrostatic repulsion would be non-existent hence allowing better adaptive behaviour to be displayed by the adsorbent while additionally the negative surface charges of Cs/SD-Ma-Tk and the positively charged BG dye molecules would have electrostatic attraction to further improve the dye removal. The electrostatic attraction between Cs/SD-Ma-Tk and BG dye molecules is simply illustrated below (4.2).

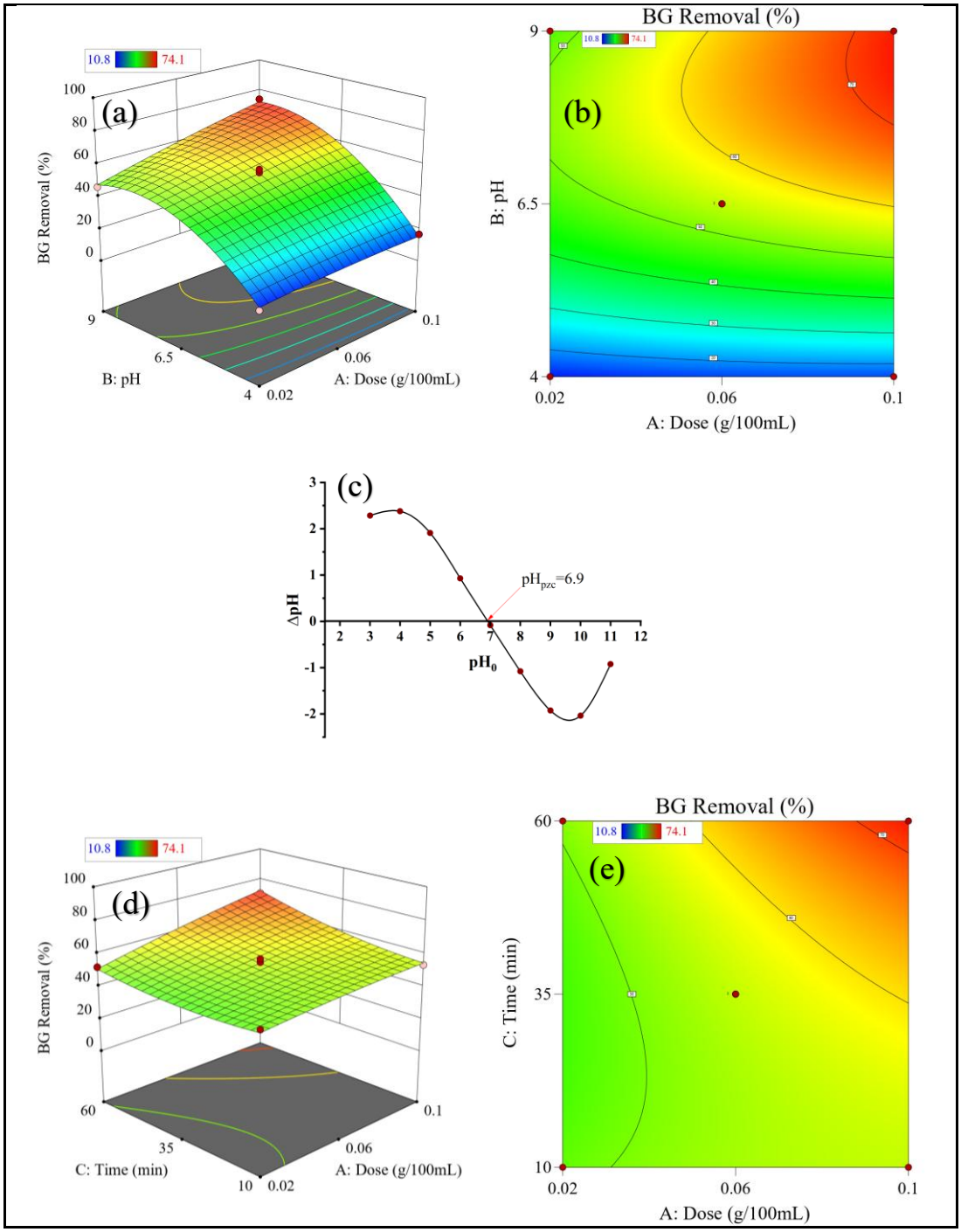


(4.2)

Figure 4.8d and e exhibit the 3D surface plot and 2D contour curve of the interactive impact of time and dosage (AC) while pH is kept constant at 6.5. It can be seen from the figures that the increase in Cs/SD-Ma-Tk dose from 0.02 to 0.1(g/100 mL) at minimum time duration caused a mild increase from 50.5% to 53.5% in BG removal. Similarly, the increase of time from 10 to 60 min while using minimum adsorbent dose only caused a mild increase in BG removal from 50.5% to 52.1%. However, the simultaneous increase of these two variables prompted a sharper increase in BG removal from 50.5% to 70.9%.

The interactive impact of time and pH (BC) while Cs/SD-Ma-Tk dosage is kept constant at 0.06 (g/100 mL) is presented in the 3D surface plot and 2D contour curve displayed in Figure 4.8f and g. The increase of pH from 4 to 9 while keeping time at its minimum value had a strong impact on BG removal, increasing it from 16.4% to 55.2% which can be attributed to the electrostatic attractions as discussed above. Whereas the

increase of time from 10 to 60 minutes caused a mild increase in BG removal from 16.4% to 20.6%. Nevertheless, the simultaneous increase of both time and pH variables resulted into a very sharp increase in BG removal from 16.4% to 72.8%.



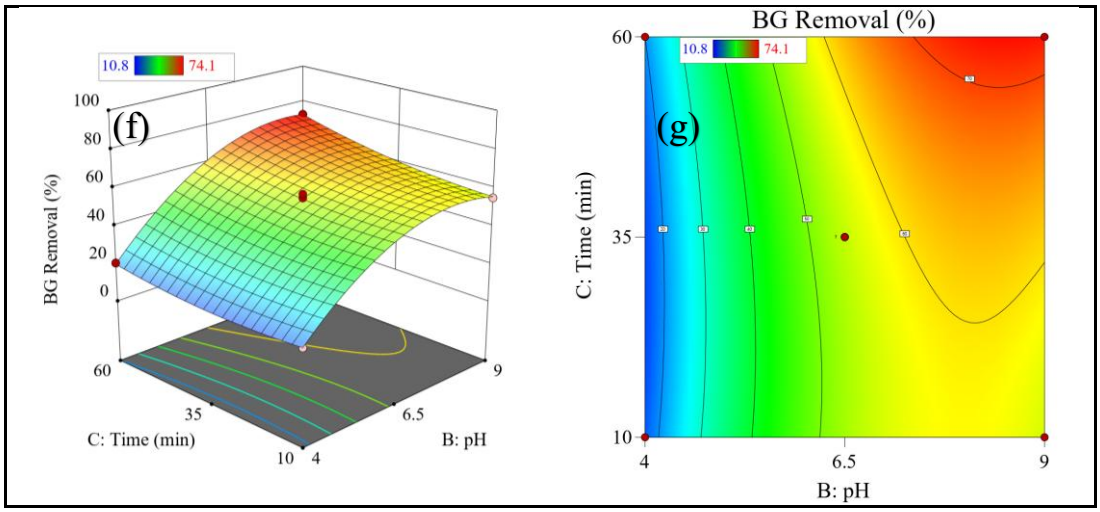


Figure 4.8 3D Surface Plots and 2D Contour Curves of the Interactive Impact of Variable Pairs with Significant Impact on BG Removal Response by Cs/SD-Ma-Tk (Plus pHpzc Plot of Cs/SD-Ma-Tk)

4.1.6 Adsorption Equilibrium Studies of BG Removal by Cs/SD-Ma-Tk

4.1.6.1 Initial BG Concentration and Kinetic Study of BG Removal by Cs/SD-Ma-Tk

The adsorption capacity of Cs/SD-Ma-Tk towards BG dye at different initial dye concentrations (20, 50, 80, 120, 150, 200 and 250 mg/L) using the optimum variable conditions obtained from the desirability test is displayed in Figure 4.9. The distribution of the plot points representing the experimental data for each concentration at different time points always reveals that the adsorptive capabilities of Cs/SD-Ma-Tk improve with the increase in the initial dye concentration; from 33.5 to 386.1 mg/g with the increase of initial dye concentration from 20 to 250 mg/L. Thus, it can be concluded that the increase in the concentration gradient creates a driving force to better diffuse the dye molecules into the inner pores and active adsorption sites of Cs/SD-Ma-Tk [296].

The non-linear regressions of PFO and PSO kinetic models are illustrated in Figure 4.9 alongside the experimental data points. The computed model parameters for PFO and PSO models (displayed in Table 4.5) show that the experimental values for equilibrium adsorption capacity for all initial dye concentrations are closer to the calculated values of adsorption capacity obtained through PSO kinetic model. Likewise, the coefficients of determination for all initial BG concentrations achieved a higher

value in PSO model. Thus, it can be derived that the PSO kinetic model can better fit the obtained results for BG removal by Cs/SD-Ma-Tk and hence it can be derived that the adsorption process of BG dye by Cs/SD-Ma-Tk is through chemisorption and the sharing of electrons of the active functional groups on the surface of Cs/SD-Ma-Tk with the cationic dye molecules [297].

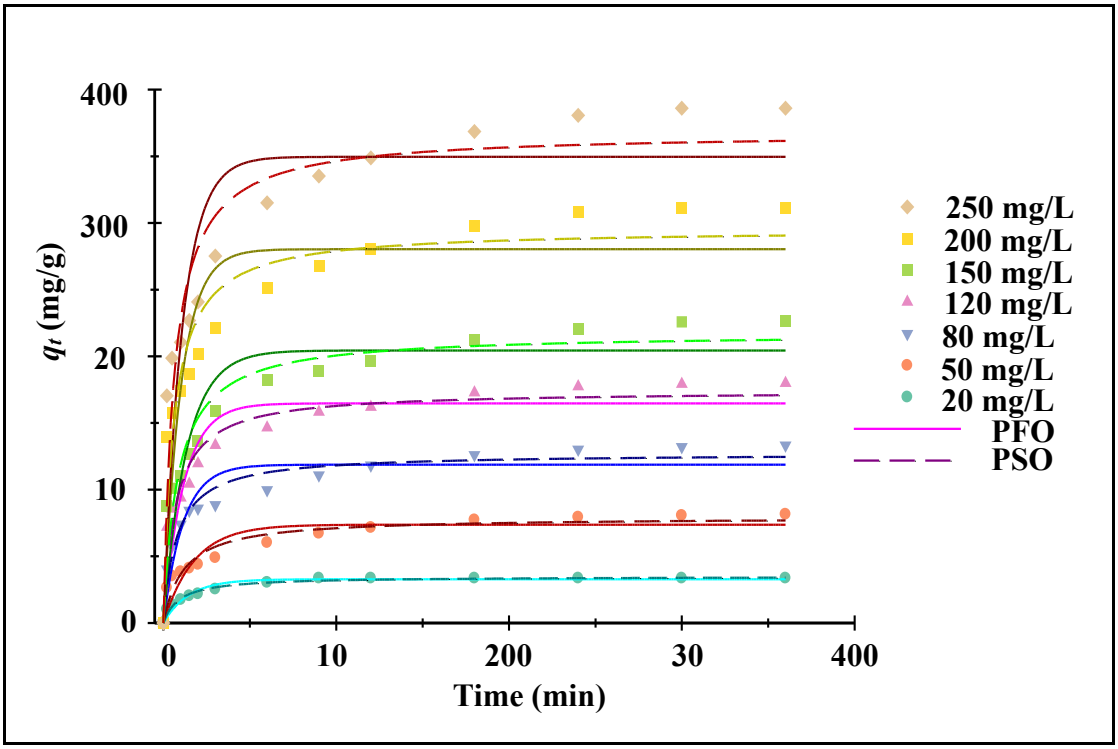


Figure 4.9 Impact of Initial Concentration and Kinetic Model Regressions of BG Removal by Cs/SD-Ma-Tk

Table 4.5
Kinetic Model Data for BG Adsorption by Cs/SD-Ma-Tk

Concentration (mg/L)	$q_{e.exp}$ (mg/g)	PFO			PSO		
		$q_{e.cal}$ (mg/g)	k_1 (1/min)	R^2	$q_{e.cal}$ (mg/g)	k_2 x 10^{-2} (g/mg.min)	R^2
20	33.5	32.8	0.068	0.95	34.9	0.311	0.98
50	81.4	73.7	0.056	0.85	79.4	0.108	0.93
80	133.2	118.7	0.087	0.88	127.2	0.103	0.96
120	179.9	164.7	0.085	0.87	174.2	0.082	0.94
150	226.3	204.4	0.075	0.86	217.4	0.055	0.93
200	311.0	280.4	0.098	0.81	295.3	0.058	0.91
250	386.1	349.7	0.092	0.81	367.9	0.044	0.91

4.1.6.2 Isotherm Study of BG Removal by Cs/SD-Ma-Tk

The compatibility of the acquired equilibrium data with the three most widely applied Langmuir, Freundlich, and Temkin isotherm models is reported in Fig. 10 and the calculated model parameters are tabulated in Table 4.6. Figure 4.10 visibly illustrates that the two Langmuir and Freundlich isotherm models can better fit the experimental data, which can be proven by the coefficients of determination of 0.98 and 0.99, respectively as stated in Table 4.6. The high coefficients of determination for both Langmuir and Freundlich isotherm models reveal that the adsorption process would firstly occur on the surface of the adsorbent as a monolayer process and after the occupation of the active adsorption sites on the surface layer the adsorption continues in a multi-layered fashion till equilibrium [298]. Furthermore, the value of *n* being greater than unity signifies the favourability of the adsorption process. The Langmuir maximum adsorption capacity obtained for BG removal by Cs/SD-Ma-Tk is 957.0 mg/g which proves the high efficiency and great potential of this adsorbent to be employed for the removal of BG dye from effluents.

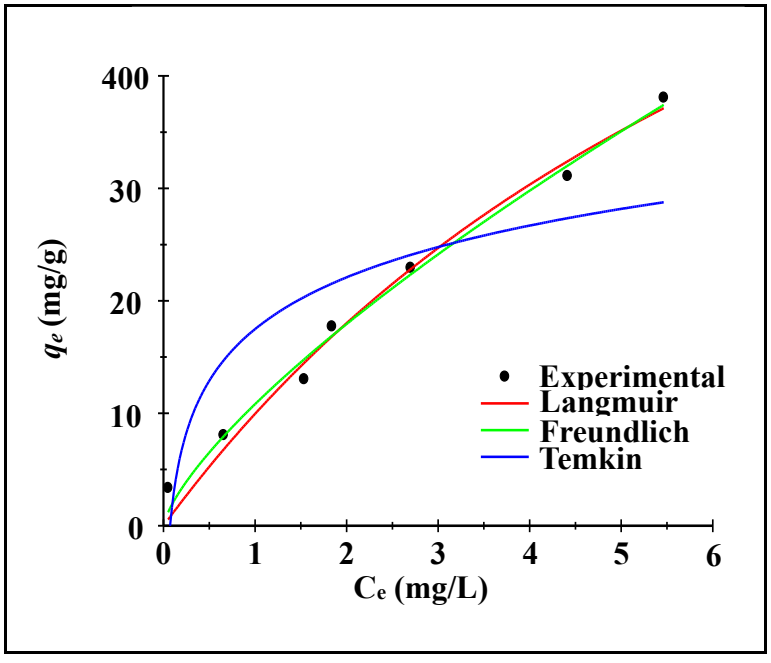


Figure 4.10 Langmuir, Freundlich and Temkin Isotherm Regressions for BG Removal by Cs/SD-Ma-Tk

Table 4.6
Isotherm Model Parameters for BG Removal by Cs/SD-Ma-Tk

Adsorption isotherm	Parameter	Value
Langmuir	q_{max} (mg/g)	957.0
	K_a (L/mg)	0.12
	R^2	0.98
Freundlich	K_f (mg/g) (L/mg)$^{1/n}$	108.1
	n	1.4
	R^2	0.99
Temkin	K_T (L/mg)	13.9
	b_T (J/mol)	37.6
	R^2	0.73

4.1.6.3 Thermodynamic Study of BG Removal by Cs/SD-Ma-Tk

The thermodynamic parameters Gibbs free energy change (ΔG°), entropy change (ΔS°), and enthalpy change (ΔH°) were calculated utilising the slope and intercept of the Van't Hoff plot (Figure 4.11) and tabulated in Table 4.7. The increase in the negativity of ΔG° values with the increase in temperature proves the spontaneity and feasibility of the adsorption process [299]. Moreover, the positive $\Delta H°$ value represents the endothermic nature of the adsorption process, which increases the adsorption rate and capacity of Cs/SD-Ma-Tk with the increase of temperature, occurring due the heat transfer to the system [300]. Furthermore, the positive value of ΔS° signifies that the increase in the temperature of the environment results into an increased randomness in the adsorbent/adsorbate interface [301].

Table 4.7
Thermodynamic Parameters of BG Removal by Cs/SD-Ma-Tk

Temperature (K)	k_d	ΔG (kJ/mol)	ΔH (kJ/mol)	ΔS (J/mol.K)
298.15	1.90	-1.1	93.9	318.6
308.15	5.15	-4.3		
318.15	9.62	-7.5		
328.15	74.1	-10.7		

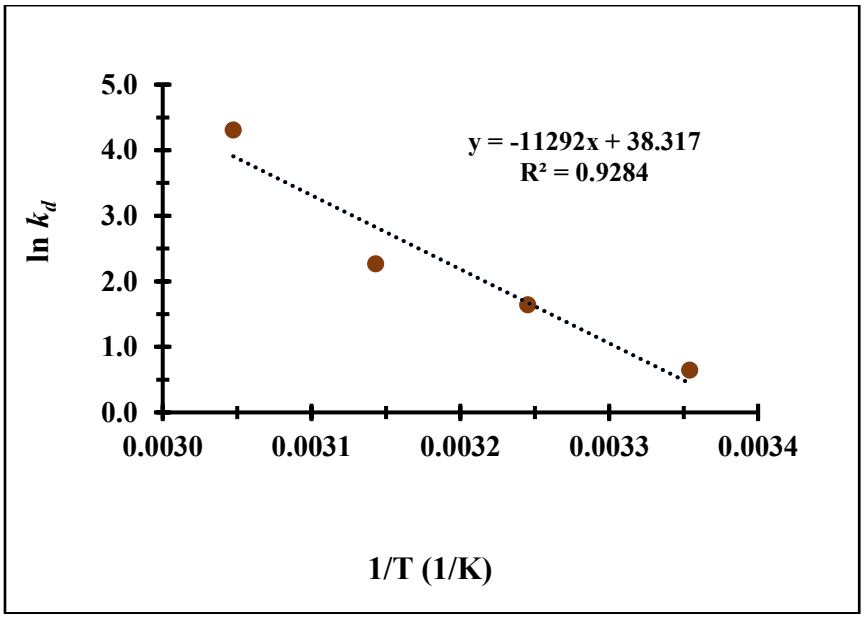


Figure 4.11 Van't Hoff Plot of BG Removal by Cs/SD-Ma-Tk

4.1.7 Proposed Mechanism of BG Removal by Cs/SD-Ma-Tk

The FT-IR spectra of Cs/SD-Ma-Tk revealed an abundance of functional groups that can be negatively charged in environments with pH>pH_{pzc} and form electrostatic bonds with the positively charged BG dye molecules. Based on the investigations throughout this research, it was found that the most impactful variable affecting BG removal by Cs/SD-Ma-Tk is pH, hence it can be derived that the electrostatic attractions play the most significant role in the removal of BG by Cs/SD-Ma-Tk. Furthermore, the abundant presence of amino (NH_2) and hydroxyl (OH) groups on the polymeric chain of Cs/SD-Ma-Tk provides the opportunity for the formation of hydrogen bonds between the hydrogen atoms of these groups and the nitrogen atoms of the BG dye molecules [302]. Similarly, Yoshida-H bonds can be formed between the hydrogen atoms of the hydroxyl groups and the aromatic rings of BG dye molecules [11]. Additionally, n-π and π-π stacking interactions would further improve the adsorptive behaviour of Cs/SD-Ma-Tk toward BG dye molecules. n-π stacking interactions can be occurred between the electron donating nitrogen atoms of Cs/SD-Ma-Tk and the electron accepting aromatic groups of BG dye molecules [288], while π-π stacking interactions occur between the aromatic group of salicylaldehyde grafted onto Cs/SD-Ma-Tk and the aromatic rings of the BG dye molecules [303]. The schematic of the interactions

responsible for the adsorption of BG dye molecules by Cs/SD-Ma-Tk is illustrated in Figure 4.12.

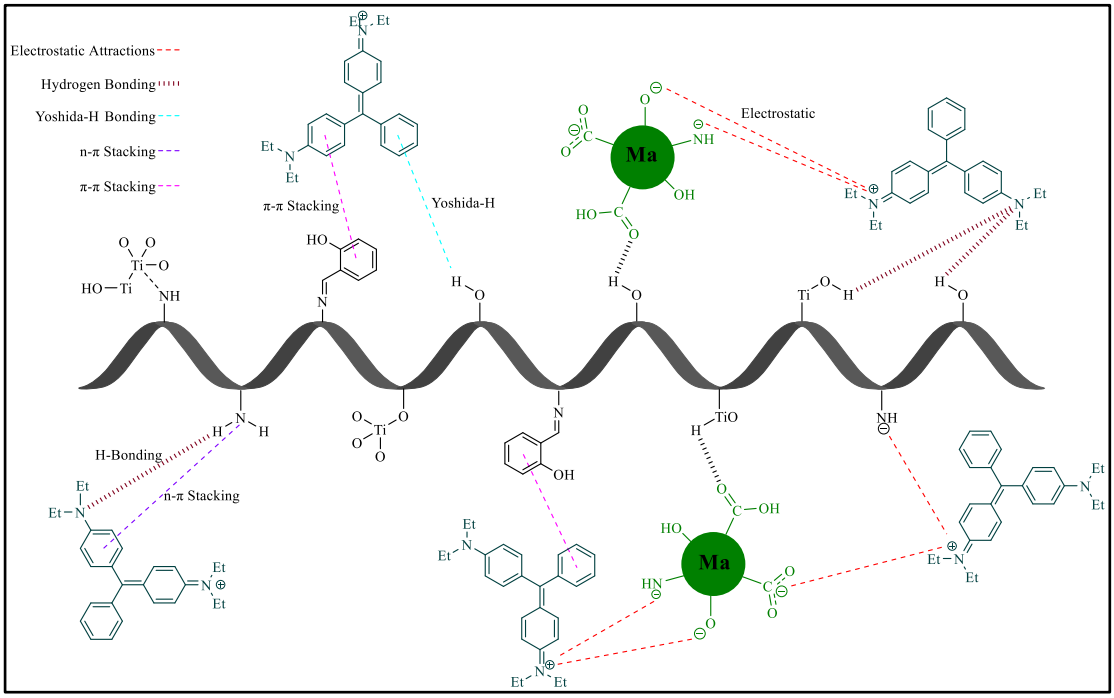


Figure 4.12 Suggested Mechanism of Adsorption for the Removal of BG Dye by Cs/SD-Ma-Tk

4.2 Benzaldehyde grafted Cs-Ma-Tk (Cs/BD-Ma-Tk)

In this section, a new composite material of Chitosan- Microalgae- Kronos TiO_2 was synthesised and put through a hydrothermal grafting process to create salicylaldehyde-grafted Chitosan- Microalgae- Kronos TiO_2 (henceforth referred to as Cs/BD-Ma-Tk) for the adsorption of brilliant green dye. The use of biodegradable and abundantly available resources in this study is an effort to achieve a cost-efficient and biofriendly adsorbent with high efficiency towards the removal of pollutants (specifically BG dye in this study) from effluents. The addition of Tk and Ma would help alleviate chemical instability and low affinity of Cs towards cationic pollutant species, while the Schiffbase reaction occurring during the grafting process would further enhance the structural stability of the resultant composite. The dye removal conditions (adsorbent dosage, pH, contact time) have been optimised using RSM-BBD methodology and the optimal conditions have been applied for kinetic, isotherm, and thermodynamic studies. Based on the findings of the analyses, a plausible adsorption mechanism has been proposed.

4.2.1 Surface Properties of Cs/BD-Ma-Tk

The BET analysis finding is presented in Figure 4.13 and Table 4.8. The N_2 adsorption-desorption curves of Cs/BD-Ma-Tk (shown in Figure 4.13) display compatibility with type IV isotherm and H3 hysteresis loops confirming that Cs/BD-Ma-Tk is a mesoporous material [280], [304]. Moreover, Table 4.8 shows the Cs/BD-Ma-Tk composite's pore size distribution and the BET surface area, which is found to be 6.21 nm and 8.77 m^2/g, respectively. This discovery further substantiates that the Cs/BD-Ma-Tk composite has a mesoporous architecture as confirmed by the International Union of Pure and Applied Chemistry (IUPAC) standard with the pore size in the range 2.0 to 50 nm [280]. The advantageous average pore size of Cs/BD-Ma-Tk facilitates the easy penetration of BG dye molecules into its pores [112] efficiently employed for water pollutant removal. Furthermore, the elemental analysis of Cs/BD-Ma-Tk confirmed the presence of carbon, hydrogen, oxygen, nitrogen, and sulphur, with respective quantities of 38.75%, 5.18%, 50.15%, 5.48%, and 0.08%.

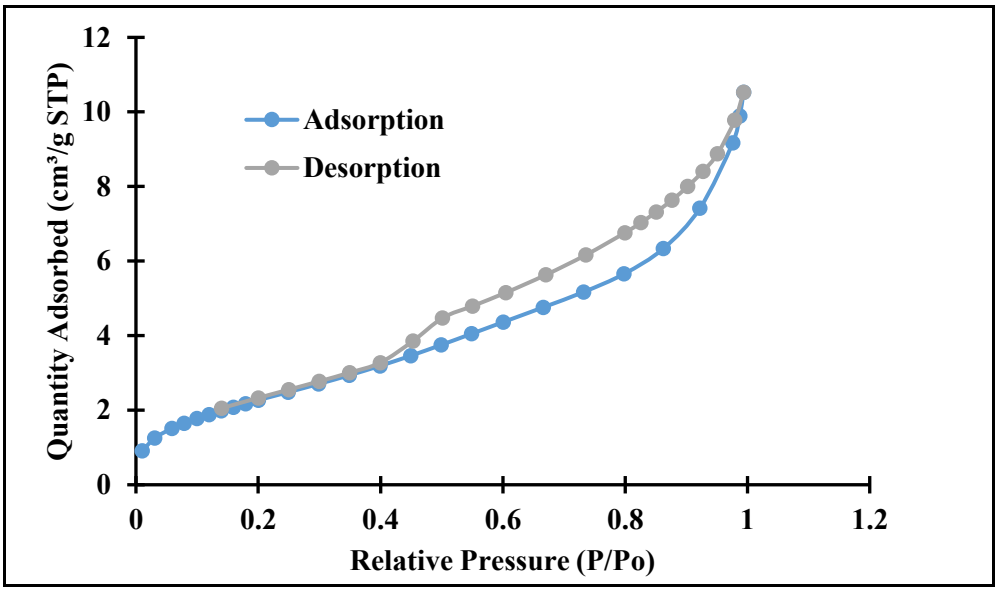


Figure 4.13 N_2 Adsorption/Desorption Profile of Cs/BD-Ma-Tk

Table 4.8
Surface Properties of Cs/BD-Ma-Tk

Parameter(s)	Value
C	38.75%
H	5.18%
N	5.84%
S	0.08%
O (by difference)	50.15%
BET surface area (m^2/g)	8.77
Langmuir surface area (m^2/g)	13.12
Total volume in pores (cm^3/g)	0.016
Mean pore diameter (nm)	6.21

4.2.2 X-Ray Diffraction Analysis of

The crystal phase of Cs/BD-Ma-Tk was analysed by XRD analysis, as depicted in Figure 4.14. The diffraction pattern of Cs/BD-Ma-Tk has a prominent peak at 2θ = 20.3°, indicative of the (110) crystal planes of Cs [305], [306]. The XRD spectrum of Ma has a peak at $2\theta \approx 22°$, signifying the crystalline phase of cellulose, which has been overshadowed by the broad characteristic peak of CT in the XRD spectrum of Cs/BD-Ma-Tk [190]. The crystal planes of TiO_2 are discerned by the peaks observed at 2θ = 25.6° (101), 38.2° (004), 48.3° (209), 54.1° (105), 55° (211), 62° (213), 70.5° (220),

75.3° (215), and 82.9° (224), respectively which are identified on the XRD spectrum of Cs/BD-Ma-Tk [282], [283], [284]. The detection of these characteristic peaks in the XRD pattern of Cs/BD-Ma-Tk signifies the effective incorporation of Tk and Ma into the chitosan matrix.

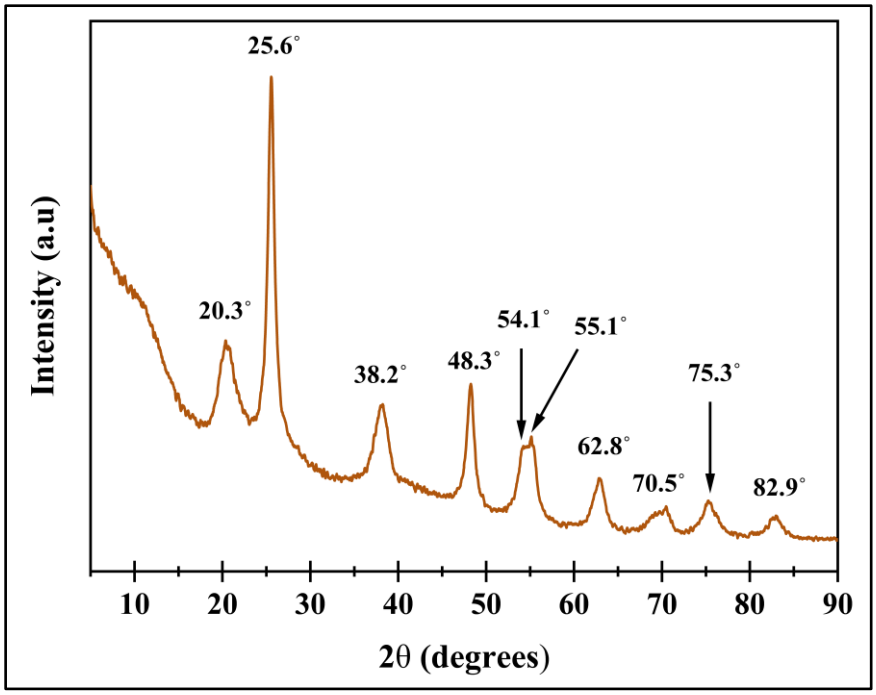


Figure 4.14 XRD Pattern of Cs/BD-Ma-Tk

4.2.3 FT-IR Spectrum Analysis of Cs/BD-Ma-Tk

FT-IR analysis was employed to identify a key property of Cs/BD-Ma-Tk, specifically the nature of the functional groups presents on its surface, thereby assessing the composite's capacity to adsorb cationic contaminants. Figure 4.15 presents the FTIR spectra of Cs/BD-Ma-Tk and Cs/BD-Ma-Tk+BG. The FTIR spectra of the Cs/BD-Ma-Tk composite (Figure 4.15a) exhibits distinctive peaks in the 3261-3724 cm^{-1} region, which are attributed to the vibrations of amino (-NH_2) and hydroxyl (-OH) groups [307], [308]. Moreover, several peaks were identified on the FTIR spectrum of Cs/BD-Ma-Tk, including the peaks at 2919 cm^{-1} and 2872 cm^{-1} (C-H symmetric and asymmetric stretching vibrations, respectively), 1656 cm^{-1} (C=O and C=N due to the Schiff's base reaction), 1543 cm^{-1} (C=C), 1414 cm^{-1} (-O-P due to the presence of Ma), 1160 cm^{-1} (C-O-C bridge), 1054 cm^{-1} (C-O), 766 cm^{-1} (Ti-O), and 652 cm^{-1} (O-P) [132], [133], [144], [307], [308], [309], [310], [311]. Furthermore, the IR spectra of the Cs/BD-Ma-Tk+BG

(Figure 4.15b) exhibits a broadly analogous spectrum to that of the Cs/BD-Ma-Tk composite, with minor shifts in certain bands, particularly -OH and -NH_2, indicating these groups as the principal functional groups of the Cs/BD-Ma-Tk composite which participated in the adsorption of BG dye molecules.

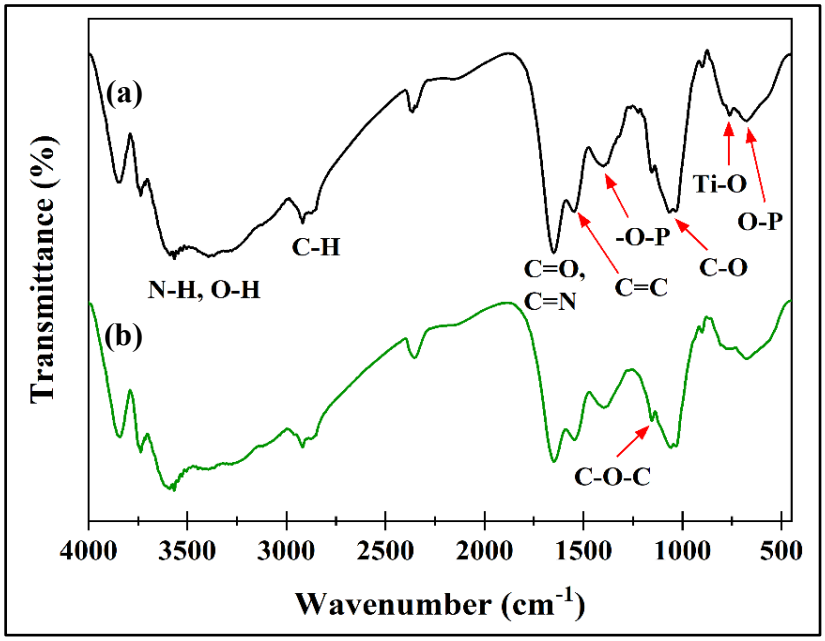
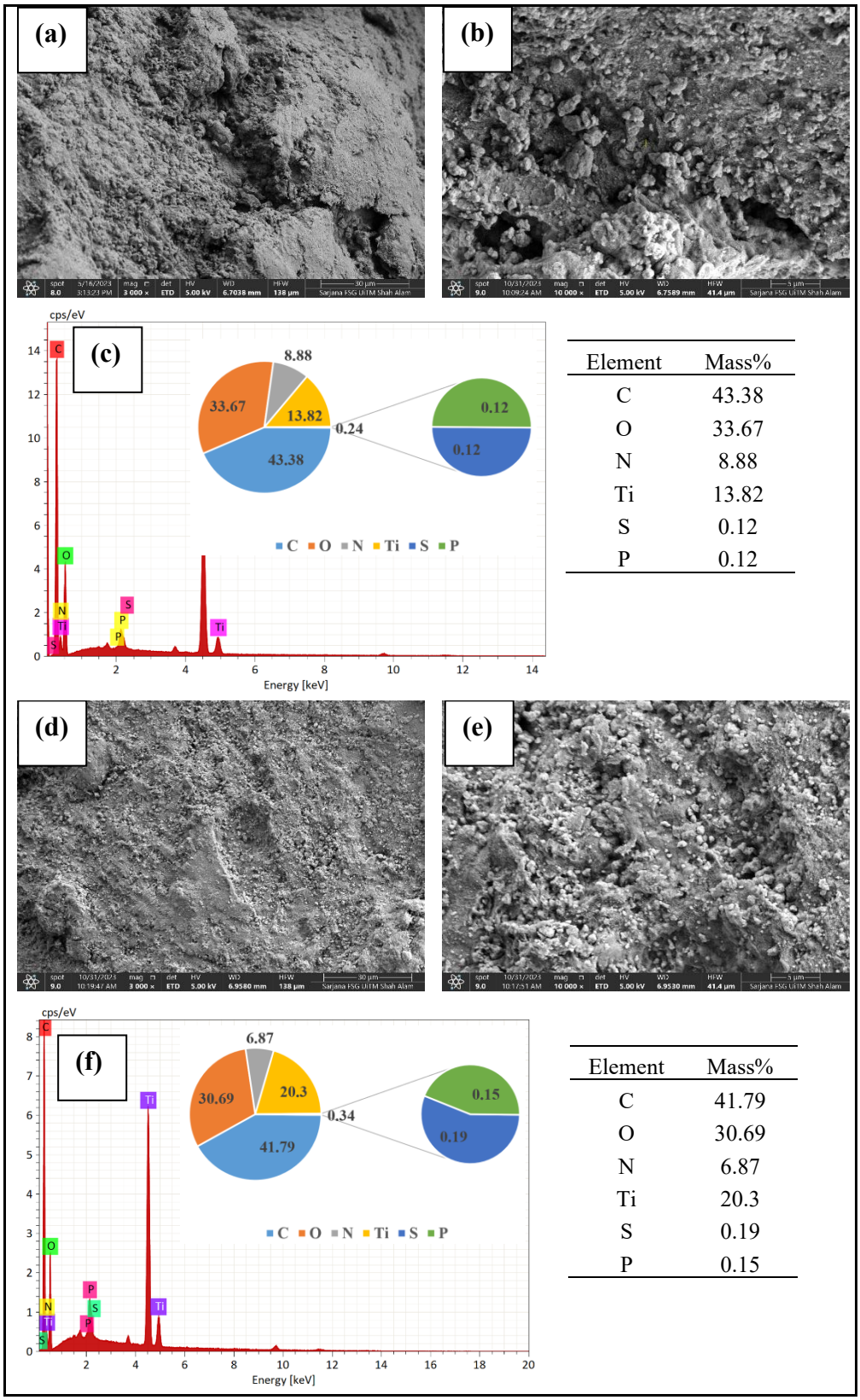


Figure 4.15 FT-IR Analysis of (a) Cs/BD-Ma-Tk, and (b) Cs/BD-Ma-Tk+BG dye

4.2.4 Surface Morphology of Cs/BD-Ma-Tk

FE-SEM/EDX analysis was employed to characterise the morphology and elemental composition on the surfaces of Cs/BD-Ma-Tk and Cs/BD-Ma-Tk+BG as shown in Figure 4.16 at two magnification levels (3kx and 10kx).



Element	Mass%
C	43.38
O	33.67
N	8.88
Ti	13.82
S	0.12
P	0.12

Element	Mass%
C	41.79
O	30.69
N	6.87
Ti	20.3
S	0.19
P	0.15

Figure 4.16 FE-SEM Images at Two Magnification Powers of 3kx (a and d) and 10kx (b and e) of (a-b) Cs/BD-Ma-Tk, (d-e) Cs/BD-Ma-Tk+BG and EDX Profiles of (c) Cs/BD-Ma-Tk and (f) Cs/BD-Ma-Tk+BG

Figure 4.16a and b illustrate that the surface morphology of Cs/BD-Ma-Tk is irregular with several prominent cracks. The EDX analysis (Figure 4.16c) indicates that nitrogen, oxygen, and carbon are the predominant constituents of the Cs/BD-Ma-Tk. The microstructure of Cs/BD-Ma-Tk was significantly altered to exhibit increased compactness following BG absorption (Figure 4.16d and e), accompanied by a notable reduction in fractures, thereby validating the deposition of BG on the surface of Cs/BD-Ma-Tk. The EDX data (Figure 4.16f) displays changes in the elemental contents on the surface of Cs/BD-Ma-Tk and the increase in S content indicates BG adsorption and accumulation of the dye molecules on the surface of Cs/BD-Ma-Tk.

4.2.5 Statistical Optimisation and Analysis

4.2.5.1 Experimental Design and Process Optimisation for BG dye Removal by Cs/BD-Ma-Tk

The optimisation and statistical analysis of three adsorption factors (pH, contact time, and Cs/BD-Ma-Tk dosage) were conducted using Box Behnken Design (BBD) from Response Surface Methodology (RSM) and formulated utilising the Design Expert (ver. 13.0, Stat-Ease, USA) software, resulting in 17 runs of experiments. A preliminary study was conducted to define the key factors with their code and values. The codes and levels of the three input variables are provided in Table 4.9.

Table 4.9
Factor Levels of the BBD Design for BG Removal by Cs/BD-Ma-Tk

Factor name	**Factor code**	**Level of factor**		
		-1	**0**	**1**
Cs/BD-Ma-Tk Dose (g/100mL)	A	0.02	0.06	0.1
pH	B	4	6.5	9
Time (min)	C	10	35	60

Furthermore, Table 4.10 provides the generated experimental design including the coded and actual values of the three variables as well as the experimental and predicted values for the response. A desirability test was conducted to compare trial outcomes with expected results computed from analysing the ideal conditions obtained through Design Expert software and to evaluate the reliability of the employed BBD

model [312]. Figure 4.17 illustrates that the optimal removal of BG necessitates a dosage of 0.06 g/100 mL of Cs/BD-Ma-Tk, a pH of 8.5, and a contact time of 60 min with anticipated result for the removal of BG dye by Cs/BD-Ma-Tk being 88.7%. Consequently, the experiment was conducted with a removal result of 87% obtained which is consistent with the anticipated conclusion based on the proposed model. Thus, the result of this experiment confirms that the proposed model is reliable and precise in predicting the outcome withing the studied range of the parameters. Furthermore, the acquired optimal parameter values (Cs/BD-Ma-Tk dose=0.06 g/100 and pH=8.5) were used for the adsorption experiments.

Table 4.10
Experimental Matrix Based on BBD Approach for Designing Experiments and the Corresponding Response (BG Removal (%) by Cs/BD-Ma-Tk)

Run	A: Dose (g)	B: pH	C: Time (min)	BG removal (%)	
				Predicted	Actual
1	0.02	4	35	5.7	5.4
2	0.1	4	35	27.5	27.1
3	0.02	9	35	70.5	70.9
4	0.1	9	35	81.9	82.2
5	0.02	6.5	10	54.3	53.9
6	0.1	6.5	10	67.6	67.3
7	0.02	6.5	60	66.4	66.7
8	0.1	6.5	60	86.3	86.7
9	0.06	4	10	11.7	12.4
10	0.06	9	10	66.5	66.5
11	0.06	4	60	22.3	22.3
12	0.06	9	60	86.6	85.9
13	0.06	6.5	35	69.9	69.4
14	0.06	6.5	35	69.9	68.2
15	0.06	6.5	35	69.9	70.1
16	0.06	6.5	35	69.9	71.2
17	0.06	6.5	35	69.86	70.4

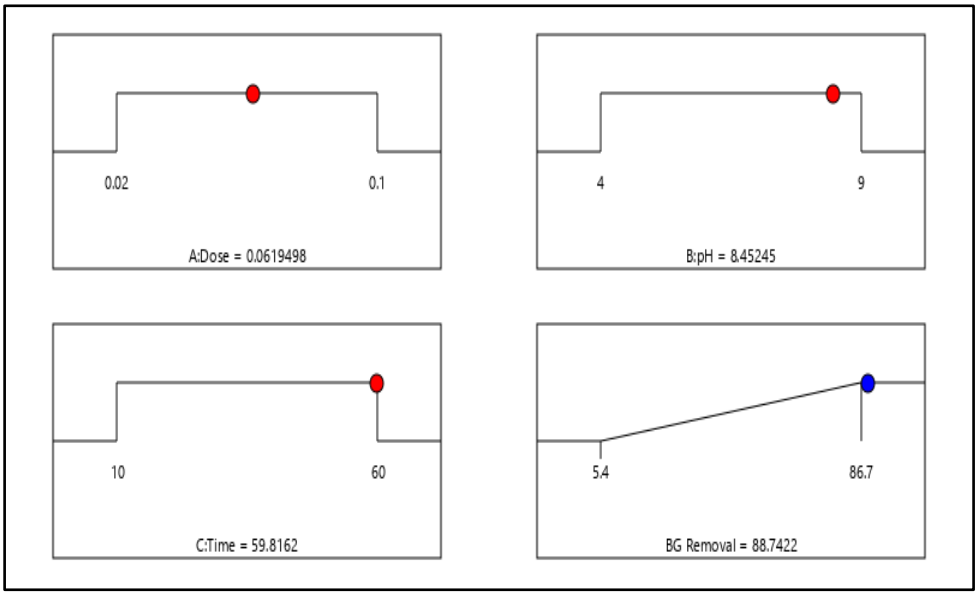


Figure 4.17 Desirability Ramps of BG Removal by Cs/BD-Ma-Tk

4.2.5.2 Statistical Analysis of BG Removal by Cs/BD-Ma-Tk

The ANOVA approach was employed to validate the proposed quadratic model for BG removal and to evaluate the efficacy of the parameters. The findings presented in Table 4.11 indicate the significance of the applied BG removal model, evidenced by an F-value of 1115.45 (p-value < 0.0001). Moreover, an R^2 value of 0.99 was obtained for the developed quadratic model, indicating statistical acceptability and demonstrating a reasonable concordance between the actual and anticipated values of BG removal. In addition, the ANOVA finding demonstrated the Lack of Fit p-value = 0.5536, which is considered non-significant, confirming the appropriateness of the developed model [313]. A p-value exceeding 0.05 for the variables is deemed statistically insignificant towards the response (BG removal), hence the model terms A, B, C, AB, AC, BC, and B^2 were identified as statistically significant for the removal of BG. The model's three factors and outcome (BG removal) yield the final quadratic function (4.3):

$$\text{BG Removal (\%)} = +69.86 + 8.30A + 29.79B + 7.69C - 2.60AB + 1.65AC + 2.37BC - 22.67B^2 \quad (4.3)$$

Table 4.11
Analysis of Variances (ANOVA) for BG Dye Removal by Cs/BD-Ma-Tk

Source	Sum of Squares	df	Mean Square	F-value	p-value	Remark
Model	10375.38	9	1152.82	1115.45	< 0.0001	significant
A-Dose	551.12	1	551.12	533.26	< 0.0001	significant
B-pH	7098.36	1	7098.36	6868.27	< 0.0001	significant
C-Time	472.78	1	472.78	457.46	< 0.0001	significant
AB	27.04	1	27.04	26.16	0.0014	significant
AC	10.89	1	10.89	10.54	0.0141	significant
BC	22.56	1	22.56	21.83	0.0023	significant
A^2	2.64	1	2.64	2.56	0.1537	not significant
B^2	2163.43	1	2163.43	2093.31	< 0.0001	significant
C^2	0.7339	1	0.7339	0.7101	0.4273	not significant
Residual	7.23	7	1.03			
Lack of Fit	2.12	3	0.7075	0.5536	0.6727	not significant
Pure Error	5.11	4	1.28			
Cor Total	10382.61	16				

The graph in Figure 4.18a illustrates the standard probability associated with the BG removal model. The spots (Figure 4.18a) closely align with a single line indicating that the errors are normally distributed, further confirming the suitability of the model [314].

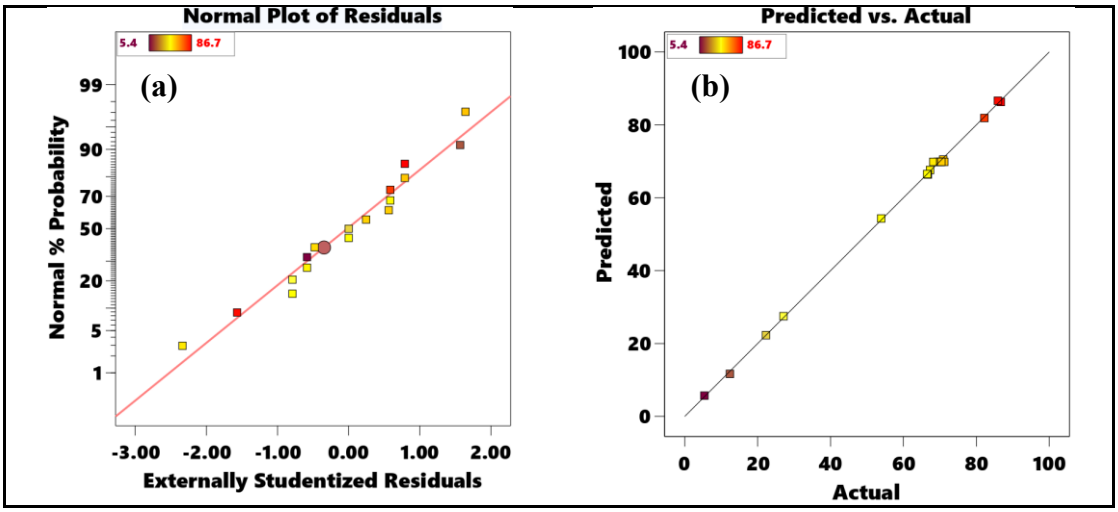
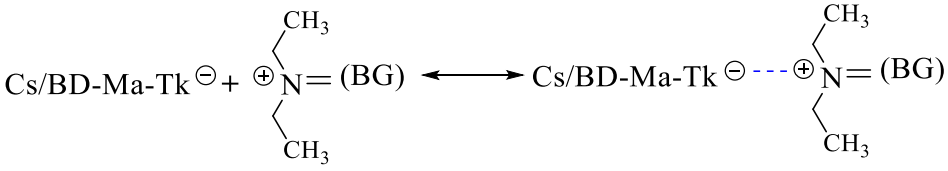


Figure 4.18 BBD Model Validation Plots of (a) Normal Plot of Residual (b) Predicted vs Actual for BG Dye Removal by Cs/BD-Ma-Tk

Moreover, Figure 4.18b illustrates the relation between observed and the anticipated values of BG dye removal, displaying a significant association between the actual outcome of BG removal and the hypothetically calculated values, thereby confirming the validity of the data from the developed models.

4.2.5.3 Interactive Impact of Variables

Three-dimensional (3D) response surfaces were constructed to analyse the influence of the investigated factors on the BG removal procedure and to identify significant relationships among these factors. The interaction effects of AB (Cs/BD-Ma-Tk dose vs. pH) on the BG removal rate are illustrated in Figure 4.19a, with time remaining constant at 35 min. Figure 4.19a indicates that the adsorption efficiency of Cs/BD-Ma-Tk was higher for the removal of BG under pH ≥ 6.5 conditions. The Cs/BD-Ma-Tk exhibits a pH_{pzc} value of 7 (refer to Figure 4.19d), pH levels higher than 7, its surface is characterised by negative charges, favouring the adsorption of cationic BG molecules. This study demonstrates that electrostatic interactions, as outlined in equation (4.4), significantly influence the adsorption when the pH is similar or above the pH_{pzc} of the Cs/BD-Ma-Tk adsorbent.



(4.4)

Furthermore, Figure 4.19a illustrates that adsorbent exhibited superior adsorption performance towards BG dye at elevated Cs/BD-Ma-Tk quantities (0.1 g). The observed effect results from an increase in the adsorption sites of Cs/BD-Ma-Tk with higher doses of the compound. Moreover, Figure 4.19b illustrates the cumulative impact of Cs/BD-Ma-Tk dosage and the duration of the adsorption process (AC) on the percentage of BG elimination while maintaining a constant pH of 6.5. The results presented in Figure 4.19b demonstrate that the efficacy of BG removal was marginally enhanced by prolonging the period from 35 to 60 min. This phenomenon is attributed to the quick adsorption of BG molecules on the Cs/BD-Ma-Tk surface, followed by their swift migration inside the mesopores. The interaction effect of BC (pH against

time) on the BG removal rate is illustrated in Figure 4.19c, while the Cs/BD-Ma-Tk dosage (0.06 g) remained constant. The results depicted in Figure 4.19c indicate that the effectiveness of BG removal improved as the pH climbed from 4 to 9 despite a reduction in time from 60 to 35 min. The binding of BG molecules to the Cs/BD-Ma-Tk surface is contingent upon a suitable pH, with successful attachment occurring within the pH range of 6.5 to 9.

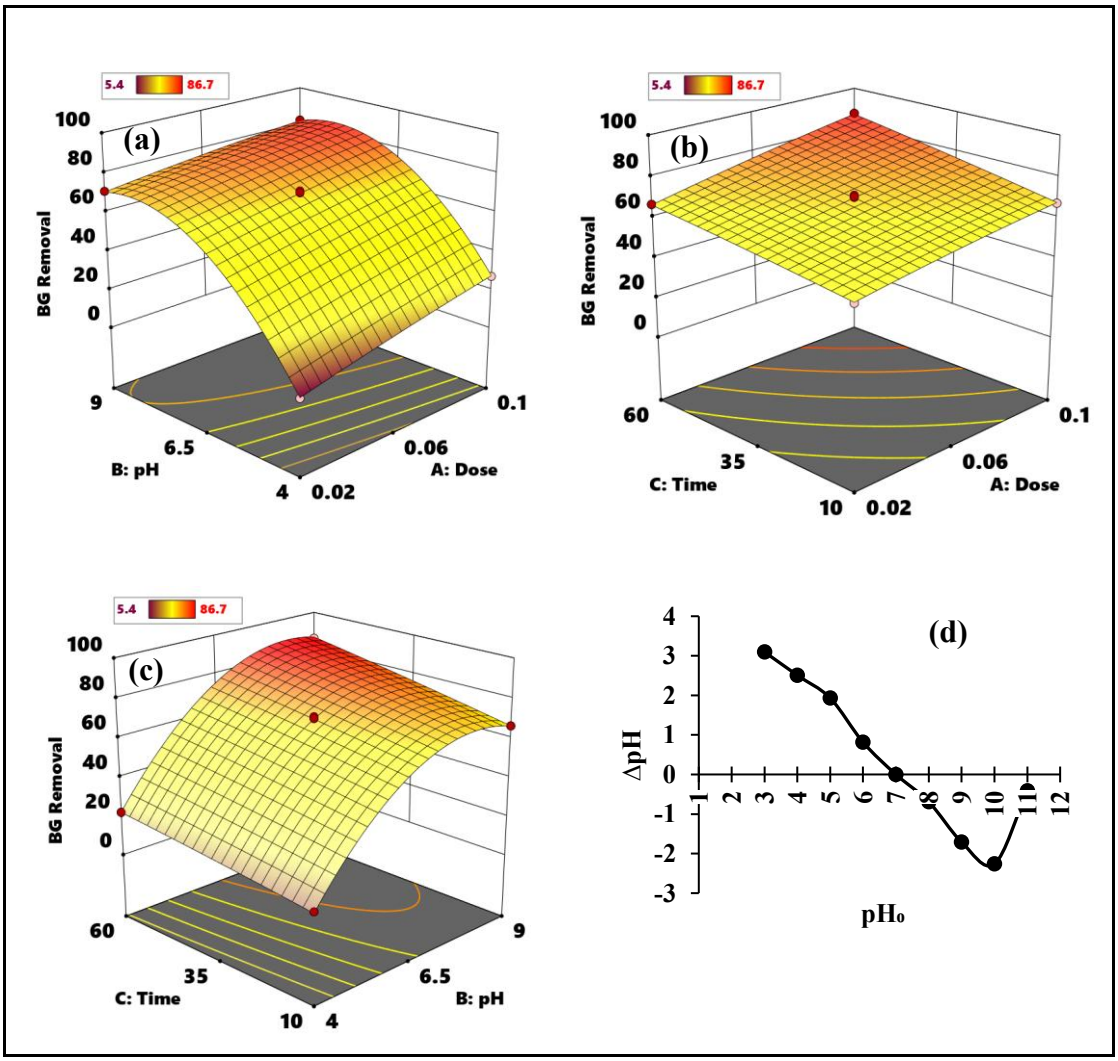


Figure 4.19 3D Images of Interactive Effects Of Parameters (a) AB (Dose vs pH), (b) AC (Dose vs Time), and (c) BC (pH vs Time) on BG Removal by Cs/BD-Ma-Tk and (d) pH_{pzc} Test of Cs/BD-Ma-Tk

4.2.6 Adsorption Equilibrium Studies of BG Removal by Cs/BD-Ma-Tk

4.2.6.1 Initial BG Concentration and Kinetic Study of BG Removal by Cs/BD-Ma-Tk

The effect of initial BG concentration on the adsorption capacity of Cs/BD-Ma-Tk was examined using the optimal adsorption conditions obtained through desirability function (a specified quantity of 0.06g/100mL, an alkaline pH of 8.5), and ranging of the contact time and concentration levels from 0 to 360 min, and 20-250 mg/L, respectively. Figure 4.20 illustrates the adsorption capacity of Cs/BD-Ma-Tk (q_t, mg/g) for the adsorption of BG at varying initial BG concentrations. Figure 4.20 indicates that the accumulation of BG molecules on the surface of Cs/BD-Ma-Tk increased from 31.6 to 413 mg/g as the BG dye concentration raised from 20 to 250 mg/L. This finding correlated with the elevation in the concentration gradient generating a driving force for the BG dye molecules to occupy the active adsorption sites of the Cs/BD-Ma-Tk [315].

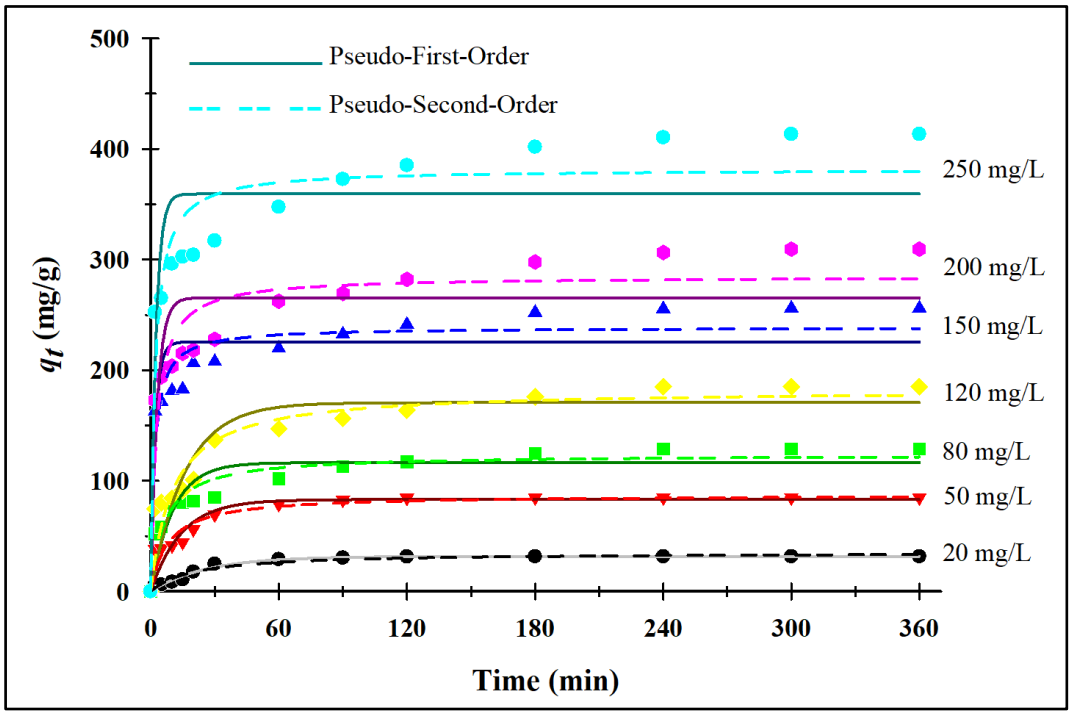


Figure 4.20 Effect of Concentration and Time Variations on Cs/BD-Ma-Tk Adsorption Capacity Alongside the Regression Fits of the PFO and PSO Kinetic Models to the Experimental Data

The kinetic study offers valuable insights for advancing and scaling up the adsorption technology for the adsorptive removal of BG utilising Cs/BD-Ma-Tk. Two

widely used kinetic models, pseudo-first order and pseudo-second-order, were utilised to assess the adsorption data. Table 4.12 summarises the data regarding the kinetic parameters and Figure 4.20 illustrates the regressions fits of the PFO and PSO kinetic models to the experimental data.

Table 4.12
Kinetic Model Parameters for BG Dye Removal by Cs/BD-Ma-Tk

Concentration (mg/L)	$q_{e.exp}$ (mg/g)	PFO			PSO		
		$q_{e.cal}$ (mg/g)	k_1 (1/min)	R^2	$q_{e.cal}$ (mg/g)	$k_2 \times 10^{-2}$ (g/mg min)	R^2
20	31.6	31.6	0.04	0.98	35.2	0.13	0.96
50	84.8	82.9	0.07	0.87	87.2	0.14	0.92
80	128	116	0.09	0.83	123	0.12	0.92
120	185	170	0.06	0.84	182	0.05	0.91
150	256	225	0.46	0.83	248	0.24	0.91
200	309	265	0.33	0.80	291	0.13	0.90
250	413	359	0.42	0.81	394	0.13	0.91

The significantly elevated R^2 values (see Table 4.12) observed in the PSO model compared to the PFO model, and the calculated values of q_e for the PSO kinetic model closely matching the actual values of q_e, indicate that the PSO model effectively characterises the binding of BG onto Cs/BD-Ma-Tk. This outcome suggests that the chemisorption mechanism, resulting from interactions between the BG cationic groups and the anionic groups of Cs/BD-Ma-Tk, is responsible for the adsorption of BG [316].

4.2.6.2 Isotherm Study of BG Removal by Cs/BD-Ma-Tk

The Freundlich, Langmuir, and Temkin mathematical equations have been employed (in their non-linear forms) to elucidate the adsorption isotherm data. Table 4.13 presents the calculated values associated with the isotherm models, while the graphs depicting BG adsorption onto the surface of Cs/BD-Ma-Tk are provided in Figure 4.21. The results indicate that the Freundlich model can effectively describe the BG adsorption by Cs/BD-Ma-Tk, as evidenced by the high R^2 value = 0.98. Consequently, it can be concluded that heterogeneous multilayer adsorption of BG dye molecules by Cs/BD-Ma-Tk occurs in this adsorption system [317]. The maximum monolayer BG uptake by Cs/BD-Ma-Tk in this study was calculated to be 441 mg/g.

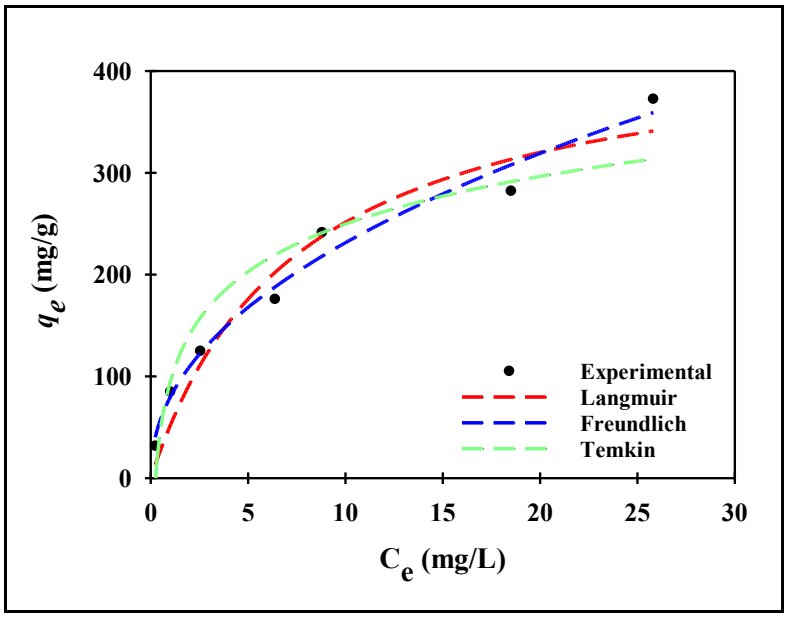


Figure 4.21 Isotherm Model (Langmuir, Freundlich and Temkin) Regression Fits to the Equilibrium Data of BG Adsorption by Cs/BD-Ma-Tk

Table 4.13
The Parameters of Isotherm Models for BG Dye Adsorption by Cs/BD-Ma-Tk

Adsorption isotherm	**Parameter**	**Value**
Langmuir	q_{max} (mg/g)	441
	K_a (L/mg)	0.13
	R^2	0.94
Freundlich	K_f(mg/g) (L/mg)$^{1/n}$	79.6
	n	2.15
	R^2	0.98
Temkin	K_T (L/mg)	2.71
	b_T (J/mol)	33.6
	R^2	0.90

4.2.6.3 Thermodynamic Study of BG Removal by Cs/BD-Ma-Tk

The analysis of adsorption thermodynamic parameters was conducted to analyse irregularity and the spontaneity of BG adsorption by Cs/BD-Ma-Tk across four temperatures (298.15 to 328.15 K) under the optimal experimental condition (Cs/BD-

Ma-Tk dose = 0.06 g/100 mL, and pH = 8.5). Using the intercept and slope of the van't Hoff plot enthalpy change (ΔH°), entropy change (ΔS°), and Gibbs free energy change (ΔG°), were calculated. The van't Hoff plot (Figure 4.22) was generated by plotting 1/T vs. the lnk_d obtained through the adsorption data. Moreover, the calculated adsorption isotherm parameters are displayed in Table 4.14. According to the presented results, the adsorption of BG dye by Cs/BD-Ma-Tk is viable and spontaneous, as confirmed by the negative ΔG° results [318]. Moreover, the positive ΔH° value of 71.5 kJ/mol validated the endothermic process of BG dye adsorption using Cs/BD-Ma-Tk. These results correlated with the increase of temperature influencing the increase in both the adsorption capacity and rate of BG adsorption by Cs/BD-Ma-Tk. This phenomenon arises from the transfer of heat to the system, which facilitates the rapid diffusion of BG dye molecules into the mesoporous structure of Cs/BD-Ma-Tk [319]. The positive ΔS° value (241 J/mol.K) indicates that with an increase in temperature, there is an increase of randomness in the adsorbent/adsorbate interface allowing a greater number of binding configurations for BG on the surface of Cs/BD-Ma-Tk [320]

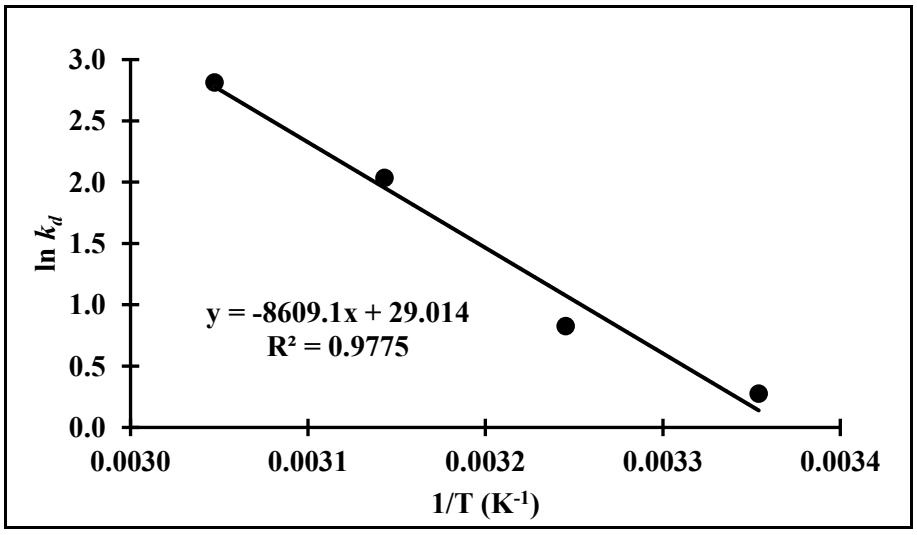


Figure 4.22 Van't Hoff Plot of BG Removal by Cs/BD-Ma-Tk

Table 4.14
Thermodynamic Parameters for the Adsorption of BG Dye by Cs/BD-Ma-Tk

T (K)	k_d	ΔG (kJ/mol)	ΔH (kJ/mol)	ΔS (J/mol.K)
298.15	1.31	-0.34	71.5	241
308.15	2.28	-2.75		
318.15	7.66	-5.16		
328.15	16.6	-7.58		

4.2.7 Proposed Mechanism of BG Removal by

Various possible interactions facilitating the binding process of BG dye onto the surface of Cs/BD-Ma-Tk are illustrated in Figure 4.23. As per the findings of the FT-IR analysis, the surface of Cs/BD-Ma-Tk contains various functional groups (-OH, Ti-O, -COOH, and C-O-C) that demonstrate a negative charge under alkaline conditions, with a point of zero charge (pHpzc) of 7. Due to the presence of these functional groups (-NH, -OH) electrostatic attraction occurs between the negatively charged surface of Cs/BD-Ma-Tk and the positively charged BG dye molecules. Furthermore, hydrogen bonding can occur between the hydrogen atoms in the structure of Cs/BD-Ma-Tk and the nitrogen atoms of the BG dye molecules, contributing to an increase in the efficiency of BG dye removal by Cs/BD-Ma-Tk. In addition, Yoshida-H bonds could be formed through the interaction of BG and Cs/BD-Ma-Tk via the attraction of hydrogen from Cs/BD-Ma-Tk with the benzene rings of the BG dye molecules. Moreover, the ion-pair electrons of the nitrogen and oxygen heteroatoms in the Cs/BD-Ma-Tk complex can engage with the aromatic rings of the BG dye through n–π interactions [321]. Lastly, the aromatic rings of the BG dye molecule and the aromatic rings of benzaldehyde can produce π–π stacking contact in an electron donor/acceptor system to further enhance the removal efficiency of BG dye by Cs/BD-Ma-Tk [320].

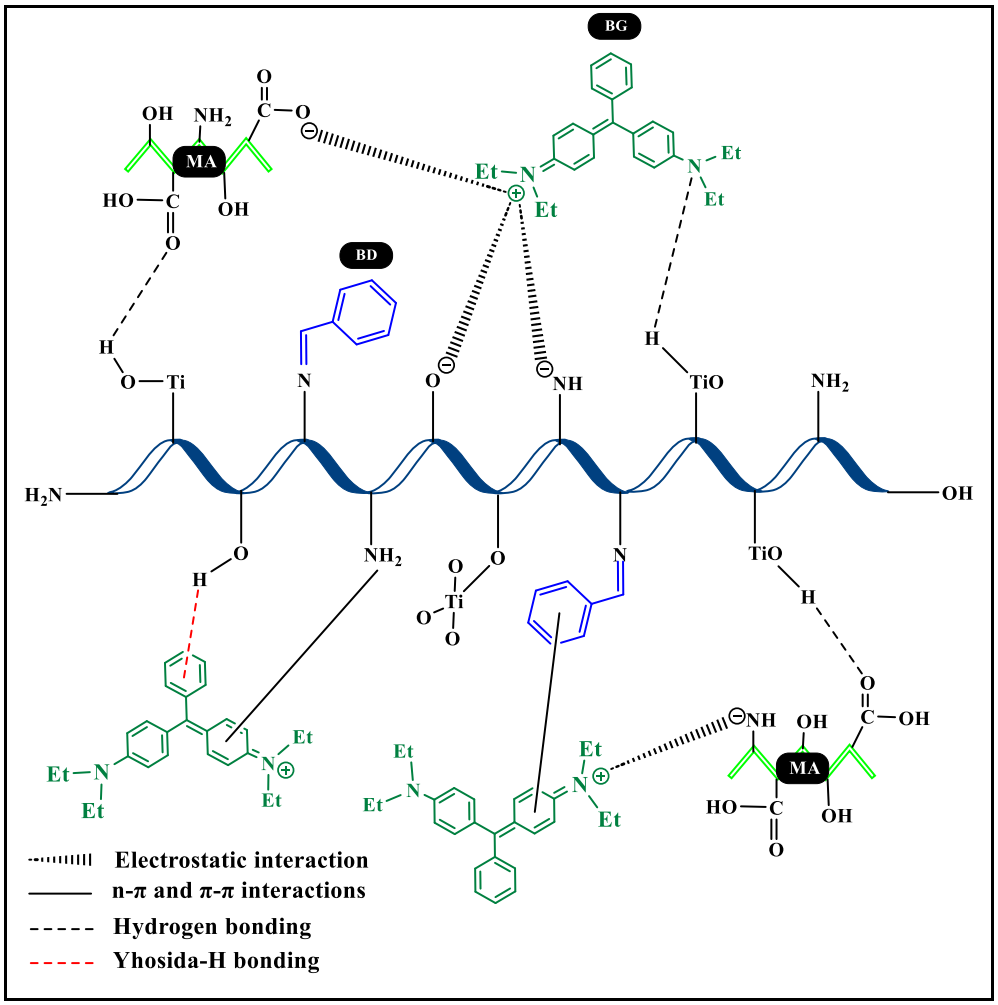


Figure 4.23 The Proposed Interaction Mechanism of BG Dye with Cs/BD-Ma-Tk

4.3 Glyoxal Crosslinked Cs-Ma-Tk (Cs/Gly-Ma-Tk)

In this section, a new composite material of Chitosan- Microalgae- Kronos TiO_2 was synthesised and put through a hydrothermal crosslinking process to create glyoxal-crosslinked Chitosan- Microalgae- Kronos TiO_2 (henceforth referred to as Cs/Gly-Ma-Tk) for the adsorption of brilliant green dye. The use of biodegradable and abundantly available resources in this study is an effort to achieve a cost-efficient and biofriendly adsorbent with high efficiency towards the removal of pollutants (specifically BG dye in this study) from effluents. The addition of Tk and Ma would help alleviate chemical instability and low affinity of Cs towards cationic pollutant species, while the Schiff's base reaction occurring during the grafting process would further enhance the structural stability of the resultant composite. The dye removal conditions (adsorbent dosage, pH, contact time) have been optimised using RSM-BBD methodology and the optimal conditions have been applied for kinetic, isotherm, and thermodynamic studies. Based on the findings of the analyses, a plausible adsorption mechanism has been proposed.

4.3.1 Surface Properties of Cs/Gly-Ma-Tk

The component composition and surface properties of Cs/Gly-Ma-Tk are presented in Table 4.15. The elemental analysis data for carbon, hydrogen, nitrogen, sulphur, and oxygen (by difference) content (%) in Cs/Gly-Ma-Tk were found at 32.09%, 3.9%, 5.95%, 0.32%, and 57.74%, respectively. Moreover, the BET surface study indicates that Cs/Gly-Ma-Tk possesses a surface area of 2.79 m^2/g and an average pore diameter of 10.16 nm. Cs/Gly-Ma-Tk exhibits a pore diameter ranging from 2 to 50 nm, indicating the mesoporous structure of the adsorbent [304]. Furthermore, Figure 4.24 illustrates the isotherm of the nitrogen (N2) adsorption and desorption process on the Cs/Gly-Ma-Tk composite. The mesoporous structure of Cs/Gly-Ma-Tk is further confirmed as the isotherm aligns with the attributes of a Type-IV isotherm [322]. In addition, Figure 4.24 illustrates a hysteresis loop classified as H3, indicating the existence of mesopores in the Cs/Gly-Ma-Tk system. The findings indicate that the Cs/Gly-Ma-Tk generated exhibits high porosity allowing the BG dye molecules into the porous structure of the adsorbent and leading their capture by the active adsorption sites resulting to the efficient removal of BG by Cs/Gly-Ma-Tk.

Table 4.15
Surface Properties of Cs/Gly-Ma-Tk

Parameter(s)	Value
C	32.09%
H	3.9%
N	5.95%
S	0.32%
O (by difference)	57.74%
BET surface area (m^2/g)	2.79
Langmuir surface area (m2/g)	4.08
Total volume in pores (cm3/g)	0.01
Mean pore diameter (nm)	10.16

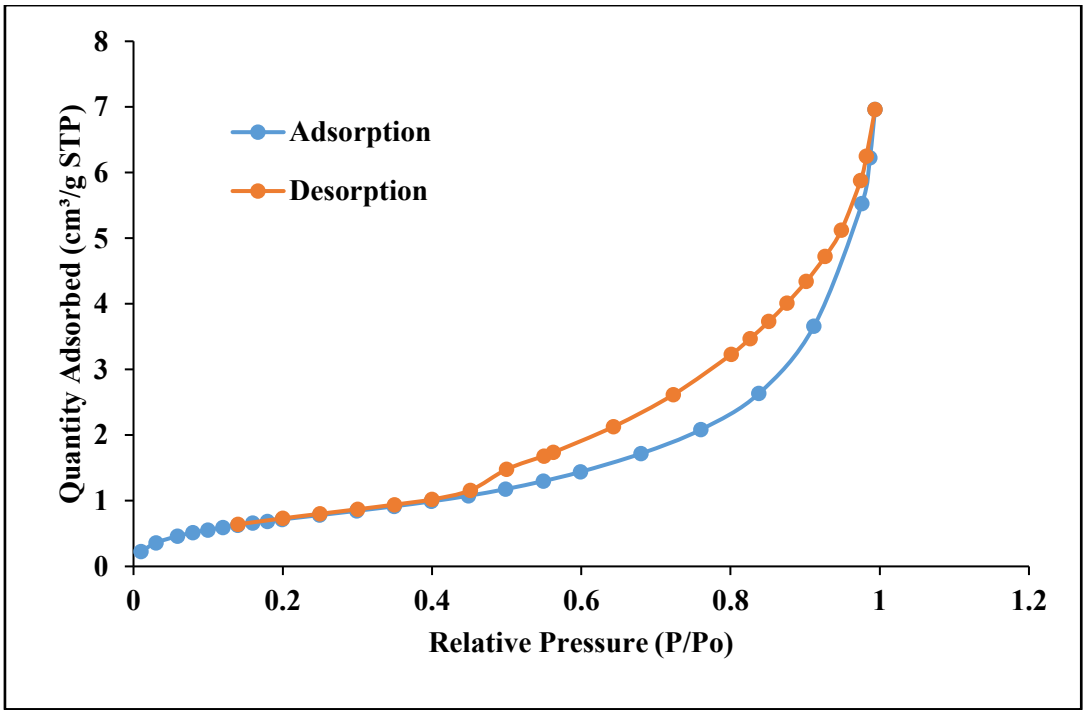


Figure 4.24 N_2 Adsorption-Desorption Isotherm of Cs/Gly-Ma-Tk

4.3.2 X-Ray Diffraction Analysis of Cs/Gly-Ma-Tk

The morphological characteristics of Cs/Gly-Ma-Tk were analysed using XRD, as illustrated in Figure 4.25. The characteristic peaks of Cs at 2θ = 10.9° and 20°, corresponding to the (020) and (200) crystal planes can be seen with a weak intensity due to the introduction of Ma, and Tk into the polymeric matrix of Cs in addition to the crosslinking process with Gly, similar results were observed by Bashal et al., (2023) when introducing cobalt nanoparticles into the polymeric matrix of Cs [323]. The

characteristic peak of Ma, generally observed at $2\theta \approx 22°$, corresponding to (101) crystal plane of cellulose, is observed with a very weak intensity in the XRD pattern of Cs/Gly-Ma-Tk [190], [306]. Additionally, the crystal planes of TiO_2 are identified by the peaks of 2θ = 25.7°, 38.2°, 48.2°, 54.1°, 55.3°, 62.9°, 70.6°, 75.7°, and 83.4° corresponding to the (101), (004), (200), (105), (211), (213), (220), (215) and (224) planes, respectively [282], [283], [284], which are observed in the XRD pattern of Cs/Gly-Ma-Tk as highlighted in Figure 4.25. The presence of Ma, Cs, and Tk in the XRD pattern of Cs/Gly-Ma-Tk indicates the successful integration of Tk and Ma into the chitosan matrix.

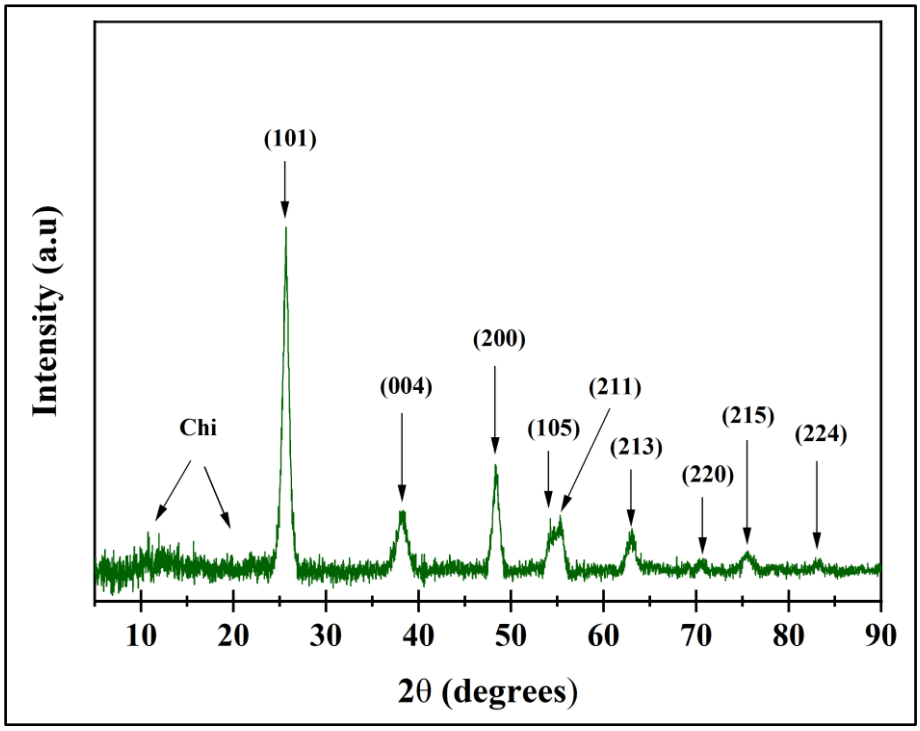


Figure 4.25 XRD Pattern of Cs/Gly-Ma-Tk

4.3.3 FT-IR Spectrum Analysis of Cs/Gly-Ma-Tk

The functional group analysis of Cs/Gly-Ma-Tk before and following the removal of BG is shown in Figure 4.26a and b, respectively. Figure 4.26a (the FT-IR spectrum of Cs/Gly-Ma-Tk), broad peaks observed in the range of 3470-3274 cm^{-1} correspond to the stretching vibrations of -NH and -OH groups from Cs and Ma. The C-H stretching vibrations of the aliphatic groups can be characterised by the prominent peak at 2929 cm^{-1}. The peak observed at 1651 cm^{-1} signifies the stretching vibrations of

C=O (in esters and carboxylic acids) and the stretching vibrations of C=N due to the occurrence of the Schiff's base reaction and formation of imine groups [132], [144]. The FT-IR spectrum of Cs/Gly-Ma-Tk displays a peak at 1235 cm^{-1}, which corresponds to the asymmetric stretching vibrations of the O-P-O bands, thereby confirming the presence of Ma [310]. Additionally, the peaks detected at 1409 cm^{-1}, 1072 cm^{-1}, and 690 cm^{-1} correspond to the bending vibrations of C-H and O-H, asymmetric stretching vibrations of C-O, and the stretching vibrations of the Ti-O-Ti groups, respectively [133], [151], [309].

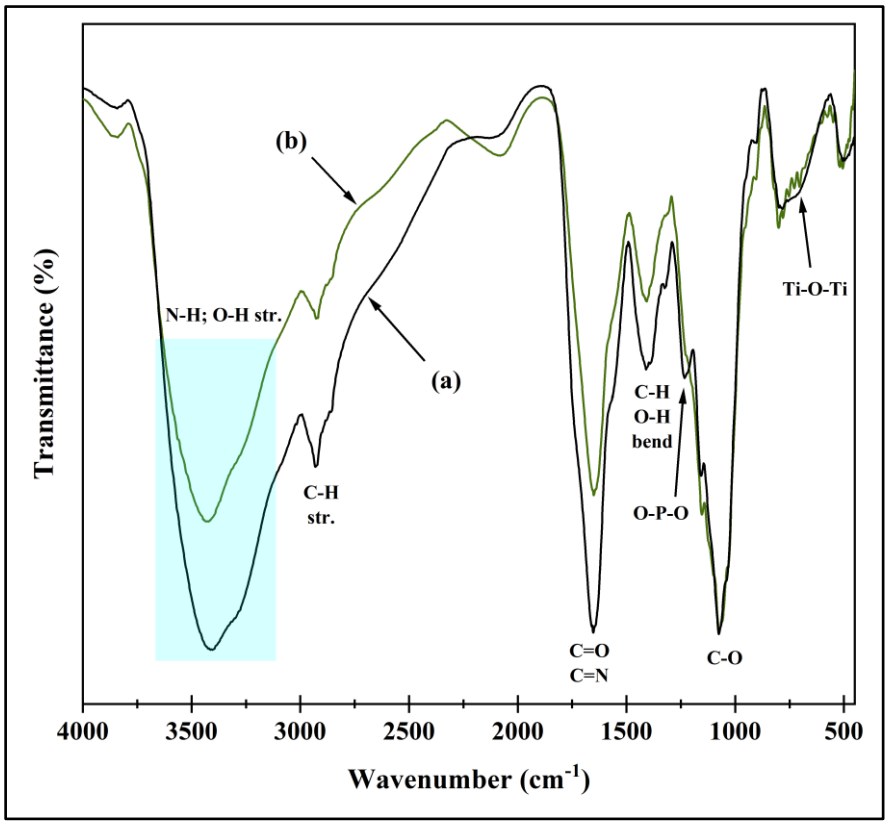
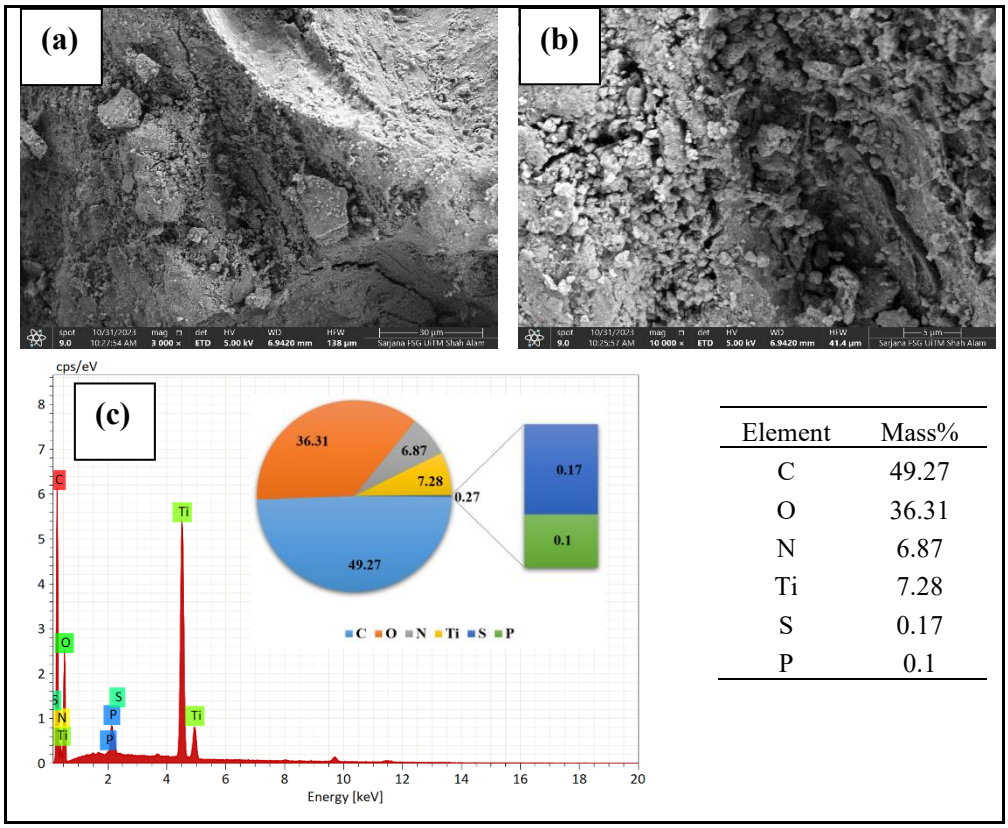


Figure 4.26 FT-IR Spectra of (a) Cs/Gly-Ma-Tk, and (b) Cs/Gly-Ma-Tk+BG

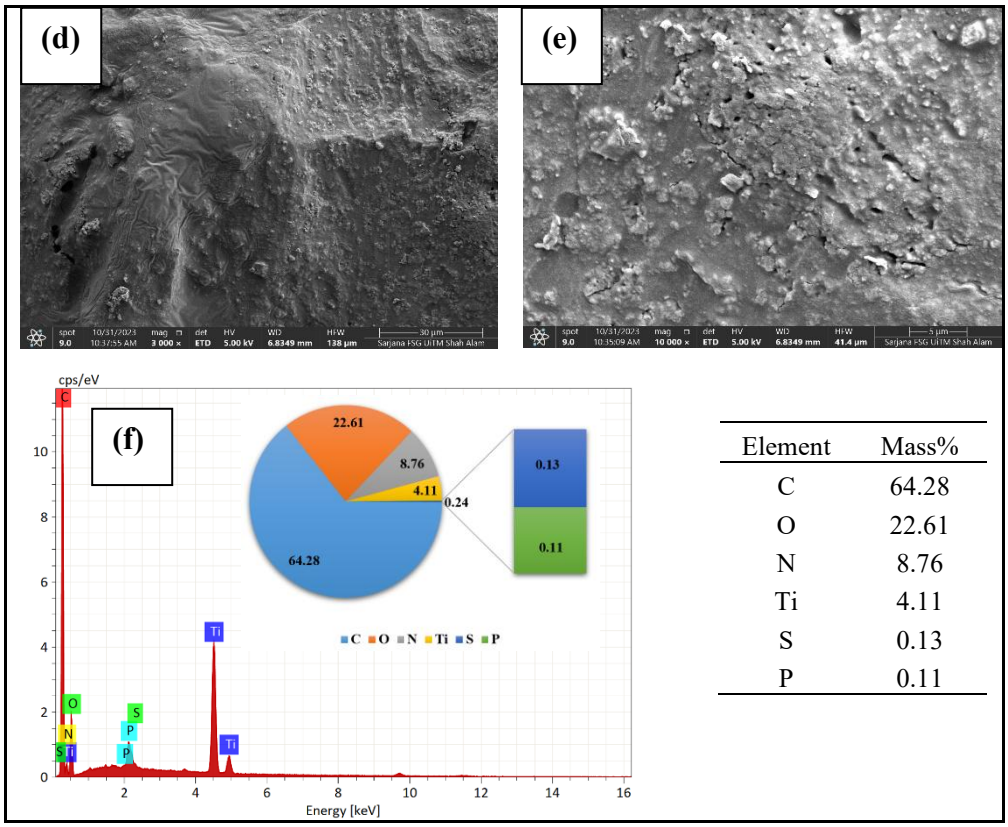
Figure 4.26b displays the IR spectrum of Cs/Gly-Ma-Tk following the adsorption of BG dye, indicating that the principal peaks in Cs/Gly-Ma-Tk are consistent with those observed before adsorption (Figure 4.26a). The intensity of multiple peaks related to surface functional groups, such as -NH, O-H, C=O, and C-H, diminishes, as illustrated in Figure 4.26b indicating that the numerous functional groups present in the structure of Cs/Gly-Ma-Tk play a significant role in the removal of BG from the dye solution.

4.3.4 Surface Morphology of Cs/Gly-Ma-Tk

The FE-SEM/EDX characterisation provided critical insights into the surface structure and elemental composition of Cs/Gly-Ma-Tk both before and after the adsorption of BG. Figure 4.27a and b display the FE-SEM image of the Cs/Gly-Ma-Tk before BG dye adsorption, illustrating an irregular and heterogeneous surface marked by numerous cavities. The surface irregularities and heterogeneity of Cs/Gly-Ma-Tk make it a favourable substrate for BG adsorption. The EDX spectrum of Cs/Gly-Ma-Tk (Figure 4.27c) reveals the presence of multiple elements within its polymeric matrix, specifically carbon (C), oxygen (O), nitrogen (N), titanium (Ti), sulphur (S), and phosphorus (P). Figure 4.27d and e display the FE-SEM images of the surface of Cs/Gly-Ma-Tk following the adsorption of BG dye molecules, demonstrating that the surface of Cs/Gly-Ma-Tk has become more compact, showing a reduction in cavities. The alteration in the surface morphology of Chi-Gly/Ma/TiO_2 is due to the incorporation of BG molecules onto its surface. The EDX analysis supports the adsorption of BG, as indicated by the increase observed in the C content as the BG dye molecules captured on the surface of Cs/Gly-Ma-Tk are dominantly comprised of carbon.



Element	Mass%
C	49.27
O	36.31
N	6.87
Ti	7.28
S	0.17
P	0.1



Element	Mass%
C	64.28
O	22.61
N	8.76
Ti	4.11
S	0.13
P	0.11

Figure 4.27 FE-SEM Images at Two Magnification Powers of 3kx (a and d) and 10kx (b and e) of (a-b) Cs/Gly-Ma-Tk and (d-e) Cs/Gly-Ma-Tk After BG Adsorption and EDX Mapping of (c) Cs/Gly-Ma-Tk and (f) Cs/Gly-Ma-Tk after BG Dye Adsorption

4.3.5 Statistical Optimisation and Analysis

4.3.5.1 Experimental Design and Process Optimisation for BG dye Removal by Cs/Gly-Ma-Tk

Box Behnken Design (BBD) from Response Surface Methodology (RSM) was utilised for statistical analysis and optimisation of three input factor (A: Cs/Gly-Ma-Tk dose, B: pH, and C: contact time) to maximise the output (BG dye removal%). The experimental design was developed using the computer software Design Expert (ver. 13.0, Stat-Ease, USA) which generated 17 experiments for three levels of the three input factors. The range of the input variables were initially determined by performing premonitory experiments prior to the experimental design. The value of the three levels of the input variables (-1, 0 and 1) are illustrated in Table 4.16.

Table 4.16
Factor Levels of the BBD Design for BG Removal by Cs/Gly-Ma-Tk

Factor name	Factor code	Level of factor		
		-1	0	1
Cs/Gly-Ma-Tk dose (g/100mL)	A	0.05	0.125	0.2
pH	B	4	6.5	9
Time (min)	C	30	105	180

Furthermore, Table 4.17 provides the generated experimental design including the values of the three variables as well as the experimental and predicted values for the response. A desirability test was conducted to compare experimental outcomes with expected results computed from analysing the ideal conditions obtained through Design Expert software and to evaluate the reliability of the employed BBD model [324]. Figure 4.28 illustrates the suggested optimal variable values to maximise the removal of BG by Cs/Gly-Ma-Tk within the range of the model parameters (pH = 4.1; Cs/Gly-Ma-Tk dose = 0.2 g/100 mL; time = 180 min, resulting in a BG removal percentage of 81.1%). The outcome of the desirability test performed was found to be 80.5% and close to the predicted BG removal value, thereby validating the reliability of the developed model.

Table 4.17
Experimental Design Based on BBD for BG Removal (%) by Cs/Gly-Ma-Tk

Run	A: Dose (g)	B: pH	C: Time (min)	BG removal (%)	
				Predicted	Actual
1	0.05	4	105	51	52.1
2	0.2	4	105	69.6	69.1
3	0.05	9	105	30.1	30.6
4	0.2	9	105	59.8	58.7
5	0.05	6.5	30	22.44	20.6
6	0.2	6.5	30	50.84	50.6
7	0.05	6.5	180	49.4	49.6
8	0.2	6.5	180	69.3	71.1
9	0.125	4	30	49.1	49.8
10	0.125	9	30	42.6	43.9
11	0.125	4	180	80.6	79.3
12	0.125	9	180	56.3	55.6

Run	A: Dose (g)	B: pH	C: Time (min)	BG removal (%)	
				Predicted	Actual
13	0.125	6.5	105	54.4	55.6
14	0.125	6.5	105	54.4	53.4
15	0.125	6.5	105	54.4	51.7
16	0.125	6.5	105	54.4	54.5
17	0.125	6.5	105	54.4	56.9

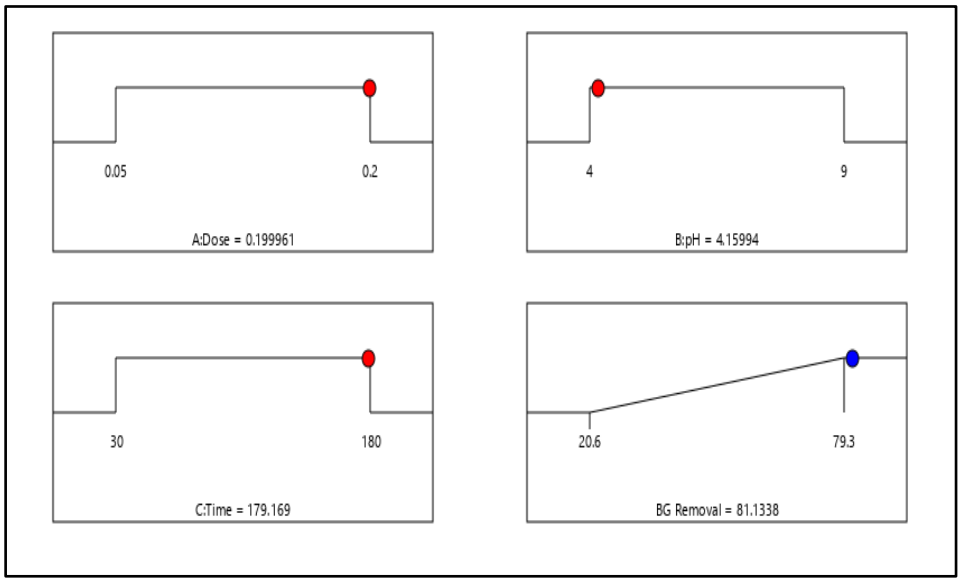


Figure 4.28 Desirability Ramps of BG Removal by Cs/Gly-Ma-Tk

4.3.5.2 Statistical Analysis of BG Removal by Cs/Gly-Ma-Tk

The developed model's efficiency and accuracy of factors and their interactions were evaluated using an analysis of variance (ANOVA) as displayed in Table 4.18. The R^2 value of 0.99 for the model indicates a strong correlation, demonstrating alignment between the reported BG removal and computed results and the credibility of the model to explain the experimental results. Moreover, the high F-value of 76.19 (with pp-value<0.0001) for the model further confirms the suitability of the obtained model to describe the experimentally obtained data. The low F-value of 1.20 for the lack of fit suggests that there is potential to decrease pure error through enhancements [325].

Table 4.18
Analysis of Variance (ANOVA) for BG Dye Removal by Cs/Gly-Ma-Tk

Source	Sum of Squares	df	Mean Square	F-value	p-value	Remark
Model	2975.89	9	330.65	76.19	< 0.0001	significant
A-Dose	1166.45	1	1166.45	268.76	< 0.0001	significant
B-pH	472.78	1	472.78	108.93	< 0.0001	significant
C-Time	1028.31	1	1028.31	236.93	< 0.0001	significant
AB	30.80	1	30.80	7.10	0.0323	significant
AC	18.06	1	18.06	4.16	0.0807	not significant
BC	79.21	1	79.21	18.25	0.0037	Significant
A^2	126.67	1	126.67	29.19	0.0010	Significant
B^2	57.33	1	57.33	13.21	0.0083	Significant
C^2	3.88	1	3.88	0.8941	0.3759	not significant
Residual	30.38	7	4.34			
Lack of Fit	14.39	3	4.80	1.20	0.4165	not significant
Pure Error	15.99	4	4.00			
Cor Total	3006.27	16				

The model can be utilised to enhance the response via optimisation, while the model terms yielding a p-value of less than 0.05 are considered to have had a significant statistical impact on the model's response, hence the terms A, B, C, AB, BC, A^2, and B^2 significantly contribute to the substantial adsorption of BG by Cs/Gly-Ma-Tk. Equation (4.5) delineates a quadratic polynomial that quantifies BG's theoretical removal by Cs/Gly-Ma-Tk based on the values of the input variables with statistically significant impact on the response.

$$\text{BG Removal (\%)} = + 54.42 + 12.07A - 7.69B + 11.34C + 2.78AB - 4.45BC - 5.49A^2 + 3.69B^2 \quad (4.5)$$

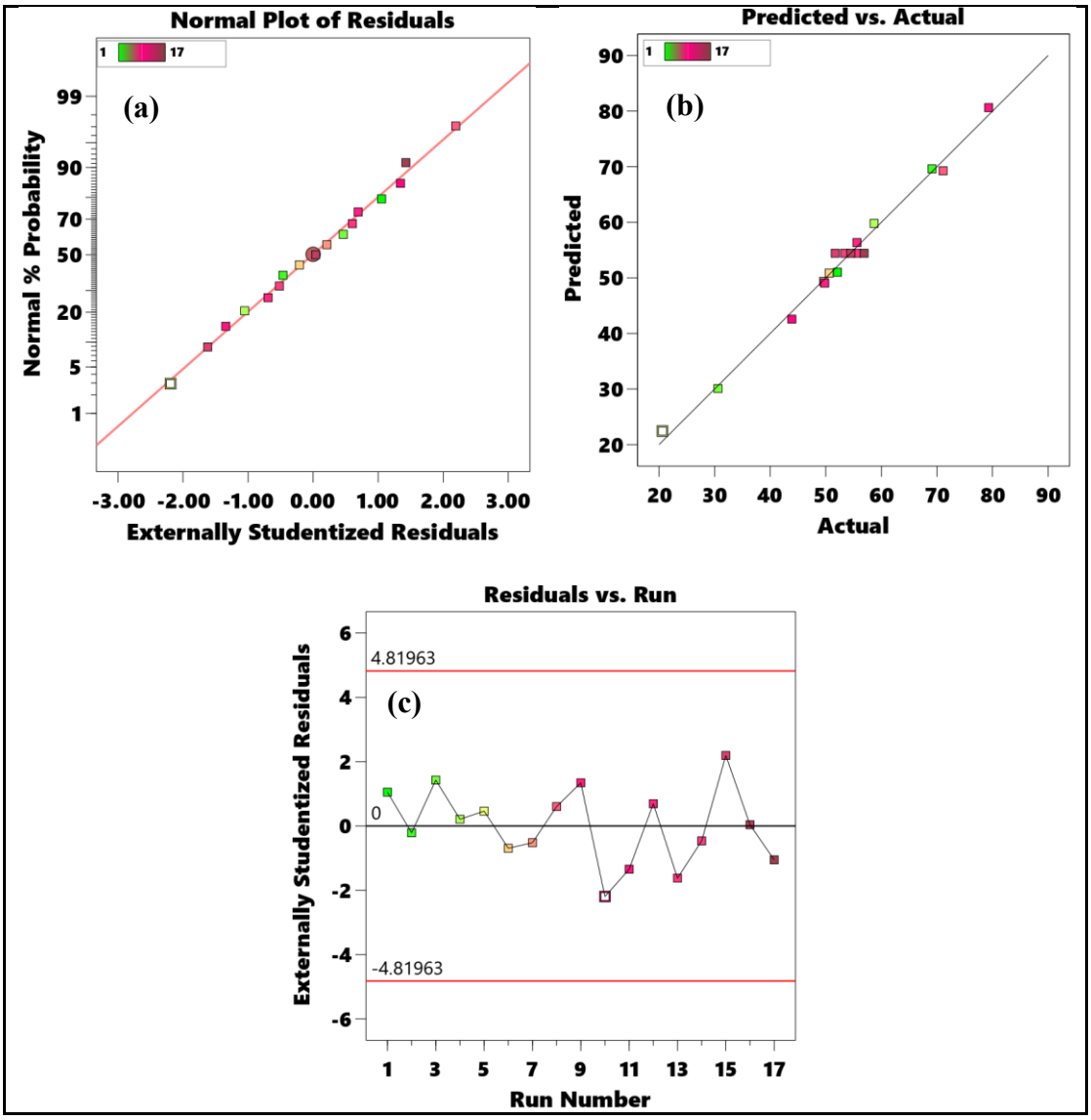


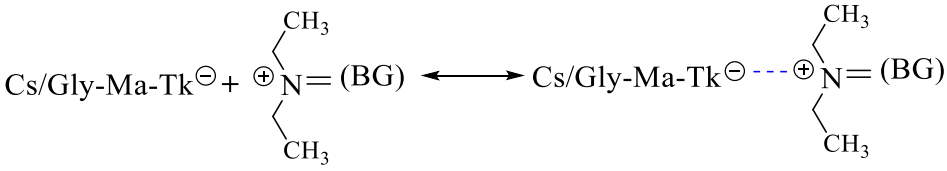
Figure 4.29 (a) Normal Plot of Residual (b) Predicted versus Actual Removal of BG Dye with Cs/Gly-Ma-Tk (c) Residual vs Run of BG Removal

Furthermore, employing a graphical tool enhances the verification of model accuracy and provides a visual representation of residual dispersion. Average probability charts serve to evaluate the distributions of model's residual. The distribution of the dots in Figure 4.29a, randomly positioned along the 45° line, suggests the validity of both the model structures and the ANOVA findings and the errors have a normal distribution [326]. The strong alignment between the experimental data of BG removal and the projected values supports the model's applicability, as illustrated in Figure 4.29b. Additionally, Figure 4.29c presents the residuals plotted against the run numbers to minimise the background dye. The data points in Figure 4.29c exhibit a

random distribution around the initial point, indicating that the model is both reliable and precise.

4.3.5.3 Interactive Impact of Variables

Figure 4.30 illustrates the pairings of factors that demonstrate statistically significant interacting effects on BG removal response, specifically dose versus pH and pH versus time, through 3D surface plots and 2D contours. Figure 4.30a and b illustrate that, at a constant duration of 105 min, the response value increases from 30.6% to 58.7% as the Cs/Gly-Ma-Tk dosage is raised from 0.05 to 0.125 g/100mL at pH 9. Reducing the pH from 9 to 4, with a constant Cs/Gly-Ma-Tk dosage of 0.05 g/100mL, leads to an enhancement in BG removal from 30.6% to 52.1%. The simultaneous increase in Cs/Gly-Ma-Tk dosage and reduction in pH yields a reaction value of 69.1%, clearly demonstrating the synergistic effect of these two variables on the response value. The influence of pH on the removal of BG dye is associated with the changes in the Cs/Gly-Ma-Tk's surface charges at different pH levels. Figure 4.30c demonstrates that the point of zero charge (pH_{pzc}) for Cs/Gly-Ma-Tk is observed at a pH=3.2. This suggests that pH values exceeding pH_{pzc} (pH> 3.2) result in the Cs/Gly-Ma-Tk's surface acquiring negative charges, which facilitate binding with the BG dye molecules with positive charges through electrostatic forces, as illustrated below (4.6).



(4.6)

The low pH_{pzc} observed for Cs/Gly-Ma-Tk may be due to the major consumption of the amine groups through the crosslinking process and Schiff base formation, which reduces the basic sites available on the polymeric matrix of Cs/Gly-Ma-Tk and ultimately causes the pH_{pzc} to lower. Additionally, the presence of acidic functional groups, such as carboxylates (–COOH/–COO^-), phosphoryl groups (–PO_4H/–PO_4^{2-}) in the chemical structure of Ma which deprotonate at moderate pH levels and create negative surface charge can further contribute to lowering the pH_{pzc} of the Cs/Gly-Ma-Tk adsorbent. Moreover, the hydroxyl functional groups in Kronos (Ti-OH)

can act as Lewis acid sites which further contributes to the shift of pH_{pzc} to lower pH values. Finally, it can be expected that not all glyoxal molecules have successfully crosslinked (considering the small size of the molecules) and a part of the attached glyoxal molecules might have been grafted to a Cs chain through Schiff base reaction, meaning that the aldehyde group on one side can be oxidized (or further reacted) to carboxyl-containing products (e.g., glyoxylic/glyoxalic-type moieties) or form aldehyde-derived species that hydrolyse/oxidize to acids. These new acidic groups (–COOH, hydrated aldehydes) increase anionic sites and push pH_{pzc} lower.

As the pH_{pzc} value found for Cs/Gly-Ma-Tk is lower than all pH values used in this study (using pH values lower than 3.2 would be an extremely acidic environment and in this study efforts have been made to avoid extreme conditions as they will not be practical for industrial applications) best adsorption performance was observed in acidic environments (pH=4) which can be attributed to the presence of deprotonated -OH groups in higher pH values which would compete with the Cs/Gly-Ma-Tk adsorbent in forming ionic bonds with the BG dye molecules through electrostatic attractions and consequently reduce the adsorption efficiency. Hence, the higher performance of Cs/Gly-Ma-Tk in more acidic environments can be justified by the lack of competition for creating electrostatic attractions with the BG dye molecules.

In addition, the interaction effects of pH and time on the removal of BG dye by Cs/Gly-Ma-Tk are illustrated in Figure 4.30d and e, utilising a constant dosage of 0.125 g/100 mL of Cs/Gly-Ma-Tk. An increase in pH from 4 to 9, with a constant duration of 30 min, results in a reduction of the response value from 49.8% to 43.9%. This observation supports the conclusion that optimal removal occurs under acidic conditions (pH = 4). Extending the contact time between Cs/Gly-Ma-Tk and BG dye solution from 30 to 180 min at pH=9 increases the BG dye removal response from 43.9% to 55.6%. The simultaneous increase in pH and time factors facilitates the BG dye removal reaction, achieving a removal rate of 79.3%. This enhancement is correlated with a sufficient contact time being required for BG dye molecules to penetrate the porous structure of Cs/Gly-Ma-Tk.

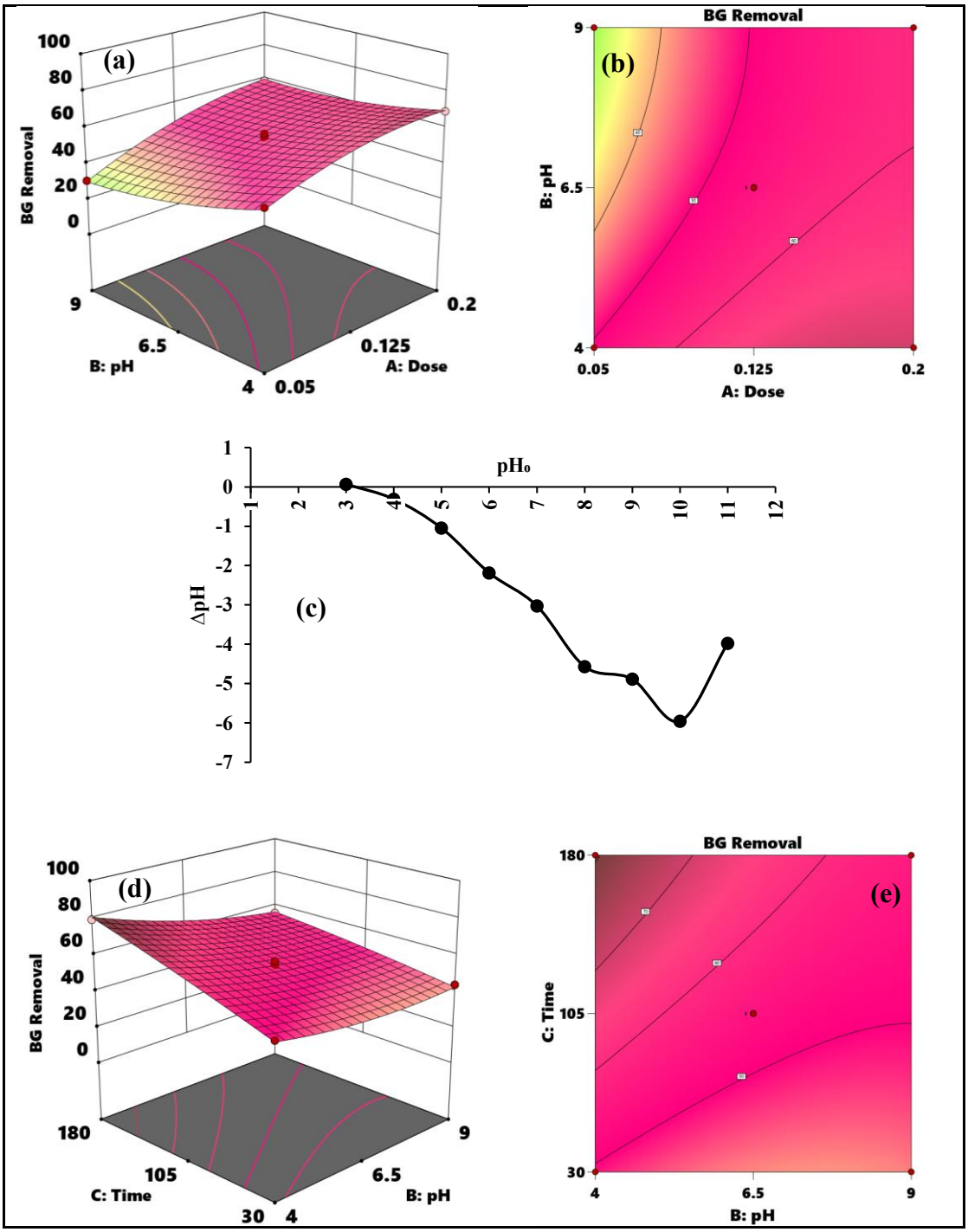


Figure 4.30 3D Surface Plots and 2D Contours of (a-b) AB (Adsorbent Dose*pH), and (d-e) BC (pH*Time) Interactions on BG Dye Removal by Cs/Gly-Ma-Tk (and (c) pH_{pzc} Test of Cs/Gly-Ma-Tk)

4.3.6 Adsorption Equilibrium Studies of BG Removal by Cs/Gly-Ma-Tk

4.3.6.1 Initial BG Concentration and Kinetic Study of BG Removal by Cs/Gly-Ma-Tk

Various initial concentrations of BG (20, 50, 80, 120, 150, 200, and 250 mg/L) were utilised with samples taken at varying times (0-240 min) while the solution pH (4), Cs/Gly-Ma-Tk dosage (0.2 g/100 mL), and temperature (25 °C) remained constant. Figure 4.31 presents the adsorption capacities of Cs/Gly-Ma-Tk (q_t (mg/g)) over time (min) at different initial concentrations of BG, where the Cs/Gly-Ma-Tk adsorption capacity was increased from 11.8 to 73 mg/g as the BG dye concentration rose from 20 mg/L to 250 mg/L. The attained result is attributed to the mass transfer phenomenon happening due to the increase in the concentration gradient. The increased concentration of the BG dye in the solution would create a strong driving force which subsequently enhances the diffusion of BG molecules within the internal pores of the Cs/Gly-Ma-Tk, facilitating the movement of BG molecules to the active adsorption sites [327].

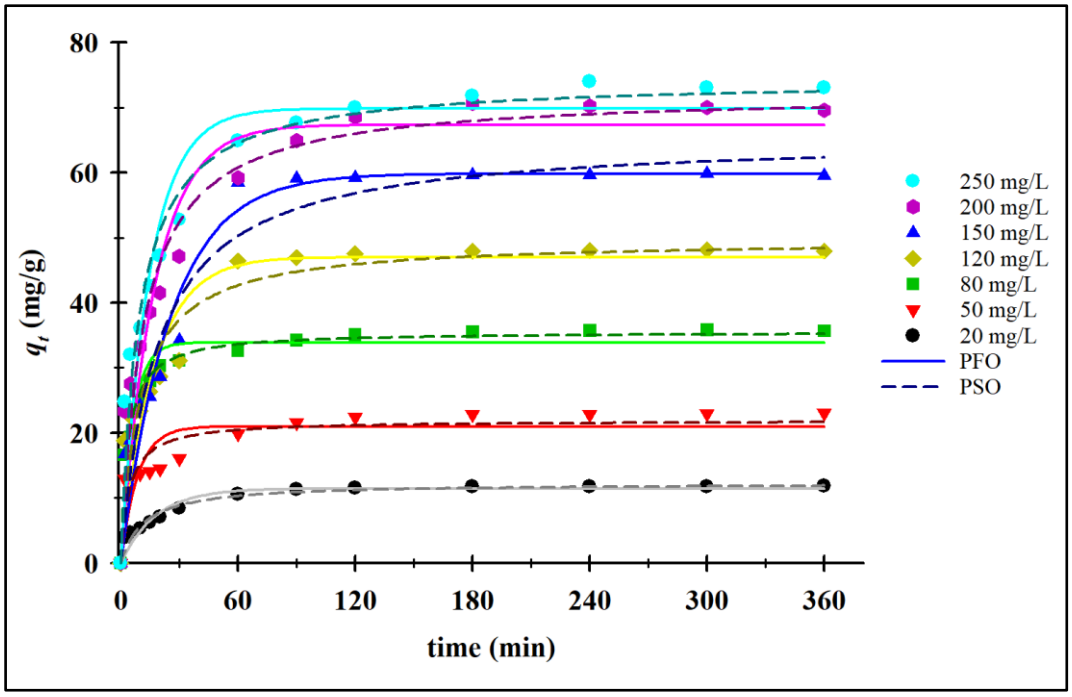


Figure 4.31 Effect of the Contact Time on BG Adsorption by Cs/Gly-Ma-Tk at Several Concentrations Alongside PFO and PSO Regression Fits to the Experimental Data

The BG adsorption behaviour on Cs/Gly-Ma-Tk's surface was investigated via adsorption kinetics analysis. Table 4.19 summarises the kinetic parameter values of PFO and PSO kinetic models for the adsorption of BG on the surface of Cs/Gly-Ma-Tk while the regression fits of the models is visually presented in Figure 4.31 for all initial BG dye concentrations.

Table 4.19 PFO and PSO Kinetic Parameters for BG Adsorption by Cs/Gly-Ma-Tk

Concentration (mg/L)	$q_{e.exp}$ **(mg/g)**	**PFO**			**PSO**		
		$q_{e.cal}$ **(mg/g)**	k_1 **(1/min)**	R^2	$q_{e.cal}$ **(mg/g)**	$k_2 \times 10^{-2}$ **(g/mg min)**	R^2
20	11.8	11.4	0.06	0.93	12.2	0.71	0.96
50	23.1	21.0	1.28	0.72	21.9	1.07	0.85
80	35.7	33.9	0.17	0.93	35.6	0.81	0.98
120	48.2	47.0	0.06	0.87	49.6	0.21	0.92
150	59.5	59.8	0.04	0.94	65.4	0.08	0.94
200	69.6	67.3	2.63	0.92	72.1	0.12	0.96
250	73.3	69.8	0.07	0.92	74.2	0.15	0.97

The kinetic data for BG adsorption (Table 4.19) on the Cs/Gly-Ma-Tk's surface shows superior alignment with the PSO model, indicated by higher R^2 values and closer calculated q_e values to the experimental q_e values, in contrast to the PFO model. This suggests that chemisorption is the predominant mechanism governing the adsorption of BG on the Cs/Gly-Ma-Tk surface [316].

4.3.6.2 Isotherm Study of BG Removal by Cs/Gly-Ma-Tk

The equilibrium isotherm data is a crucial parameter for elucidating the interactions between BG molecules and the surface of Cs/Gly-Ma-Tk. Three commonly utilised isotherms, namely Langmuir, Freundlich and Temkin in their non-linear forms were used to elucidate the interactions between BG and Cs/Gly-Ma-Tk. Figure 4.32 and Table 4.20 provide the graphical plot of non-linear fits of the isotherm models to the adsorption equilibrium data and isotherm parameters calculation results, respectively. As shown in Table 4.20 and Figure 4.32, the Langmuir isotherm model exhibits the best fit to the equilibrium adsorption data and has the closest coefficient of determination (R^2) value to unity (R^2=0.97). Hence, it can be concluded that the Langmuir isotherm model better explains the adsorption process, indicating that the adsorption of BG dye

by Cs/Gly-Ma-Tk mainly occurs on the surface layer of the adsorbent [42]. Furthermore, the Freundlich model parameter n having a value greater than unity indicates the favourability of the adsorption process and the high affinity of Cs/Gly-Ma-Tk towards BG dye. The maximum monolayer adsorption capacity (q_{max}) of BG onto the surface of Cs/Gly-Ma-Tk is computed to be 88.3 mg/g at 25 °C.

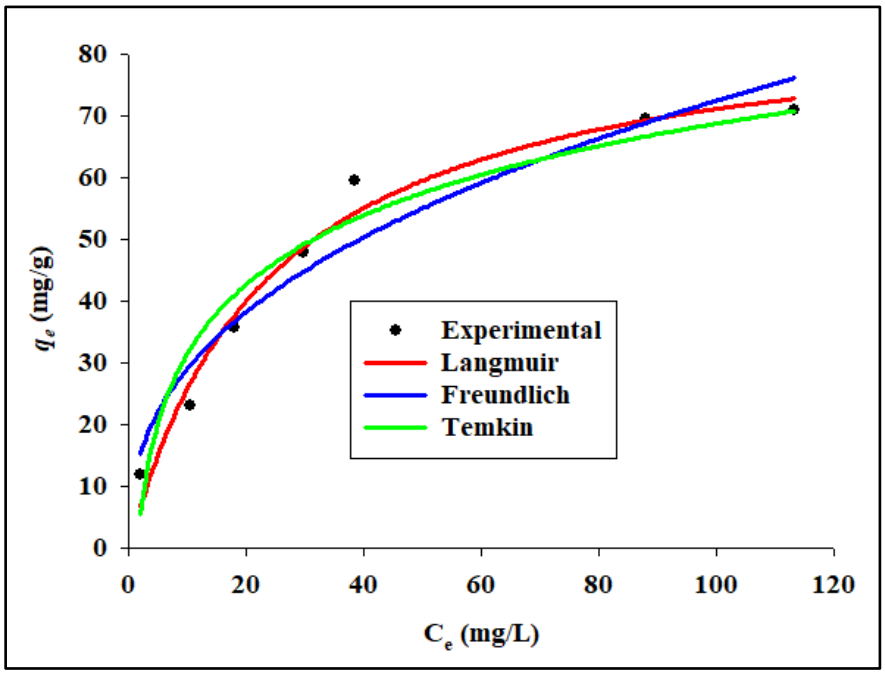


Figure 4.32 The Langmuir, Freundlich and Temkin Adsorption Isotherm Regression Fits of BG Dye Adsorption by Cs/Gly-Ma-Tk

Table 4.20
Isotherm Model Parameters for BG Adsorption by Cs/Gly-Ma-Tk

Adsorption isotherm	Parameter	Value
Langmuir	q_{max} (mg/g)	88.3
	K_a (L/mg)	0.04
	R^2	0.97
Freundlich	K_f (mg/g) (L/mg)$^{1/n}$	11.6
	n	2.51
	R^2	0.93
Temkin	K_T (L/mg)	1.49
	b_T (J/mol)	140
	R^2	0.93

4.3.6.3 Thermodynamic Study of BG Removal by Cs/Gly-Ma-Tk

to better understand the nature of BG dye adsorption by Cs/Gly-Ma-Tk and analyse the feasibility and spontaneity of the adsorption process, the thermodynamic parameters (ΔG^o: free Gibbs energy; ΔH^o: enthalpy change; ΔS^o: entropy change) were obtained through the slope and intercept of the van't Hoff plot (Figure 4.33) and the computed values are displayed in Table 4.21. The positive value of ΔH^o indicates the endothermic nature of the adsorption process, signifying that with the increase of temperature and the transfer of heat to the system the adsorption capacity of Cs/Gly-Ma-Tk towards BG increases. Moreover, the positive ΔS^o value obtained denotes the increase in randomness that occurs with the increase in the temperature. However, the positive ΔG^o values reveal the non-spontaneous nature of the process at low temperatures, meaning that for the adsorption process to be spontaneous higher temperatures are required.

Table 4.21
Thermodynamic Parameters of BG Removal by Cs/Gly-Ma-Tk

Temperature (K)	K_d	ΔG (kJ/mol)	ΔH (kJ/mol)	ΔS (J/mol.K)
298.15	0.19	4.04	11.9	26.7
308.15	0.23	3.77		
318.15	0.28	3.50		
328.15	0.30	3.23		

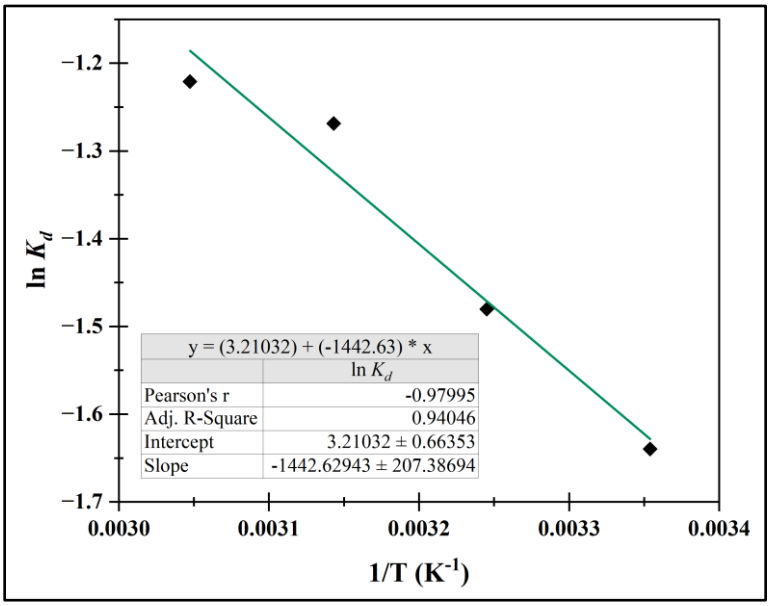


Figure 4.33 The Van't Hoff Plot of the Equilibrium Thermodynamic Data for BG Adsorption by Cs/Gly-Ma-Tk

4.3.7 Proposed Mechanism of BG Removal by Cs/Gly-Ma-Tk

The findings of all analyses performed on Cs/Gly-Ma-Tk were utilised to identify the interactions contributing to the adsorption of BG onto Cs/Gly-Ma-Tk (plausible pathways to adsorption presented in Figure 4.34). The abundance of surface functional groups identified through FT-IR analysis displayed reductions in peak intensities after the adsorption of BG dye, indicating their involvement in the adsorption process. In pH values higher than pH_{pzc} (as pH_{pzc} was found to be 3.2, all pH ranges in this study are higher than pH_{pzc}) the surface functional groups become deprotonated and gain a negative charge allowing the formation of ionic bonds through electrostatic attractions with the positively charged cationic species BG dye molecules. Furthermore, the abundance of O-H and N-H groups available on the matrix of Cs/Gly-Ma-Tk would create the opportunity for the formation of hydrogen bonds through dipole-dipole attractions between the H atoms of these groups and the electronegative nitrogen atoms in the structure of the BG dye molecules. Moreover, the electronegative N atoms in the structure of Cs/Gly-Ma-Tk can create an electron donor/acceptor system with the aromatic rings in the structure of BG dye molecules and further enhance the adsorption capabilities of Cs/Gly-Ma-Tk through n-π stacking. Additionally, Yoshida hydrogen bonds can be created between the aromatic rings of the BG dye molecules and the H atoms in the hydroxyl groups of Cs/Gly-Ma-Tk to allow for more adsorption opportunities.

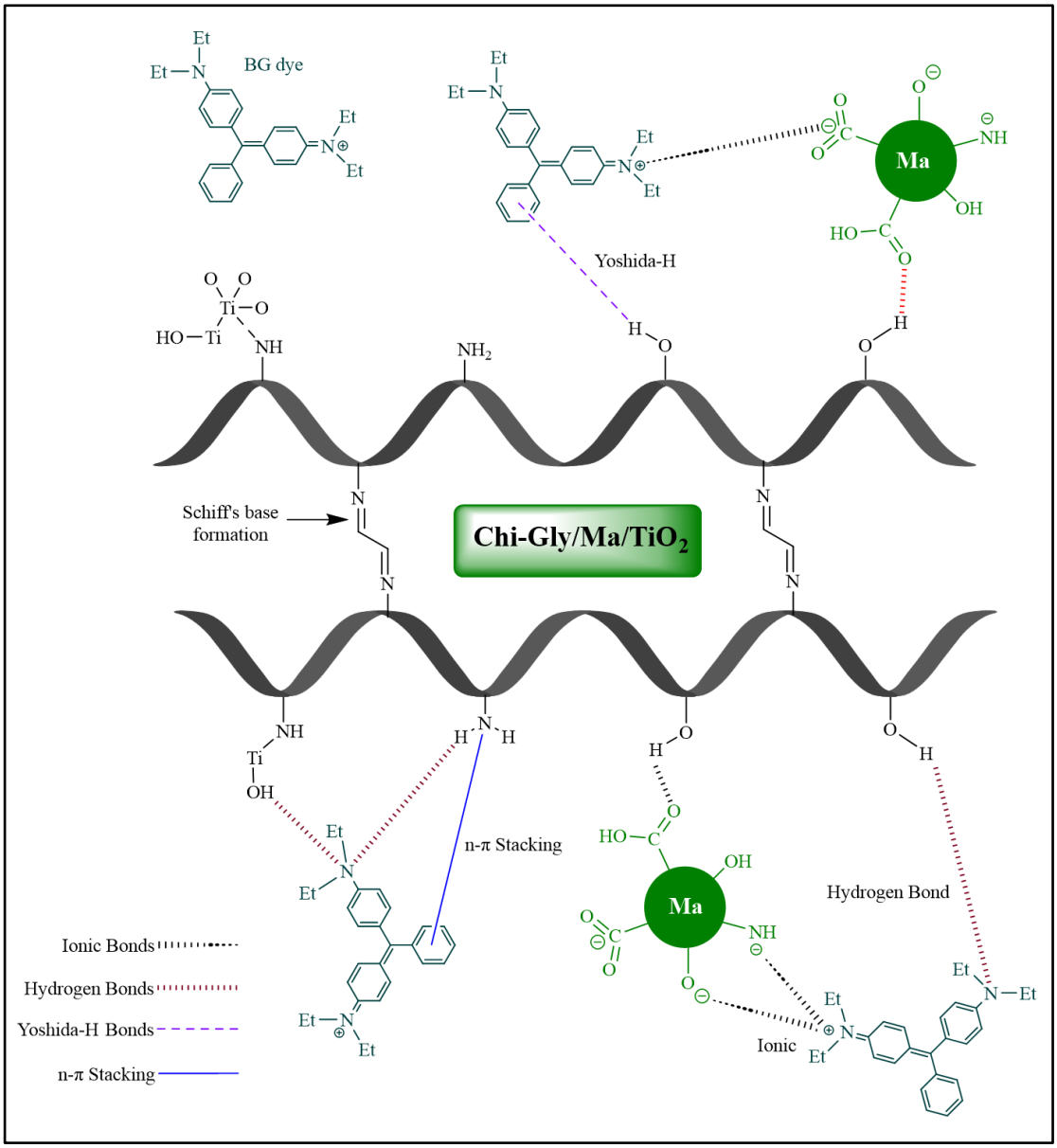


Figure 4.34 Illustration of the Plausible Interactions Contributing to the Adsorption of BG Dye by Cs/Gly-Ma-Tk

4.4 Benzil Crosslinked Cs-Ma-Tk (Cs/Bz_2-Ma-Tk)

In this section, a new composite material of Chitosan- Microalgae- Kronos TiO_2 was synthesised and put through a hydrothermal grafting process to create benzil-crosslinked Chitosan- Microalgae- Kronos TiO_2 (henceforth referred to as Cs/Bz_2-Ma-Tk) for the adsorption of brilliant green dye. The use of biodegradable and abundantly available resources in this study is an effort to achieve a cost-efficient and biofriendly adsorbent with high efficiency towards the removal of pollutants (specifically BG dye in this study) from effluents. The addition of Tk and Ma would help alleviate chemical instability and low affinity of Cs towards cationic pollutant species, while the Schiff's base reaction occurring during the grafting process would further enhance the structural stability of the resultant composite. The dye removal conditions (adsorbent dosage, pH, contact time) have been optimised using RSM-BBD methodology and the optimal conditions have been applied for kinetic, isotherm, and thermodynamic studies. Based on the findings of the analyses, a plausible adsorption mechanism has been proposed.

4.4.1 Surface Properties of Cs/Bz_2-Ma-Tk

The surface area and pore structure of Cs/Bz_2-Ma-Tk were analysed using the Brunauer, Emmett, and Teller (BET) method and tabulated in Table 4.22. The specific surface area of Cs/Bz_2-Ma-Tk was found to be 1.32 (m^2/g) with a pore volume of 0.11 (cm^3/g). On the other hand, the average pore diameter observed for Cs/Bz_2-Ma-Tk is 34.42nm, which places Cs/Bz_2-Ma-Tk in the category of mesoporous (2nm < pore width < 50nm) materials according to IUPAC (International Union of Pure and Applied Chemistry) [328]. With the increase in pore diameter, there would be more space available within the porous structure of Cs/Bz_2-Ma-Tk to capture BG dye molecules resulting in higher physisorption capabilities of the adsorbent. Furthermore, the N_2 adsorption/desorption isotherm of Cs/Bz_2-Ma-Tk was plotted and exhibited in Figure 4.35 which is found to be compatible with type IV physisorption isotherm with an H3 hysteresis loop which further affirms the mesoporous nature of the adsorbent. Furthermore, the elemental analysis of Cs/Bz_2-Ma-Tk revealed the carbon (C), hydrogen (H), nitrogen (N), Sulphur (S), and oxygen (O; by difference) content of the adsorbent (Table 4.22).

Table 4.22
Surface Properties and Elemental Composition of Cs/Bz_2-Ma-Tk

Parameters	Cs/Bz_2-Ma-Tk
Surface Area (m^2/g)	1.32
Pore Volume (cm^3/g)	0.11
Average Pore Diameter (nm)	34.42
Carbon	34.15%
Hydrogen	4.76%
Nitrogen	4.22%
Oxygen (by difference) (%)	56.87%

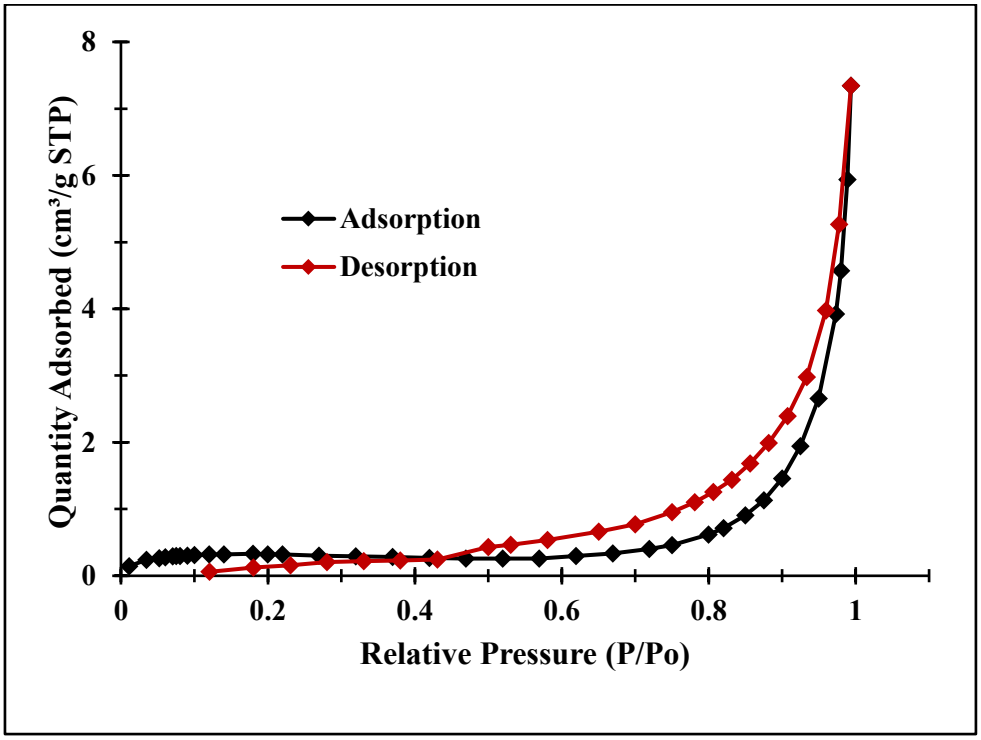


Figure 4.35 N_2 Adsorption/Desorption Plot of Cs/Bz_2-Ma-Tk

4.4.2 X-Ray Diffraction Analysis of Cs/Bz_2-Ma-Tk

The XRD pattern of Cs/Bz_2-Ma-Tk was obtained (Figure 4.36) to confirm the successful incorporation of Ma and Tk on the polymeric matrix of CS, as well as the Schiff base reaction with Bz_2 through the study of the crystalline structure of the composite. The peaks observed at $2\theta \approx 10°$ and $2\theta = 20.2°$ in Figure 4.36 are the characteristic peaks of (020) and (110) crystalline planes of Cs [329]. The peak at $2\theta \approx 10°$ appears as a minor reflection which is attributed to the effect of crosslinking with Bz_2. The peaks observed at $2\theta = 25.6°$, 38.3°, 48.2°, 54.4°, 55.2°, 63°, 70.2°, 75.5°, and

83.3° correspond to the (101), (004), (200), (105), (211), (213), (220), (215) and (224) crystalline planes of TiO_2 [282], [283], [284], respectively, further confirming the successful incorporation of the compositing materials in the polymeric matrix of CS. Furthermore, the reflection at 2θ = 18.2° is associated with the (003) crystalline plane of Bz_2, which affirms the success of the crosslinking process[330].

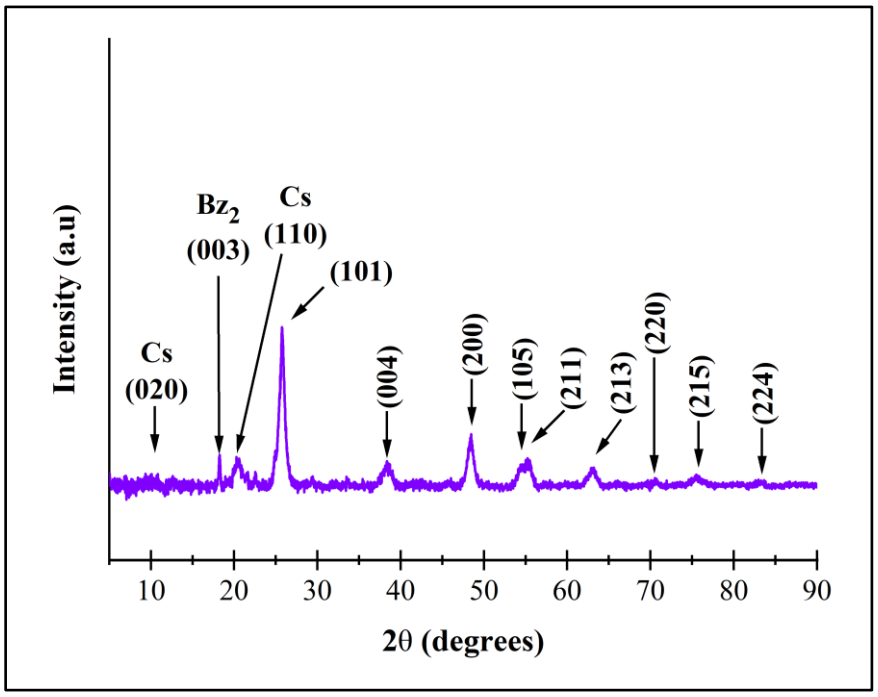


Figure 4.36 XRD Pattern of Cs/Bz_2-Ma-Tk

4.4.3 FT-IR Spectrum Analysis of Cs/Bz_2-Ma-Tk

In order to identify the functional groups available on the surface of Cs/Bz_2-Ma-Tk as well as to better understand the possible pathways to adsorption the analysis of the FT-IR spectra is a crucial step. Figure 4.37 displays the FT-IR spectra of Cs/Bz_2-Ma-Tk before (Figure 4.37a) and after (Figure 4.37b) BG dye adsorption. The peaks observed in the region of 3600-3200 cm^{-1} are attributed to the stretching vibrations of hydroxyl (-OH) and amine (-NH) functional groups, and the twin peaks observed at 2920 cm^{-1} and 2860 belong to the symmetric and asymmetric stretching vibrations of C-H of the aliphatic groups, respectively [131], [132]. Furthermore, various bands were observed in both spectra in Figure 4.37 at 1650 cm^{-1} (carbonyl (C=O) stretching vibrations in carboxylic acids, esters, etc.), 1381 cm^{-1} (vibrations of -P-O groups in Ma), 1157 cm^{-1} (asymmetric stretching vibrations of the C-O-C bridge), 1077 cm^{-1}

(stretching vibrations of C-O), 897 cm^{-1} (bending vibrations of C-H), and 797 cm^{-1} (Ti-O vibrations of Tk) [132], [133], [309], [331]. Furthermore, the sharp band located at 1650 is associated with the presence of C=N groups, which confirms the occurrence of Schiff base reaction and formations of imine groups. From Figure 4.37a and b, it can be observed that BG dye adsorption by Cs/Bz_2-Ma-Tk caused the intensity of the broad band in 3600-3200 region, characteristic of O-H and N-H to be dramatically reduced, indicating the involvement of these functional groups in the process of BG adsorption. Furthermore, the adsorption process caused a reduction in intensity and shifts in some bands (as highlighted in Figure 4.37), indicating their involvement in the adsorption process.

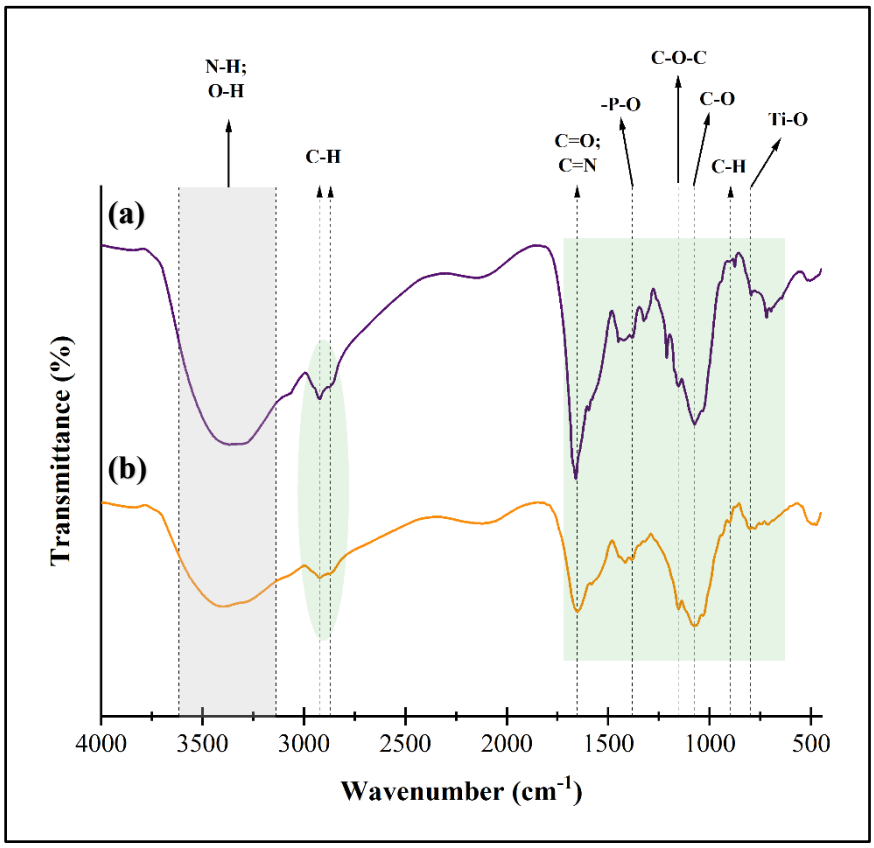
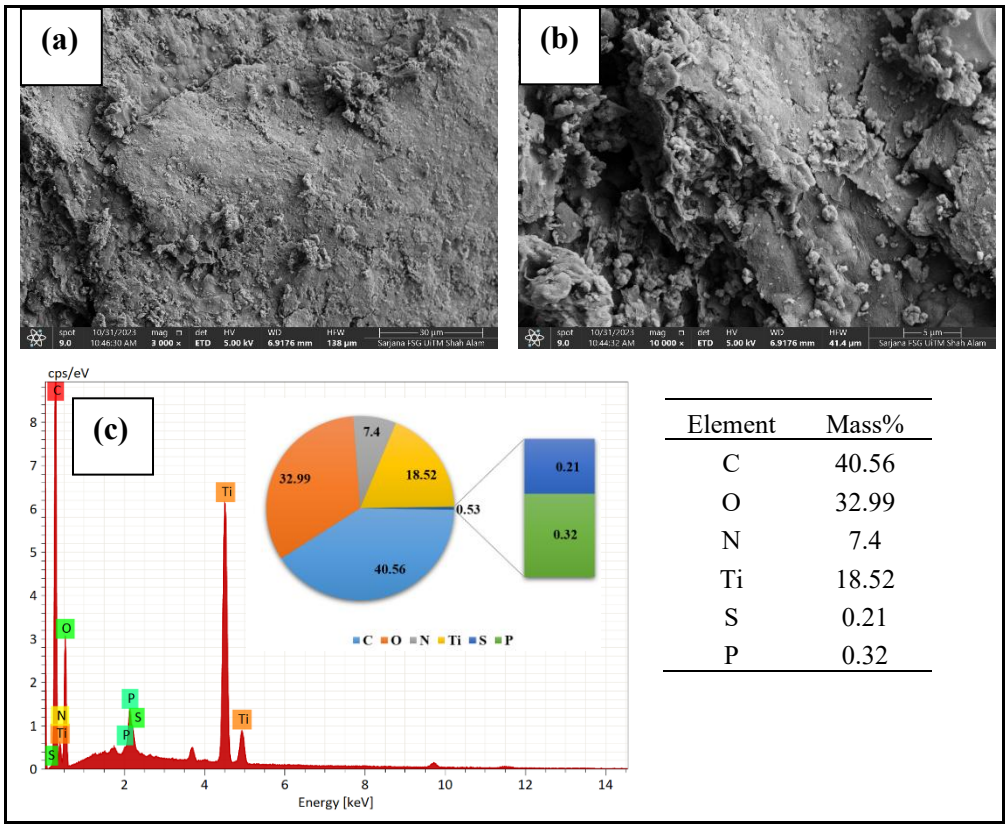


Figure 4.37 FT-IR Spectra of Cs/Bz_2-Ma-Tk (a) Before and (b) After BG Dye Adsorption

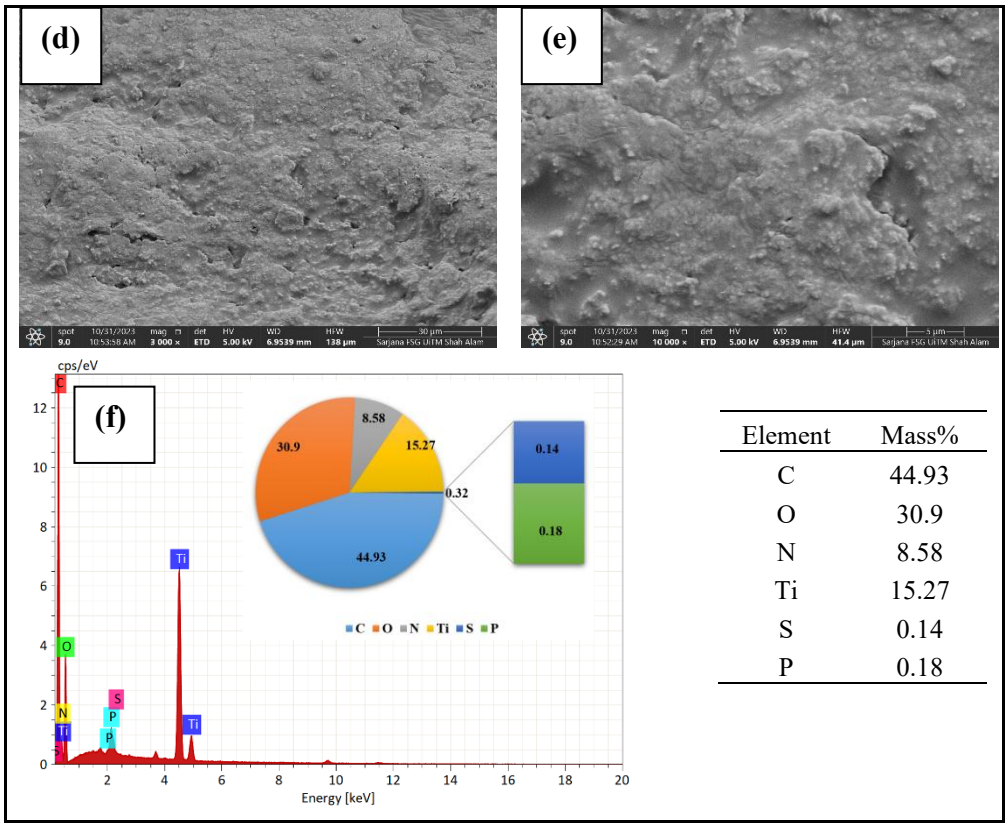
4.4.4 Surface Morphology of Cs/Bz_2-Ma-Tk

The surface topography and elemental composition on the surface of Cs/Bz_2-Ma-Tk were analysed using FE-SEM/EDX and the obtained images at two

magnification powers (3kx and 10kx) as well as the EDX data are displayed in Figure 4.38a-f. The surface images of Cs/Bz_2-Ma-Tk (Figure 4.38a and b) appear rugged with the presence of cracks and crevices whereas after BG dye adsorption (Figure 4.38d and e) the surface appears to have been coated with BG dye molecules appearing as an even surface. The EDX data of Cs/Bz_2-Ma-Tk before (Figure 4.38c) and after (Figure 4.38f) BG dye adsorption reveals an increase in C and N content while the contents of the other elements display a reduction in value. This observation is in line with the elemental composition of the BG dye molecules where they mainly consist of C and N atoms.



Element	Mass%
C	40.56
O	32.99
N	7.4
Ti	18.52
S	0.21
P	0.32



Element	Mass%
C	44.93
O	30.9
N	8.58
Ti	15.27
S	0.14
P	0.18

Figure 4.38 FE-SEM Images at Two Magnification Powers of 3kx (a and d) and 10kx (b and e) of (a-b) Cs/Bz$_2$-Ma-Tk and (d-e) Cs/Bz$_2$-Ma-Tk After BG Adsorption and EDX Mapping of (c) Cs/Bz$_2$-Ma-Tk and (f) Cs/Bz$_2$-Ma-Tk After BG Dye Adsorption

4.4.5 Statistical Optimisation and Analysis

4.4.5.1 Experimental Design and Process Optimisation for BG dye Removal by Cs/Bz$_2$-Ma-Tk

Three main parameters affecting the process of BG adsorption onto Cs/Bz$_2$-Ma-Tk; namely A: Cs/Bz$_2$-Ma-Tk dosage (g/100 mL of BG dye solution), B:pH of the adsorption media, and C: contact time (min) were used as input variables to maximise the yield (BG dye removal%) using Box Behnken design (BBD) from Response Surface Methodology (RSM). The parameters affecting the BG dye removal outcome and their effective range were determined during preliminary experiments and a three level three factor design from BBD-RSM from computer software Design Expert (ver. 13, Stat-Ease, USA) was selected as the efficient model in this study. The three levels of the input variables for Cs/Bz$_2$-Ma-Tk (tabulated in Table 4.23) were used by the software to generate 17 experimental runs to determine the statistical importance of the

independent variables on the BG dye removal outcome as well as achieving the optimal conditions for the highest BG dye removal value.

Table 4.23
Three Levels of the Three Independent Variables in the Removal of BG Dye by Cs/Bz_2-Ma-Tk

Factor name	Factor code	Level of factor		
		-1	0	1
Cs/Bz_2-Ma-Tk Dose (g/100mL)	A	0.02	0.06	0.1
pH	B	4	6.5	9
Time (min)	C	10	35	60

The generated experimental design for Cs/Bz_2-Ma-Tk is presented in Table 4.24, with the experimentally obtained and model predicted values for BG dye removal tabulated. The optimal experimental conditions were obtained through performing a desirability test on the BBD suggested parameter values with the goal of maximising the response (BG dye removal %). The suggested optimal variable values (Cs/Bz_2-Ma-Tk dose=0.09 g/100 mL; pH=8.5; time=45min; Figure 4.39) were evaluated three times to verify the consistency of the acquired results and tabulated in the last row of Table 4.24.

Table 4.24 BBD
Design Coded and Actual Values Alongside Predicted and Experimental Response for BG Removal by Cs/Bz_2-Ma-Tk (with Desirability Test Results (Last Row)

Run	Coded Values			Actual values			Removal of BG (%)	
	A	B	C	A	B	C	Observed	Predicted
1	-1	-1	0	0.02	4	35	27.1	27.4
2	+1	-1	0	0.1	4	35	56.9	56.8
3	-1	+1	0	0.02	9	35	64.5	64.6
4	+1	+1	0	0.1	9	35	95.5	95.2
5	-1	0	-1	0.02	6.5	10	40.2	40.3
6	+1	0	-1	0.1	6.5	10	68.3	68.7
7	-1	0	+1	0.02	6.5	60	62.1	61.7
8	+1	0	+1	0.1	6.5	60	93.4	93.3
9	0	-1	-1	0.06	4	10	35.6	35.3
10	0	+1	-1	0.06	9	10	68.5	68.3
11	0	-1	+1	0.06	4	60	53.4	53.5
12	0	+1	+1	0.06	9	60	95.9	96.2

Run	Coded Values			Actual values			Removal of BG (%)	
	A	B	C	A	B	C	Observed	Predicted
13	0	0	0	0.06	6.5	35	64.2	64.1
14	0	0	0	0.06	6.5	35	65.1	64.1
15	0	0	0	0.06	6.5	35	63.8	64.1
16	0	0	0	0.06	6.5	35	64.7	64.1
17	0	0	0	0.06	6.5	35	62.9	64.1
Desirability test run				0.089	8.46	45.5	93.4±1.6	96.1

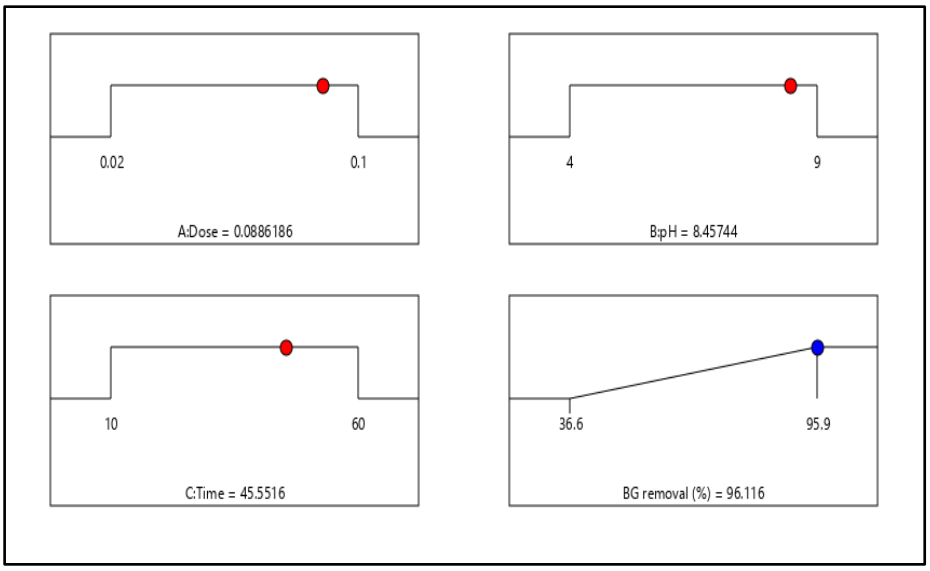


Figure 4.39 Desirability Ramps of BG Removal by Cs/Bz$_2$-Ma-Tk

4.4.5.2 Statistical Analysis of BG Removal by Cs/Bz$_2$-Ma-Tk

ANOVA test was conducted on the data obtained from the experimental design to confirm the validity of the acquired adsorption models and analyse the effect of the model terms on the response (BG dye removal %). The ANOVA test results for BG dye removal by Cs/Bz$_2$-Ma-Tk are reported in Table 4.25. The acquired model for BG removal by Cs/Bz$_2$-Ma-Tk reveals an F-value of 1260.13 (with p-value <0.0001), confirming the validity of the generated model to represent the experimental data. Generally, model terms with p-values lower than 0.05 are statistically significant on the output (response value) [332]. Furthermore, the reported R^2 value of 0.9994 affirms the accuracy of the model to predict the response. To further confirm the validity of the acquired model to describe the experimentally obtained results, the p-value obtained for Lack-of-Fit renders it statistically insignificant.

Table 4.25
ANOVA Test Results for BG Removal by Cs/Bz_2-Ma-Tk

Source	Sum of Squares	df	Mean Square	F-value	p-value	Significance
Model	5811.56	9	645.73	1260.13	<0.0001	*
A-Dose	1806.01	1	1806.01	3524.40	<0.0001	*
B-pH	2865.25	1	2865.25	5591.50	<0.0001	*
C-Time	1062.60	1	1062.60	2073.66	<0.0001	*
AB	0.3600	1	0.3600	0.7025	0.4296	#
AC	2.56	1	2.56	5.00	0.0605	#
BC	23.04	1	23.04	44.96	0.0003	*
A^2	0.2527	1	0.2527	0.4932	0.5052	#
B^2	35.29	1	35.29	68.87	<0.0001	*
C^2	18.66	1	18.66	36.41	0.0005	#
Residual	3.59	7	0.5124			
Lack of Fit	0.6950	3	0.2317	0.3204	0.8116	#
Pure Error	2.89	4	0.7230			
Cor Total	5815.14	16				

R^2 = 0.9994, * significant; # not significant.

According to Table 4.25, all individual model terms (A, B, and C) are statistically significant and affect the response value, whereas only the interactive effect of pH*time (BC) is statistically significant. Regarding the squared effect of variables, only B^2 displays statistical significance. Hence, based on the significant model terms, a 2^{nd} order polynomial expression was generated to predict the BG dye removal by Cs/Bz_2-Ma-Tk response (4.7).

$$\text{BG Removal (\%)} = 64.14 + 15.03A + 18.93B + 11.53C + 2.40BC - 2.90B^2 \quad (4.7)$$

To further confirm the ability of the generated model to predict the response values accurately, additional analytical graphs were obtained from BBD and analysed (as displayed in Figure 4.40).

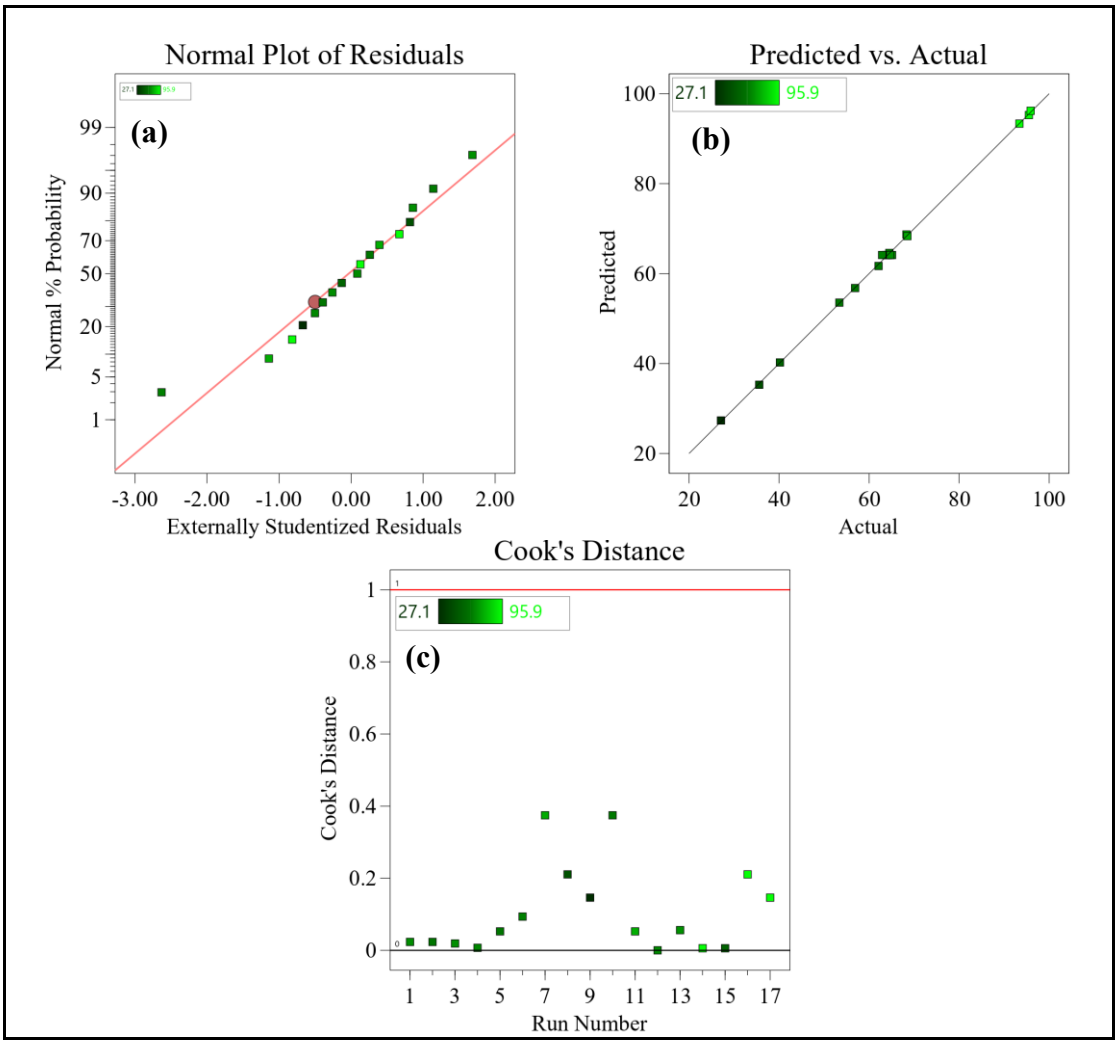


Figure 4.40 BBD Plots of (a) Normal Plot of Residuals, (b) Predicted vs. Actual, and (c) Cook's Distance; for BG Removal by Cs/Bz$_2$-Ma-Tk

The regular and precise distribution of the data points on the normal probably of residuals plot further confirms the suitability of the proposed models due to the normal distribution of errors and independence of the residuals (Figure 4.40a). The plot displaying the predicted vs. actual response values also affirms the reliability of the proposed model to accurately predict the response values as the data points are closely aligned near the linear regression line for (Figure 4.40b). Furthermore, the plot of Cook's distance was used to further validate the model and as it can be observed all data points in the Cook's distance plot are lower than unity (Figure 4.40c), providing further affirmation towards the suitability of the proposed model.

4.4.5.3 Individual Impact of Variables

The impact of individual input variables on the response (BG removal %) was analysed and the obtained plots are exhibited in Figure 4.41. It can be observed that all variables have a synergistic effect on the BG dye removal response, and the increase in all individual variables causes an increase in the response value.

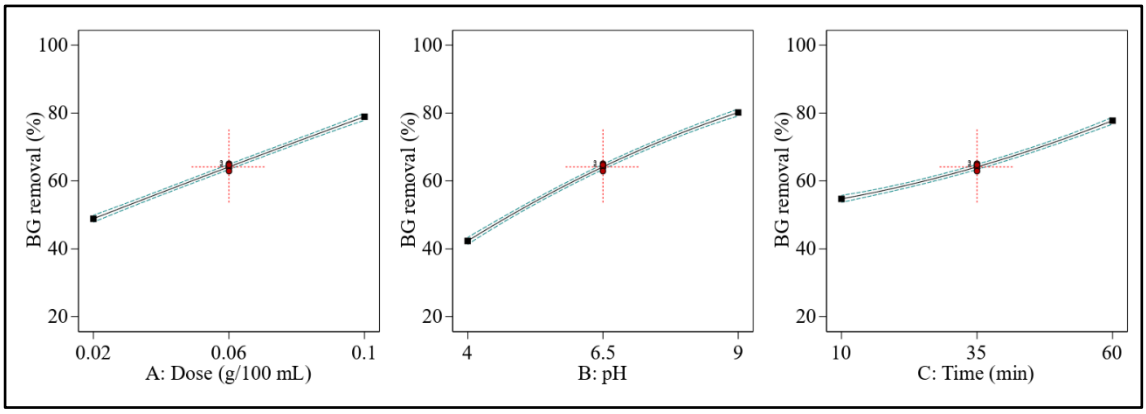
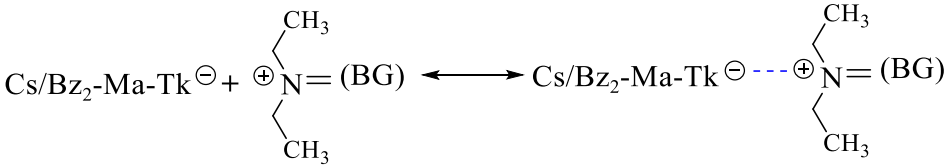


Figure 4.41 The Impact of Independent Variables on BG Removal Response by Cs/Bz$_2$-Ma-Tk

As the mass of adsorbent available in the dye solution increases, more active adsorption sites become available for the capture of BG dye molecules, hence the observed increment in the response value with the increase of Cs/Bz$_2$-Ma-Tk dosage can be explained. pH appears to have the highest impact on the BG removal response values, which is due to the changes occurring to the surface charge of the adsorbent in different pH values. For this purpose, pH_{pzc} (point of zero charge) experiments were performed to determine the point at which the surface is devoid of charge and the pH_{pzc} of Cs/Bz$_2$-Ma-Tk was found to be 7.3 (Figure 4.42). Hence, at pH values higher than 7.3 the surface of Cs/Bz$_2$-Ma-Tk acquires a negative charge resulting in the formation of electrostatic bonds between the adsorbent and BG dye molecules. Furthermore, in pH values lower than pH_{pzc}, the surface of the adsorbent is positively charged, causing electrostatic repulsion to occur between the adsorbent and the BG dye molecules, hence hindering the adsorption process. Consequently, with the increase in pH value, even in values lower than pH_{pzc}, as the positive surface charge becomes weaker, the effect of electrostatic repulsion lowers, allowing for more adsorption of BG dye molecules to

occur. The electrostatic attractions between Cs/Bz$_2$-Ma-Tk and BG dye molecules are illustrated in (4.8).



(4.8)

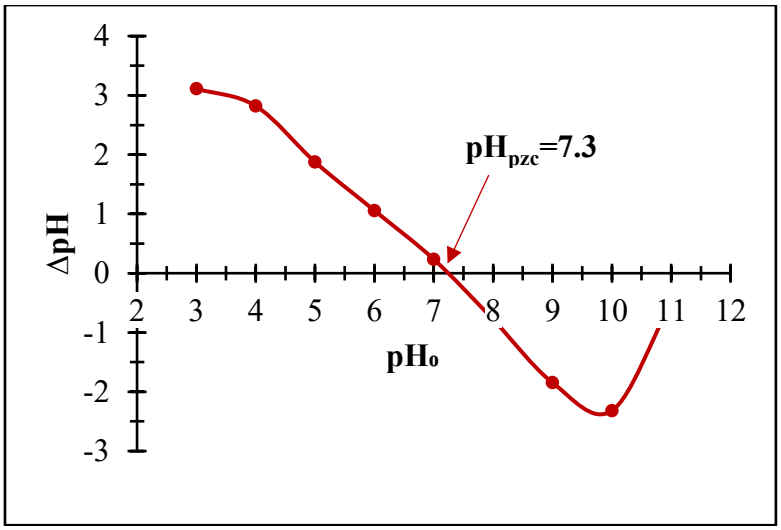


Figure 4.42 pH$_{pzc}$ Plot of Cs/Bz$_2$-Ma-Tk

Furthermore, the time variable appears to have a continuous impact on the response value (Figure 4.41). The process of adsorption of BG dye by Cs/Bz$_2$-Ma-Tk requires sufficient time to allow for the dye molecules to penetrate the porous structure of the adsorbent, hence as the contact time between the adsorbent and the dye solution increases, a continuous increment in response value is observed.

4.4.5.4 Interactive Impact of Variables

The pair of variables with statistically significant interactive impact on BG removal response by Cs/Bz$_2$-Ma-Tk (pH*time) are exhibited in the 3D surface plot and 2D contour displayed in Figure 4.43. The interactive effect of pH and time (the pair of variables with statistically significant interactive impact on BG removal response by Cs/Bz$_2$-Ma-Tk according to the ANOVA test) is portrayed in the 3D surface plot (Figure 4.43a) and 2D contour (Figure 4.43b), while Cs/Bz$_2$-Ma-Tk is kept constant at 0.06

g/100mL. The increment in pH value from 4 to 9, while time kept constant at 10min, causes the BG removal to increase from 35.6% to 68.5%, and increasing contact time between Cs/Bz$_2$-Ma-Tk and BG dye solution from 10 to 60 min, with pH kept constant at 4, allows the increase of BG removal from 35.6% to 53.4%. However, the simultaneous raise of pH and time variables causes the BG removal response value to soar to 95.9%.

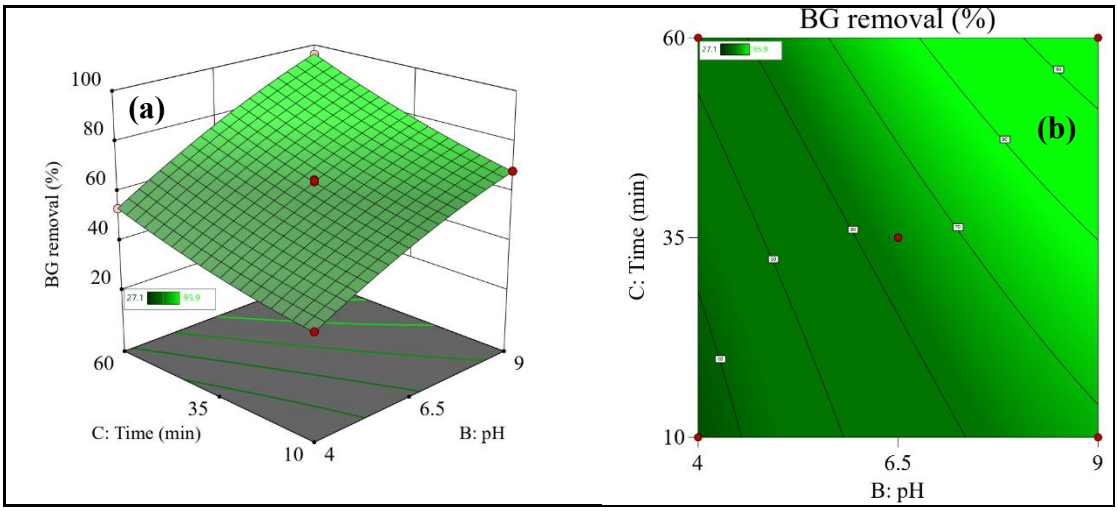


Figure 4.43 3D Plot and 2D Contour of Interactive Impact of pH and Time for BG Dye Removal Response by Cs/Bz$_2$-Ma-Tk

4.4.6 Adsorption Equilibrium Studies of BG Removal by Cs/Bz$_2$-Ma-Tk

4.4.6.1 Initial BG Concentration and Kinetic Study of BG Removal by Cs/Bz$_2$-Ma-Tk

Adsorption equilibrium studies were performed by conducting batch adsorption studies using various initial BG dye concentrations to obtain the adsorption capacity of Cs/Bz$_2$-Ma-Tk towards BG dye using the optimal operating conditions obtained through desirability test (Cs/Bz$_2$-Ma-Tk dose=0.09 g/100mL; pH=8.5). Figure 4.44 displays the adsorption capacity of Cs/Bz$_2$-Ma-Tk at different time intervals for varying initial concentrations of BG dye (20, 50, 80, 120, 150, 200, 250 mg/L). It is observed that the rise in the initial concentration of the BG dye causes an incremental growth in the adsorption capacity, from 27.62 to 269.9 mg/g with the increase of initial concentration of BG dye from 20 to 250 mg/L. This phenomenon can be attributed to the driving force

created at higher BG dye concentrations, allowing better pore diffusion and thus exhibiting higher adsorption capacities [333].

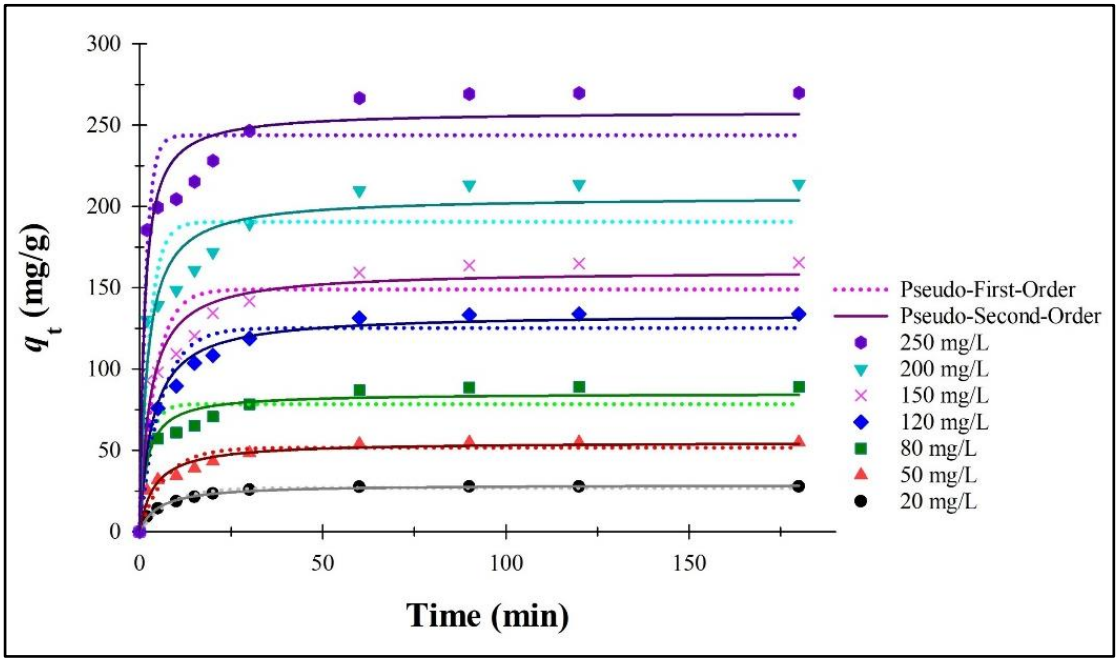


Figure 4.44 Impact of Initial Dye Concentration and Kinetic Model Regressions of BG Dye Removal by Cs/Bz$_2$-Ma-Tk

Furthermore, Figure 4.44 also exhibits the non-linear regression fits of Pseudo-First Order (PFO) and Pseudo-Second-Order (PSO) kinetic models to the experimentally obtained results. Additionally, the model terms of PFO and PSO kinetic models for BG dye removal by Cs/Bz$_2$-Ma-Tk were computed and reported in Table 4.26. The obtained data in Table 4.26 reveals the better compatibility of the experimental data with the PSO kinetic model, as the R^2 values of the PSO model at all initial BG dye concentrations are higher than their PFO counterparts and the $q_{e\ exp}$ (experimentally obtained adsorption capacity) values at all initial dye concentrations are closer in value to $q_{e\ cal}$ (calculated adsorption capacity) values of the PSO model. Hence, PSO kinetic model appears to be a better fit for the process of BG dye adsorption by Cs/Bz$_2$-Ma-Tk and it can be concluded that the adsorption process occurs mainly through chemisorption, meaning the main factor in the adsorption of BG dye by Cs/Bz$_2$-Ma-Tk is the presence of the active functional groups which can facilitate the adsorption process through electron sharing with BG dye molecules [70].

Table 4.26
PFO and PSO Kinetic Models' Terms for the Removal of BG Dye by Cs/Bz$_2$-Ma-Tk

Concentration (mg/L)	$q_{e.exp}$ (mg/g)	PFO			PSO		
		$q_{e.cal}$ (mg/g)	k_1 (1/min)	R^2	$q_{e.cal}$ (mg/g)	$k_2 \times 10^{-2}$ (g/mg min)	R^2
20	27.6	26.9	0.13	0.98	28.9	0.70	0.99
50	54.9	51.6	0.15	0.89	55.2	0.45	0.96
80	89.1	78.4	0.41	0.82	85.1	0.58	0.92
120	133.9	125.3	0.17	0.90	134.2	0.21	0.97
150	165.5	149.1	0.24	0.84	160.6	0.22	0.94
200	213.9	190.6	0.38	0.85	206.1	0.23	0.94
250	269.9	243.8	0.60	0.89	258.5	0.32	095

4.4.6.2 Isotherm Study of BG Removal by Cs/Bz$_2$-Ma-Tk

The adsorption equilibrium data were further utilised to investigate the compatibility of the experimental data with Langmuir, Freundlich, and Temkin isotherm models. The regression plots of the isotherm models are presented in Figure 4.45, while the isotherm model parameters for the removal of BG dye by Cs/Bz$_2$-Ma-Tk are reported in Table 4.27. The data obtained from Table 4.27 reveals the compatibility of the adsorption process with Langmuir isotherm model (R^2 = 0.93), and therefore, it can be concluded that the BG dye adsorption by Cs/Bz$_2$-Ma-Tk follows a monolayer system on the surface of the adsorbent. Moreover, the monolayer maximum adsorption capacity (q_{max}) for BG dye adsorption by Cs/Bz$_2$-Ma-Tk was found to be 289.23 mg/g, which attests to the potential of Cs/Bz$_2$-Ma-Tk for application towards the removal of BG dye (as a model of cationic dye). The relatively high value of K_a (Langmuir isotherm constant; 0.39 L/mg) indicates the high affinity of Cs/Bz$_2$-Ma-Tk towards BG dye molecules, whereas the Freundlich isotherm parameter n having a value higher than unity (n=2.88) signifies the favourability of the adsorption process.

Table 4.27
Isotherm Model Parameters for BG Removal by Cs/Bz2-Ma-Tk

Adsorption isotherm	Parameter	Cs-Bz2/Ma/Tk
Langmuir	q_{max} (mg/g)	289.2
	K_a (L/mg)	0.39
	R^2	0.93
Freundlich	K_f (mg/g) (L/mg)$^{1/n}$	92.4
	n	2.88
	R^2	0.78
Temkin	K_T (L/mg)	3.52
	b_T (J/mol)	39.3
	R^2	0.90

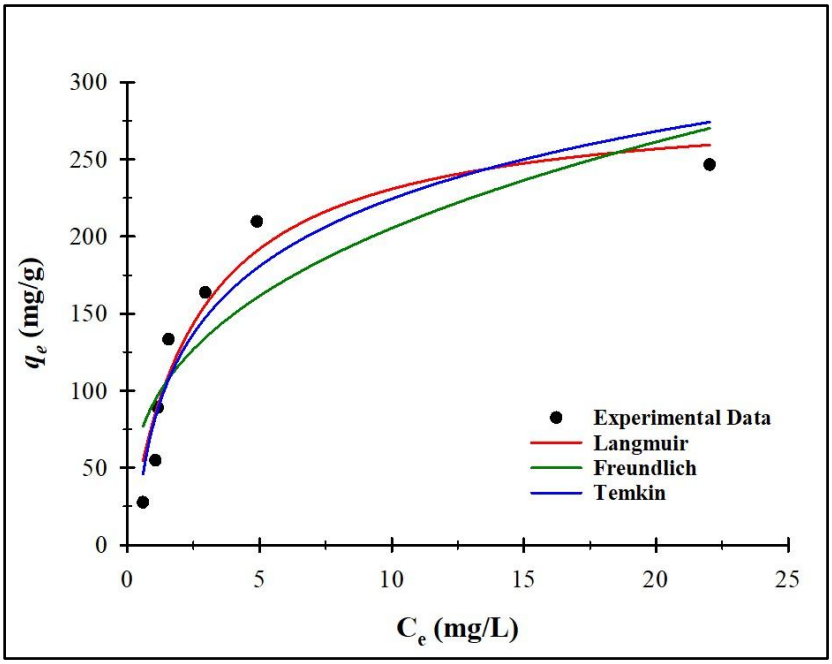


Figure 4.45 Langmuir, Freundlich and Temkin Isotherm Regressions for BG Removal by Cs/Bz2-Ma-Tk

4.4.6.3 Thermodynamic Study of BG Removal by Cs/Bz2-Ma-Tk

The feasibility and spontaneity of the adsorption process was investigated by conducting thermodynamic studies. Thermodynamic experiments were conducted using the optimal adsorption conditions acquired through desirability test in four working temperatures (298.15, 308.15, 318.15, and 328.15 K) and the slope and intercept of the van't Hoff plot (exhibited in Figure 4.46) were used to calculate the

thermodynamic parameters, namely Gibbs free energy change ($\Delta G°$), entropy change ($\Delta S°$), and enthalpy change ($\Delta H°$), while the computed values of the thermodynamic parameters are reported in Table 4.28.

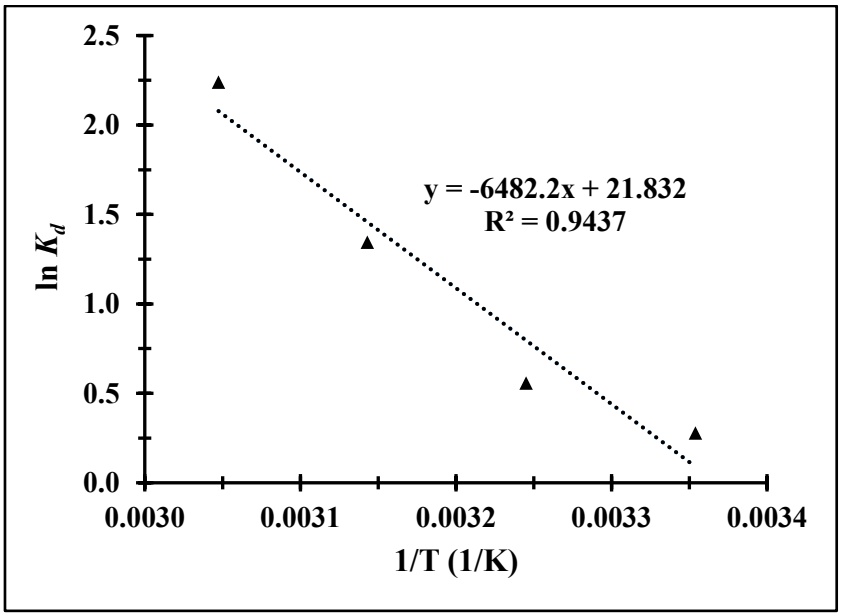


Figure 4.46 Van't Hoff Plot of BG Removal by Cs/Bz_2-Ma-Tk

The positive $\Delta H°$ value acquired denotes the endothermic nature of the adsorption process whereas the increase in temperature accelerates the rate of adsorption and the capacity of Cs/Bz_2-Ma-Tk towards BG dye due to the transfer of heat into the adsorption system. The positive value obtained for $\Delta S°$ reveals an increased disorder in the adsorbent/adsorbate interface occurring when raising the temperature of the adsorption environment. Additionally, the negative increase in $\Delta G°$ values when raising the temperature of the environment signifies that the adsorption process is spontaneous and feasible.

Table 4.28
Thermodynamic Parameters of BG Removal by Cs/Bz_2-Ma-Tk

Temperature (K)	ΔG (kJ/mol)	ΔH (kJ/mol)	ΔS (J/mol K)
298.15	-0.22	53.9	181.5
308.15	-2.04		
318.15	-3.85		
328.15	-5.67		

4.4.7 Proposed Mechanism of BG Removal by Cs/Bz_2-Ma-Tk

The FT-IR spectrum of Cs/Bz_2-Ma-Tk revealed the presence of various functional groups on the surface of the adsorbent, which have the capacity of acquiring negative charges when exposed to environments with pH lower than their pH_{pzc} values. Furthermore, it was observed that pH has the highest significance on the removal of BG dye by Cs/Bz_2-Ma-Tk and the significance of electrostatic attractions in BG dye removal was further explained. Moreover, the presence of the aforementioned functional groups detected in the FT-IR spectra of the adsorbent (amino NH_2 and hydroxyl OH) allows for the formation of hydrogen bonds between the nitrogen (N) atoms present in the chemical structure of BG dye molecules and the hydrogen (H) atoms of these functional groups in Cs/Bz_2-Ma-Tk. Furthermore, the aromatic rings available in the structure of BG dye can form Yoshida-H bonds with the H atoms of hydroxyl groups in Cs/Bz_2-Ma-Tk polymeric chains. Moreover, the N atoms of Cs/Bz_2-Ma-Tk can have n-π interactions with the aromatic groups of BG dye molecules in an electron donor/acceptor system. Additionally, the crosslinking reaction with Bz_2 facilitates formation of π-π interactions between the aromatic rings available in the structure of BG dye molecules and the aromatic rings of Bz_2. Figure 4.47 showcases the schematic of the plausible interactions that lead to the removal of BG dye by Cs/Bz_2-Ma-Tk.

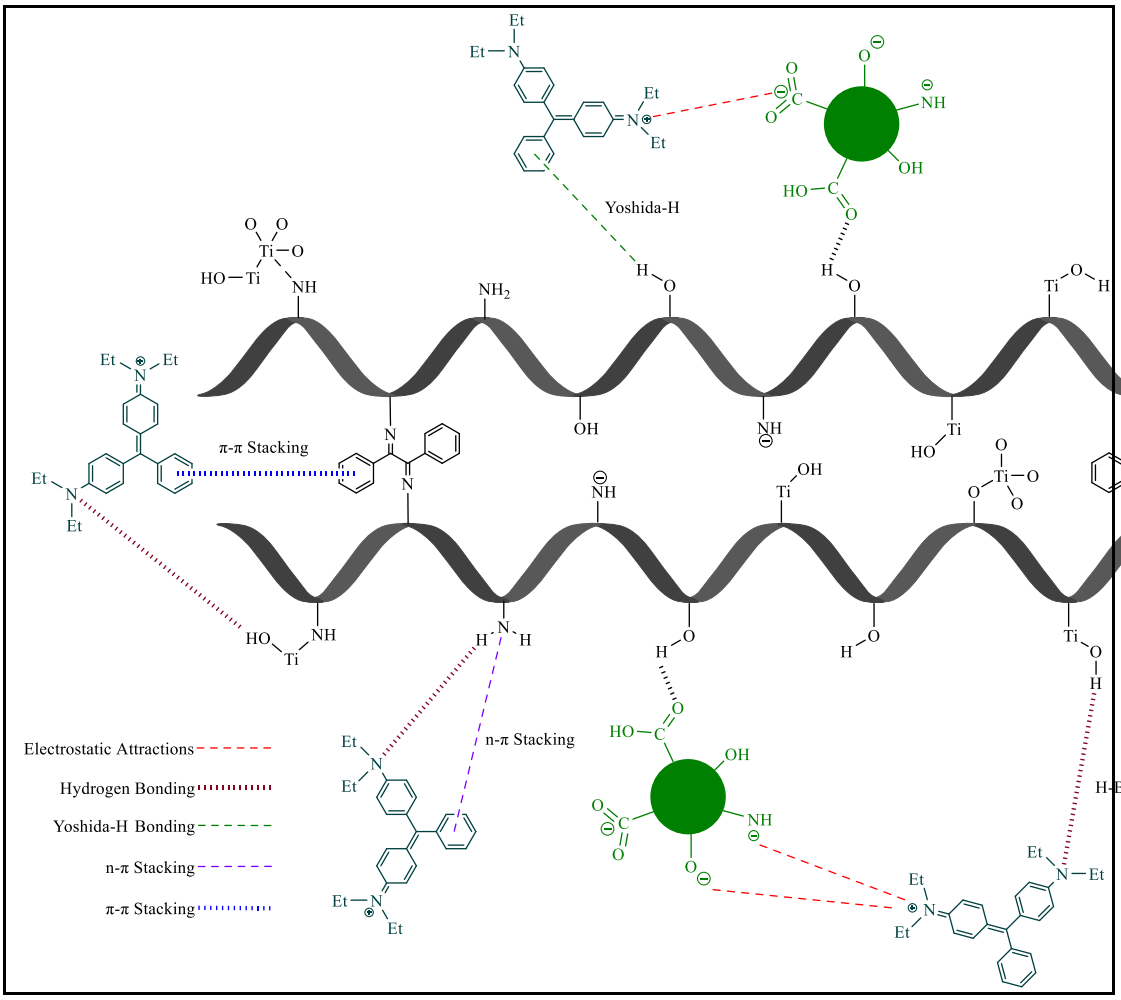


Figure 4.47 Suggested Mechanism of Adsorption for the Removal of BG Dye by Cs/Bz_2-Ma-Tk

4.5 Comparison

The comparison of the physicochemical properties and adsorption performance of the prepared composites provides insight into the influence of the modifying agents on the characteristics of the chitosan matrix. The results of various analysis performed on the four synthesised composites have been summarised in Table 4.29. The base composite, Cs-Ma-Tk, exhibited a BET surface area of 6.27 m^2/g and a Langmuir surface area of 18.02 m^2/g (see Appendix6), which serve as reference values for evaluating the effects of subsequent grafting and crosslinking modifications. Upon modification, Cs/SD-Ma-Tk and Cs/BD-Ma-Tk showed increased BET surface areas of 9.10 m^2/g and 8.77 m^2/g, respectively, indicating that the incorporation of these modifying agents contributed to the development of additional surface sites compared with the base composite. In contrast, Cs/Gly-Ma-Tk and Cs/Bz_2-Ma-Tk exhibited lower BET surface areas of 2.79 m^2/g and 1.32 m^2/g, suggesting that the structural arrangement of these modifiers may have partially reduced accessible surface area. In terms of pore characteristics, Cs-Ma-Tk displayed an average pore diameter of approximately 6.57 nm with a pore volume of 0.10 cm^3/g, indicating the presence of a mesoporous structure within the base composite. The modified composites showed variations in pore architecture, with Cs/Gly-Ma-Tk presenting a larger average pore diameter of 10.16 nm and Cs/Bz_2-Ma-Tk exhibiting a significantly larger pore diameter of 34.42 nm. These variations suggest that the grafting and crosslinking processes influence the spatial arrangement of the polymer chains and the resulting pore structure of the composites.

Elemental composition analysis further indicated that Cs-Ma-Tk contained 30.94% carbon, 5.04% hydrogen, and 5.70% nitrogen (see Appendix6), reflecting the typical elemental composition of the chitosan-based matrix. The modified composites generally showed higher carbon contents, particularly Cs/SD-Ma-Tk (40.35%) and Cs/BD-Ma-Tk (38.75%), which can be attributed to the incorporation of additional organic moieties during modification. These changes in elemental composition confirm the successful integration of the modifying agents into the chitosan framework.

The effects of grafting and crosslinking were also reflected in the adsorption performance of the materials. The base composite Cs-Ma-Tk exhibited a maximum adsorption capacity of 440.8 mg/g. A comparable adsorption capacity was observed for Cs/BD-Ma-Tk (441 mg/g), whereas Cs/SD-Ma-Tk demonstrated a significantly higher

adsorption capacity of 957.0 mg/g. The superior performance of Cs/SD-Ma-Tk may be attributed to the combined effects of increased surface area and the presence of additional functional groups introduced through salicylaldehyde grafting, which enhance the availability of active binding sites for dye molecules. Conversely, Cs/Gly-Ma-Tk exhibited a lower adsorption capacity of 88.3 mg/g, which can be attributed to the non-spontaneity of the adsorption process in lower temperatures for this material. Overall, the lower adsorption capacity obtained for the crosslinked Cs-Ma-Tk samples could be attributed to the higher rate of occupation on the $-NH_2$ functional groups on the backbone of Cs in the presence of crosslinking agents which limits the binding sites available for entrapping the BG dye molecules. Furthermore, glyoxal is the only reagent amongst the four used in this study lacking the presence of aromatic rings in its structure, which makes it unable to create π- π stacking attractions with the aromatic rings of the BG dye molecules. Hence the lower adsorption capacity observed for Cs/Gly-Ma-Tk can be attributed to the lack of aromatic rings in its structure as well. The higher adsorption capacity of Cs/SD-Ma-Tk over Cs/BD-Ma-Tk could be attributed to the extra hydroxyl group (-OH) in the structure of salicylaldehyde which can greatly attribute to the dye removal efficiency by providing more active binding sites. Overall, these results indicate that grafting tends to enhance surface accessibility and adsorption capacity, while crosslinking primarily improves structural stability but may reduce accessible surface area depending on the extent of network formation.

The kinetic model followed by all four modified adsorbents as well as the base adsorbent (Cs -Ma-Tk; see Appendix4) was the PSO model, hence it can be concluded that the adsorption of BG dye by the four modified Cs-Ma-Tk adsorbents happens through the process of chemisorption. The isotherm model analysis revealed that the adsorption process for Cs/SD-Ma-Tk occurs in a monolayer at the beginning which then proceeds into a multilayer system on the heterogenous surface of the adsorbent after the surface layer is saturated (similar to the unmodified ternary composite as shown in Appendix 5), while Cs/BD-Ma-Tk revealed a multilayered adsorption system altogether. However, the adsorption of BG dye by the crosslinked Cs-Ma-Tk derivatives (Cs/Gly-Ma-Tk and Cs/Bz_2-Ma-Tk) happens in a monolayered fashion. This observation can be attributed to the more rigid chemical structure obtained through the crosslinking process as the crosslinking agents bond with two active functional groups (of two different Cs chain or same Cs chain) and create a firm structure. The pH_{pzc} values obtained for the adsorbents are 7.3, 7, 6.9 and 3.2 for Cs/Bz_2-Ma-Tk, Cs/BD-

Ma-Tk, Cs/SD-Ma-Tk and Cs/Gly-Ma-Tk, respectively, while the unmodified Cs-Ma-Tk adsorbent exhibits a pH_{pzc} value of 7.4. The differences in the pH_{pzc} values can be attributed to the different structures of the modifying agents, where the glyoxal crosslinked Cs-Ma-Tk is the most conspicuous with a very low pH_{pzc}. The low pH_{pzc} obtained for Cs/Gly-Ma-Tk material makes it a very unique adsorbent to be employed for the removal of cationic species of contaminants in acidic environments without the need for pH adjustment. Furthermore, the optimised operation conditions for the four modified composite adsorbents once again differentiates the glyoxal crosslinked adsorbent (Cs/Gly-Ma-Tk) from the others as the pH required to achieve the highest removal is 4 and the time required to achieve efficient removal is 180min. Pn the other hand, the other three adsorbents display similar trends in the adsorption conditions required to achieve optimal BG removal in line with the observations made for the unmodified Cs-Ma-Tk. The FT-IR spectra of the four synthesised adsorbents reveal the involvements of the active functional groups in the adsorption of BG dye with most changes in peak intensity happening in the 3600-330 cm^{-1} region (-NH and -OH bonds) while confirming the formation of Schiff base (similar to the observations made for the unmodified Cs-Ma-Tk; see Appendix2). The XRD patterns of the four adsorbents confirm the successful incorporation of the composite components while the crosslinking reaction severely reduces the intensity of the peaks related to the (020) and (110) plains of Cs, indicating the more severe structural changes occurring during the crosslinking process.

Overall, the results of this study indicate that the grafted Cs-Ma-Tk composites (Cs/SD-Ma-Tk and Cs/BD-Ma-Tk) have an overall higher efficiency in the removal of BG dye. While the Cs/Bz_2-Ma-Tk containing aromatic rings and capable of forming π-π stacking attractions with the dye molecules has a noticeably higher efficiency compared to Cs/Gly-Ma-Tk. On the other hand, the practicality of the Cs/Gly-Ma-Tk in regard to deprotonation occurring at lower (acidic) pH levels which allows its application in samples with acidic pH without the need for pH adjustments (which requires the use of vast amounts of chemicals in industrial applications) makes it a unique adsorbent.

Table 4.29

Comparison of the Analyses Results for the Four Synthesised Adsorbents

		Cs-Ma-Tk (appendices)	Cs/SD-Ma-Tk	Cs/BD-Ma-Tk	Cs/Gly-Ma-Tk	Cs/Bz_2-Ma-Tk
Elemental composition	**C**	30.94%	40.35%	38.75%	32.09%	34.15%
	H	5.04%	4.56%	5.18%	3.9%	4.76%
	N	5.70%	4.51%	5.84%	5.95%	4.22%
	S	0.07%	0.05%	0.08%	0.32%	0
	O (by difference)	58.25%	50.53%	50.15%	57.74%	56.87%
Specific Surface Area (m2/g)		6.27	9.1	8.77	2.79	1.32
Langmuir Surface Area (m2/g)		18.02	13.1	13.12	4.08	1.16
Pore Volume (cm3/g)		0.10	0.02	0.016	0.01	0.11
Average Pore Diameter (nm)		6.57	8.2	6.21	10.16	34.42
pH_{pzc}		7.4	6.9	7	3.2	7.3
Optimised adsorption parameters	**Dose (g/100mL)**	0.08	0.066	0.06	0.2	0.09
	pH	8.67	8.6	8.5	4.1	8.5
	Time (min)	53.2	58	60	180	45
	BG removal (%)	92.4%	72.4%	87%	80.5%	93.4%
Kinetic model		PSO	PSO	PSO	PSO	PSO
Isotherm model		Langmuir and Freundlich	Langmuir and Freundlich	Freundlich	Langmuir	Langmuir
q_m (mg/g)		440.8	957.0	441	88.3	289.2

	Cs-Ma-Tk (appendices)	Cs/SD-Ma-Tk	Cs/BD-Ma-Tk	Cs/Gly-Ma-Tk	Cs/Bz_2-Ma-Tk
Thermodynamic behaviour	Spontaneous, endothermic	Spontaneous, endothermic	Spontaneous, endothermic	spontaneous in higher temperatures, endothermic	Spontaneous, endothermic
Mechanism	Electrostatic bonds H-bonding Yoshida-H bonding n- π stacking	Electrostatic bonds H-bonding Yoshida-H bonding n- π stacking π- π stacking	Electrostatic bonds H-bonding Yoshida-H bonding n- π stacking π- π stacking	Electrostatic bonds H-bonding Yoshida-H bonding n- π stacking	Electrostatic bonds H-bonding Yoshida-H bonding n- π stacking π- π stacking

CHAPTER 5
CONCLUSION AND FUTURE WORK

5.1 Conclusion

This study successfully investigated the synthesis, characterisation, optimisation, and adsorption performance of grafted and crosslinked chitosan–microalgae–TiO_2 (Kronos) composites for the removal of Brilliant Green (BG) dye from aqueous solutions. The findings of this research address the stated research objectives and provide insight into the influence of grafting and crosslinking modifications on the structural properties and adsorption performance of the ternary composite system.

The first objective, which aimed to synthesise Schiff base chitosan–microalgae–TiO_2 composites modified through grafting (salicylaldehyde and benzaldehyde) and crosslinking (glyoxal and benzil) via the hydrothermal method, was successfully achieved. Four modified composites were prepared: salicylaldehyde-grafted chitosan–microalgae–TiO_2 (Cs/SD-Ma-Tk), benzaldehyde-grafted chitosan–microalgae–TiO_2 (Cs/BD-Ma-Tk), glyoxal-crosslinked chitosan–microalgae–TiO_2 (Cs/Gly-Ma-Tk), and benzil-crosslinked chitosan–microalgae–TiO_2 (Cs/Bz_2-Ma-Tk). The successful incorporation of the modifying agents into the chitosan matrix confirmed that both grafting and crosslinking processes effectively altered the structure of the ternary composite system.

The second objective was to study the physicochemical properties of the synthesised composites using various analytical techniques. Characterisation through FT-IR, FE-SEM/EDX, XRD, BET surface area analysis, pH_{pzc} determination, and elemental (CHNS/O) analysis confirmed the successful formation of the modified composites and revealed differences in their structural and surface properties. FT-IR analysis verified the presence of functional groups associated with grafting and crosslinking reactions, while FE-SEM analysis demonstrated changes in surface morphology and texture. BET analysis showed variations in surface area and pore structure among the composites, indicating that grafting generally enhanced surface accessibility whereas crosslinking resulted in denser polymeric structures. The pH_{pzc} analysis further confirmed the role of surface charge in the adsorption process.

The third objective was to perform statistical optimisation of key adsorption parameters using Response Surface Methodology with Box–Behnken Design (RSM-BBD). The optimisation successfully identified the most favourable adsorption conditions for each adsorbent. Statistical analysis through ANOVA validated the reliability of the developed models and confirmed that solution pH, adsorbent dosage, and contact time significantly influence BG dye removal efficiency. Among these variables, pH was found to play a critical role in controlling the electrostatic interactions between the adsorbent surface and the cationic dye molecules.

The fourth objective was to investigate the adsorption equilibrium behaviour and determine the mechanisms governing BG adsorption. Kinetic studies demonstrated that the adsorption process for all composites followed the pseudo-second-order (PSO) kinetic model, indicating that chemisorption plays a dominant role in the adsorption mechanism. Isotherm studies revealed that the adsorption behaviour could be described by both Langmuir and Freundlich models depending on the composite, suggesting the presence of both monolayer and multilayer adsorption processes. Thermodynamic analysis further showed that the adsorption process is spontaneous and endothermic, indicating increased randomness at the solid–liquid interface during adsorption.

The final objective was to compare the adsorption performance of the grafted and crosslinked composites to determine the most effective modification strategy for BG removal. Among the synthesised materials, the salicylaldehyde-grafted composite Cs/SD-Ma-Tk exhibited the highest adsorption capacity (957.0 mg/g), demonstrating superior adsorption performance compared with the other composites. The benzaldehyde-grafted composite Cs/BD-Ma-Tk also showed strong adsorption performance with a capacity comparable to the base composite. In contrast, the crosslinked composites Cs/Gly-Ma-Tk and Cs/Bz_2-Ma-Tk exhibited lower adsorption capacities, which may be attributed to the formation of more compact polymer networks that restrict surface accessibility. These results indicate that grafting modifications, particularly with salicylaldehyde, significantly enhance adsorption efficiency by introducing additional functional groups and improving surface accessibility.

Overall, the findings of this study demonstrate that the grafted Cs-Ma-Tk composites exhibit superior efficiency for the removal of Brilliant Green (BG) dye. The Cs/Bz_2-Ma-Tk crosslinked composite, which contains aromatic structures capable of promoting π–π stacking interactions with dye molecules, also shows improved adsorption performance compared to Cs/Gly-Ma-Tk. Nevertheless, Cs/Gly-Ma-Tk

presents a notable practical advantage due to its ability to undergo deprotonation at relatively low (acidic) pH conditions. This property enables its effective application in acidic aqueous environments without requiring pH adjustment, thereby reducing the need for additional chemical reagents. Such a characteristic is particularly beneficial for large-scale industrial wastewater treatment processes, where minimising chemical consumption is an important operational consideration.

5.2 Future Work Recommendations

Future work should extend the application of the synthesised composites beyond Brilliant Green dye to provide a broader assessment of their environmental potential. In particular, further studies are recommended on the removal of heavy metals from aqueous media in order to evaluate the affinity of the materials towards inorganic contaminants and to determine whether the functional groups introduced through grafting and crosslinking can enhance metal ion binding. Special attention should be given to the salicylaldehyde-grafted composite, Cs/SD-Ma-Tk, as it exhibited the highest adsorption capacity in the present study. This material may be further examined for the removal of other classes of pollutants, including anionic and cationic dyes, pharmaceutical residues, and emerging organic contaminants, in order to assess its versatility as a high-performance adsorbent. In addition, adsorption studies involving binary or multi-pollutant systems are strongly recommended to better simulate realistic wastewater conditions and to evaluate competitive adsorption behaviour among co-existing contaminants. Continuous-flow column studies should also be conducted to determine breakthrough behaviour, bed capacity, and operational stability under dynamic conditions, thereby providing more practical information for scale-up and industrial implementation. Together, these investigations would contribute to a more comprehensive understanding of the applicability of the developed composites in complex wastewater treatment systems.

REFERENCES

[1] G. Crini and E. Lichtfouse, "Advantages and disadvantages of techniques used for wastewater treatment," *Environ. Chem. Lett.*, vol. 17, no. 1, pp. 145–155, Mar. 2019, doi: 10.1007/S10311-018-0785-9.

[2] V. Katheresan, J. Kansedo, and S. Y. Lau, "Efficiency of various recent wastewater dye removal methods: A review," *J. Environ. Chem. Eng.*, vol. 6, no. 4, pp. 4676–4697, Aug. 2018, doi: 10.1016/j.jece.2018.06.060.

[3] A. S. Abdulhameed, A. H. Jawad, and A.-T. Mohammad, "Synthesis of chitosan-ethylene glycol diglycidyl ether/TiO2 nanoparticles for adsorption of reactive orange 16 dye using a response surface methodology approach," *Bioresour. Technol.*, vol. 293, p. 122071, Dec. 2019, doi: 10.1016/j.biortech.2019.122071.

[4] S. Olivera, H. B. Muralidhara, K. Venkatesh, V. K. Guna, K. Gopalakrishna, and Y. Kumar K., "Potential applications of cellulose and chitosan nanoparticles/composites in wastewater treatment: A review," *Carbohydr. Polym.*, vol. 153, pp. 600–618, Nov. 2016, doi: 10.1016/J.CARBPOL.2016.08.017.

[5] N. I. Normi, A. S. Abdulhameed, A. H. Jawad, S. N. Surip, R. Razuan, and M. L. Ibrahim, "Hydrothermal-Assisted Grafting of Schiff base Chitosan by Salicylaldehyde for Adsorptive Removal of Acidic Dye: Statistical Modeling and Adsorption Mechanism," *J. Polym. Environ.*, vol. 31, no. 5, pp. 1925–1937, May 2023, doi: 10.1007/s10924-022-02730-9.

[6] N. I. Normi, A. S. Abdulhameed, S. N. Surip, Z. A. ALOthman, L. D. Wilson, and A. H. Jawad, "Benzil Schiff Base Side-Chain Polymer-Crosslinked Chitosan Via Hydrothermal Process for Reactive Orange 16 Dye Removal: An Optimized and Comparative Study with Chitosan," *J. Polym. Environ.*, vol. 31, no. 5, pp. 1986–2004, May 2023, doi: 10.1007/s10924-022-02727-4.

[7] M. M. Hassan and C. M. Carr, "Biomass-derived porous carbonaceous materials and their composites as adsorbents for cationic and anionic dyes: A review," *Chemosphere*, vol. 265, p. 129087, Feb. 2021, doi: 10.1016/j.chemosphere.2020.129087.

[8] U. A. Guler, M. Ersan, E. Tuncel, and F. Dügenci, "Mono and simultaneous removal of crystal violet and safranin dyes from aqueous solutions by HDTMA-

modified Spirulina sp.," *Process Safety and Environmental Protection*, vol. 99, pp. 194–206, Jan. 2016, doi: 10.1016/j.psep.2015.11.006.

[9] F. Robledo-Padilla *et al.*, "Evaluation and Predictive Modeling of Removal Condition for Bioadsorption of Indigo Blue Dye by Spirulina platensis," *Microorganisms*, vol. 8, no. 1, p. 82, Jan. 2020, doi: 10.3390/microorganisms8010082.

[10] N. M. Zain, C. M. Lim, A. Usman, N. Keasberry, R. Thotagamuge, and A. H. Mahadi, "Synergistic effect of TiO2 size on activated carbon composites for ruthenium N-3 dye adsorption and photocatalytic degradation in wastewater treatment," *Environ. Nanotechnol. Monit. Manag.*, vol. 16, p. 100567, Dec. 2021, doi: 10.1016/J.ENMM.2021.100567.

[11] A. M. Aljeboree *et al.*, "Synthesis of a new nanocomposite with the core TiO2/hydrogel: Brilliant green dye adsorption, isotherms, kinetics, and DFT studies," *Journal of Industrial and Engineering Chemistry*, vol. 109, pp. 475–485, May 2022, doi: 10.1016/j.jiec.2022.02.031.

[12] N. M. Mahmoodi, M. Oveisi, A. Taghizadeh, and M. Taghizadeh, "Synthesis of pearl necklace-like ZIF-8@chitosan/PVA nanofiber with synergistic effect for recycling aqueous dye removal," *Carbohydr. Polym.*, vol. 227, p. 115364, Jan. 2020, doi: 10.1016/J.CARBPOL.2019.115364.

[13] L. Chungkrang and S. Bhuyan, "Natural Dye Sources and its Applications in Textiles: A Brief Review," *Int. J. Curr. Microbiol. Appl. Sci.*, vol. 9, no. 10, pp. 261–269, Oct. 2020, doi: 10.20546/ijcmas.2020.910.034.

[14] K. Elsahida, A. M. Fauzi, I. Sailah, and I. Z. Siregar, "Sustainability of the use of natural dyes in the textile industry," *IOP Conf. Ser. Earth Environ. Sci.*, vol. 399, no. 1, p. 012065, Dec. 2019, doi: 10.1088/1755-1315/399/1/012065.

[15] M. M. Asai and K. Tapadia, "Biofabricated magnetic CuO@Fe3O4 nanocomposites: Synthesis, characterization and Brilliant Green dye removal from aqueous media and its kinetics study," *Journal of the Indian Chemical Society*, vol. 102, no. 5, p. 101668, May 2025, doi: 10.1016/J.JICS.2025.101668.

[16] H. Afiya, E. E. Ahmet, and M. M. Shah, "Enzymatic Decolorization of Remazol Brilliant Blue Royal (RB 19) textile dye by White Rot Fungi," *Journal of Applied and Advanced Research*, pp. 11–15, Jan. 2019, doi: 10.21839/jaar.2019.v4i1.260.

[17] F. Mashkoor, A. Nasar, and Inamuddin, “Carbon nanotube-based adsorbents for the removal of dyes from waters: A review,” *Environ. Chem. Lett.*, vol. 18, no. 3, pp. 605–629, May 2020, doi: 10.1007/s10311-020-00970-6.

[18] N. El Messaoudi *et al.*, “Regeneration and reusability of non-conventional low-cost adsorbents to remove dyes from wastewaters in multiple consecutive adsorption–desorption cycles: a review,” *Biomass Convers. Biorefin.*, vol. 14, no. 11, pp. 11739–11756, Jun. 2024, doi: 10.1007/s13399-022-03604-9.

[19] I. A. Shah, M. Bilal, I. W. Almanassra, and I. Ihsanullah, “A comprehensive review of graphene oxide-based membranes for efficient dye removal from water sources,” *Sep. Purif. Technol.*, vol. 330, p. 125277, Feb. 2024, doi: 10.1016/j.seppur.2023.125277.

[20] V. K. Parida, N. Singh, M. Priyadarshini, P. Kumari, D. Datta, and A. Tambi, “Insights into the synthetic dye contamination in textile wastewater: Impacts on aquatic ecosystems and human health, and eco-friendly remediation strategies for environmental sustainability,” *Journal of Industrial and Engineering Chemistry*, vol. 150, pp. 247–264, Oct. 2025, doi: 10.1016/j.jiec.2025.04.019.

[21] A. G. B. Pereira, F. H. A. Rodrigues, A. T. Paulino, A. F. Martins, and A. R. Fajardo, “Recent advances on composite hydrogels designed for the remediation of dye-contaminated water and wastewater: A review,” *J. Clean. Prod.*, vol. 284, p. 124703, Feb. 2021, doi: 10.1016/j.jclepro.2020.124703.

[22] F. P. Andrew, T. R. Papo, and P. A. Ajibade, “Optimization of trypan blue and brilliant green dyes photocatalytic degradation and adsorption of lead(II) and chromium (VI) heavy metal ions by copper sulfide nanoparticles,” *Environmental Advances*, vol. 17, p. 100575, Oct. 2024, doi: 10.1016/j.envadv.2024.100575.

[23] Y.-C. An *et al.*, “A critical review on graphene oxide membrane for industrial wastewater treatment,” *Environ. Res.*, vol. 223, p. 115409, Apr. 2023, doi: 10.1016/j.envres.2023.115409.

[24] A. Deb, A. Debnath, and B. Saha, “Sono-assisted enhanced adsorption of eriochrome Black-T dye onto a novel polymeric nanocomposite: kinetic, isotherm, and response surface methodology optimization,” *J. Dispers. Sci. Technol.*, vol. 42, no. 11, pp. 1579–1592, Aug. 2021, doi: 10.1080/01932691.2020.1775093.

[25] R. Jasrotia, J. Singh, S. Mittal, and H. Singh, “Synthesis of CTAB modified

ferrite composite for the efficient removal of brilliant green dye," *Int. J. Environ. Anal. Chem.*, vol. 104, no. 16, pp. 4126–4142, Dec. 2024, doi: 10.1080/03067319.2022.2098485.

[26] A. M. Aljeboree and A. F. Alkaim, "Studying removal of anionic dye by prepared highly adsorbent surface hydrogel nanocomposite as an applicable for aqueous solution," *Scientific Reports 2024 14:1*, vol. 14, no. 1, pp. 1–17, Apr. 2024, doi: 10.1038/s41598-024-59545-y.

[27] Y. Zhou, J. Lu, Y. Zhou, and Y. Liu, "Recent advances for dyes removal using novel adsorbents: A review," *Environmental Pollution*, vol. 252, pp. 352–365, Sep. 2019, doi: 10.1016/j.envpol.2019.05.072.

[28] S. Mishra and A. Maiti, "The efficacy of bacterial species to decolourise reactive azo, anthroquinone and triphenylmethane dyes from wastewater: a review," *Environmental Science and Pollution Research*, vol. 25, no. 9, pp. 8286–8314, Mar. 2018, doi: 10.1007/s11356-018-1273-2.

[29] B. Lellis, C. Z. Fávaro-Polonio, J. A. Pamphile, and J. C. Polonio, "Effects of textile dyes on health and the environment and bioremediation potential of living organisms," *Biotechnology Research and Innovation*, vol. 3, no. 2, pp. 275–290, Jul. 2019, doi: 10.1016/J.BIORI.2019.09.001.

[30] A. H. Jawad, A. S. Abdulhameed, E. Kashi, Z. M. Yaseen, Z. A. ALOthman, and M. R. Khan, "Cross-Linked Chitosan-Glyoxal/Kaolin Clay Composite: Parametric Optimization for Color Removal and COD Reduction of Remazol Brilliant Blue R Dye," *J. Polym. Environ.*, vol. 30, no. 1, 2022, doi: 10.1007/s10924-021-02188-1.

[31] S. P. Bera, "Bioremediation of Remazol Blue RGB by Newly Isolated Bacillus Strain," *Austin Journal of Microbiology*, vol. 5, no. 1, Feb. 2019, doi: 10.26420/austinjmicrobiol.1024.2019.

[32] D. A. Yaseen and M. Scholz, "Textile dye wastewater characteristics and constituents of synthetic effluents: a critical review," *International Journal of Environmental Science and Technology*, vol. 16, no. 2, pp. 1193–1226, Feb. 2019, doi: 10.1007/s13762-018-2130-z.

[33] A. Tkaczyk, K. Mitrowska, and A. Posyniak, "Synthetic organic dyes as contaminants of the aquatic environment and their implications for ecosystems: A review," *Science of The Total Environment*, vol. 717, p. 137222, May 2020, doi: 10.1016/j.scitotenv.2020.137222.

[34] F. M. D. Chequer *et al.*, “Textile Dyes: Dyeing Process and Environmental Impact,” *Eco-Friendly Textile Dyeing and Finishing*, Jan. 2013, doi: 10.5772/53659.

[35] A. Singh *et al.*, “Biological remediation technologies for dyes and heavy metals in wastewater treatment: New insight,” *Bioresour. Technol.*, vol. 343, p. 126154, Jan. 2022, doi: 10.1016/j.biortech.2021.126154.

[36] H. Ben Slama *et al.*, “Diversity of Synthetic Dyes from Textile Industries, Discharge Impacts and Treatment Methods,” *Applied Sciences 2021, Vol. 11, Page 6255*, vol. 11, no. 14, p. 6255, Jul. 2021, doi: 10.3390/APP11146255.

[37] Kusumlata, B. Ambade, A. Kumar, and S. Gautam, “Sustainable Solutions: Reviewing the Future of Textile Dye Contaminant Removal with Emerging Biological Treatments,” *Limnological Review 2024, Vol. 24, Pages 126-149*, vol. 24, no. 2, pp. 126–149, Apr. 2024, doi: 10.3390/LIMNOLREV24020007.

[38] J. Sharma, S. Sharma, and V. Soni, “Classification and impact of synthetic textile dyes on Aquatic Flora: A review,” *Reg. Stud. Mar. Sci.*, vol. 45, p. 101802, Jun. 2021, doi: 10.1016/J.RSMA.2021.101802.

[39] P. Dutta, M. Razaya Rabbi, M. A. Sufian, and S. Mahjebin, “Effects of textile dyeing effluent on the environment and its treatment: A review,” *Engineering and Applied Science Letters (EASL)*, vol. 5, no. 1, pp. 1–17, Dec. 2022, doi: 10.30538/PSRP-EASL2022.0080.

[40] K. Ramamurthy, P. S. Priya, R. Murugan, and J. Arockiaraj, “Hues of risk: investigating genotoxicity and environmental impacts of azo textile dyes,” *Environ. Sci. Pollut. Res. Int.*, vol. 31, no. 23, pp. 33190–33211, May 2024, doi: 10.1007/S11356-024-33444-1.

[41] K. F. Kayani, S. J. Mohammed, M. S. Mustafa, and S. B. Aziz, “Dyes and their toxicity: removal from wastewater using carbon dots/metal oxides as hybrid materials: a review,” *Mater. Adv.*, vol. 6, no. 16, pp. 5391–5409, Aug. 2025, doi: 10.1039/D5MA00572H.

[42] S. Singh, H. Gupta, S. Dhiman, and N. K. Sahu, “Decontamination of cationic dye brilliant green from the aqueous media,” *Appl. Water Sci.*, vol. 12, no. 4, p. 61, Apr. 2022, doi: 10.1007/s13201-022-01596-5.

[43] C. G. Kumar, P. Mongolla, J. Joseph, and V. U. M. Sarma, “Decolorization and biodegradation of triphenylmethane dye, brilliant green, by Aspergillus sp. isolated from Ladakh, India,” *Process Biochemistry*, vol. 47, no. 9, pp. 1388–

1394, Sep. 2012, doi: 10.1016/j.procbio.2012.05.015.

[44] R. Ahmad and K. Ansari, “Chemically treated Lawsonia inermis seeds powder (CTLISP): An eco-friendly adsorbent for the removal of brilliant green dye from aqueous solution,” *Groundw. Sustain. Dev.*, vol. 11, p. 100417, Oct. 2020, doi: 10.1016/j.gsd.2020.100417.

[45] “Brilliant Green | C27H34N2O4S | CID 12449 - PubChem.” Accessed: Mar. 10, 2026. [Online]. Available: https://pubchem.ncbi.nlm.nih.gov/compound/Brilliant-Green

[46] B. K. Nandi and S. Patel, “Effects of operational parameters on the removal of brilliant green dye from aqueous solutions by electrocoagulation,” *Arabian Journal of Chemistry*, vol. 10, pp. S2961–S2968, May 2017, doi: 10.1016/j.arabjc.2013.11.032.

[47] S. J. Ukkund *et al.*, “Adsorption Method for the Remediation of Brilliant Green Dye Using Halloysite Nanotube: Isotherm, Kinetic and Modeling Studies,” *Applied Sciences*, vol. 11, no. 17, p. 8088, Aug. 2021, doi: 10.3390/app11178088.

[48] P. Samiyammal *et al.*, “Adsorption of brilliant green dye onto activated carbon prepared from cashew nut shell by KOH activation: Studies on equilibrium isotherm,” *Environ. Res.*, vol. 212, p. 113497, Sep. 2022, doi: 10.1016/j.envres.2022.113497.

[49] R. A. Mansour, A. El Shahawy, A. Attia, and M. S. Beheary, “Brilliant green dye biosorption using activated carbon derived from guava tree wood,” *Wiley Online Library*, vol. 2020, 2020, doi: 10.1155/2020/8053828.

[50] Y. A. Aggour, E. R. Kenawy, M. Magdy, and E. Elbayoumy, “Multifunctional copolymers for brilliant green dye removal: adsorption kinetics, isotherm and process optimization,” *Environmental Science: Advances*, 2025, doi: 10.1039/D4VA00404C.

[51] R. Fiaz, M. Hafeez, and R. Mahmood, “Removal of brilliant green (BG) from aqueous solution by using low cost biomass Salix alba leaves (SAL): thermodynamic and kinetic studies,” *Journal of Water Reuse and Desalination*, vol. 10, no. 1, pp. 70–81, Mar. 2020, doi: 10.2166/wrd.2020.054.

[52] A. Ragab, I. Ahmed, and D. Bader, “The Removal of Brilliant Green Dye from Aqueous Solution Using Nano Hydroxyapatite/Chitosan Composite as a Sorbent,” *Molecules*, vol. 24, no. 5, p. 847, Feb. 2019, doi:

10.3390/molecules24050847.

[53] E. Zabłocka-Godlewska and W. Przystaś, "Fed-Batch Decolourization of Mixture of Brilliant Green and Evans Blue by Bacteria Species Applied as Pure and Mixed Cultures: Influence of Growth Conditions," *Water Air Soil Pollut.*, vol. 231, no. 2, p. 75, Feb. 2020, doi: 10.1007/s11270-020-4441-1.

[54] S. Pang *et al.*, "Insights into the Toxicity and Degradation Mechanisms of Imidacloprid Via Physicochemical and Microbial Approaches," *Toxics*, vol. 8, no. 3, p. 65, Sep. 2020, doi: 10.3390/toxics8030065.

[55] H. Zhang, K. Zhang, M. Gao, Z. An, C. Tang, and X. Yan, "Degradation efficiency of the azo dye acid orange 2 and microbial community characteristics in a rotating algal biofilm reactor," *Journal of Water Process Engineering*, vol. 50, p. 103233, Dec. 2022, doi: 10.1016/j.jwpe.2022.103233.

[56] S. S. Ali, R. Al-Tohamy, and J. Sun, "Performance of Meyerozyma caribbica as a novel manganese peroxidase-producing yeast inhabiting wood-feeding termite gut symbionts for azo dye decolorization and detoxification," *Science of The Total Environment*, vol. 806, p. 150665, Feb. 2022, doi: 10.1016/j.scitotenv.2021.150665.

[57] J. M. Solaiman, N. Rajamohan, M. Yusuf, and H. Kamyab, "Nanocomposite ceramic membranes as novel tools for remediation of textile dye waste water – A review of current applications, machine learning based modeling and future perspectives," *J. Environ. Chem. Eng.*, vol. 12, no. 2, p. 112353, Apr. 2024, doi: 10.1016/j.jece.2024.112353.

[58] R. S. Vieira and M. M. Beppu, "Interaction of natural and crosslinked chitosan membranes with Hg(II) ions," *Colloids Surf. A Physicochem. Eng. Asp.*, vol. 279, no. 1–3, pp. 196–207, May 2006, doi: 10.1016/j.colsurfa.2006.01.026.

[59] J. Wang *et al.*, "Fabrication of Bioinspired Gallic Acid-Grafted Chitosan/Polysulfone Composite Membranes for Dye Removal *via* Nanofiltration," *ACS Omega*, vol. 5, no. 22, pp. 13077–13086, Jun. 2020, doi: 10.1021/acsomega.0c01013.

[60] R. Bouchareb, Z. Bilici, and N. Dizge, "Water recovery from yarn fabric dyeing wastewater using electrochemical oxidation and membrane processes," *Water Environment Research*, vol. 94, no. 1, Jan. 2022, doi: 10.1002/wer.1681.

[61] S. K. Muniasamy, A. A. AlObaid, I. Warad, and G. Ravindiran, "Removal of Brilliant Green dye in aqueous solution using synthetic coagulation and

flocculation technique," *Desalination Water Treat.*, vol. 314, pp. 231–240, Dec. 2023, doi: 10.5004/dwt.2023.30093.

[62] M. C. Menkiti, P. C. Nnaji, and O. D. Onukwuli, "Coag-flocculation kinetics and functional parameters response of periwinkle shell coagulant (PSC) to pH variation in organic rich coal effluent medium," *Nat. Sci. (East. Lansing).*, vol. 7, no. 6, pp. 1–18, 2009.

[63] J. Dotto, M. R. Fagundes-Klen, M. T. Veit, S. M. Palácio, and R. Bergamasco, "Performance of different coagulants in the coagulation/flocculation process of textile wastewater," *J. Clean. Prod.*, vol. 208, pp. 656–665, Jan. 2019, doi: 10.1016/j.jclepro.2018.10.112.

[64] S. Ihaddaden, D. Aberkane, A. Boukerroui, and D. Robert, "Removal of methylene blue (basic dye) by coagulation-flocculation with biomaterials (bentonite and Opuntia ficus indica)," *Journal of Water Process Engineering*, vol. 49, p. 102952, Oct. 2022, doi: 10.1016/j.jwpe.2022.102952.

[65] F. Rehman, M. Sayed, J. A. Khan, N. S. Shah, H. M. Khan, and D. D. Dionysiou, "Oxidative removal of brilliant green by UV/S2O82–, UV/HSO5– and UV/H2O2 processes in aqueous media: A comparative study," *J. Hazard. Mater.*, vol. 357, pp. 506–514, Sep. 2018, doi: 10.1016/j.jhazmat.2018.06.012.

[66] A. R. Quaff, S. Venkatesh, and K. Venkatesh, "Degradation of Azo Dye by Ozone Oxidation: Cost Analysis and Buffering Effects on Dye Decomposition," *National Academy Science Letters*, vol. 44, no. 4, pp. 339–341, Aug. 2021, doi: 10.1007/s40009-020-01008-9.

[67] M. A. Hassaan *et al.*, "Advanced oxidation of acid yellow 11 dye; detoxification and degradation mechanism," *Toxin Rev.*, vol. 40, no. 4, pp. 1472–1480, Oct. 2021, doi: 10.1080/15569543.2020.1736098.

[68] Y. Dadban Shahamat, M. Masihpour, P. Borghei, and S. Hoda Rahmati, "Removal of azo red-60 dye by advanced oxidation process O3/UV from textile wastewaters using Box-Behnken design," *Inorg. Chem. Commun.*, vol. 143, p. 109785, Sep. 2022, doi: 10.1016/j.inoche.2022.109785.

[69] S. Kalidhasan, D.-G. Park, K. S. Jin, and H.-Y. Lee, "Engineered polymer–clay–copper oxides catalyst for the oxidation and reduction of organic molecules: synergy of degradation and instinctive interface stability by polymer self-healing function," *Surfaces and Interfaces*, vol. 39, p. 102934, Jul. 2023, doi: 10.1016/j.surfin.2023.102934.

[70] S. Gul *et al.*, “Removal of Brilliant Green Dye from Water Using Ficus benghalensis Tree Leaves as an Efficient Biosorbent,” *Materials*, vol. 16, no. 2, p. 521, Jan. 2023, doi: 10.3390/ma16020521.

[71] P. Samiyammal *et al.*, “Adsorption of brilliant green dye onto activated carbon prepared from cashew nut shell by KOH activation: Studies on equilibrium isotherm,” *Environ. Res.*, vol. 212, p. 113497, Sep. 2022, doi: 10.1016/J.ENVRES.2022.113497.

[72] A. Venkatesan *et al.*, “High adsorption capacities of rhodamine B dye by activated carbon synthesized from cotton stalks agricultural waste by chemical activation,” *Ceram. Int.*, vol. 51, no. 10, pp. 13345–13354, Apr. 2025, doi: 10.1016/J.CERAMINT.2025.01.178.

[73] N. Y. Donkadokula, A. K. Kola, and D. Saroj, “Modelling and optimization studies on decolorization of brilliant green dye using integrated nanofiltration and photocatalysis,” *Sustainable Environment Research*, vol. 30, no. 1, p. 9, Dec. 2020, doi: 10.1186/s42834-020-00050-y.

[74] H. Xu *et al.*, “Recent advances in anaerobic biological processes for textile printing and dyeing wastewater treatment: a mini-review,” *World J. Microbiol. Biotechnol.*, vol. 34, no. 11, pp. 1–9, Nov. 2018, doi: 10.1007/S11274-018-2548-Y/FIGURES/5.

[75] C. Bouasla, “Optimization of electrochemical oxidation for the degradation of acid yellow 99 via sulfate and hydroxyl radicals activation: A study using Plackett–Burman and Box–Behnken designs,” *Journal of Water Process Engineering*, vol. 68, p. 106362, Dec. 2024, doi: 10.1016/j.jwpe.2024.106362.

[76] A. Alkhouzaam and M. Khraisheh, “Towards sustainable management of end-of-life membranes: Novel transformation of end of life (EoL) reverse osmosis membranes for efficient dye/salt separation,” *Desalination*, vol. 571, p. 117104, Feb. 2024, doi: 10.1016/J.DESAL.2023.117104.

[77] P. Kumari, S. Malik, J. Bora, S. Mondal, R. Rani, and A. Kapoor, “Applied aspects of reverse osmosis technology for industrial wastewater treatment,” *Development in Wastewater Treatment Research and Processes: Advanced Oxidation Processes for Tannery Effluent*, pp. 341–366, Jan. 2024, doi: 10.1016/B978-0-323-95656-7.00011-7.

[78] Ruslan, E. Wulandari, F. Sagita, W.-S. Hung, and G. T. M. Kadja, “Recent advances in MXenes and their functionalization for highly effective

ultrafiltration, nanofiltration, and reverse osmosis," *Inorg. Chem. Commun.*, vol. 170, p. 113152, Dec. 2024, doi: 10.1016/J.INOCHE.2024.113152.

[79] P. Mahajan, D. Jaspal, and N. Zari, "Application of Electron Beam Irradiation for the Removal of Dye from Textile Effluents: A Review," *Ind. Eng. Chem. Res.*, vol. 63, no. 22, pp. 9611–9618, Jun. 2024, doi: 10.1021/acs.iecr.4c00072.

[80] S. Juabrum *et al.*, "Magnetically separable TiO2/SnO2/Fe3O4-based nanocomposite photocatalyst for organic dye removal under low-power ultraviolet-visible light irradiation," *Journal of Water Process Engineering*, vol. 66, p. 105883, Sep. 2024, doi: 10.1016/J.JWPE.2024.105883.

[81] R. Riaz *et al.*, "NiFe2O4/CuO heterostructures optical, magnetic and photocatalytic properties: Methylene blue dye degradation under solar light irradiation," *J. Mol. Struct.*, vol. 1309, p. 138174, Aug. 2024, doi: 10.1016/J.MOLSTRUC.2024.138174.

[82] D. M. Aboelkhir, A. Sayed, L. S. Eldondaity, V. Joseph, A. Amin, and G. A. Mahmoud, "Multiwalled carbon nanotubes@pectin/κ-carrageenan-based nanocomposite biohydrogel prepared by gamma irradiation for efficient methylene blue dye sequestration," *J. Appl. Polym. Sci.*, vol. 141, no. 22, p. e55452, Jun. 2024, doi: 10.1002/app.55452.

[83] N. Tajat *et al.*, "Facile synthesis of Ag2CO3/Ag2O@NiFe LDH nanohetrostructure with enhanced photocatalytic performance for MB dye degradation under visible light irradiation," *Colloids Surf. A Physicochem. Eng. Asp.*, vol. 681, p. 132789, Jan. 2024, doi: 10.1016/J.COLSURFA.2023.132789.

[84] A. H. Ragab, N. F. Gumaah, A. A. El Aziz Elfiky, and M. F. Mubarak, "Exploring the sustainable elimination of dye using cellulose nanofibrils- vinyl resin based nanofiltration membranes," *BMC Chem.*, vol. 18, no. 1, pp. 1–15, Dec. 2024, doi: 10.1186/S13065-024-01211-5/TABLES/5.

[85] S. Guo, X. Yan, Z. Luo, J. Zhang, and C. Yuan, "Preparation of positively charged nanofiltration membranes: Manipulation of the positive charge," *Desalination*, vol. 586, p. 117780, Oct. 2024, doi: 10.1016/J.DESAL.2024.117780.

[86] A. A. E. A. Elfiky, M. F. Mubarak, M. Keshawy, I. E. T. El Sayed, and T. A. Moghny, "Novel nanofiltration membrane modified by metal oxide nanocomposite for dyes removal from wastewater," *Environ. Dev. Sustain.*, vol. 26, no. 8, pp. 19935–19957, Aug. 2024, doi: 10.1007/S10668-023-03444-

1/TABLES/5.

[87] Y. Rakcho *et al.*, “Fabrication of low-cost ceramic nanofiltration membrane from natural resources for the removal of cationic and anionic dyes: Experimental and DFT investigations,” *Chemical Engineering Journal*, vol. 505, p. 159779, Feb. 2025, doi: 10.1016/J.CEJ.2025.159779.

[88] S. Saja *et al.*, “Fabrication of low-cost ceramic ultrafiltration membrane made from bentonite clay and its application for soluble dyes removal,” *J. Eur. Ceram. Soc.*, vol. 40, no. 6, pp. 2453–2462, Jun. 2020, doi: 10.1016/j.jeurceramsoc.2020.01.057.

[89] B. Dehingia, R. Lahkar, and H. Kalita, “Efficient removal of both cationic and anionic dyes from water using a single rGO/PSS nanocomposite membrane with superior permeability and high aqueous stability,” *J. Environ. Chem. Eng.*, vol. 12, no. 2, p. 112393, Apr. 2024, doi: 10.1016/J.JECE.2024.112393.

[90] R. M. Paixão, L. H. B. R. da Silva, M. F. Vieira, M. T. P. de Amorim, R. Bergamasco, and A. M. S. Vieira, “Enhanced filtration membranes with graphene oxide and tannic acid for textile industry wastewater dye removal,” *Environmental Technology (United Kingdom)*, Mar. 2024, doi: 10.1080/09593330.2024.2369733.

[91] H. Jang, C. S. Lee, J. H. Kim, and J. Kim, “Optimization of photocatalytic ceramic membrane filtration by response surface methodology: Effects of hydrodynamic conditions on organic fouling and removal efficiency,” *Chemosphere*, vol. 356, p. 141885, May 2024, doi: 10.1016/J.CHEMOSPHERE.2024.141885.

[92] M. Chebbi *et al.*, “Single and combined treatment processes for rhodamine B removal by coagulation–flocculation and adsorption,” *RSC Adv.*, vol. 14, no. 51, pp. 37833–37845, Nov. 2024, doi: 10.1039/D4RA06882C.

[93] A. Zourif, A. Benbiyi, S. Kouniba, and M. El Guendouzi, “Avocado seed as a natural coagulant for removing dyes and turbidity from wastewater: Behnken Box design, sustainable reuse, and economic evaluation,” *Sustain. Chem. Pharm.*, vol. 39, p. 101621, Jun. 2024, doi: 10.1016/J.SCP.2024.101621.

[94] I. Dobrosz-Gómez, J. D. Quintero-Arias, and M. Á. Gómez-García, “Coagulation-Flocculation - Fenton-Neutralization sequential process for the treatment of industrial effluent polluted with AB194 dye,” *Case Studies in Chemical and Environmental Engineering*, vol. 9, p. 100720, Jun. 2024, doi:

10.1016/J.CSCEE.2024.100720.

[95] M. Khajavian and S. Ismail, “Deep eutectic solvent-modified polyvinyl alcohol/chitosan thin film membrane for dye adsorption: Machine learning modeling, experimental, and density functional theory calculations,” *Int. J. Biol. Macromol.*, vol. 294, p. 139479, Mar. 2025, doi: 10.1016/J.IJBIOMAC.2025.139479.

[96] R. T. Mogharbel *et al.*, “Fabrication of Cerium Metal–Organic Frameworks Functionalized with Glutamic Acid for Adsorption of Basic Red 46 from Aqueous Solutions: Kinetics, Thermodynamics, and Optimization,” *ACS Omega*, Apr. 2025, doi: 10.1021/acsomega.4c10666.

[97] A. S. Abdulhameed, R. H. Al Omari, S. Althahban, Y. Jazaa, M. Abualhaija, and S. Algburi, “Green vegetable waste composited with chitosan as a bioadsorbent for effective removal of methylene blue dye from water: Insight into physicochemical and adsorption characteristics,” *Biomass Bioenergy*, vol. 193, p. 107528, Feb. 2025, doi: 10.1016/j.biombioe.2024.107528.

[98] S. Hussain *et al.*, “Adsorption, kinetics and thermodynamics studies of methyl orange dye sequestration through chitosan composites films,” *Int. J. Biol. Macromol.*, vol. 168, pp. 383–394, Jan. 2021, doi: 10.1016/j.ijbiomac.2020.12.054.

[99] A. Hashem, C. O. Aniagor, L. A. Mohamed, A. M. Abdelgawad, and A. A. Aly, “Hydroxypropyl sulfonated starch and Asperlligus oryzae biomass for cationic dye adsorption: characterization, mechanism, sorption modelling,” *Biomass Convers. Biorefin.*, vol. 15, no. 1, pp. 1211–1227, Jan. 2024, doi: 10.1007/S13399-023-05248-9/TABLES/6.

[100] A. Salah Omer *et al.*, “Adsorption of crystal violet and methylene blue dyes using a cellulose-based adsorbent from sugercane bagasse: characterization, kinetic and isotherm studies,” *Journal of Materials Research and Technology*, vol. 19, pp. 3241–3254, Jul. 2022, doi: 10.1016/J.JMRT.2022.06.045.

[101] A. M. Aljeboree, A. F. Alkaim, F. H. Alsultany, and S. K. Issa, “Highly Reusable Nano Adsorbent Based on Clay-Incorporated Hydrogel Nanocomposite for Cationic Dye Adsorption,” *Journal of Inorganic and Organometallic Polymers and Materials 2024 35:2*, vol. 35, no. 2, pp. 1165–1186, Aug. 2024, doi: 10.1007/S10904-024-03344-5.

[102] N. Shah *et al.*, “Fabrication and Characterization of Montmorillonite Clay/Agar-

Based Magnetic Composite and Its Biological and Electrical Conductivity Evaluation," *ACS Omega*, vol. 9, no. 14, pp. 15904–15914, Apr. 2024, doi: 10.1021/acsomega.3c08708.

[103] G. George, A. M. Ealias, and M. P. Saravanakumar, "Advancements in textile dye removal: a critical review of layered double hydroxides and clay minerals as efficient adsorbents," *Environmental Science and Pollution Research*, vol. 31, no. 9, pp. 12748–12779, Jan. 2024, doi: 10.1007/s11356-024-32021-w.

[104] E. Mosaffa, R. I. Patel, A. Banerjee, B. B. Basak, and M. Oroujzadeh, "Comprehensive analysis of cationic dye removal from synthetic and industrial wastewater using a semi-natural curcumin grafted biochar/poly acrylic acid composite hydrogel," *RSC Adv.*, vol. 14, no. 11, pp. 7745–7762, Feb. 2024, doi: 10.1039/D3RA08521J.

[105] A. Bambal, R. Jugade, M. Khapre, and D. Saravanan, "Carbonization of golden shower pods to high surface area biochar for decontamination of cationic dyes and regeneration study by gamma radiations," *Next Sustainability*, vol. 5, p. 100064, 2025, doi: 10.1016/j.nxsust.2024.100064.

[106] M. Laxmi Deepak Bhatlu, P. S. Athira, N. Jayan, D. Barik, and M. S. Dennison, "Preparation of Breadfruit Leaf Biochar for the Application of Congo Red Dye Removal from Aqueous Solution and Optimization of Factors by RSM-BBD," *Adsorption Science & Technology*, vol. 2023, pp. 1–17, Feb. 2023, doi: 10.1155/2023/7369027.

[107] R. Foroutan, R. Mohammadi, A. Ahmadi, G. Bikhabar, F. Babaei, and B. Ramavandi, "Impact of ZnO and Fe3O4 magnetic nanoscale on the methyl violet 2B removal efficiency of the activated carbon oak wood," *Chemosphere*, vol. 286, p. 131632, Jan. 2022, doi: 10.1016/j.chemosphere.2021.131632.

[108] G. N. Murthy and U. K. Sahu, "Methylene Blue Dye Removal from Aqueous Solution Using Activated Carbon Prepared from Corn Cob Stem: Kinetics, Isotherms and Mechanism Studies," *AUIQ Complementary Biological System*, vol. 2, no. 1, pp. 35–48, Mar. 2025, doi: 10.70176/3007-973X.1024.

[109] N. Atirah Shamsudin *et al.*, "Oil Palm Fronds Activated Carbon via Microwave-assisted H3PO4 Activation: Box-Behnken Optimization for Crystal Violet Dye Removal," *AUIQ Complementary Biological System*, vol. 1, no. 1, pp. 77–88, Aug. 2024, doi: 10.70176/3007-973X.1008.

[110] A. M. Aljeboree, A. F. Alkaim, S. A. Hussein, F. H. Alsultany, and M. A. Jawad,

"Ecofriendly k-Carrageenan-Based Hydrogel with Strong Adsorption and Higher Abilities to Remove Crystal Violet from Aqueous Solution: Thermodynamic, Isotherm and Kinetic Investigation," *J. Inorg. Organomet. Polym. Mater.*, vol. 35, no. 4, pp. 2921–2942, Oct. 2024, doi: 10.1007/S10904-024-03434-4.

[111] E. Mosaffa, D. Patel, N. A. Ramsheh, R. I. Patel, A. Banerjee, and H. Ghafuri, "Bacterial cellulose microfiber reinforced hollow chitosan beads decorated with cross-linked melamine plates for the removal of the Congo red," *Int. J. Biol. Macromol.*, vol. 254, p. 127794, Jan. 2024, doi: 10.1016/J.IJBIOMAC.2023.127794.

[112] G. Bayramoglu, S. Burcu Angi, I. Acikgoz-Erkaya, and M. Yakup Arica, "Preparation of effective green sorbents using O. Princeps alga biomass with different composition of amine groups: Comparison to adsorption performances for removal of a model acid dye," *J. Mol. Liq.*, vol. 347, p. 118375, Feb. 2022, doi: 10.1016/j.molliq.2021.118375.

[113] B. Ramesh *et al.*, "A review on algae biosorption for the removal of hazardous pollutants from wastewater: Limiting factors, prospects and recommendations," *Environmental Pollution*, vol. 327, p. 121572, Jun. 2023, doi: 10.1016/j.envpol.2023.121572.

[114] A. Saravanan *et al.*, "Adsorption performance and modelling of malachite green dye removal from aqueous solution using sulphuric acid–modified Ipomoea pes caprae biomass," *Biomass Convers. Biorefin.*, vol. 15, no. 1, pp. 341–357, Jan. 2023, doi: 10.1007/S13399-023-05067-Y.

[115] F. Hoppe-Seyler, "Ueber Chitin und Cellulose," *Berichte der deutschen chemischen Gesellschaft*, vol. 27, no. 3, pp. 3329–3331, Oct. 1894, doi: 10.1002/CBER.189402703135.

[116] J. Wang and S. Zhuang, "Chitosan-based materials: Preparation, modification and application," *J. Clean. Prod.*, vol. 355, p. 131825, Jun. 2022, doi: 10.1016/J.JCLEPRO.2022.131825.

[117] C. K. S. Pillai, W. Paul, and C. P. Sharma, "Chitin and chitosan polymers: Chemistry, solubility and fiber formation," *Prog. Polym. Sci.*, vol. 34, no. 7, pp. 641–678, Jul. 2009, doi: 10.1016/J.PROGPOLYMSCI.2009.04.001.

[118] I. Aranaz *et al.*, "Chitosan: An Overview of Its Properties and Applications," *Polymers (Basel).*, vol. 13, no. 19, p. 3256, Sep. 2021, doi:

10.3390/polym13193256.

[119] S. (Gabriel) Kou, L. M. Peters, and M. R. Mucalo, “Chitosan: A review of sources and preparation methods,” *Int. J. Biol. Macromol.*, vol. 169, pp. 85–94, Feb. 2021, doi: 10.1016/j.ijbiomac.2020.12.005.

[120] M. K. A. Khan, A. S. Abdulhameed, H. Alshahrani, and S. Algburi, “Chitosan/functionalized fruit stones as a highly efficient adsorbent biomaterial for adsorption of brilliant green dye: Comprehensive characterization and statistical optimization,” *Int. J. Biol. Macromol.*, vol. 263, p. 130465, Apr. 2024, doi: 10.1016/j.ijbiomac.2024.130465.

[121] R. Siala, I. Hammemi, S. Sellimi, T. Vallaeys, A. S. Kamoun, and M. Nasri, “Arthrobacter arilaitensis Re117 as a Source of Solvent-Stable Proteases: Production, Characteristics, Potential Application in the Deproteinization of Shrimp Wastes,” *Advances in Bioscience and Biotechnology*, no. 6, pp. 105–119, 2015, doi: 10.4236/abb.2015.62011.

[122] J. Nilsen-Nygaard, S. Strand, K. Vårum, K. Draget, and C. Nordgård, “Chitosan: Gels and Interfacial Properties,” *Polymers (Basel).*, vol. 7, no. 3, pp. 552–579, Mar. 2015, doi: 10.3390/polym7030552.

[123] A. K. Rana, V. K. Gupta, P. Hart, F. Scarpa, and V. K. Thakur, “Sustainable MXene-chitosan/chitin composites for Interdisciplinary applications in water purification, bio-medical, bio-sensing and electronic fields,” *Materials Today Sustainability*, vol. 25, p. 100671, Mar. 2024, doi: 10.1016/j.mtsust.2024.100671.

[124] R. Jiang *et al.*, “Sustainable chitosan-based materials as heterogeneous catalyst for application in wastewater treatment and water purification: An up-to-date review,” *Int. J. Biol. Macromol.*, vol. 273, p. 133043, Jul. 2024, doi: 10.1016/j.ijbiomac.2024.133043.

[125] X. Zang *et al.*, “A review on the progress of magnetic chitosan-based materials in water purification and solid-phase extraction of contaminants,” *Sep. Purif. Technol.*, vol. 330, p. 125521, Feb. 2024, doi: 10.1016/j.seppur.2023.125521.

[126] I. Younes and M. Rinaudo, “Chitin and Chitosan Preparation from Marine Sources. Structure, Properties and Applications,” *Mar. Drugs*, vol. 13, no. 3, pp. 1133–1174, Mar. 2015, doi: 10.3390/md13031133.

[127] G. I. Edo, E. Yousif, and M. H. Al-Mashhadani, “Modified chitosan: Insight on biomedical and industrial applications,” *Int. J. Biol. Macromol.*, vol. 275, p.

133526, Aug. 2024, doi: 10.1016/j.ijbiomac.2024.133526.

[128] C. L. Ke, F. S. Deng, C. Y. Chuang, and C. H. Lin, "Antimicrobial Actions and Applications of Chitosan," *Polymers 2021, Vol. 13, Page 904*, vol. 13, no. 6, p. 904, Mar. 2021, doi: 10.3390/POLYM13060904.

[129] Z. Shariatinia, "Pharmaceutical applications of chitosan," *Adv. Colloid Interface Sci.*, vol. 263, pp. 131–194, Jan. 2019, doi: 10.1016/J.CIS.2018.11.008.

[130] R. Ramya, J. Venkatesan, S. K. Kim, and P. N. Sudha, "Biomedical Applications of Chitosan: An Overview," *J. Biomater. Tissue Eng.*, vol. 2, no. 2, pp. 100–111, Jun. 2012, doi: 10.1166/JBT.2012.1030.

[131] M. A. Khapre, S. Pandey, and R. M. Jugade, "Glutaraldehyde-cross-linked chitosan–alginate composite for organic dyes removal from aqueous solutions," *Int. J. Biol. Macromol.*, vol. 190, pp. 862–875, Nov. 2021, doi: 10.1016/j.ijbiomac.2021.09.026.

[132] R. M. Eltabey, F. T. Abdelwahed, M. M. Eldefrawy, and M. M. Elnagar, "Fabrication of poly(maleic acid)-grafted cross-linked chitosan/montmorillonite nanospheres for ultra-high adsorption of anionic acid yellow-17 and cationic brilliant green dyes in single and binary systems," *J. Hazard. Mater.*, vol. 439, p. 129589, Oct. 2022, doi: 10.1016/j.jhazmat.2022.129589.

[133] J. Kurczewska, "Chitosan-montmorillonite hydrogel beads for effective dye adsorption," *Journal of Water Process Engineering*, vol. 48, p. 102928, Aug. 2022, doi: 10.1016/j.jwpe.2022.102928.

[134] H. Demirtaş, Ş. Taşar, F. Kaya, and A. Özer, "Removal of BB41 dye molecules onto cross-linked chitosan microspheres: synthesis, characterization, and sorption/desorption," *Biomass Convers. Biorefin.*, Mar. 2023, doi: 10.1007/s13399-023-04047-6.

[135] G. Dodi, D. Hritcu, G. Lisa, and M. I. Popa, "Core–shell magnetic chitosan particles functionalized by grafting: Synthesis and characterization," *Chemical Engineering Journal*, vol. 203, pp. 130–141, Sep. 2012, doi: 10.1016/j.cej.2012.06.133.

[136] I. Tahira, Z. Aslam, A. Abbas, M. Monim-ul-Mehboob, S. Ali, and A. Asghar, "Adsorptive removal of acidic dye onto grafted chitosan: A plausible grafting and adsorption mechanism," *Int. J. Biol. Macromol.*, vol. 136, pp. 1209–1218, Sep. 2019, doi: 10.1016/j.ijbiomac.2019.06.173.

[137] R. Chanajaree, M. Sriuttha, V. S. Lee, and K. Wittayanarakul,

"Thermodynamics and kinetics of cationic/anionic dyes adsorption on cross-linked chitosan," *J. Mol. Liq.*, vol. 322, p. 114507, Jan. 2021, doi: 10.1016/j.molliq.2020.114507.

[138] N. N. A. Malek, A. H. Jawad, K. Ismail, R. Razuan, and Z. A. ALOthman, "Fly ash modified magnetic chitosan-polyvinyl alcohol blend for reactive orange 16 dye removal: Adsorption parametric optimization," *Int. J. Biol. Macromol.*, vol. 189, pp. 464–476, Oct. 2021, doi: 10.1016/j.ijbiomac.2021.08.160.

[139] A. S. Abdulhameed, A.-T. Mohammad, and A. H. Jawad, "Application of response surface methodology for enhanced synthesis of chitosan tripolyphosphate/TiO2 nanocomposite and adsorption of reactive orange 16 dye," *J. Clean. Prod.*, vol. 232, pp. 43–56, Sep. 2019, doi: 10.1016/j.jclepro.2019.05.291.

[140] A. H. Jawad, N. S. A. Mubarak, and A. S. Abdulhameed, "Tunable Schiff's base-cross-linked chitosan composite for the removal of reactive red 120 dye: Adsorption and mechanism study," *Int. J. Biol. Macromol.*, vol. 142, pp. 732–741, Jan. 2020, doi: 10.1016/j.ijbiomac.2019.10.014.

[141] Y. Wang, H. Wang, H. Peng, Z. Wang, J. Wu, and Z. Liu, "Dye adsorption from aqueous solution by cellulose/chitosan composite: Equilibrium, kinetics, and thermodynamics," *Fibers and Polymers*, vol. 19, no. 2, pp. 340–349, Feb. 2018, doi: 10.1007/S12221-018-7520-9.

[142] T. K. Arumugam, P. Krishnamoorthy, N. R. Rajagopalan, S. Nanthini, and D. Vasudevan, "Removal of malachite green from aqueous solutions using a modified chitosan composite," *Int. J. Biol. Macromol.*, vol. 128, pp. 655–664, May 2019, doi: 10.1016/j.ijbiomac.2019.01.185.

[143] S. T. Akar, E. San, and T. Akar, "Chitosan–alunite composite: An effective dye remover with high sorption, regeneration and application potential," *Carbohydr. Polym.*, vol. 143, pp. 318–326, Jun. 2016, doi: 10.1016/j.carbpol.2016.01.066.

[144] M. A. Khapre, S. Pandey, and R. M. Jugade, "Glutaraldehyde-cross-linked chitosan–alginate composite for organic dyes removal from aqueous solutions," *Int. J. Biol. Macromol.*, vol. 190, pp. 862–875, Nov. 2021, doi: 10.1016/J.IJBIOMAC.2021.09.026.

[145] T. J. Al-Musawi, N. Mengelizadeh, O. Al Rawi, and D. Balarak, "Capacity and Modeling of Acid Blue 113 Dye Adsorption onto Chitosan Magnetized by Fe2O3 Nanoparticles," *J. Polym. Environ.*, vol. 30, no. 1, pp. 344–359, Jan.

2022, doi: 10.1007/S10924-021-02200-8.

[146] J. C. S. da Silva *et al.*, “What happens when chitosan meets bentonite under microwave-assisted conditions? Clay-based hybrid nanocomposites for dye adsorption,” *Colloids Surf. A Physicochem. Eng. Asp.*, vol. 609, p. 125584, Jan. 2021, doi: 10.1016/j.colsurfa.2020.125584.

[147] F. Wang, L. Li, J. Iqbal, Z. Yang, and Y. Du, “Preparation of magnetic chitosan corn straw biochar and its application in adsorption of amaranth dye in aqueous solution,” *Int. J. Biol. Macromol.*, vol. 199, pp. 234–242, Feb. 2022, doi: 10.1016/j.ijbiomac.2021.12.195.

[148] A. Mokhtar *et al.*, “Adsorption behavior of cationic and anionic dyes on magadiite-chitosan composite beads,” *Carbohydr. Polym.*, vol. 229, p. 115399, Feb. 2020, doi: 10.1016/j.carbpol.2019.115399.

[149] D. Han *et al.*, “Preparation of carboxymethyl chitosan/phytic acid composite hydrogels for rapid dye adsorption in wastewater treatment,” *Colloids Surf. A Physicochem. Eng. Asp.*, vol. 628, p. 127355, Nov. 2021, doi: 10.1016/j.colsurfa.2021.127355.

[150] A. S. Abdulhameed, R. H. Al Omari, M. Abualhaija, and S. Algburi, “Novel bionanocomposite of grafted chitosan-phthalic anhydride/Co2O3 nanoparticles for efficient removal of brilliant green dye: Adsorption optimization using Box-Behnken design,” *Int. J. Biol. Macromol.*, vol. 283, p. 137645, Dec. 2024, doi: 10.1016/J.IJBIOMAC.2024.137645.

[151] H. M. Aghaa *et al.*, “Biocomposite Adsorbent of Grafted Chitosan-benzaldehyde/*Lactobacillus Casei* Bacteria for Removal of Acid Red 88 Dye: Box-Benken Design Optimization and Mechanism Approach,” *AUIQ Complementary Biological System*, vol. 2, no. 1, pp. 1–14, Mar. 2025, doi: 10.70176/3007-973X.1020.

[152] N. I. Normi *et al.*, “One-Step Functionalization of Chitosan Using Aromatic Groups via Hydrothermal Assisted Grafting for Removal of Reactive Orange 16 Dye: Optimization and Adsorption Mechanism,” *J. Polym. Environ.*, vol. 31, no. 4, pp. 1292–1307, Apr. 2023, doi: 10.1007/s10924-022-02688-8.

[153] A. H. Jawad, A. S. Abdulhameed, S. N. Surip, and Z. A. Alothman, “Hybrid multifunctional biocomposite of chitosan grafted benzaldehyde/montmorillonite/algae for effective removal of brilliant green and reactive blue 19 dyes: Optimization and adsorption mechanism,” *J. Clean.*

Prod., vol. 393, p. 136334, Mar. 2023, doi: 10.1016/j.jclepro.2023.136334.

[154] V. Vaid *et al.*, "Removal of Organic Dyes from Aqueous Solutions by Adsorption of Chitosan-Guar Gum-Based Glyoxal Crosslinked Hydrogel," *Fibers and Polymers*, vol. 24, no. 2, pp. 383–401, Feb. 2023, doi: 10.1007/S12221-023-00080-4/FIGURES/4.

[155] V. Gomase, T. Rathi, D. Saravanan, and R. Jugade, "Amputation of Remazol brilliant blue dye on crosslinked chitosan hydrogel: Statistical treatment and experimental evaluation," *Environ. Res.*, vol. 252, p. 118764, Jul. 2024, doi: 10.1016/j.envres.2024.118764.

[156] M. A. Kiechel and C. L. Schauer, "Non-covalent crosslinkers for electrospun chitosan fibers," *Carbohydr. Polym.*, vol. 95, no. 1, pp. 123–133, Jun. 2013, doi: 10.1016/J.CARBPOL.2013.02.034.

[157] Z. Shao *et al.*, "Novel green chitosan-pectin gel beads for the removal of Cu(II), Cd(II), Hg(II) and Pb(II) from aqueous solution," *Int. J. Biol. Macromol.*, vol. 176, pp. 217–225, Apr. 2021, doi: 10.1016/J.IJBIOMAC.2021.02.037.

[158] M. Rajabi, M. McConnell, J. Cabral, and M. A. Ali, "Chitosan hydrogels in 3D printing for biomedical applications," *Carbohydr. Polym.*, vol. 260, p. 117768, May 2021, doi: 10.1016/J.CARBPOL.2021.117768.

[159] E. M. Saad, R. F. Elshaarawy, S. A. Mahmoud, and K. M. El-Moselhy, "New Ulva lactuca Algae Based Chitosan Bio-composites for Bioremediation of Cd(II) Ions," *Journal of Bioresources and Bioproducts*, vol. 6, no. 3, pp. 223–242, Aug. 2021, doi: 10.1016/j.jobab.2021.04.002.

[160] B. Li, X. Lin, and Y. Zhao, "Facile preparation and application of magnetic chitosan/fly ash composite as a hybrid biosorbent for the effective removal of direct dyes," *J. Mol. Liq.*, vol. 397, p. 124148, Mar. 2024, doi: 10.1016/J.MOLLIQ.2024.124148.

[161] E. Binaeian, S. Babaee Zadvarzi, and D. Yuan, "Anionic dye uptake via composite using chitosan-polyacrylamide hydrogel as matrix containing TiO2 nanoparticles; comprehensive adsorption studies," *Int. J. Biol. Macromol.*, vol. 162, pp. 150–162, Nov. 2020, doi: 10.1016/j.ijbiomac.2020.06.158.

[162] A. A. Ismail *et al.*, "Self-cleaning application of mesoporous ZnO, TiO2 and Fe2O3 films with the accommodation of silver nanoparticles for antibacterial activity," *J. Taiwan Inst. Chem. Eng.*, vol. 142, p. 104627, Jan. 2023, doi: 10.1016/j.jtice.2022.104627.

[163] K. Ashok Kumar Raju and A. Biswas, “Corrosion behavior of self-organized TiO2 nanotubular arrays grown on Ti6Al4V for biomedical applications,” *Mater. Chem. Phys.*, vol. 305, p. 128011, Sep. 2023, doi: 10.1016/j.matchemphys.2023.128011.

[164] T. V. Nguyen *et al.*, “Effects of nano-TiO2 and nano-SiO2 particles on the reflectance and weathering durability of solar heat reflectance coating,” *J. Photochem. Photobiol. A Chem.*, vol. 442, p. 114752, Aug. 2023, doi: 10.1016/j.jphotochem.2023.114752.

[165] Y. J. Park *et al.*, “Selective Control of Novel TiO $_2$ Nanorods: Excellent Building Blocks for the Electron Transport Layer of Mesoscopic Perovskite Solar Cells,” *ACS Appl. Mater. Interfaces*, vol. 15, no. 7, pp. 9447–9456, Feb. 2023, doi: 10.1021/acsami.2c21731.

[166] N. Kumari, S. Chintakula, I. Sai Sonali Anantha, and S. Maddila, “An efficient P3TA/Fe doped TiO2 catalyst for photo-degradation of Brilliant green dye and inactivation of pathogens under visible light,” *Results Chem.*, vol. 5, p. 100759, Jan. 2023, doi: 10.1016/j.rechem.2022.100759.

[167] A. K. Inamdar *et al.*, “Flame synthesized tetragonal TiO2 nanoparticles for Methylene Blue and Congo Red dye removal applications,” *Results Chem.*, vol. 5, p. 100854, Jan. 2023, doi: 10.1016/j.rechem.2023.100854.

[168] C. Su, A. K. Berekute, and K.-P. Yu, “Chitosan@TiO2 composites for the adsorption of copper(II) and antibacterial applications,” *Sustainable Environment Research*, vol. 32, no. 1, p. 27, Dec. 2022, doi: 10.1186/s42834-022-00138-7.

[169] J. Gubitosa, V. Rizzi, P. Fini, S. Nuzzo, and P. Cosma, “The Adsorption Efficiency of Regenerable Chitosan-TiO2 Composite Films in Removing 2,4-Dinitrophenol from Water,” *Int. J. Mol. Sci.*, vol. 24, no. 10, p. 8552, May 2023, doi: 10.3390/ijms24108552.

[170] L. M. Anaya-Esparza *et al.*, “Chitosan-TiO2: A Versatile Hybrid Composite,” *Materials*, vol. 13, no. 4, p. 811, Feb. 2020, doi: 10.3390/ma13040811.

[171] T. Miyazaki, K. Ishikawa, Y. Shirosaki, and C. Ohtsuki, “Organic–inorganic composites designed for biomedical applications,” *Biol. Pharm. Bull.*, vol. 36, no. 11, pp. 1670–1675, 2013, Accessed: Jun. 11, 2025. [Online]. Available: https://www.jstage.jst.go.jp/article/bpb/36/11/36_b13-00424/_article/-char/ja/

[172] G. Xiao, X. Zhang, Y. Zhao, H. Su, and T. Tan, “The behavior of active

bactericidal and antifungal coating under visible light irradiation," *Appl. Surf. Sci.*, vol. 292, pp. 756–763, Feb. 2014, doi: 10.1016/j.apsusc.2013.12.044.

[173] T. Qian, H. Su, and T. Tan, "The bactericidal and mildew-proof activity of a TiO2–chitosan composite," *J. Photochem. Photobiol. A Chem.*, vol. 218, no. 1, pp. 130–136, Feb. 2011, doi: 10.1016/j.jphotochem.2010.12.012.

[174] R. Jayakumar, R. Ramachandran, V. V. Divyarani, K. P. Chennazhi, H. Tamura, and S. V. Nair, "Fabrication of chitin–chitosan/nano TiO2-composite scaffolds for tissue engineering applications," *Int. J. Biol. Macromol.*, vol. 48, no. 2, pp. 336–344, Mar. 2011, doi: 10.1016/j.ijbiomac.2010.12.010.

[175] B. Lin, Y. Luo, Z. Teng, B. Zhang, B. Zhou, and Q. Wang, "Development of silver/titanium dioxide/chitosan adipate nanocomposite as an antibacterial coating for fruit storage," *LWT - Food Science and Technology*, vol. 63, no. 2, pp. 1206–1213, Oct. 2015, doi: 10.1016/J.LWT.2015.04.049.

[176] K. Kavitha, M. Prabhu, V. Rajendran, P. Manivasankan, P. Prabu, and T. Jayakumar, "Optimization of nano-titania and titania–chitosan nanocomposite to enhance biocompatibility," *Curr. Nanosci.*, vol. 9, no. 3, pp. 308–317, 2013, doi: 10.2174/1573413711309030003.

[177] S. S. Behera, U. Das, A. Kumar, A. Bissoyi, and A. K. Singh, "Chitosan/TiO 2 composite membrane improves proliferation and survival of L929 fibroblast cells: Application in wound dressing and skin regeneration," *Int. J. Biol. Macromol.*, vol. 98, pp. 329–340, May 2017, doi: 10.1016/j.ijbiomac.2017.02.017.

[178] A. Sarwer *et al.*, "Algal biomass valorization for biofuel production and carbon sequestration: a review," *Environ. Chem. Lett.*, vol. 20, no. 5, pp. 2797–2851, Oct. 2022, doi: 10.1007/s10311-022-01458-1.

[179] S. Arun, A. Sinharoy, K. Pakshirajan, and P. N. L. Lens, "Algae based microbial fuel cells for wastewater treatment and recovery of value-added products," *Renewable and Sustainable Energy Reviews*, vol. 132, p. 110041, Oct. 2020, doi: 10.1016/j.rser.2020.110041.

[180] A. Kartik *et al.*, "A critical review on production of biopolymers from algae biomass and their applications," *Bioresour. Technol.*, vol. 329, p. 124868, Jun. 2021, doi: 10.1016/j.biortech.2021.124868.

[181] P. Bhatt, G. Bhandari, R. F. Turco, Z. Aminikhoei, K. Bhatt, and H. Simsek, "Algae in wastewater treatment, mechanism, and application of biomass for

production of value-added product," *Environmental Pollution*, vol. 309, p. 119688, Sep. 2022, doi: 10.1016/j.envpol.2022.119688.

[182] T. A. Aragaw and F. M. Bogale, "Biomass-Based Adsorbents for Removal of Dyes From Wastewater: A Review," *Front. Environ. Sci.*, vol. 9, pp. 1–24, Dec. 2021, doi: 10.3389/fenvs.2021.764958.

[183] G. Bayramoglu, S. Burcu Angi, I. Acikgoz-Erkaya, and M. Yakup Arica, "Preparation of effective green sorbents using O. Princeps alga biomass with different composition of amine groups: Comparison to adsorption performances for removal of a model acid dye," *J. Mol. Liq.*, vol. 347, p. 118375, Feb. 2022, doi: 10.1016/j.molliq.2021.118375.

[184] H. M. Abumelha, "Enhancing brilliant green dye removal via bio composite chitosan and food-grade algae capsulated ruthenium metal-organic framework: Optimization of adsorption parameters by box-behnken design," *Int. J. Biol. Macromol.*, vol. 264, p. 130635, Apr. 2024, doi: 10.1016/j.ijbiomac.2024.130635.

[185] A. Jiang *et al.*, "Chitosan Based Biodegradable Composite for Antibacterial Food Packaging Application," *Polymers (Basel).*, vol. 15, no. 10, p. 2235, May 2023, doi: 10.3390/polym15102235.

[186] A. R. Deshmukh *et al.*, "Biodegradable films based on chitosan and defatted Chlorella biomass: Functional and physical characterization," *Food Chem.*, vol. 337, p. 127777, Feb. 2021, doi: 10.1016/j.foodchem.2020.127777.

[187] F.-N. Allouche, "A user-friendly Ulva lactuca/chitosan composite bead for mercury removal," *Inorg. Chem. Commun.*, vol. 130, p. 108747, Aug. 2021, doi: 10.1016/j.inoche.2021.108747.

[188] İ. Sargın, G. Arslan, and M. Kaya, "Efficiency of chitosan–algal biomass composite microbeads at heavy metal removal," *React. Funct. Polym.*, vol. 98, pp. 38–47, Jan. 2016, doi: 10.1016/j.reactfunctpolym.2015.11.007.

[189] E. Kashi *et al.*, "High adsorptive performance of chitosan-microalgae-carbon-doped TiO2 (kronos)/ salicylaldehyde for brilliant green dye adsorption: Optimization and mechanistic approach," *Int. J. Biol. Macromol.*, vol. 259, p. 129147, Feb. 2024, doi: 10.1016/j.ijbiomac.2023.129147.

[190] Y. W. Chen, H. V. Lee, J. C. Juan, and S.-M. Phang, "Production of new cellulose nanomaterial from red algae marine biomass Gelidium elegans," *Carbohydr. Polym.*, vol. 151, pp. 1210–1219, Oct. 2016, doi:

10.1016/j.carbpol.2016.06.083.

[191] R. Gerhardt *et al.*, “Development of chitosan/Spirulina sp. blend films as biosorbents for Cr6+ and Pb2+ removal,” *Int. J. Biol. Macromol.*, vol. 155, pp. 142–152, Jul. 2020, doi: 10.1016/j.ijbiomac.2020.03.201.

[192] D. C. S. Alves, B. B. Coseglio, L. A. A. Pinto, and T. R. S. Cadaval, “Development of Spirulina/chitosan foam adsorbent for phenol adsorption,” *J. Mol. Liq.*, vol. 309, p. 113256, Jul. 2020, doi: 10.1016/j.molliq.2020.113256.

[193] J. M. Silva *et al.*, “Development of chitosan/Spirulina bio-blend films and its biosorption potential for dyes,” *J. Appl. Polym. Sci.*, vol. 134, no. 11, Mar. 2017, doi: 10.1002/APP.44580.

[194] E. Tekay, D. Aydınoğlu, and S. Şen, “Effective adsorption of Cr (VI) by high strength chitosan/montmorillonite composite hydrogels involving spirulina biomass/microalgae,” *J. Polym. Environ.*, vol. 27, no. 8, pp. 1828–1842, Aug. 2019, doi: 10.1007/S10924-019-01481-4.

[195] R. Balti *et al.*, “Development and characterization of bioactive edible films from spider crab (Maja crispata) chitosan incorporated with Spirulina extract,” *Int. J. Biol. Macromol.*, vol. 105, pp. 1464–1472, Dec. 2017, doi: 10.1016/j.ijbiomac.2017.07.046.

[196] S. Solanki, S. Sinha, K. Bisaria, R. Singh, and R. Saxena, “Accurate data prediction by fuzzy inference model for adsorption of hazardous azo dyes by novel algal doped magnetic chitosan bionanocomposite,” *Environ. Res.*, vol. 214, p. 113844, Nov. 2022, doi: 10.1016/j.envres.2022.113844.

[197] M. L. G. Vieira, C. P. Pinheiro, K. A. Silva, T. R. S. Cadaval, G. L. Dotto, and L. A. A. Pinto, “Development of adsorbent rigid structure based on Spirulina sp./chitosan bioblends coatings for dye adsorption in fixed bed column,” *Environmental Science and Pollution Research*, vol. 29, no. 52, pp. 79466–79477, Nov. 2022, doi: 10.1007/S11356-022-21372-X/TABLES/3.

[198] T. Fathipoor, M. Emtyazjoo, A. Kazemi, and M. S. Sadeghi, “Investigating the efficacy of chitosan-modified magnetic Spirulina biosorbent for mercury removal from aqueous solutions: isotherm model analysis,” *International Journal of Environmental Science and Technology*, vol. 21, no. 5, pp. 4807–4816, Mar. 2024, doi: 10.1007/S13762-023-05395-6/FIGURES/3.

[199] M. Ben Yahia *et al.*, “An emerging application of chitosan and chitosan/spirulina films for Pb2+ adsorption: New physicochemical insights via

experimental and theoretical studies," *Sep. Purif. Technol.*, vol. 337, p. 126451, Jun. 2024, doi: 10.1016/J.SEPPUR.2024.126451.

[200] L. Sellaoui *et al.*, "Novel films prepared from spirulina and chitosan for textile pollutant removal: Experiments and theoretical study of adsorption equilibrium via an advanced theoretical approach," *Sep. Purif. Technol.*, vol. 329, p. 125158, Jan. 2024, doi: 10.1016/J.SEPPUR.2023.125158.

[201] E. M. Elnaggar *et al.*, "Insight into divergent chemical modifications of chitosan biopolymer: Review," *Int. J. Biol. Macromol.*, vol. 277, p. 134347, Oct. 2024, doi: 10.1016/J.IJBIOMAC.2024.134347.

[202] I. O. Saheed, W. Da Oh, and F. B. M. Suah, "Chitosan modifications for adsorption of pollutants – A review," *J. Hazard. Mater.*, vol. 408, p. 124889, Apr. 2021, doi: 10.1016/j.jhazmat.2020.124889.

[203] F. Alakhras *et al.*, "Adsorptive removal of cationic rhodamine B dye from aqueous solutions using chitosan-derived schiff base," *Sep. Sci. Technol.*, vol. 57, no. 4, pp. 542–554, 2022, doi: 10.1080/01496395.2021.1931326.

[204] A. A. Alamri *et al.*, "Synthesis of Schiff bases based on Chitosan, thermal stability and evaluation of antimicrobial and antitumor activities," *Sci. Rep.*, vol. 15, no. 1, pp. 1–14, Dec. 2025, doi: 10.1038/S41598-024-73610-6.

[205] T. Abdul-Kader Saleh, E. T. B. Al-Tikrity, E. Yousif, M. H. Al-Mashhadani, and A. H. Jawad, "Preparation of Schiff bases derived from chitosan and investigate their photostability and thermal stability," *Physical Chemistry Research*, vol. 10, no. 4, pp. 549–557, 2022, doi: 10.22036/PCR.2022.333808.2051.

[206] G. Crini, G. Torri, E. Lichtfouse, G. Z. Kyzas, L. D. Wilson, and N. Morin-Crini, "Dye removal by biosorption using cross-linked chitosan-based hydrogels," *Environmental Chemistry Letters 2019 17:4*, vol. 17, no. 4, pp. 1645–1666, Jul. 2019, doi: 10.1007/S10311-019-00903-Y.

[207] M. Sadeghi-Kiakhani, M. Arami, and K. Gharanjig, "Preparation of chitosan-ethyl acrylate as a biopolymer adsorbent for basic dyes removal from colored solutions," *J. Environ. Chem. Eng.*, vol. 1, no. 3, pp. 406–415, Sep. 2013, doi: 10.1016/j.jece.2013.06.001.

[208] K. Rathinam, S. P. Singh, C. J. Arnusch, and R. Kasher, "An environmentally-friendly chitosan-lysozyme biocomposite for the effective removal of dyes and heavy metals from aqueous solutions," *Carbohydr. Polym.*, vol. 199, pp. 506–

515, Nov. 2018, doi: 10.1016/j.carbpol.2018.07.055.

[209] I. A. Mohammed, A. H. Jawad, A. S. Abdulhameed, and M. S. Mastuli, “Physicochemical modification of chitosan with fly ash and tripolyphosphate for removal of reactive red 120 dye: Statistical optimization and mechanism study,” *Int. J. Biol. Macromol.*, vol. 161, pp. 503–513, Oct. 2020, doi: 10.1016/j.ijbiomac.2020.06.069.

[210] A. H. Jawad, A. S. Abdulhameed, N. N. A. Malek, and Z. A. ALOthman, “Statistical optimization and modeling for color removal and COD reduction of reactive blue 19 dye by mesoporous chitosan-epichlorohydrin/kaolin clay composite,” *Int. J. Biol. Macromol.*, vol. 164, pp. 4218–4230, Dec. 2020, doi: 10.1016/j.ijbiomac.2020.08.201.

[211] F. Marrakchi, B. H. Hameed, and E. H. Hummadi, “Mesoporous biohybrid epichlorohydrin crosslinked chitosan/carbon–clay adsorbent for effective cationic and anionic dyes adsorption,” *Int. J. Biol. Macromol.*, vol. 163, pp. 1079–1086, Nov. 2020, doi: 10.1016/j.ijbiomac.2020.07.032.

[212] J. Yang *et al.*, “Synthesis of honeycomb-like citric acid-crosslinked chitosan hydrogel beads (cCHBs): Insight into structural characteristics of Cu(II)-loaded cCHBs (cCHBs-Cu(II)),” *Int. J. Biol. Macromol.*, vol. 301, p. 140244, Apr. 2025, doi: 10.1016/J.IJBIOMAC.2025.140244.

[213] K. Stanković *et al.*, “Citric acid functionalized chitosan hydrogel beads for enhanced Cr(VI) removal: Experimental assessment and COMSOL modelling of adsorption in a fixed-bed system,” *Journal of Industrial and Engineering Chemistry*, vol. 144, pp. 512–525, Apr. 2025, doi: 10.1016/J.JIEC.2024.09.051.

[214] B. Kjidaa, Z. Mchich, K. Aziz, N. Saffaj, T. Saffaj, and R. Mamouni, “Flexible Synthesis of Bio-Hydroxyapatite/Chitosan Hydrogel Beads for Highly Efficient Orange G Dye Removal: Batch and Recirculating Fixed-Bed Column Study,” *ACS Omega*, 2023, doi: 10.1021/ACSOMEGA.3C10054.

[215] E. Igberase, A. Ofomaja, and P. O. Osifo, “Enhanced heavy metal ions adsorption by 4-aminobenzoic acid grafted on chitosan/epichlorohydrin composite: Kinetics, isotherms, thermodynamics and desorption studies,” *Int. J. Biol. Macromol.*, vol. 123, pp. 664–676, Feb. 2019, doi: 10.1016/j.ijbiomac.2018.11.082.

[216] B. Tanhaei, A. Ayati, and M. Sillanpää, “Magnetic xanthate modified chitosan as an emerging adsorbent for cationic azo dyes removal: Kinetic,

thermodynamic and isothermal studies," *Int. J. Biol. Macromol.*, vol. 121, pp. 1126–1134, Jan. 2019, doi: 10.1016/j.ijbiomac.2018.10.137.

[217] G. H. Al-Hazmi, L. A. Albedair, R. A. S. Alatawi, J. S. Alnawmasi, A. M. Alsuhaibani, and M. G. El-Desouky, "Enhancing trimethoprim pollutant removal from wastewater using magnetic metal-organic framework encapsulated with poly (itaconic acid)-grafted crosslinked chitosan composite sponge: Optimization through Box-Behnken design and thermodynamics of adsorption parameters," *Int. J. Biol. Macromol.*, vol. 268, p. 131947, May 2024, doi: 10.1016/j.ijbiomac.2024.131947.

[218] J. Zhou, B. Hao, L. Wang, J. Ma, and W. Cheng, "Preparation and characterization of nano-TiO2/chitosan/poly(N-isopropylacrylamide) composite hydrogel and its application for removal of ionic dyes," *Sep. Purif. Technol.*, vol. 176, pp. 193–199, Apr. 2017, doi: 10.1016/j.seppur.2016.11.069.

[219] N. Parshi, D. Pan, V. Dhavle, B. Jana, S. Maity, and J. Ganguly, "Fabrication of lightweight and reusable salicylaldehyde functionalized chitosan as adsorbent for dye removal and its mechanism," *Int. J. Biol. Macromol.*, vol. 141, pp. 626–635, Dec. 2019, doi: 10.1016/j.ijbiomac.2019.09.025.

[220] I. M. M. Kenawy, M. M. Eldeframy, R. M. Eltabey, and E. G. Zaki, "Melamine grafted chitosan-montmorillonite nanocomposite for ferric ions adsorption: Central composite design optimization study," *J. Clean. Prod.*, vol. 241, p. 118189, Dec. 2019, doi: 10.1016/j.jclepro.2019.118189.

[221] A.-T. Mohammad, A. S. Abdulhameed, and A. H. Jawad, "Box-Behnken design to optimize the synthesis of new crosslinked chitosan-glyoxal/TiO2 nanocomposite: Methyl orange adsorption and mechanism studies," *Int. J. Biol. Macromol.*, vol. 129, pp. 98–109, May 2019, doi: 10.1016/j.ijbiomac.2019.02.025.

[222] A. Reghioua, D. Barkat, A. H. Jawad, A. S. Abdulhameed, A. A. Al-Kahtani, and Z. A. ALOthman, "Parametric optimization by Box–Behnken design for synthesis of magnetic chitosan-benzil/ZnO/Fe3O4 nanocomposite and textile dye removal," *J. Environ. Chem. Eng.*, vol. 9, no. 3, p. 105166, Jun. 2021, doi: 10.1016/j.jece.2021.105166.

[223] A. Reghioua, D. Barkat, A. H. Jawad, A. S. Abdulhameed, and M. R. Khan, "Synthesis of Schiff's base magnetic crosslinked chitosan-glyoxal/ZnO/Fe3O4 nanoparticles for enhanced adsorption of organic dye: Modeling and mechanism

study," *Sustain. Chem. Pharm.*, vol. 20, p. 100379, May 2021, doi: 10.1016/j.scp.2021.100379.

[224] M. E. A. El-Aziz, A. M. Youssef, K. H. Kamal, I. Kelnar, and S. Kamel, "Preparation and performance of bionanocomposites based on grafted chitosan, GO and TiO2-NPs for removal of lead ions and basic-red 46," *Carbohydr. Polym.*, vol. 305, p. 120571, Apr. 2023, doi: 10.1016/j.carbpol.2023.120571.

[225] A. H. Jawad, S. S. A. Norrahma, B. H. Hameed, and K. Ismail, "Chitosan-glyoxal film as a superior adsorbent for two structurally different reactive and acid dyes: Adsorption and mechanism study," *Int. J. Biol. Macromol.*, vol. 135, pp. 569–581, Aug. 2019, doi: 10.1016/j.ijbiomac.2019.05.127.

[226] A. H. Jawad, N. F. H. Mamat, B. H. Hameed, and K. Ismail, "Biofilm of cross-linked Chitosan-Ethylene Glycol Diglycidyl Ether for removal of Reactive Red 120 and Methyl Orange: Adsorption and mechanism studies," *J. Environ. Chem. Eng.*, vol. 7, no. 2, p. 102965, Apr. 2019, doi: 10.1016/j.jece.2019.102965.

[227] B. P. Kafle, *Chemical analysis and material characterization by spectrophotometry*. Elsevier, 2019.

[228] S. Subramaniam, K. Y. Foo, E. N. Md Yusof, A. H. Jawad, L. D. Wilson, and S. Sabar, "Hydrothermal synthesis of phosphorylated chitosan and its adsorption performance towards Acid Red 88 dye," *Int. J. Biol. Macromol.*, vol. 193, pp. 1716–1726, Dec. 2021, doi: 10.1016/j.ijbiomac.2021.11.009.

[229] N. S. Abishek and K. Gopalakrishna Naik, "Structural and morphological properties of bismuth telluride nanoparticles synthesized by two-step hydrothermal method," *Mater. Today Proc.*, vol. 49, pp. 1319–1322, 2022, doi: 10.1016/j.matpr.2021.06.390.

[230] A. A. H. Faisal, S. S. Alquzweeni, L. A. Naji, and M. Naushad, "Predominant Mechanisms in the Treatment of Wastewater Due to Interaction of Benzaldehyde and Iron Slag Byproduct," *Int. J. Environ. Res. Public Health*, vol. 17, no. 1, p. 226, Dec. 2019, doi: 10.3390/ijerph17010226.

[231] M. A. Andrade and L. M. D. R. S. Martins, "Selective Styrene Oxidation to Benzaldehyde over Recently Developed Heterogeneous Catalysts," *Molecules*, vol. 26, no. 6, p. 1680, Mar. 2021, doi: 10.3390/molecules26061680.

[232] H. Li, Y. Meng, C. Shu, X. Li, A. A. Kiss, and X. Gao, "Innovative Reactive Distillation Process for the Sustainable Synthesis of Natural Benzaldehyde," *ACS Sustain. Chem. Eng.*, vol. 6, no. 11, pp. 14114–14124, Nov. 2018, doi:

10.1021/acssuschemeng.8b02686.

[233] F. Brühne and E. Wright, "Benzaldehyde," *Ullmann's Encyclopedia of Industrial Chemistry*, Oct. 2011, doi: 10.1002/14356007.A03_463.PUB2.

[234] J. P. Losada, I. Heckl, B. Bertok, F. Friedler, J. C. Garcia-Ojeda, and A. Argoti, "Process network synthesis for benzaldehyde production: P-graph approach," *Chem. Eng. Trans.*, vol. 45, pp. 1369–1374, 2015, doi: 10.3303/CET1545229.

[235] F. Damiri, Y. Bachra, C. Bounacir, A. Laaraibi, and M. Berrada, "Synthesis and Characterization of Lyophilized Chitosan-Based Hydrogels Cross-Linked with Benzaldehyde for Controlled Drug Release," *J. Chem.*, vol. 2020, pp. 1–10, May 2020, doi: 10.1155/2020/8747639.

[236] C. Maliverney and M. Mulhauser, "Hydroxybenzaldehydes," *Kirk-Othmer Encyclopedia of Chemical Technology*, Dec. 2000, doi: 10.1002/0471238961.0825041813011209.A01.

[237] A. M. Saeed, A. G. Taha, H. M. Dardeer, and M. F. Aly, "One-pot synthesis of novel chitosan-salicylaldehyde polymer composites for ammonia sensing," *Sci. Rep.*, vol. 14, no. 1, p. 239, Jan. 2024, doi: 10.1038/s41598-023-50243-9.

[238] P. G. Cozzi, "Metal–Salen Schiff base complexes in catalysis: practical aspects," *Chem. Soc. Rev.*, vol. 33, no. 7, pp. 410–421, Sep. 2004, doi: 10.1039/B307853C.

[239] E. Frollini, C. G. Silva, and E. C. Ramires, "Phenolic resins as a matrix material in advanced fiber-reinforced polymer (FRP) composites," *Advanced Fibre-Reinforced Polymer (FRP) Composites for Structural Applications*, pp. 7–43, Jan. 2013, doi: 10.1533/9780857098641.1.7.

[240] B. Kaczmarek-Szczepańska, O. Mazur, M. Michalska-Sionkowska, K. Łukowicz, and A. M. Osyczka, "The Preparation and Characterization of Chitosan-Based Hydrogels Cross-Linked by Glyoxal," *Materials*, vol. 14, no. 9, p. 2449, May 2021, doi: 10.3390/ma14092449.

[241] Q. YANG, F. DOU, B. LIANG, and Q. SHEN, "Studies of cross-linking reaction on chitosan fiber with glyoxal," *Carbohydr. Polym.*, vol. 59, no. 2, pp. 205–210, Jan. 2005, doi: 10.1016/j.carbpol.2004.09.013.

[242] C.-C. Tsai, T.-H. Young, G.-S. Chen, and N.-C. Cheng, "Developing a Glyoxal-Crosslinked Chitosan/Gelatin Hydrogel for Sustained Release of Human Platelet Lysate to Promote Tissue Regeneration," *Int. J. Mol. Sci.*, vol. 22, no. 12, p. 6451, Jun. 2021, doi: 10.3390/ijms22126451.

[243] A. S. Abdulhameed, A.-T. Mohammad, and A. H. Jawad, “Modeling and mechanism of reactive orange 16 dye adsorption by chitosan-glyoxal/TiO2 nanocomposite: application of response surface methodology,” *Desalination Water Treat.*, vol. 164, pp. 346–360, 2019, doi: 10.5004/dwt.2019.24384.

[244] N. N. A. Malek, A. H. Jawad, A. S. Abdulhameed, K. Ismail, and B. H. Hameed, “New magnetic Schiff’s base-chitosan-glyoxal/fly ash/Fe3O4 biocomposite for the removal of anionic azo dye: An optimized process,” *Int. J. Biol. Macromol.*, vol. 146, pp. 530–539, Mar. 2020, doi: 10.1016/j.ijbiomac.2020.01.020.

[245] E. Igberase, P. Ogbemudia Osifo, T. Seodigeng, and I. Emeji, “Use of Diethylenetriamine Grafted onto Glyoxal Cross-Linked Chitosan Beads for Efficient Batch System Adsorption,” *Engineering Materials*, pp. 135–157, 2021, doi: 10.1007/978-3-030-71722-3_7.

[246] M. Qin, D. Dou, Y. Zhu, M. Zhang, J. Deng, and T. Zhou, “High-effective, convenient and environmental-friendly MOFs-chitosan-glyoxal composite film for ceftizoxime adsorption: Behavior and mechanisms,” *Int. J. Biol. Macromol.*, vol. 282, p. 137077, Dec. 2024, doi: 10.1016/J.IJBIOMAC.2024.137077.

[247] R. Chigare, J. Patil, and S. Kamat, “Synthesis of Benzil and Its Various Derivatives,” *International Research Journal of Engineering and Technology*, vol. 7, pp. 3764–3766, May 2020, Accessed: Jun. 13, 2025. [Online]. Available: https://www.researchgate.net/profile/Siddharth-Kamat-2/publication/341821250_Synthesis_of_Benzil_and_its_Various_Derivatives/links/5ed603af4585152945280e15/Synthesis-of-Benzil-and-its-Various-Derivatives.pdf

[248] N. Kanagathara, K. Senthilkumar, V. Sabari, V. Ragavendran, and S. Elangovan, “Structural and Vibrational Investigation of Benzil-(1,2-Diphenylethane-1,2-Dione): Experimental and Theoretical Studies,” *J. Chem.*, vol. 2022, pp. 1–11, Apr. 2022, doi: 10.1155/2022/5968496.

[249] D. Mitrogiannis, G. Markou, A. Çelekli, and H. Bozkurt, “Biosorption of methylene blue onto Arthrospira platensis biomass: Kinetic, equilibrium and thermodynamic studies,” *J. Environ. Chem. Eng.*, vol. 3, no. 2, pp. 670–680, Jun. 2015, doi: 10.1016/j.jece.2015.02.008.

[250] R. A. Soni, K. Sudhakar, and R. S. Rana, “Spirulina – From growth to nutritional product: A review,” *Trends Food Sci. Technol.*, vol. 69, pp. 157–171, Nov. 2017, doi: 10.1016/j.tifs.2017.09.010.

[251] I. Y. López-Pacheco *et al.*, "Removal and biotransformation of 4-nonylphenol by Arthrospira maxima and Chlorella vulgaris consortium," *Environ. Res.*, vol. 179, p. 108848, Dec. 2019, doi: 10.1016/j.envres.2019.108848.

[252] M. H. Sayadi, N. Salmani, A. Heidari, and M. R. Rezaei, "Bio-synthesis of palladium nanoparticle using Spirulina platensis alga extract and its application as adsorbent," *Surfaces and Interfaces*, vol. 10, pp. 136–143, Mar. 2018, doi: 10.1016/j.surfin.2018.01.002.

[253] J. Masojídek, J. Kopecký, L. Giannelli, and G. Torzillo, "Productivity correlated to photobiochemical performance of Chlorella mass cultures grown outdoors in thin-layer cascades," *J. Ind. Microbiol. Biotechnol.*, vol. 38, no. 2, pp. 307–317, Feb. 2011, doi: 10.1007/s10295-010-0774-x.

[254] Y. A. R. Lebron, V. R. Moreira, and L. V. S. Santos, "Studies on dye biosorption enhancement by chemically modified Fucus vesiculosus, Spirulina maxima and Chlorella pyrenoidosa algae," *J. Clean. Prod.*, vol. 240, p. 118197, Dec. 2019, doi: 10.1016/J.JCLEPRO.2019.118197.

[255] W. Z. Wu, R. Li, Z. Q. L. Ma, C. X. Liu, and W. T. Zhao, "Biochar-algae microspheres based on sodium alginate for the highly efficient adsorption of malachite green dye: Kinetics, isotherms, and mechanism of adsorption," *J. Contam. Hydrol.*, vol. 272, p. 104547, May 2025, doi: 10.1016/J.JCONHYD.2025.104547.

[256] H. Arshad, M. Imran, M. Ashraf, A. Naeem, and M. A. Riaz, "Removal of structurally different textile dyes from water by adsorption onto biomass of non-viable Chlorella sorokiniana strain HIN-3: Kinetics and adsorption isotherms," *J. Appl. Phycol.*, vol. 37, no. 2, pp. 973–985, Apr. 2025, doi: 10.1007/S10811-025-03445-9/TABLES/4.

[257] J. T. Ferreira *et al.*, "Evaluating the removal of the tetra-azo dye direct black-22 in Chlorella vulgaris closed-cultivation systems," *Environ. Technol.*, May 2025, doi: 10.1080/09593330.2024.2406989.

[258] S. Mirizadeh, A. A. Casazza, and A. Converti, "Removal of tetracycline and crystal violet from aqueous solutions by magnetic chitosan-lipid free Chlorella vulgaris biocomposite," *Sep. Purif. Technol.*, vol. 368, p. 132919, Sep. 2025, doi: 10.1016/J.SEPPUR.2025.132919.

[259] M. H. Marzbali, A. A. Mir, M. Pazoki, R. Pourjamshidian, and M. Tabeshnia, "Removal of direct yellow 12 from aqueous solution by adsorption onto

spirulina algae as a high-efficiency adsorbent," *J. Environ. Chem. Eng.*, vol. 5, no. 2, pp. 1946–1956, Apr. 2017, doi: 10.1016/j.jece.2017.03.018.

[260] K. Wei, Y. Faraj, G. Yao, R. Xie, and B. Lai, "Strategies for improving perovskite photocatalysts reactivity for organic pollutants degradation: A review on recent progress," *Chemical Engineering Journal*, vol. 414, p. 128783, Jun. 2021, doi: 10.1016/J.CEJ.2021.128783.

[261] T. R. Esch, I. Gadaczek, and T. Bredow, "Surface structures and thermodynamics of low-index of rutile, brookite and anatase – A comparative DFT study," *Appl. Surf. Sci.*, vol. 288, pp. 275–287, Jan. 2014, doi: 10.1016/j.apsusc.2013.10.021.

[262] X. Jaramillo-Fierro, L. F. Capa, F. Medina, and S. González, "DFT Study of Methylene Blue Adsorption on ZnTiO3 and TiO2 Surfaces (101)," *Molecules*, vol. 26, no. 13, p. 3780, Jun. 2021, doi: 10.3390/molecules26133780.

[263] B. Rouhi Broujeni, A. Nilchi, and F. Azadi, "Adsorption modeling and optimization of thorium (IV) ion from aqueous solution using chitosan/TiO2 nanocomposite: Application of artificial neural network and genetic algorithm," *Environ. Nanotechnol. Monit. Manag.*, vol. 15, p. 100400, May 2021, doi: 10.1016/j.enmm.2020.100400.

[264] K. S. Abdullah Al Balushi, G. Devi, A. Saif Al Hudaifi, and A. S. R. Khamis Al Garibi, "Development of chitosan-TiO2 thin film and its application for methylene blue dye degradation," *Int. J. Environ. Anal. Chem.*, vol. 103, no. 17, pp. 6062–6075, 2023, doi: 10.1080/03067319.2021.1948540.

[265] A. H. Jawad, N. S. A. Mubarak, and A. S. Abdulhameed, "Hybrid Crosslinked Chitosan-Epichlorohydrin/TiO2 Nanocomposite for Reactive Red 120 Dye Adsorption: Kinetic, Isotherm, Thermodynamic, and Mechanism Study," *J. Polym. Environ.*, vol. 28, no. 2, pp. 624–637, Feb. 2020, doi: 10.1007/s10924-019-01631-8.

[266] M. A. Ahmed, N. M. Abdelbar, and A. A. Mohamed, "Molecular imprinted chitosan-TiO2 nanocomposite for the selective removal of Rose Bengal from wastewater," *Int. J. Biol. Macromol.*, vol. 107, pp. 1046–1053, Feb. 2018, doi: 10.1016/j.ijbiomac.2017.09.082.

[267] R. Mashabi, Z. Khan, K. E.-M. Advances, and undefined 2022, "Chitosan-or glycidyl methacrylate-based adsorbents for the removal of dyes from aqueous solutions: a review," *pubs.rsc.org*, vol. 2022, p. 5645, 2022, doi:

10.1039/d2ma00320a.

[268] A. H. Jawad, A. S. Abdulhameed, and M. S. Mastuli, “Mesoporous Crosslinked Chitosan-Activated Charcoal Composite for the Removal of Thionine Cationic Dye: Comprehensive Adsorption and Mechanism Study,” *J. Polym. Environ.*, vol. 28, no. 3, pp. 1095–1105, Mar. 2020, doi: 10.1007/s10924-020-01671-5.

[269] E. Kashi, A. H. Jawad, S. N. Surip, R. Wu, and Z. A. ALOthman, “Crosslinked chitosan-benzil/microalgae/kronos (titanium dioxide) biocomposite for the removal of brilliant green dye: Response surface methodology optimisation and mechanism,” *Int. J. Biol. Macromol.*, vol. 312, p. 144005, Jun. 2025, doi: 10.1016/J.IJBIOMAC.2025.144005.

[270] S. Karimifard and M. R. Alavi Moghaddam, “Application of response surface methodology in physicochemical removal of dyes from wastewater: A critical review,” *Science of The Total Environment*, vol. 640–641, pp. 772–797, Nov. 2018, doi: 10.1016/j.scitotenv.2018.05.355.

[271] S. Lagergren, “Zur theorie der sogenannten adsorption geloster stoffe,” *K. Sven. vetenskapsakademiens. Handl.*, vol. 24, pp. 1–39, 1898.

[272] Y. HO and G. MCKAY, “Sorption of dye from aqueous solution by peat,” *Chemical Engineering Journal*, vol. 70, no. 2, pp. 115–124, Jun. 1998, doi: 10.1016/S1385-8947(98)00076-X.

[273] U. Habiba, J. J. L. Lee, T. C. Joo, B. C. Ang, and A. M. Afifi, “Degradation of methyl orange and congo red by using chitosan/polyvinyl alcohol/TiO2 electrospun nanofibrous membrane,” *Int. J. Biol. Macromol.*, vol. 131, pp. 821–827, Jun. 2019, doi: 10.1016/j.ijbiomac.2019.03.132.

[274] I. Langmuir, “THE ADSORPTION OF GASES ON PLANE SURFACES OF GLASS, MICA AND PLATINUM.,” *J. Am. Chem. Soc.*, vol. 40, no. 9, pp. 1361–1403, Sep. 1918, doi: 10.1021/ja02242a004.

[275] H. M. F. Freundlich, “Over the adsorption in solution,” *J. Phys. chem* , vol. 57, no. 385471, pp. 1100–1107, 1906.

[276] M. J. Temkin and V. Pyzhev, “Recent modifications to Langmuir isotherms,” 1940.

[277] T. A. Osmari, R. Gallon, M. Schwaab, E. Barbosa-Coutinho, J. B. Severo, and J. C. Pinto, “Statistical Analysis of Linear and Non-Linear Regression for the Estimation of Adsorption Isotherm Parameters,” *Adsorption Science & Technology*, vol. 31, no. 5, pp. 433–458, May 2013, doi: 10.1260/0263-

6174.31.5.433.

[278] M. E. González-López, C. M. Laureano-Anzaldo, A. A. Pérez-Fonseca, M. Arellano, and J. R. Robledo-Ortíz, "A Critical Overview of Adsorption Models Linearization: Methodological and Statistical Inconsistencies," *Separation & Purification Reviews*, vol. 51, no. 3, pp. 358–372, Jul. 2022, doi: 10.1080/15422119.2021.1951757.

[279] S. Daikh, D. Ouis, A. Benyoucef, and B. Mouffok, "Equilibrium, kinetic and thermodynamic studies for evaluation of adsorption capacity of a new potential hybrid adsorbent based on polyaniline and chitosan for Acetaminophen," *Chem. Phys. Lett.*, vol. 798, p. 139565, Jul. 2022, doi: 10.1016/j.cplett.2022.139565.

[280] M. Thommes *et al.*, "Physisorption of gases, with special reference to the evaluation of surface area and pore size distribution (IUPAC Technical Report)," *Pure and Applied Chemistry*, vol. 87, no. 9–10, pp. 1051–1069, Oct. 2015, doi: 10.1515/pac-2014-1117.

[281] M. Imani, L. Radmanesh, and A. Tadjarodi, "Synthesis and study of the pseudocapacitive behavior of heterojunctional NiTiO3-based chitosan nanocomposite," *Journal of Physics and Chemistry of Solids*, vol. 139, p. 109309, Apr. 2020, doi: 10.1016/j.jpcs.2019.109309.

[282] A. K. Inamdar *et al.*, "Flame synthesized tetragonal TiO2 nanoparticles for Methylene Blue and Congo Red dye removal applications," *Results Chem.*, vol. 5, p. 100854, Jan. 2023, doi: 10.1016/j.rechem.2023.100854.

[283] H. Kaur, S. Kaur, J. Singh, M. Rawat, and S. Kumar, "Expanding horizon: green synthesis of TiO_2 nanoparticles using Carica papaya leaves for photocatalysis application," *Mater. Res. Express*, vol. 6, no. 9, p. 095034, Jul. 2019, doi: 10.1088/2053-1591/ab2ec5.

[284] A. S. AlShammari, M. M. Halim, F. K. Yam, and N. H. M. Kaus, "Synthesis of Titanium Dioxide (TiO2)/Reduced Graphene Oxide (rGO) thin film composite by spray pyrolysis technique and its physical properties," *Mater. Sci. Semicond. Process.*, vol. 116, p. 105140, Sep. 2020, doi: 10.1016/j.mssp.2020.105140.

[285] M. A. Khapre, S. Pandey, and R. M. Jugade, "Glutaraldehyde-cross-linked chitosan–alginate composite for organic dyes removal from aqueous solutions," *Int. J. Biol. Macromol.*, vol. 190, pp. 862–875, Nov. 2021, doi: 10.1016/j.ijbiomac.2021.09.026.

[286] R. M. Eltabey, F. T. Abdelwahed, M. M. Eldefrawy, and M. M. Elnagar,

"Fabrication of poly(maleic acid)-grafted cross-linked chitosan/montmorillonite nanospheres for ultra-high adsorption of anionic acid yellow-17 and cationic brilliant green dyes in single and binary systems," *J. Hazard. Mater.*, vol. 439, p. 129589, Oct. 2022, doi: 10.1016/j.jhazmat.2022.129589.

[287] J. Kurczewska, "Chitosan-montmorillonite hydrogel beads for effective dye adsorption," *Journal of Water Process Engineering*, vol. 48, p. 102928, Aug. 2022, doi: 10.1016/j.jwpe.2022.102928.

[288] A. S. Abdulhameed, A. H. Jawad, E. Kashi, K. A. Radzun, Z. A. ALOthman, and L. D. Wilson, "Insight into adsorption mechanism, modeling, and desirability function of crystal violet and methylene blue dyes by microalgae: Box-Behnken design application," *Algal Res.*, vol. 67, 2022, doi: 10.1016/j.algal.2022.102864.

[289] A.-T. Mohammad, A. S. Abdulhameed, and A. H. Jawad, "Box-Behnken design to optimize the synthesis of new crosslinked chitosan-glyoxal/TiO2 nanocomposite: Methyl orange adsorption and mechanism studies," *Int. J. Biol. Macromol.*, vol. 129, pp. 98–109, May 2019, doi: 10.1016/j.ijbiomac.2019.02.025.

[290] D. C. L. Vasconcelos, V. C. Costa, E. H. M. Nunes, A. C. S. Sabioni, M. Gasparon, and W. L. Vasconcelos, "Infrared Spectroscopy of Titania Sol-Gel Coatings on 316L Stainless Steel," *Materials Sciences and Applications*, vol. 02, no. 10, pp. 1375–1382, 2011, doi: 10.4236/msa.2011.210186.

[291] M. Laxmi Deepak Bhatlu, P. S. Athira, N. Jayan, D. Barik, and M. S. Dennison, "Preparation of Breadfruit Leaf Biochar for the Application of Congo Red Dye Removal from Aqueous Solution and Optimization of Factors by RSM-BBD," *Adsorption Science & Technology*, vol. 2023, pp. 1–17, Feb. 2023, doi: 10.1155/2023/7369027.

[292] J. Flores-Gómez, V. H. Romero-Arellano, M. Vazquez-Lepe, Á. de J. Martínez-Gómez, and J. Morales-Rivera, "Modeling and Optimization of the Adsorption of Cr (VI) in a Chitosan-Resole Aerogel Using Response Surface Methodology," *Gels*, vol. 9, no. 3, p. 197, Mar. 2023, doi: 10.3390/gels9030197.

[293] H. Khan *et al.*, "Multiple design and modelling approaches for the optimisation of carbon felt electro-Fenton treatment of dye laden wastewater," *Chemosphere*, p. 139510, Jul. 2023, doi: 10.1016/j.chemosphere.2023.139510.

[294] E. Natarajan and G. P. Ponnaiah, "Optimization of process parameters for the

decolorization of Reactive Blue 235 dye by barium alginate immobilized iron nanoparticles synthesized from aluminum industry waste," *Environ. Nanotechnol. Monit. Manag.*, vol. 7, pp. 73–88, May 2017, doi: 10.1016/j.enmm.2017.01.002.

[295] A. E. D. Mahmoud, M. Hosny, N. El-Maghrabi, and M. Fawzy, "Facile synthesis of reduced graphene oxide by Tecoma stans extracts for efficient removal of Ni (II) from water: batch experiments and response surface methodology," *Sustainable Environment Research*, vol. 32, no. 1, p. 22, Mar. 2022, doi: 10.1186/s42834-022-00131-0.

[296] V. O. Njoku, M. A. Islam, M. Asif, and B. H. Hameed, "Preparation of mesoporous activated carbon from coconut frond for the adsorption of carbofuran insecticide," *J. Anal. Appl. Pyrolysis*, vol. 110, pp. 172–180, Nov. 2014, doi: 10.1016/j.jaap.2014.08.020.

[297] S. Gul *et al.*, "Removal of Brilliant Green Dye from Water Using Ficus benghalensis Tree Leaves as an Efficient Biosorbent," *Materials*, vol. 16, no. 2, p. 521, Jan. 2023, doi: 10.3390/ma16020521.

[298] S. Singh, H. Gupta, S. Dhiman, and N. K. Sahu, "Decontamination of cationic dye brilliant green from the aqueous media," *Appl. Water Sci.*, vol. 12, no. 4, p. 61, Apr. 2022, doi: 10.1007/s13201-022-01596-5.

[299] M. T. Alotaibi, R. T. Mogharbel, A. Q. Alorabi, N. A. Alamrani, A. Shahat, and N. M. El-Metwaly, "Superior adsorption and removal of toxic industrial dyes using cubic Pm3n aluminosilica form an aqueous solution, Isotherm, Kinetic, thermodynamic and mechanism of interaction," *J. Mol. Liq.*, vol. 379, p. 121672, Jun. 2023, doi: 10.1016/j.molliq.2023.121672.

[300] S. Zghal, I. Jedidi, M. Cretin, S. Cerneaux, and M. Abdelmouleh, "Adsorptive Removal of Rhodamine B Dye Using Carbon Graphite/CNT Composites as Adsorbents: Kinetics, Isotherms and Thermodynamic Study," *Materials*, vol. 16, no. 3, p. 1015, Jan. 2023, doi: 10.3390/ma16031015.

[301] H. Zhu, S. Chen, H. Duan, J. He, and Y. Luo, "Removal of anionic and cationic dyes using porous chitosan/carboxymethyl cellulose-PEG hydrogels: Optimization, adsorption kinetics, isotherm and thermodynamics studies," *Int. J. Biol. Macromol.*, vol. 231, p. 123213, Mar. 2023, doi: 10.1016/j.ijbiomac.2023.123213.

[302] A. H. Jawad, A. S. Abdulhameed, E. Kashi, Z. M. Yaseen, Z. A. ALOthman,

and M. R. Khan, “Cross-Linked Chitosan-Glyoxal/Kaolin Clay Composite: Parametric Optimization for Color Removal and COD Reduction of Remazol Brilliant Blue R Dye,” *J. Polym. Environ.*, vol. 30, no. 1, 2022, doi: 10.1007/s10924-021-02188-1.

[303] K. Sukla Baidya and U. Kumar, “Adsorption of brilliant green dye from aqueous solution onto chemically modified areca nut husk,” *S. Afr. J. Chem. Eng.*, vol. 35, pp. 33–43, Jan. 2021, doi: 10.1016/j.sajce.2020.11.001.

[304] K. S. W. Sing *et al.*, “Reporting Physisorption Data for Gas/Solid Systems with Special Reference to the Determination of Surface Area and Porosity,” *Pure and Applied Chemistry*, vol. 57, no. 4, pp. 603–619, Jan. 1985, doi: 10.1351/PAC198557040603.

[305] C. S. Thatte, M. V. Rathnam, and A. C. Pise, “Chitosan-based Schiff base-metal complexes (Mn, Cu, Co) as heterogeneous, new catalysts for the β-isophorone oxidation,” *Journal of chemical sciences*, vol. 126, no. 3, pp. 727–737, 2014, doi: 10.1007/S12039-014-0601-4.

[306] F. A. R. Pereira *et al.*, “Green biosorbents based on chitosan-montmorillonite beads for anionic dye removal,” *J. Environ. Chem. Eng.*, vol. 5, no. 4, pp. 3309–3318, Aug. 2017, doi: 10.1016/j.jece.2017.06.032.

[307] F. Marrakchi, W. A. Khanday, M. Asif, and B. H. Hameed, “Cross-linked chitosan/sepiolite composite for the adsorption of methylene blue and reactive orange 16,” *Int. J. Biol. Macromol.*, vol. 93, pp. 1231–1239, Dec. 2016, doi: 10.1016/j.ijbiomac.2016.09.069.

[308] W. Sun, W. Sun, and Y. Wang, “Biosorption of Direct Fast Scarlet 4BS from aqueous solution using the green-tide-causing marine algae Enteromorpha prolifera,” *Spectrochim. Acta A Mol. Biomol. Spectrosc.*, vol. 223, p. 117347, Dec. 2019, doi: 10.1016/j.saa.2019.117347.

[309] D. C. L. Vasconcelos, V. C. Costa, E. H. M. Nunes, A. C. S. Sabioni, M. Gasparon, and W. L. Vasconcelos, “Infrared Spectroscopy of Titania Sol-Gel Coatings on 316L Stainless Steel,” *Materials Sciences and Applications*, vol. 02, no. 10, pp. 1375–1382, 2011, doi: 10.4236/msa.2011.210186.

[310] L. S. Ferreira *et al.*, “Adsorption of Ni2+, Zn2+ and Pb2+ onto dry biomass of Arthrospira (Spirulina) platensis and Chlorella vulgaris. I. Single metal systems,” *Chemical Engineering Journal*, vol. 173, no. 2, pp. 326–333, Sep. 2011, doi: 10.1016/j.cej.2011.07.039.

[311] A. Spoială *et al.*, "Preparation and Characterization of Chitosan/TiO2 Composite Membranes as Adsorbent Materials for Water Purification," *Membranes (Basel).*, vol. 12, no. 8, p. 804, Aug. 2022, doi: 10.3390/membranes12080804.

[312] R. Razuan Raja Derisa *et al.*, "Thermal Carbonization of Biomass Wood Dust and Algae Wastes *via* Microwave-Assisted H_3PO_4: Desirability Function and Statistical Optimization," *AUIQ Complementary Biological System*, vol. 2, no. 1, pp. 60–76, Mar. 2025, doi: 10.70176/3007-973X.1023.

[313] T. A. Rathi, V. Gomase, D. Saravanan, and R. Jugade, "Novel chitosan encapsulated nitrogen-doped multiwalled carbon nanotube composite for enhanced cyanide removal," *J. Mol. Liq.*, vol. 413, p. 125922, Nov. 2024, doi: 10.1016/J.MOLLIQ.2024.125922.

[314] S. K. Shukla *et al.*, "Removal of crystal violet by Cu-chitosan nano-biocomposite particles using Box–Behnken design," *J. Environ. Chem. Eng.*, vol. 9, no. 5, p. 105847, Oct. 2021, doi: 10.1016/j.jece.2021.105847.

[315] A. M. Elgarahy, A. Akhdhar, A. S. Al-Bogami, and K. Z. Elwakeel, "Magnetically separable solid phase extractor for static anionic dyes adsorption from aqueous solutions," *Surfaces and Interfaces*, vol. 30, p. 101962, Jun. 2022, doi: 10.1016/j.surfin.2022.101962.

[316] W.-R. Wang, P.-Y. Chen, J. Deng, Y. Chen, and H.-J. Liu, "Carbon-dot hydrogels as superior carbonaceous adsorbents for removing perfluorooctane sulfonate from water," *Chemical Engineering Journal*, vol. 435, p. 135021, May 2022, doi: 10.1016/j.cej.2022.135021.

[317] W. Wang *et al.*, "Efficient dye removal using fixed-bed process based on porous montmorillonite nanosheet/poly(acrylamide-co-acrylic acid)/sodium alginate hydrogel beads," *Appl. Clay Sci.*, vol. 219, p. 106443, Mar. 2022, doi: 10.1016/j.clay.2022.106443.

[318] N. Velinov *et al.*, "Wood residue reuse for a synthesis of lignocellulosic biosorbent: characterization and application for simultaneous removal of copper (II), Reactive Blue 19," *Wood Sci. Technol.*, vol. 53, no. 3, pp. 619–647, May 2019, doi: 10.1007/S00226-019-01093-0.

[319] T. A. Saleh, S. H. Al-Ruwayshid, A. Sarı, and M. Tuzen, "Synthesis of silica nanoparticles grafted with copolymer of acrylic acrylamide for ultra-removal of methylene blue from aquatic solutions," *Eur. Polym. J.*, vol. 130, p. 109698,

May 2020, doi: 10.1016/j.eurpolymj.2020.109698.

[320] R. Wu *et al.*, "Functionalization of chitosan biopolymer with SiO2 nanoparticles and benzaldehyde via hydrothermal process for acid red 88 dye adsorption: Box-Behnken design optimization," *Int. J. Biol. Macromol.*, vol. 247, p. 125806, Aug. 2023, doi: 10.1016/j.ijbiomac.2023.125806.

[321] S. Korde, S. Tandekar, and R. M. Jugade, "Novel mesoporous chitosan-zirconia-ferrosoferric oxide as magnetic composite for defluoridation of water," *J. Environ. Chem. Eng.*, vol. 8, no. 5, p. 104360, Oct. 2020, doi: 10.1016/j.jece.2020.104360.

[322] K. Malini, D. Selvakumar, and N. S. Kumar, "Enhanced CO2 uptake of mesoporous activated carbon derived from chitosan/casein coacervate," *Chemical Papers*, vol. 77, no. 8, pp. 4179–4192, Aug. 2023, doi: 10.1007/S11696-023-02768-6.

[323] A. H. Bashal, K. D. Khalil, A. M. Abu-Dief, and M. A. El-Atawy, "Cobalt oxide-chitosan based nanocomposites: Synthesis, characterization and their potential pharmaceutical applications," *Int. J. Biol. Macromol.*, vol. 253, p. 126856, Dec. 2023, doi: 10.1016/j.ijbiomac.2023.126856.

[324] Ç. Doğar, A. Gürses, M. Açıkyıldız, and E. Özkan, "Thermodynamics and kinetic studies of biosorption of a basic dye from aqueous solution using green algae Ulothrix sp.," *Colloids Surf. B Biointerfaces*, vol. 76, no. 1, pp. 279–285, Mar. 2010, doi: 10.1016/j.colsurfb.2009.11.004.

[325] S. D. Ashrafi, G. H. Safari, K. Sharafi, H. Kamani, and J. Jaafari, "Adsorption of 4-Nitrophenol on calcium alginate-multiwall carbon nanotube beads: Modeling, kinetics, equilibriums and reusability studies," *Int. J. Biol. Macromol.*, vol. 185, pp. 66–76, Aug. 2021, doi: 10.1016/j.ijbiomac.2021.06.081.

[326] F. Liang, L. Sun, Z. Zeng, and J. Kang, "Treatment of surfactant wastewater by foam separation: Combining the RSM method and WOA-BP neural network to explore optimal process conditions," *Chemical Engineering Research and Design*, vol. 193, pp. 85–98, May 2023, doi: 10.1016/j.cherd.2023.03.023.

[327] U. Baig, M. K. Uddin, and M. A. Gondal, "Removal of hazardous azo dye from water using synthetic nano adsorbent: Facile synthesis, characterization, adsorption, regeneration and design of experiments," *Colloids Surf. A Physicochem. Eng. Asp.*, vol. 584, p. 124031, Jan. 2020, doi:

10.1016/j.colsurfa.2019.124031.

[328] B. Zdravkov, J. Čermák, M. Šefara, and J. Janků, “Pore classification in the characterization of porous materials: A perspective,” *Open Chem.*, vol. 5, no. 2, pp. 385–395, Jun. 2007, doi: 10.2478/s11532-007-0017-9.

[329] M. M. Rahman and M. Maniruzzaman, “A new route of production of the meso-porous chitosan with well-organized honeycomb surface microstructure from shrimp waste without destroying the original structure of native shells: Extraction, modification and characterization study,” *Results in Engineering*, vol. 19, p. 101362, Sep. 2023, doi: 10.1016/j.rineng.2023.101362.

[330] F. Stanculescu, M. Socol, E. Matei, and A. Stanculescu, “Effect of heavy ions irradiation on the properties of benzil crystals,” *Crystal Research and Technology*, vol. 52, no. 8, Aug. 2017, doi: 10.1002/crat.201700047.

[331] F. Almomani and R. R. Bhosale, “Bio-sorption of toxic metals from industrial wastewater by algae strains Spirulina platensis and Chlorella vulgaris: Application of isotherm, kinetic models and process optimization,” *Science of The Total Environment*, vol. 755, p. 142654, Feb. 2021, doi: 10.1016/j.scitotenv.2020.142654.

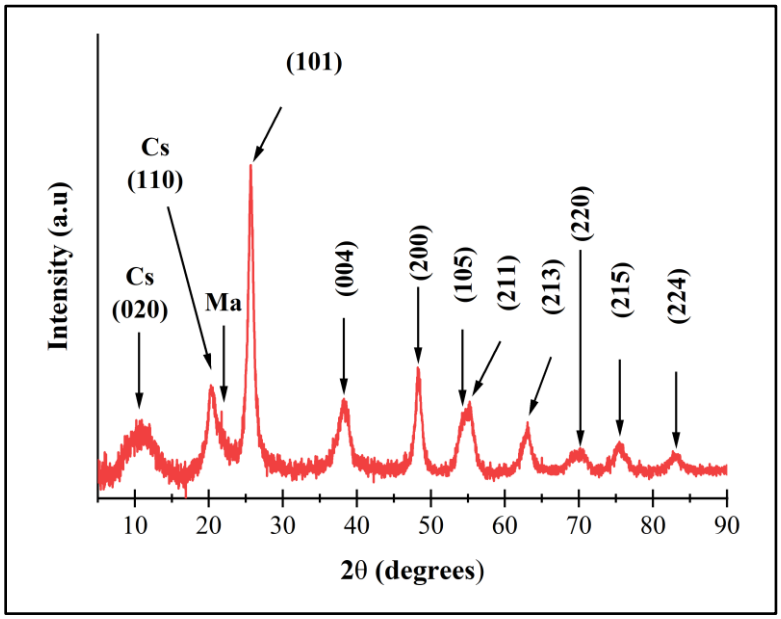
[332] J. Flores-Gómez, V. H. Romero-Arellano, M. Vazquez-Lepe, Á. de J. Martínez-Gómez, and J. Morales-Rivera, “Modeling and Optimization of the Adsorption of Cr (VI) in a Chitosan-Resole Aerogel Using Response Surface Methodology,” *Gels*, vol. 9, no. 3, p. 197, Mar. 2023, doi: 10.3390/gels9030197.

[333] V. O. Njoku, M. A. Islam, M. Asif, and B. H. Hameed, “Preparation of mesoporous activated carbon from coconut frond for the adsorption of carbofuran insecticide,” *J. Anal. Appl. Pyrolysis*, vol. 110, pp. 172–180, Nov. 2014, doi: 10.1016/j.jaap.2014.08.020.

APPENDICES

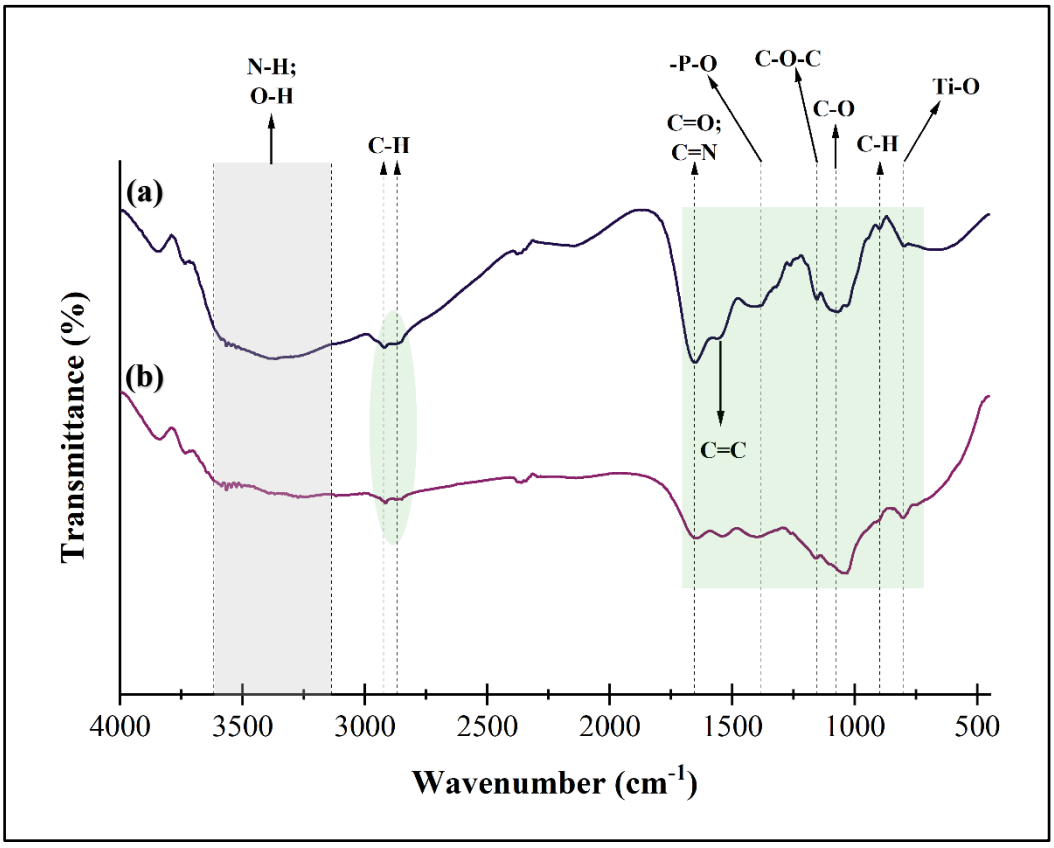
APPENDIX 1

XRD pattern of Cs-Ma-Tk



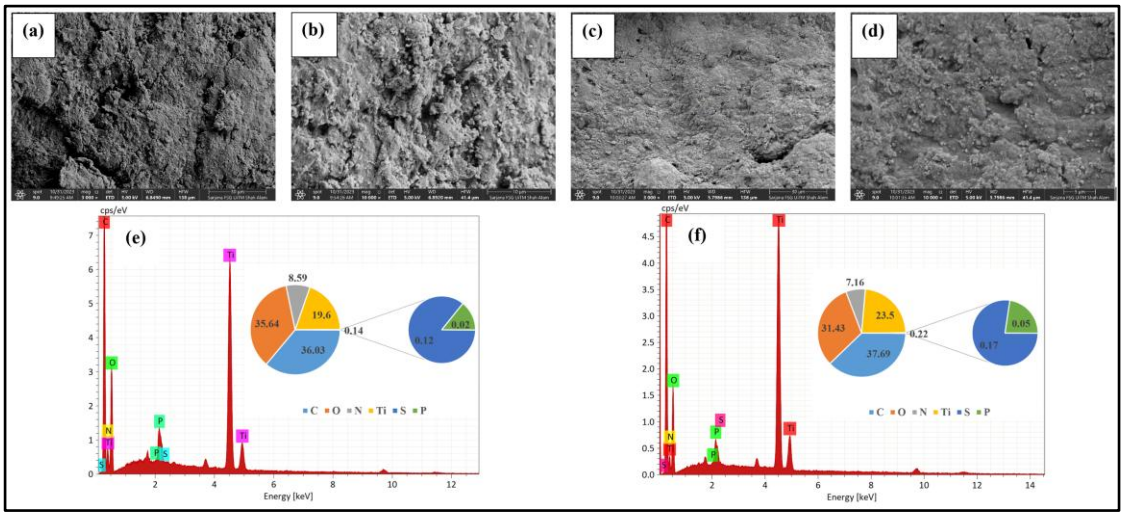
APPENDIX 2

FT-IR spectra of Cs-Ma-Tk (a) before and (b) after BG dye adsorption



APPENDIX 3

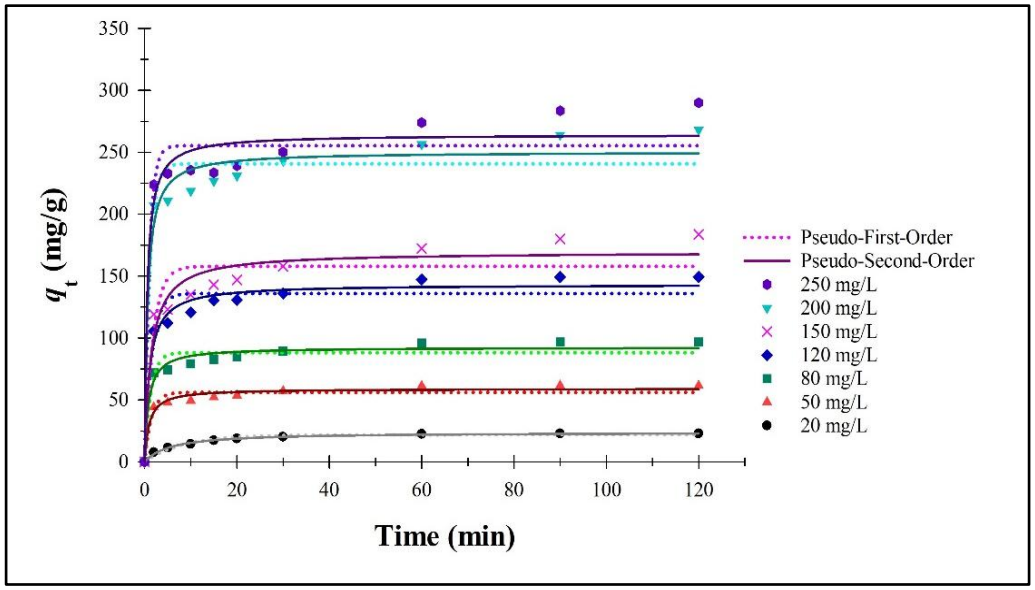
FESEM images and EDX data of Cs-Ma-Tk before (a and b) and after (c and d) BG dye adsorption at x3k (a and c) and x10k (b and d) magnification powers and EDX data of Cs-Ma-Tk before (e) and after (d) BG dye adsorption



APPENDIX 4

Impact of initial dye concentration and kinetic model regressions and parameters of BG dye removal by Cs-Ma-Tk

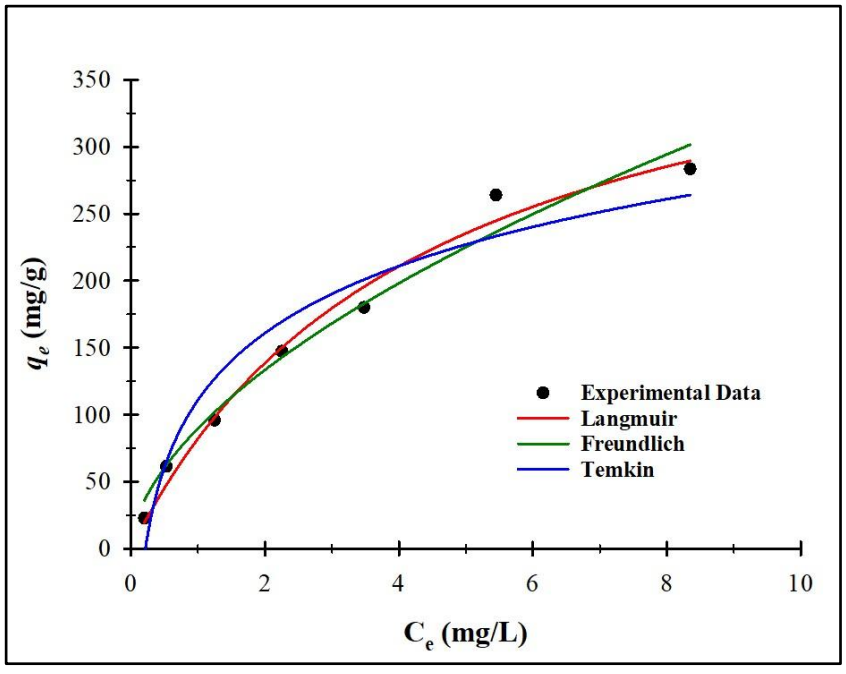
Concentration (mg/L)	$q_{e\ exp.}$ (mg/g)	PFO			PSO		
		$q_{e\ cal}$ (mg/g)	k_1 (1/min)	R^2	$q_{e\ cal}$ (mg/g)	$k_2 \times 10^{-2}$ *(g/mg min)*	R^2
20	22.8	21.8	0.12	0.964	23.9	0.75	0.993
50	61.6	56.0	0.69	0.933	59.0	1.82	0.971
80	96.6	88.0	0.76	0.936	92.4	1.32	0.971
120	149.4	135.9	0.65	0.933	143.4	0.70	0.974
150	183.7	157.9	0.55	0.881	169.6	0.43	0.944
200	268.1	240.7	0.92	0.943	250.4	0.65	0.969
250	289.9	255.3	1.01	0.936	264.4	0.73	0.956



APPENDIX 5

Langmuir, Freundlich and Temkin isotherm regressions and parameters for BG removal by Cs-Ma-Tk

Adsorption isotherm	Parameter	Chi-Ma-K
Langmuir	q_{max} (mg/g)	440.8
	K_a (L/mg)	0.23
	R^2	0.981
Freundlich	K_f (mg/g) $(L/mg)^{1/n}$	89.9
	n	1.75
	R^2	0.979
Temkin	K_T (L/mg)	4.66
	b_T (J/mol)	34.4
	R^2	0.931



APPENDIX 6

Physicochemical characteristics of Cs-Ma-Tk

Parameters	Chi-Ma-K
Surface Area (m^2/g)	6.27
Pore Volume (cm^3/g)	0.10
Average Pore Diameter (nm)	6.57
Carbon	30.94%
Hydrogen	5.04%
Nitrogen	5.70%
Sulphur	0.07%
Oxygen (by difference) (%)	58.25%

APPENDIX 7

BBD design coded and actual values alongside predicted and experimental response for BG removal by Cs-Ma-Tk with desirability test results (last row)

Run no.	Coded Values			Actual values			Removal of BG (%)	
	A	B	C	A	B	C	Observed	Predicted
1	-1	-1	0	0.02	4	35	33.9	35
2	+1	-1	0	0.1	4	35	73.9	72.9
3	-1	+1	0	0.02	9	35	73.6	74.6
4	+1	+1	0	0.1	9	35	94.8	93.7
5	-1	0	-1	0.02	6.5	10	45.5	44.3
6	+1	0	-1	0.1	6.5	10	73.3	74.2
7	-1	0	+1	0.02	6.5	60	69.2	68.3
8	+1	0	+1	0.1	6.5	60	94.1	95.3
9	0	-1	-1	0.06	4	10	40.2	40.3
10	0	+1	-1	0.06	9	10	75.6	75.8
11	0	-1	+1	0.06	4	60	68.3	68.1
12	0	+1	+1	0.06	9	60	93.2	93.1
13	0	0	0	0.06	6.5	35	73.5	74.3
14	0	0	0	0.06	6.5	35	75.5	74.3
15	0	0	0	0.06	6.5	35	73.3	74.3
16	0	0	0	0.06	6.5	35	74.6	74.3
17	0	0	0	0.06	6.5	35	74.8	74.3
Desirability test run				0.08	8.67	53.2	92.4±0.9	94.9

AUTHOR'S PROFILE



Elmira Kashi obtained her bachelor's degree in Textile Engineering (Chemistry of Textiles and Fibre Science) in 2013 from University of Guilan, Iran, MSc in Textile Engineering (Chemistry of Textiles and Fibre Science) in 2016 from Amirkabir University of Technology, Iran.

LIST OF PUBLICATIONS:

[1] E. Kashi, A. H. Jawad, R. Wu, and Z. A. ALOthman, "Desirability numerical optimisation for cationic dye removal by Schiff base chitosan-glyoxal/microalgae/titanium dioxide: Application of response surface methodology," Int. J. Biol. Macromol., vol. 339, p. 149831, Jan. 2026, doi: 10.1016/J.IJBIOMAC.2025.149831.

[2] E. Kashi, A. H. Jawad, S. N. Surip, R. Wu, and Z. A. AlOthman, "Hydrothermally grafted chitosan/organic/inorganic composite adsorbent for optimised removal of brilliant green dye: Desirability function, equilibrium and mechanism study," Int. J. Biol. Macromol., vol. 323, p. 146998, Sep. 2025, doi: 10.1016/J.IJBIOMAC.2025.146998.

[3] E. Kashi, A. H. Jawad, S. N. Surip, R. Wu, and Z. A. ALOthman, "Crosslinked chitosan-benzil/microalgae/kronos (titanium dioxide) biocomposite for the removal of brilliant green dye: Response surface methodology optimisation and mechanism," Int. J. Biol. Macromol., vol. 312, p. 144005, Jun. 2025, doi: 10.1016/J.IJBIOMAC.2025.144005.

[4] R. H. Wu, E. Kashi, A. H. Jawad, S. A. Musa, Z. A. ALOthman, and L. D. Wilson, “Polymeric Matrix of Modified Chitosan with Algae and Coal Fly Ash for a Toxic Cationic Dye Removal: Multivariable Optimization by Box-Behnken Design,” J. Inorg. Organomet. Polym. Mater., vol. 35, no. 4, pp. 2300–2314, Apr. 2024, doi: 10.1007/S10904-024-03241-X.

[5] M. S. Sando, A. M. Farhan, A. Hapiz, E. Kashi, S. A. Musa, and A. H. Jawad, “Adsorptive Performance of High Surface Area Date Palm Bunch Activated Carbon Towards Methyl Violet and Fuchsin Basic Dyes Removal: Thermochemical Activation And Statistical Optimization,” Water Air Soil Pollut., vol. 236, no. 3, pp. 1–23, Mar. 2025, doi: 10.1007/S11270-025-07834-1.

[6] R. Wu, A. H. Jawad, E. Kashi, S. A. Musa, and Z. A. ALOthman, “Zwitterion Adsorbent of Crosslinked Chitosan-Benzil/Algae/Coal Fly Ash for Anionic (Remazol Brilliant Blue R) and Cationic (Thionine) Dyes Removal: Box–Behnken Design Optimization,” J. Polym. Environ., vol. 32, no. 12, pp. 6390–6404, Dec. 2024, doi: 10.1007/S10924-024-03388-1.

[7] R. Wu, E. Kashi, A. H. Jawad, S. A. Musa, Z. A. ALOthman, and L. D. Wilson, “Organic and inorganic polymeric matrix of modified chitosan with algae and coal fly ash for cationic toxic dye removal: Multivariable optimization by Box-Behnken Design,” Jun. 2024, doi: 10.21203/RS.3.RS-4508283/V1.

[8] E. Kashi et al., “High adsorptive performance of chitosan-microalgae-carbon-doped TiO2 (kronos)/ salicylaldehyde for brilliant green dye adsorption: Optimization and mechanistic approach,” Int. J. Biol. Macromol., vol. 259, p. 129147, Feb. 2024, doi: 10.1016/j.ijbiomac.2023.129147.

[9] A. S. Abdulhameed et al., “Organically modified montmorillonite composited with magnetic glyoxal-chitosan Schiff base for reactive blue 19 dye removal: Process optimization and adsorptive mechanism,” Int. J. Biol. Macromol., vol. 256, p. 128463, Jan. 2024, doi: 10.1016/J.IJBIOMAC.2023.128463.

[10] A. S. Abdulhameed, A. H. Jawad, E. Kashi, K. A. Radzun, Z. A. ALOthman, and L. D. Wilson, “Insight into adsorption mechanism, modeling, and desirability function of crystal violet and methylene blue dyes by microalgae: Box-Behnken design application,” Algal Res., vol. 67, 2022, doi: 10.1016/j.algal.2022.102864.

[11] A. H. Jawad, A. S. Abdulhameed, E. Kashi, Z. M. Yaseen, Z. A. ALOthman, and M. R. Khan, “Cross-Linked Chitosan-Glyoxal/Kaolin Clay Composite: Parametric Optimization for Color Removal and COD Reduction of Remazol Brilliant Blue R Dye,” J. Polym. Environ., vol. 30, no. 1, 2022, doi: 10.1007/s10924-021-02188-1.